SEDIMENTOLOGY AND SEQUENCE STRATIGRAPHY OF THE LATE CRETACEOUS LOWER FERRON SANDSTONE: APPLICATION OF 3-D GEOCELLULAR MODELLING TO THE DRUNKARDS WASH CBM-FIELD IN CENTRAL UTAH, USA

Tore Klausen

Thesis for the Masters Degree in

Petroleum Geology

Department of Earth Science

University of Bergen

Bergen, Norway

June 2010

Acknowledgements

This thesis is a part of a Masters Degree in petroleum geology at the University of Bergen, to which I owe gratitude for funding my field work.

First of all, I would like to express my profound appreciation for being introduced to this exciting project by my supervisor Professor John Anthony Howell, and for the excellent supervision and his review of my draft. His network, experience, and thought-provoking discussions were all extremely valuable to this thesis.

I am very grateful to Roy Davies and Simon Buckley for sharing their software expertise that enabled me to build the model, and for being patient and approachable with questions.

My two field assistants, Christian Haug Eide and Jonas Aas Torland, are both thanked for taking time out of their busy schedule to help out during my field work.

Michael Laine and the staff at Utah Geological Survey Core Research Centre in Salt Lake City are thanked for pulling the Drunkards Wash core and for the friendly atmosphere I experienced while working there.

Thomas A. Ryer is thanked for inviting me along for a day looking at the Upper Ferron, and for the subsequent discussions in the field and at the Core Research Centre.

I would like to thank my family for all their support and encouragement during the five years I have spent at the University.

Finally, I would like to thank all my friends and fellow students at the University and 'Bakevja' for making these years fly by. None mentioned, none forgotten.

Tore Klausen

Bergen, June 2010

Abstract

Keywords: Wave dominated shoreface, Coal Deposits, Lower Ferron, Subsurface modelling, Sequence Stratigraphy

Deposition of the Ferron Sandstone Member occurred during a widespread regression of the Western Interior Seaway during the Turonian. The Ferron is informally subdivided into two units. The Upper Ferron, ferronensis sequence is well exposed as a shallow marine and coastal plain clastic wedge along the edge of the Wasatch Plateau in central Utah. In contrast the Lower Ferron, hyatti sequence, has previously only been documented in the outcrop and as a basal sandstone in the subsurface Drunkards Wash, Buzzard Bench and Helper fields around the town of Price, where the Upper Ferron is interpreted to form a major coal bed methane accumulation in non-marine deposits overlying the Lower Ferron sandstone.

The aim of this study is to improve the current understanding of the stratigraphy and sedimentology of the Lower Ferron unit. Correlation of 55 borehole logs coupled with outcrop studies have resulted in a new depositional model for the system. The correlations suggest that the Lower Ferron is comprised of a series of progradational to aggradational shoreface parasequences which prograded in an east to south-easterly direction. Modelling also suggests that a series of outcrops, previously interpreted as long shore bars, are in fact the downdip expression of these shorefaces. This model is supported by extrapolation of the facies tracts mapped in the subsurface, geometric reconstruction of the large scale structures and correlation of bentonite horizons. The final model suggests a more prominent Lower Ferron depositional system than previous studies and suggests a dynamic transition between the informally named Upper and Lower Ferron Sandstone.

Table of Contents

1 Introduction

1.1 Aim of the study

The Late Cretaceous Ferron Sandstone Member of the Mancos Shale is a well exposed, shallow marine to paralic, clastic wedge which crops out along the western edge of the San Rafael Swell in eastern Utah. Outcrops of the unit have been extensively studied as analogues for sub-surface reservoirs (Corbeanu et al., 2001; Li and White, 2003; Forster et al., 2004; van den Bergh and Garrison, 2004). There has been a long tradition on coal mining from the unit and more recently it has become commercially important as a Coal Bed Methane (CBM) play. The Ferron clastic wedge represents a highstand system tract (Ryer, 2004) within the Mancos Shale of the Mesaverde Group, deposited in a period of regression during peak Cretaceous flooding of the Western Interior Seaway in North America. The Ferron is informally subdivided into upper and lower units. The Upper Ferron comprises the majority of the outcrops and has been extensively studied over the past century (e.g. Lupton, 1916; Katich, 1953; Davis, 1954; Hale and Van De Graaff, 1964; Hale, 1972; Cotter, 1976; Ryer, 1980, 1981, 1984, 1994; Ryer and McPhillips, 1983; Gardner, 1993, 1995a, 1995b; Garrison and van den Bergh, 1997), and culminated with the publication of an AAPG memoir (Chidsey et al., 2004) which captures the current understanding. In contrast, the Lower Ferron, which is said to underlie the recent CBM fields, has been largely ignored.

The aims of the present study are:

1. To describe the sedimentology and stratigraphy of the Lower Ferron, especially the portion that lies within the subsurface.
2. To determine the relationship between the Lower Ferron in the subsurface and a series of outcrops in the San Rafael Swell.
3. To clarify the stratigraphy relationship between the Upper and Lower Ferron
4. To build a geocellular model of the Lower Ferron which captures and illustrates the relationships described above.

Data for the study have included 55 geophysical well logs and 12 outcrops that were not previously related to the subsurface field. The model focuses on the Drunkards Wash CBM-field, which is the largest field in Castle Valley and one of the most productive of its kind in

North America (Montgomery et al., 2001). The coal-bearing deposits from which the methane gas is extracted are related to a large coal-fairway in Castle Valley that stretches from beneath the Book Cliffs in the north to the Upper Ferron outcrops 100 km south.

1.2 The Study Area

The Ferron Sandstone Member crops out in Castle Valley along the northwestern rim of the San Rafael Swell (SRS), southeast of Price (Figure 1.1), The Castle Valley is bordered by the escarpment of the Wasatch Plateau to the east and the Book Cliffs to the north. The present day climate is arid, which limits vegetation cover and results in good quality outcrops. The Ferron Sandstone Member outcrop stretches as a near continuous ridge, cut by rivers and small canyons, south-southwest from the Book Cliffs for about 120 km to Indian Canyon in the south. The Ferron Sandstone Member includes up to 180 m of Turonian to Cenomanian strata.

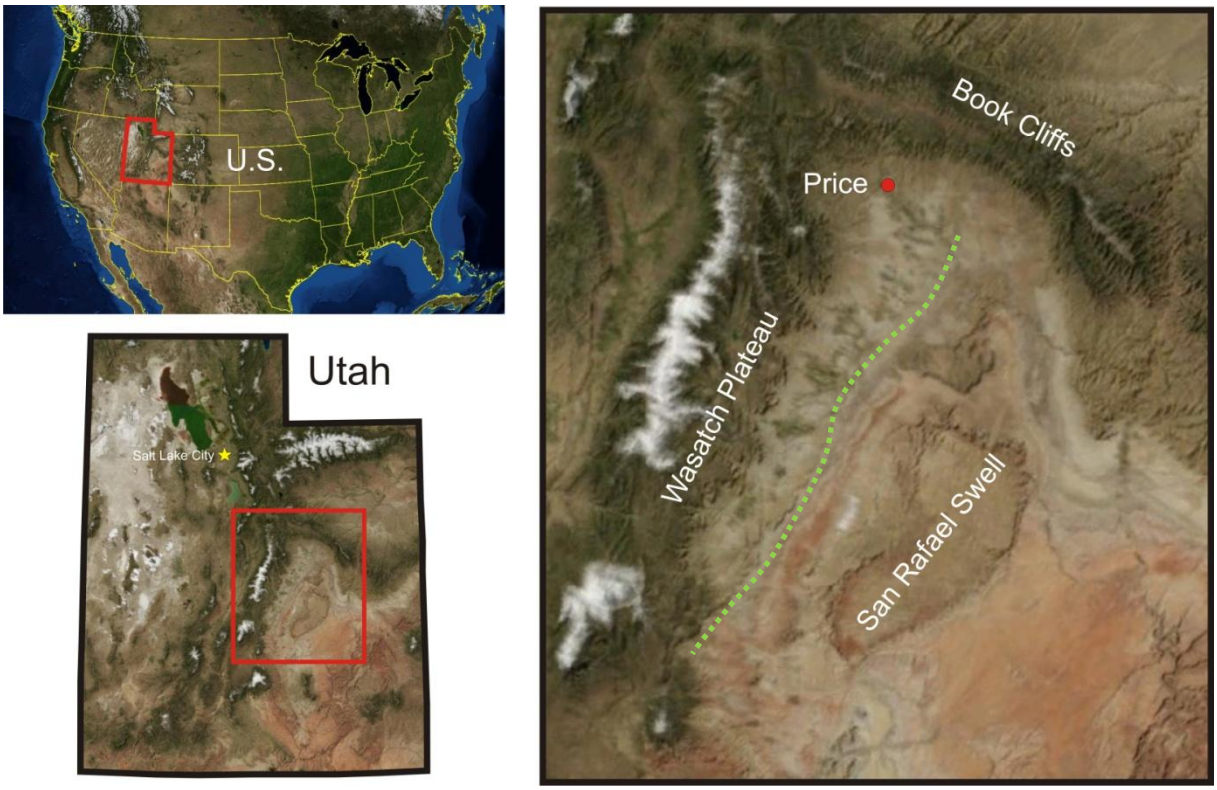

Figure 1.1: Overview maps of the study area. All images courtesy of NASA. Approximate location of Turonian Ferron Sandstone Member outcrop belt along dotted green line.

The majority of this study is focused on the Lower Ferron which is present in a series of CBM fields(Figure 1.2 B) around the town of Price and crops out in a near continuous ridge that runs for 35 km from Wellington to Castle Dale (Figure 1.3). The Lower Ferron is on average 90 m thick in the subsurface, and close to 30 meter high outcrops are recorded along the western rim of the SRS (Figure 1.2 A). Additionally studies were also undertaken on the Upper Ferron Sandstone which crops crop out along Interstate 70 south of Castle Valley. This was used as an analogue for the proximal parts of the Lower Ferron which lie within the subsurface and do not occur at outcrop.

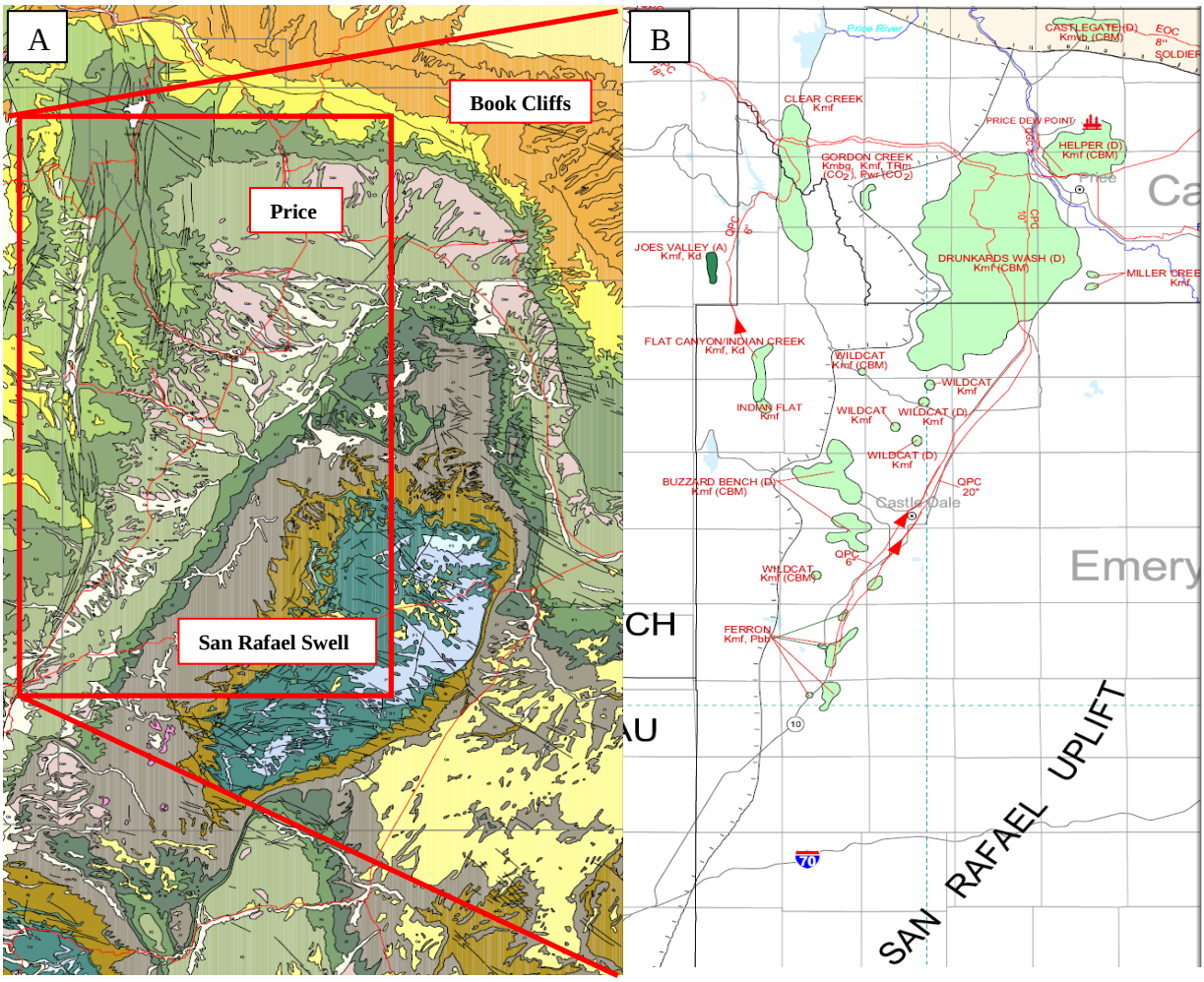

Figure 1.2: A) Geological map of the study area in Castle Valley. Central feature is the San Rafael Swell, northern escarpment is the Book Cliffs, and to the west is the Wasatch Plateau (Hintze et al., 2000). B) Map showing the position of the CBM-fields located in Castle Valley (Chidsey et al., 2004). The relationship between outcrop and the CBM-field is shown in Figure 1.3, along with the model grid-outline.

The main focus of the study is the strata in the Drunkards Wash CBM field which is located, to the east and southeast of the town of Price. Figure 1.3, and Figure 1.2 B, shows the CBM-fields of Carbon and Emery County which follow the coal bed play of the Ferron Sandstone Member where it stretches southward along the western rim of SRS and the escarpment of the Wasatch Plateau in Castle Valley. The Drunkards Wash field is the largest of the CBM-fields in Castle Valley, and one of the most productive of its kind in North America.

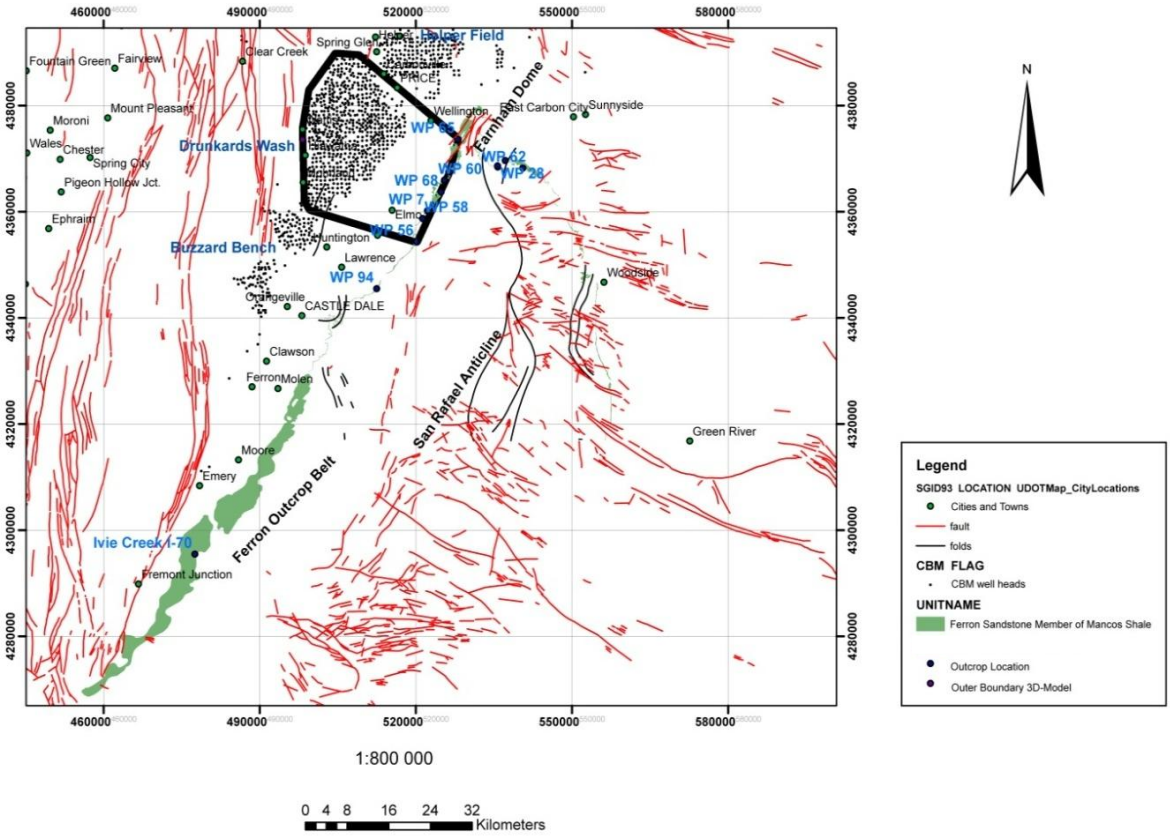

Figure 1.3: Overview map of Castle Valley and the San Rafael Swell. The map highlights the most important geological features, outcrop localities, the model outline and the producing CBM-wells.

1.3 Previous work

Most of the previous work on the Ferron Sandstone Member has focused on the Upper Ferron due to the superb quality of outcrops found in the southern part of Castle Valley and further south. The Lower Ferron at outcrop was described by Cotter, (1975) and Edwards et al. (2005) although neither of these papers considering the stratigraphic relationship between the outcrops and the producing strata CBM-fields. Following the discoveries of commercially producible gas fields in Castle Valley, Henry and Finn (2003) described the Ferron Sandstone Member in the northern part of the Ferron coal-fairway with the aid of well correlation panels. Montgomery et al. (2004) provide a summary of the work that has been carried out on the northern part of the Ferron Sandstone Member (the Lower Ferron), and suggested that more work was needed to fully appreciate the stratigraphic relationship between the Upper and Lower Ferron.

The Lower Ferron, represented by the Kf-Washboard unit of Anderson and Ryer (2004), has been interpreted to occur as far south as Mesa Butte, more than 70 km south of the Lower Ferron recognized in this study, in their study on the Upper Ferron. The proposed explanation for the southward extent of the Lower Ferron, to where the sandstones come to underlay the Upper Ferron, invokes the southward migration of a shelf sand plume (Thompson et al., 1986; Ryer, 2004) from the northern Vernal deltaic complex to be discussed in more detail later. The southward extent of the Lower Ferron and its relation to the overlying Upper Ferron is only vaguely addressed, and a source for controversy. Further, their terminology Kf-Washboard highlights a second problem encountered in the Lower Ferron literature, namely the differentiation between the Clawson and Washboard units of Cotter (1975). Originally lithostratigraphic units, these names are applied to the parasequences of the Lower Ferron hyatti sequence without consistency; compare for example the schematic cross sections of Anderson and Ryer (2004) with that of Barton et al. (2004). All of these issues will be addressed in this thesis.

1.4 Methodology

A variety of different methods were applied to the present study. They include traditional field work, digital datasets and 3D geocellular modelling. Each method will be covered in more detail in the chapter to which they apply, a short summary include:

- Compilation of existing data on the Ferron Sandstone Member from papers, published literature, field guides and maps.
- Downloading and processing available log data and cultural information for the Drunkards Wash CBM-field.
- Field work including logging, bed tracing and digital mapping (two field seasons)
- Core logging of a well section from the Drunkards Wash CBM-field to establish facies associations for the subsurface well logs.
- Combining digital datasets with outcrop and core observations to construct a digital, subsurface 3D model.

2 Geological Setting

2.1 Palaeogeography

The Cretaceous Ferron Sandstone Member was deposited within the western interior seaway in a regressive phase during a Turonian highstand of sea-level (Kauffman, 1984). During this time, the central and eastern part of the state of Utah was covered by an epeiric sea with a northwest to northeast striking western shoreline. The shoreline lay about 60 km east of the active foreland basin margin and responded to changes in both sediment-supply and relative sea-level. The sea-level was influenced by both global sea-level and regional tectonic events, (Figure 2.1) and the tectonic activity in the Sevier Orogenic belt to the west impacted both sediment supply and regional subsidence patterns.

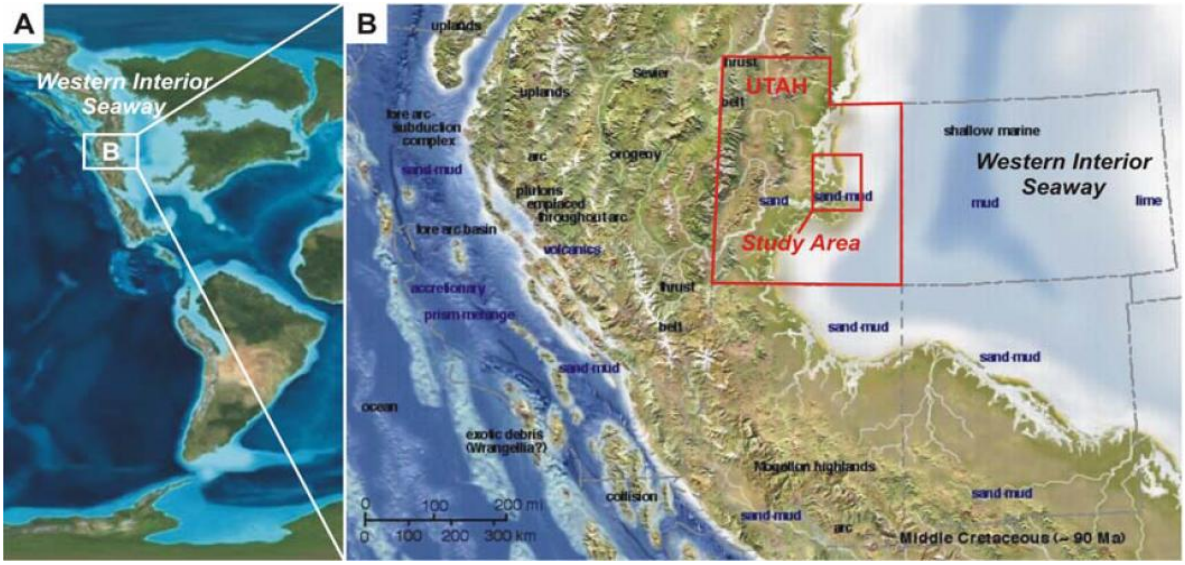

Figure 2.1: Palaeogeographic reconstruction of North America and close-up of western North America, in the Late Cretaceous. Modified after Blakely, http://jan.ucc.nau.edu/~rcb7/crepaleo.html 25/10-2009

The Cordilleran thrust belt at the western margin of North America extended for about 6000 km from Canada to Mexico, and existed as a continent-ocean convergent margin from the Late Jurassic 155 Ma to the middle Eocene (DeCelles 2004). The breakup of the supercontinent Pangaea, initiated by an ancestral North Atlantic spreading centre, forced the North American craton westward (Dietz and Holden, 1970). This motion was counteracted by contractional forces along the western margin where the craton met the eastward moving

component of the Farallon oceanic plate. Dense oceanic crust which made up the Farallon plate, being less buoyant than the continental craton, was forced to subside and led to the development of a volcanic arc and associated accretion of foreign terrains. The mountain belt that formed in response to the accreted terrains and magmatism is now part of the present day state of California. A series of orogenic events including oblique collision, the accretion of microcontinents and changes in the angle of slab subduction led to the present day situation. The Sevier and Laramide orogenies were the most important of these tectonic events and spanned the Cretaceous to early Tertiary (app. 119 - 45Ma). The Sevier Orogeny was associated with an increase in the rate at which the Farallon Plate was subducted underneath the North American craton (DeCelles 2004) and the accretion of exotic terrains from the subducting Farallon plate. This activity which stacked Proterozoic-Palaeozoic rocks at the western margin of the North American craton, forced the continent to bulge and flex creating an Andean style foreland basin (Jordan, 1981; Figure 2.2 and Figure 2.4).

The western margin of this foreland basin was located in the centre of the present day state of Utah. The basin had an asymmetric profile with a steep western margin proximal to the thrust front and a gentler dipping margin towards its foreland bulge. The onset of this foreland basin, coupled with a major eustatic sea-level rise forced by elevated global temperatures and increased seafloor spreading rates (Haq et al., 1987), led to the flooding of the basin to produce the Western Interior Seaway in the Aptian. Flooding first occurred from the Arctic Ocean through the Mowry Sea in the north, and eventually linked up with The Gulf of Mexico and Thethy's ocean in the middle Late Albian. This epicontinental ocean is estimated to have had a maximum width of 1620 km, but never reached depths of more than 500 m (Kauffman, 1984). Due to the mountain belt in the west, the seaway was partially sheltered from the prevailing wind direction and thus the fetch did not resemble open-ocean conditions thus limiting the influence of storms on the sedimentary deposits (Cotter, 1975).

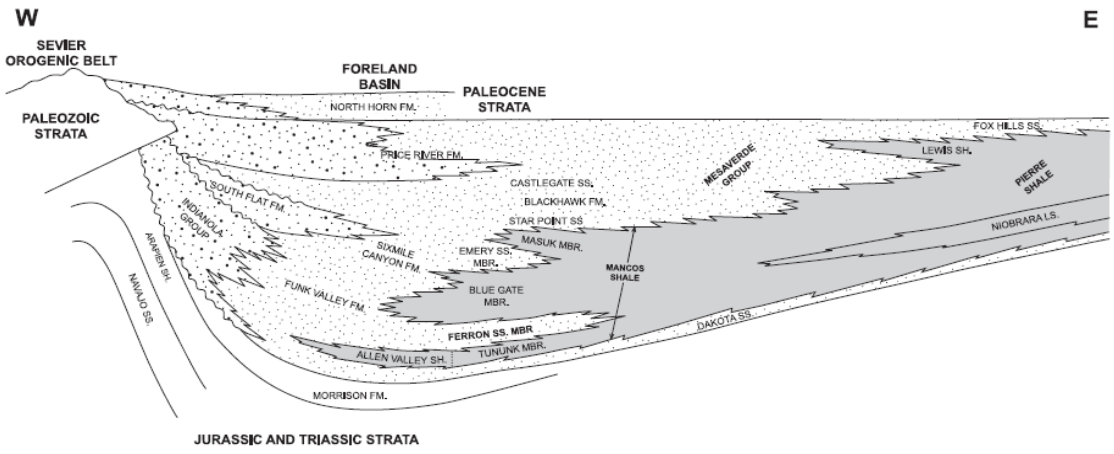

Figure 2.2: Regional schematic cross section from west to east, western Utah to western Colorado. Intertonguing Cretaceous strata, marine shale and limestone (shaded) and non-marine to marine-clastic (dotted). Modified by Henry and Finn, 2003, from Armstrong, 1968.

Elevated global temperatures were the norm for the Late Cretaceous (Hay et al., 1997) and the study area experienced a warm and humid climate throughout the period of deposition, something that is evident from the high carbonate content within the marine deposits, and thick deposits of coal in the non-marine strata.

The uplifting Sevier mountain range supplied significant volumes of sediment to the western part of the basin where the Indianola and Mesa Verde groups were deposited as a large clastic wedge (Figure 2.2). The eastern part of the seaway was dominated by carbonate deposits which included the Niobrara Limestone. The Mancos Shale was deposited throughout the central part of the basin.

The onset of Laramide uplift, and falling global sea-level resulted in the end of the epeiric seaway, after a period of about 35 my. The Laramide Orogeny resulted in uplift of more than 6000 m (Howell and Flint, 2003) to its present day topography.

2.2 Tectonic framework

Continental shortening initiated in the Late Jurassic and shortened the North American craton by as much as 350 km. Eastward migration of the Cordilleran thrust front by 1000 km was associated with the discontinuous to overlapping orogenic events, including the Sevier and Laramide orogenies (Decelles, 2004).

The Sevier Orogeny has its easternmost thrust front in east-central Utah where it is named after a type locality in Sevier County. A detailed map of the regional extent of the respective orogenies associated with the Late Jurassic to Eocene Cordilleran thrust belt is presented in Figure 2.3, where the Sevier thrust front may be seen as a narrow, extensive grey band through the North American continent. The Sevier Orogeny was initiated in the Albian, about 105 million years ago (Stokes, 1988). It spanned a north-south distance of 2000 km along the the entire North American continent, and is estimated to have been between 200 and 350 km wide (east-west) in central Utah and eastern Nevada (Miller et al., 1983; DeCelles 2004). The style of shortening during this orogenic event was mainly thin-skinned tectonics (Armstrong, 1968). The tectonic history included regional-scale mega-thrust sheets of Palaoezoic to Proterozoic age in the Early Cretaceous to multiple closely spaced Palaeozoic to Mesozoic thrust sheets in the Late Cretaceous to Palaeocene time. The frontal wedge of the Sevier thrust, consisting of the Palaeozoic to Mesozoic sedimentary strata, followed a regional basal décollement propagating through weak horizons such as the Lower Cambrian shale unit and the salt interval in the Jurassic Preuss Formation (DeCelles and Mitra, 1995). This stacking and loading of rocks on the western margin of the North American craton caused the flexure and the development of the foreland basin. This foreland basin inherited an asymmetric morphology (Jordan, 1981; Beaumont, 1981), as well as an asymmetric sedimentary accumulation which contributed to further subsidence within the basin. Syn-tectonic erosion contributed to the deposition of a thick clastic wedge at the western margin of the foreland basin (Sinclair et al., 1991).

Flexural subsidence contributed with important control on sites of erosion and deposition within the foreland basin (Decelles, 2004; Pang and Nummedal, 1995) during the Early Cretaceous through Turonian (~142-89Ma). Differences in subsidence are attributed to differential rigidity of the basement rocks, which would favour emplacement of thrust loads in areas of less rigidity, and thus affect subsidence indirectly but notably. Additionally, Pang and Nummedal (1995) suggest strike variation in magnitude and timing along the thrust front as a geodynamic factor that would have contributed to the flexural subsidence pattern. The impact

of differential subsidence on sediment dispersal in the Vernal deltaic-complex was suggested by Ryer and Lovekin (1986).

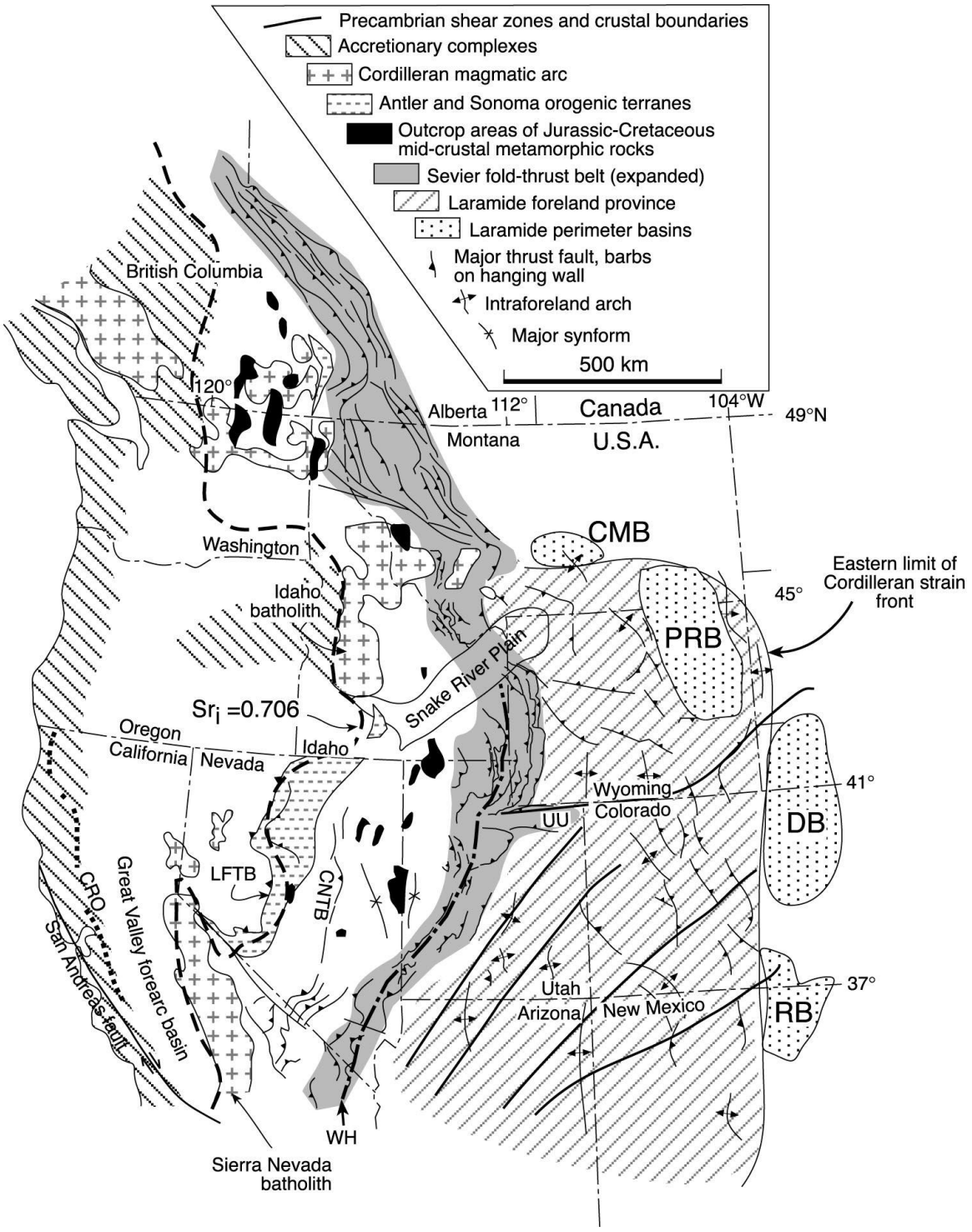

Figure 2.3: Tectonic map of the major components of the Cordilleran orogenic belt in the western United States, from DeCelles, 2004: *Abbreviations as follows: CRO, Coast Range ophiolite; LFTB, Luning-Fencemaker thrust belt; CNTB, Central Nevada thrust belt; WH,Wasatch hinge line; UU, Uinta Mountains uplift; CMB, Crazy Mountains basin; PRB, Powder River basin; DB,Denver basin; RB, Raton basin.*

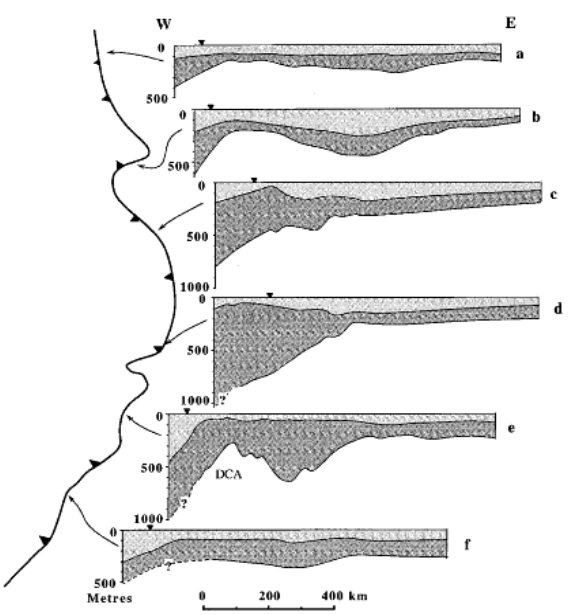

Figure 3. Flexurally backstripped subsidence profiles across basin. Light shading marks magnitude of subsidence from 97 (94 on e and f) to 90 Ma, and dark shading marks magnitude of subsidence from 90 to 80 Ma (83 on c and d). Vertical scale is tectonic subsidence in metres. Triangles indicate locations of subsidence curves discussed in Figure 4. DCA is Douglas Creek arch.

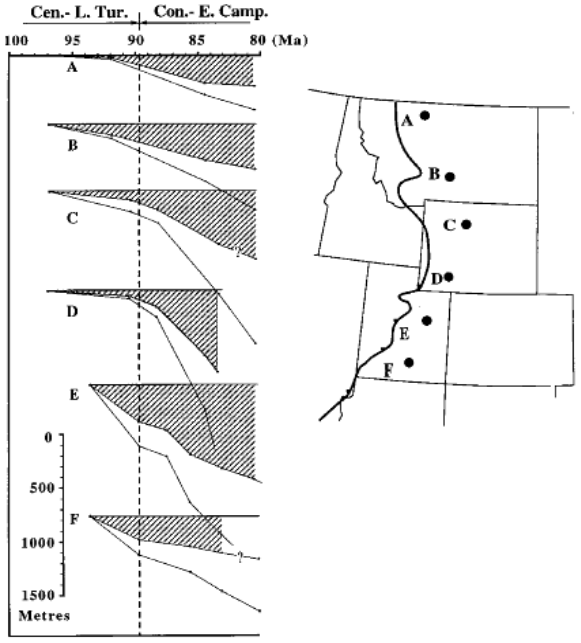

Figure 4. Temporal subsidence trends at six locations 100–150 km east of thrust belt (see Fig. 3). Diagonal-rule areas represent cumulative tectonic subsidence through time. Solid lines below represent total (uncorrected) subsidence. Cen—Cenomanian; L. Tur.—lower Turonian; Con—Coniacian; E. Camp.—early Campanian.

Figure 2.4: Pang and Nummedal, 1995. The Western Interior foreland basin, and its relationship between sediment accumulation and flexural subsidence of bedrock along the easternmost margin of the Sevier Orogeny.

The Laramide Orogeny followed the Sevier Orogeny resulting in a transition from flexural subsidence to dynamic topographic effects caused by the subducted plate. The style of deformation, and shortening changed from the thin-skinned tectonics of the Sevier Orogeny to a more deeply rooted tectonic event where reactivation of faults from the ancestral Rocky Mountain Orogeny resulted in a series of basement-cored uplifts which include the San Rafael Swell (SRS) in the study area. The overlap from the Sevier to the Laramide Orogeny was accompanied by a change in stress regimes, from a southeastward compressional regime exerted by the Sevier Fold and Thrust belt to basement-cored northeastward compression following the onset of the Laramide Orogeny around 75 Ma. This resulted in a complex interplay between two major compressional directions.

The Farnham Dome is located in the north of the San Rafael Swell in Castle Valley, and is interpreted to consist of several reverse faults that have offset the Ferron Sandstone east of the town of Wellington (Figure 2.5 C). The faults and folds in Castle Valley have been suggested by various studies to be of either Laramide (Tripp, 1989; Montgomery et al., 2001), or Sevier

(Neuhauser, 1988; Willis, 1999) age. The majority of workers suggest that the uplift post dates the deposition of the study interval (e.g, Montgomery et al. 2001) while Edwards et al. (2005) suggested that the Farnham Dome might have been a site of sediment bypass related to the deposition of the Lower Ferron Sandstone.

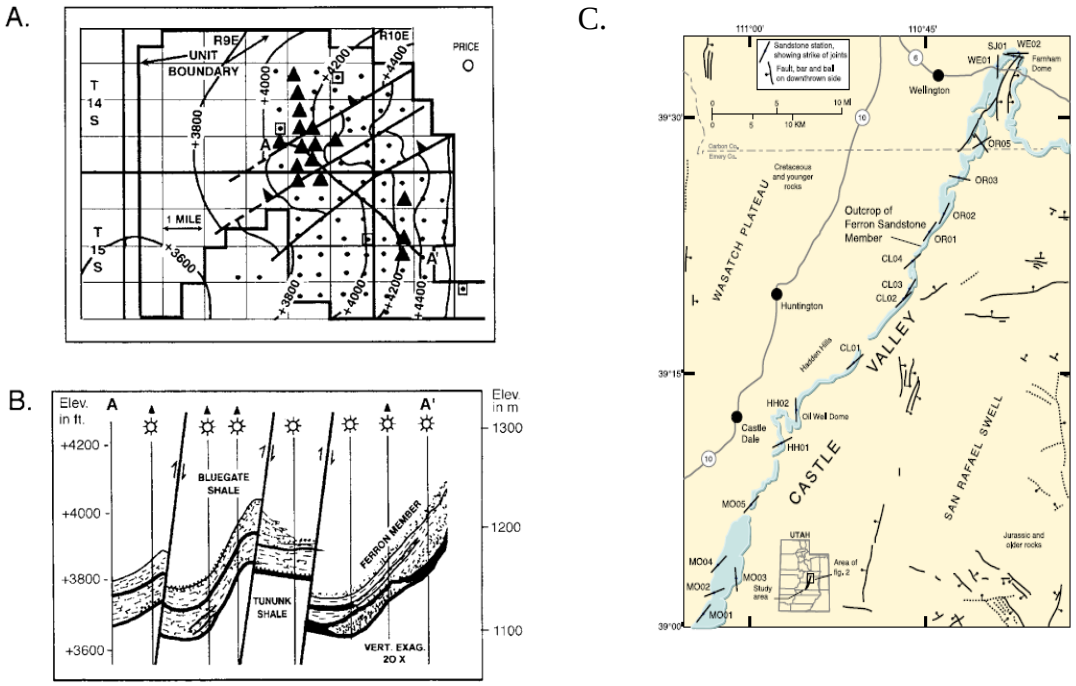

Figure 2.5: Montgomery et al., 2001, modified from Burns and Lamarre (1997): A) Map view of the Drunkards Wash Coal Bed Methane field, with transect A-A' marked as a line stretching northwest-southeast. B) Profile A-A' illustrating the fault segments encountered in the gas field. C) Structure map for Castle Valley, from Condon (2003).

The Laramide tectonic event affected the Lower Ferron on three scales:

- In the coal deposits of the Ferron Sandstone Member the Laramide stress regime resulted in the imprint of northeast striking microfractures called ‘cleats’ (Laubach et al., 1997). Condon (2003) showed that these northeast trending cleats have cross-cut northwest striking cleats related to the Sevier Orogeny. He also notes that the Ferron had to be buried to depths up to 1000 m necessary to produce microfractures in coal, which is consistent with the rapid burial history of the area.

- Reverse faulting has been observed within the subsurface Drunkards Wash field (Figure 2.5 B). The Ferron coals are deformed by a southwest plunging anticline, which is cut by several northeast striking reverse faults. The faults show up to 45 meters of vertical displacement (Montgomery et al., 2001).

- The anticline that is the San Rafael Swell caused the present dip of the Lower Ferron Deposits, gently to the west/northwest away from the anticline, and underneath Castle Valley and the Wasatch Plateau.

After the Laramide Orogeny (since 35 Ma) the region has been mildly influenced by the post orogenic collapse which generated in the Basin and Range regime to the west. Within the San Rafael Swell area the impact of this extensional tectonic regime, is mainly restricted to the Joe’s Valley Graben system west of the study area. Minor extensional faults displace the strata in Drunkards Wash and the outcrops around Wellington. Faults may also have acted as conduits for groundwater recharge in Drunkards Wash (Rice, 2003), with implication for gas production from the field.

2.3 Stratigraphy

Sediment for the Ferron Sandstone Member was sourced from the Sevier fold and thrust belt to the west (Figure 2.6). The clastic wedge of the Ferron pinches interfingers with and passes basinward into, the Mancos Shale. The Ferron Sandstone Member rests conformably on the Tununk Shale Member and is capped by the Blue Gate Shale Member. In a palaeolandward direction the deposits of the Ferron Sandstone Member grade into the fluvial and alluvial deposits of the Indianola Group.

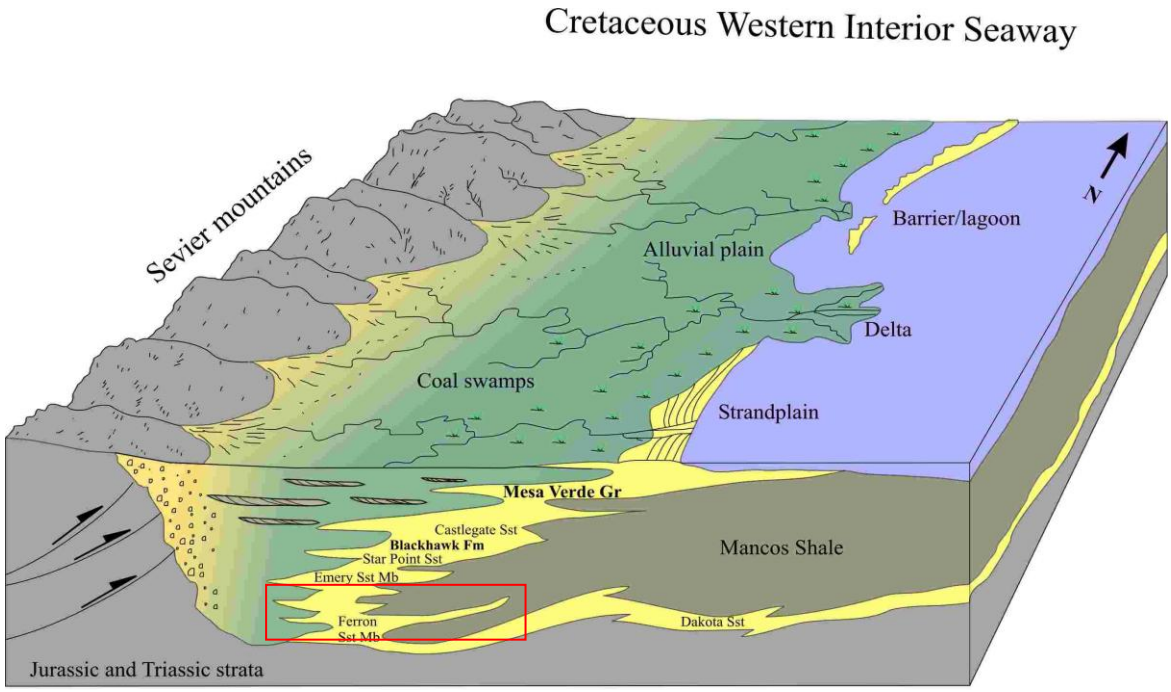

Figure 2.6: Schematic representation of the relative stratigraphic relationship, and the various depositional environments, for the deposits of the Western Interior Basin in central-eastern Utah and eastern Colorado. Relative position for the Ferron Sandstone highlighted in red. Modified by Howell and Flint (2003) from Hintze (1988).

Two depositional sequences have been identified in the Late Cretaceous Turonian Ferron Sandstone Member (Figure 2.8). The thin, Lower Ferron Sandstone of the Vernal deltaic complex (Cotter, 1976), which is the focus of the present study, outcrops in the north of Castle Valley while the Upper Ferron Sandstone of the Last Chance Delta (Hale, 1972) outcrops in the south around I-70 and was initially defined by Lupton (1916) as paralic deposits in the coal fields near the towns of Ferron and Emery (Figure 2.7).

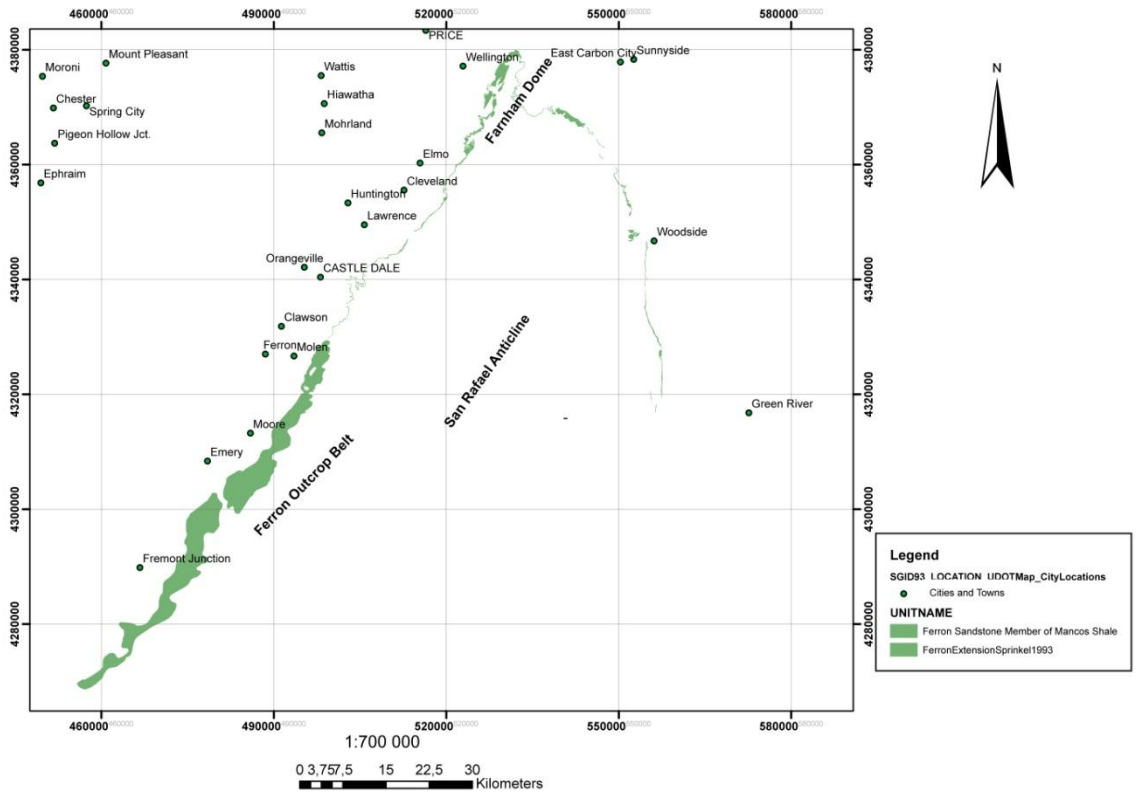

Figure 2.7: Overview map of the study area, showing the Ferron Sandstone Member outcrop belt. The Lower Ferron is located mainly north of Castle Dale, Upper Ferron deposits crop out to the south as indicated by the relatively thick outcrop belt and the Ivie Creek log locality.

Cotter (1975) described the Lower Ferron deposits that crops out along the western and eastern rim of the San Rafael Swell, in Castle Valley and from Wellington south to Green River respectively (Figure 2.7). The southernmost outcrop locality in Castle Valley was recorded just east of the town of Moore, whereas the southernmost outcrop along Highway 6 and 80 southeast to Green River was located west of Woodside Canyon. In his detailed work on these outcrops, he divided the Lower Ferron into units and named them based on their geographic locations; Woodside, Farnham, Clawson and Washboard units respectively. The Woodside Unit was interpreted to be deposits from an offshore sand bar environment, the Farnham Unit to be of a tidal inlet environment, Clawson Unit being deposited in an offshore (shelf) environment, whereas the Washboard represents relatively more proximal deposits ranging from offshore shelf to lower shoreface environment. The Washboard and Farnham units were interpreted to be time equivalent and they were along with the Clawson unit only recorded along the western rim of the SRS, in Castle Valley, where the Clawson unit was the southernmost exposed unit of the Lower Ferron.

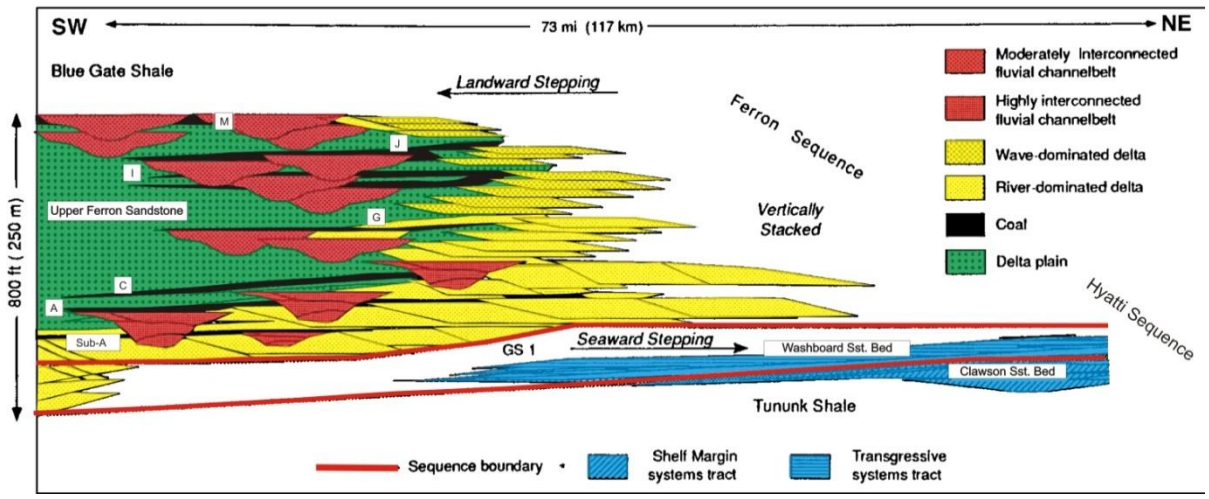

Figure 2.8: Schematic cross section displaying the relationship between the Upper and Lower Ferron Sandstone. Lower Ferron is commonly divided into the seaward stepping Clawson and Washboard beds (modified by Montgomery et al. 2001 from Fisher et al., 1993).

Gardner (1995a), estimated an age span for the deposition of the Upper Ferron Last Chance Delta to be between approximately 90,3 Ma and 88.0 Ma (Upper Turonian to Lower Coniacian) based on volcanic ash layers in coal, and biomarkers. . The Lower Ferron is dated to between 90.5 to 90.3 Ma (Middle Turonian), i.e. a period of about 200.000 years. Gardner (1995a) termed the Lower Ferron the hyatti sequence and the upper Ferron the ferronesis sequence. Garrison and van den Bergh, 2004, redefine the hyatti genetic sequence of Gardner (1995a) to a depositional composite sequence which also includes the lower part of the Last Chance Delta.

Gardner (1995b) also defined the Ferron Sandstone Member in terms of a hierarchy of base-level rise and fall cycles. The Lower Ferron, hyatti sequence, was defined as "intermediate-term cycle" (3rd order cycle following the classification of Vail et al., 1977), whereas the Ferron Sandstone Member as a whole were classified as a "long-term cycle" (2nd order), recording the turnaround from falling to rising relative sea-level.

Cotter (1976) interpreted the Lower Ferron Sandstone to be distal deposits in the southern part of a wave dominated delta which prograded in an east-southeastward direction at the western margin of the Cretaceous Interior Seaway (Figure 2.6). The parasequences recorded in these deposits represents a minor Highstand System Tract (Gardner, 1995b) within the Mancos Shale; it was deposited on a shallow, ramp margin morphology. Cotter (1976) proposed that a Late Cretaceous Vernal delta served as the sediment source for the shoreline. The delta was

later abandoned as the sea rose, and led to the deposition of the overlying Blue Gate Shale. Foci of sediment supply shifted to the above mentioned Last Chance Delta in the south, which kept pace with the rising sea-level and deposited the Upper Ferron Sandstone (Ryer, 1994).

Ryer and Lovekin, (1986) attributed the deposition of the Lower Ferron and parts of the northern, contemporaneous Frontier Formation (Winn, 1991) , to a regressive wedge that was deposited over an area that had lower subsidence than the surrounding basin due to differential flexural subsidence associated with the Sevier Orogeny. They refuted the idea of one distinct Vernal delta in the north which was proposed by Cotter (1976) due to the lack of evidence for a sufficiently large deltaic feature to have supplied such a widespread shoreline with enough sediments. They suggest that the lower part of the Turonian clastic wedge which includes the Lower Ferron, and parts of the Frontier Formation, is too thin to be related to any such delta and that the differential outbuilding along the coastline was caused by the prograding shoreline moving over an ancestral up-doming in the area of the present Uinta Mountains. This geomorphological bulge in the palaeoshoreline, inferred by Ryer and Lovekin (1986), caused the eastward migration of deltaic sediments supplied by numerous smaller river systems rather than one pronounced delta.

Given that the lower part of the Turonian clastic wedge is too thin to warrant a single delta distributary, the northwest-southeast progradation of the Lower Ferron shoreline is considered as part of a northern shoreline complex which was comprised of numerous shoreface and small, deltaic units informally termed the Vernal deltaic complex. This issue will be discussed further in the discussion chapter.

Two deltaic elements, or lobe equivalents, developed in the Vernal deltaic complex; one deltaic element, interpreted as part of the Frontier Formation, prograded northeastward into the Uinta Basin, while a southern deltaic element, the Lower Ferron Sandstone, prograded towards the south-east (Figure 2.9 A).

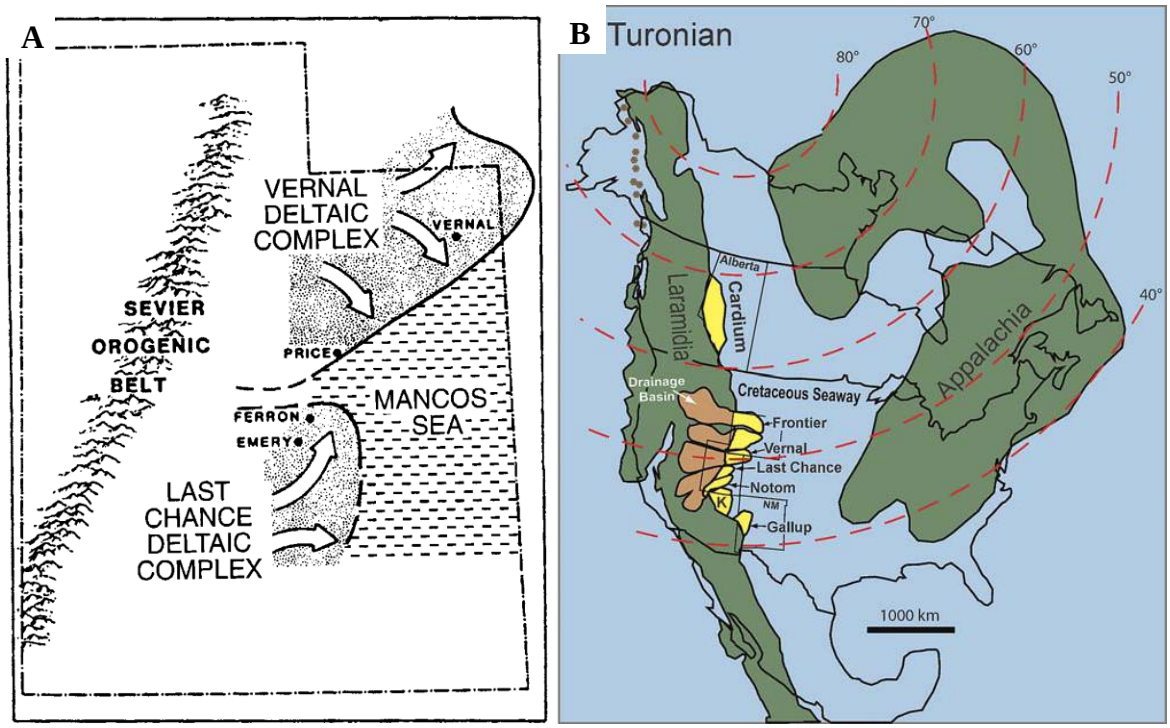

Figure 2.9: A) Schematic overview of the two proposed deltas or delta complexes of the Turonian Western Interior Seaway in East-Central Utah (Cotter, 1976). B) Schematic relationship between the Turonian deltas of the Western Interior Seaway, and latitudes. Important to note is the inclusion of a Vernal delta that was proposed by Cotter (1976), but later reclassified by Ryer and Lovekin (1986). From Bhattacharya and MacEachern (2009).

The Lower Ferron hyatti sequence was eventually transgressed, and the Last Chance Delta developed from the south west. This delta deposited the extensively studied Upper Ferron sandstone, (ferronensis sequence of Garner 1995a). The Last Chance delta prograded north-northeastwards towards and partially over the older Lower Ferron sandstone, of the Vernal deltaic complex, which at its position in the southern Castle Valley is interpreted to have been deposited offshore sands carried south as geostrophic currents sourced from a northern sedimentary source (Thompson et al., 1986). The offshore marine equivalent of the Upper Ferron sandstone is the Blue Gate Shale, which overlies the hyatti sequence.

The Upper Ferron sandstone was deposited as a clastic wedge during a period when both the sediment supply and the creation of accommodation space are thought to have been high (Gardner et al., 2004). Time equivalent strata elsewhere in the basin record a transgression and the progradation is attributed to an autogenic increase in sediment supply (Ryer, 1994). The subsequent transgression that followed in the Coniacian shifted the shoreline west of the Wasatch Plateau and led to deposit of the thick Blue Gate Shale Member in Castle Valley.

A humid climate allowed large swamps to develop on the coastal plain (Figure 2.6). The well studied outcrops of the Upper Ferron Sandstone and the CBM play in Drunkards Wash contain thick deposits of coal. In their work on the remaining petroleum potential for the Ferron Coal Play, Henry and Finn (2003) includes a stratigraphic correlation panel that illustrates that the Upper Ferron deposits continue into the subsurface in the northern part in Castle Valley and below the Wasatch Plateau. The panel shows that the Lower Ferron extends to the outcrop level as a prograding shoreline, and that the subsequent Upper Ferron retrogradational deposits are well represented within the Drunkards Wash CBM field and beneath the Wasatch Plateau (Figure 2.10). This correlation will be discussed later.

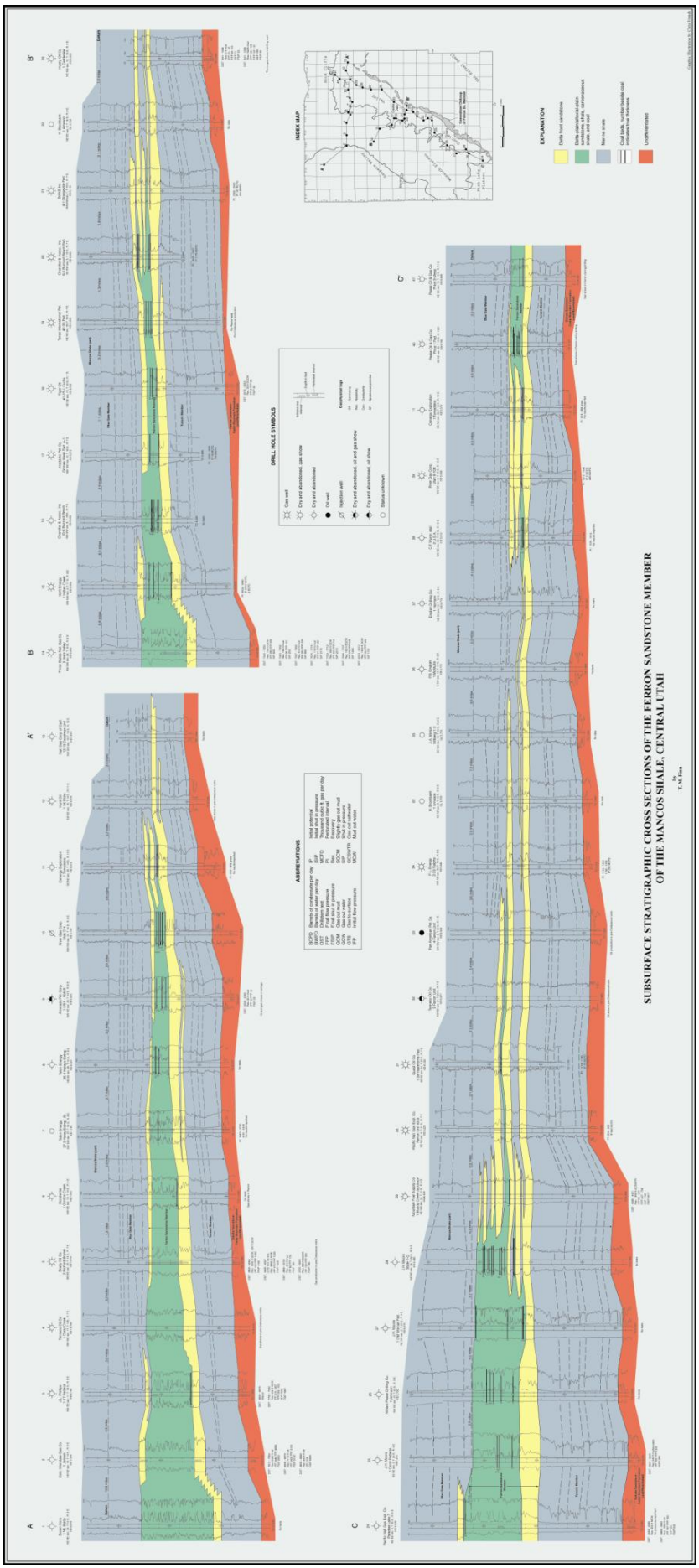

Figure 2.10: Regional well correlation panels describing the relationship between the Upper and Lower Ferron Sandstone deposits in Castle Valley, Finn, 2003. Red: undifferentiated Dakota sandstone, Grey: Mancos Shale, Yellow: Marine Ferron Sandstone, Green: Non-Marine Ferron sandstone. The Lower Ferron is interpreted as the widespread basal sandstone body that marks the onset of the Ferron clastic wedge. The Upper Ferron is characterized by seaward, through aggradational, to landward stepping parasequences with associated non-marine deposits in their proximal reach. Correlation based on widely spaced well logs, both geophysical and cored wells have been utilized. The datum, on which the correlation panel is flattened, is a distinct marker bed inferred from geophysical well logs in the lower 100-130m of the Blue Gate Shale Member.

2.4 Modern analogue

The search for a modern analogue for the Turonian Lower Ferron deposits of Central Utah is complicated by the comparably low global sea-level of the post Late Cretaceous World. Deposition occurred on a ramp margin in a continent interior seaway, for which there are no modern examples. Ryer and Lovekin (1986), proposed a hypothetical analogue in which they considered a flooded South American interior where the Andean mountains would correspond to the ancient Sevier mountain belt of the Late Cretaceous central Utah. This feature would have yielded a gentle ramp shelf margin similar to that on which the Lower Ferron was deposited.

Bhattacharya and Tye (2004) offer a careful review of the lower part of the Upper Ferron, the wave dominated Kf-1 and Kf-2 of the Last Chance Delta, and compare the delta to modern equivalents. They conclude that the Last Chance Delta was orders of magnitude smaller than the continental scale distributary deltas such as the Mississippi and Ganges-Brahmaputra in terms of river discharge, drainage area and channel height. As modern analogues to this ancient delta, they suggest the deltas Rhône, Brazo, Ebro or the St. George lobe of the Danube delta.

The Paraiba do Sul delta in Brazil (Figure 2.11), provides a reasonable analogue to the Central Utah coastline at the time of deposition of the Lower Ferron sandstone. This is a wave dominated shoreline, supplied with sediments from two rivers that cross a low-lying coastal plain. The beachfront protects the vegetated coastal plain, subject to a humid to sub-tropical climate.

Figure 2.11: Paraiba do Sul wave dominated shoreline, image courtesy of NASA. The shoreline protects a vegetated coastal plain. Paleoshoreline location and point of deposition and erosion could be inferred from the image.

2.5 The Drunkards Wash Coal Bed Methane Field

The Drunkards Wash CBM field provides a critical insight into the stratigraphy of the Lower Ferron. Despite relatively thin coal beds, the field is one of the most productive fields of its kind in North America, with individual wells showing averaged production rates of 500 mcf/day (Montgomery et al. 2001) and a cumulative production of over 760 BCF (http://oilgas.ogm.utah.gov/Statistics/PROD_CBM_field.cfm as of 31/03-2010). The field contains 234 closely spaced gas-producing wells a selection of which served as the basis for the subsurface model described below.

Gas recovered from a coal bed methane field differs from the conventional gas recoveries in a variety of ways. The organic rich coal offers rapid maturation and thus gas is produced at shallower burial depths than conventional hydrocarbon systems. The coal acts as both the source and reservoir in which the gas is absorbed to the surface of the coal rather than being contained in intra-lithological pore volumes.

The producing coal layers in the Drunkards Wash CBM-field range in depth from 330 to 1060 m, following the gentle eastward dip away from the San Rafael Swell. The coal layers range in thickness from <1 m to 7 m and consists of low-rank, high-volatile, B bituminous coal.

Drilling history began with the discovery of methane gas in the sandstone reservoirs on the Clear Creek field in 1951 (Ryer, 2004). Exploration was expanded further east, when Texaco Exploration and Production drilled two wells close to the Drunkards Wash field in 1988. Drilling on what was later to become the Drunkards Wash field was started in 1991, when the River Gas Corporation bought the property from Texaco and confirmed the high gas content within the field (Montgomery et al., 2001).

Burns and Lamarre (1997) recorded vitrinite reflectance values (R_0) of 0,7% for the Drunkards Wash field, while the value near the town of Emery to the south show R_0 to be 0,5% equal to C bituminous coal. Suggesting differences in the coal rank within the Ferron ‘coal-fairway’ in Castle Valley (Figure 2.12).

Based on crossplots of R_0 values measured against sample depths, Tabet (1998) suggested that the Ferron coals where subject to burial at depths up to 2820 meters necessary to yield values such as those present within the CBM-play. According to the model of the present day Drunkard Wash field, where the coal layers are recorded at maximum depths around 1600 meters, this suggests and exhumation of more than 1200 meters. The difference between

northern and southern coals, in terms of R_0 values and production data, have been proposed by Tabet (1998) to be the result of different burial history. This notion was backed by Cretaceous and Tertiary formation thicknesses from Hintze (1988) and by burial history reconstructions by Barker and Dallegge (1998).

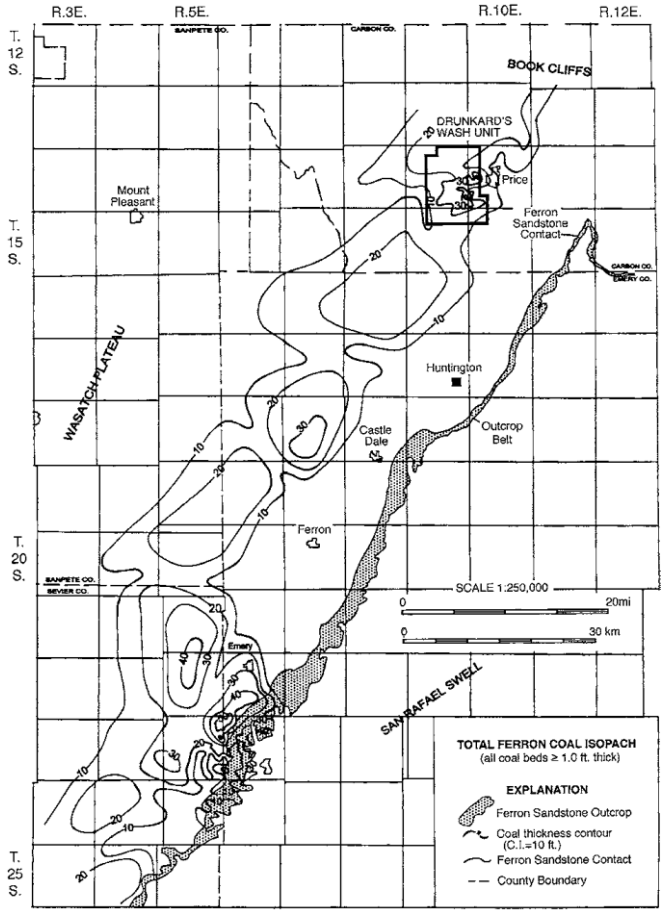

Figure 2.12: Coal-thickness isopach map of the Ferron coal fairway in Castle Valley. Montgomery et al. (2001), modified from Tabet et al., (1995).

Southern coals (Buzzard Bench and southward) show poorer production data than do the northern, this has been linked to the southern coals being exhumated from the water table and exposed to weathering according to Barker (2004). His study of the presence of sulfate in the coals south of the town of Emery linked the different levels of sulphuric content to varying degrees of weathering.

3 Subsurface Study

The subsurface data available for the investigation of the Drunkards Wash CBM-field include a large amount of geophysical well data publically available on Utah Geological Survey's on line archive, and a drilled core from the well RGU-1. The cored well section was logged and interpreted and then correlated with the well logs in order to define the wireline facies in the remaining wells used in the study.

The geophysical well logs on the UGS site are image files which once downloaded, had to be converted into digital well log data (LAS files). This was done with the use of Neuralog digitizing software, which offered partially automatic tracking of the log response. The process is laborious and time consuming consequently only the gamma ray and neutron logs were converted and only for the key interval. Fifty five wells were digitized, each one taking 2 to 3 hours. LAS files were then imported to the modelling software, Petrel, and a series of correlation strike and dip orientated correlation panels were generated. These were used as the basis for the geomodelling.

3.1 Core Section RGU-1

Over 130 m of cored well section was logged at the UGS core store in Salt Lake City. This package includes more than 95 m of the Turonian Ferron Sandstone Member clastic wedge, and a bentonitic ash layer in the Blue Gate Shale that lies above the Lower Ferron unit.

The detailed facies descriptions are summarized in Table 1. This table includes the observed lithofacies, and their interpreted facies association and depositional environments. The facies associations have been added to the geophysical well log display and used to aid interpretation in areas where core data are lacking.

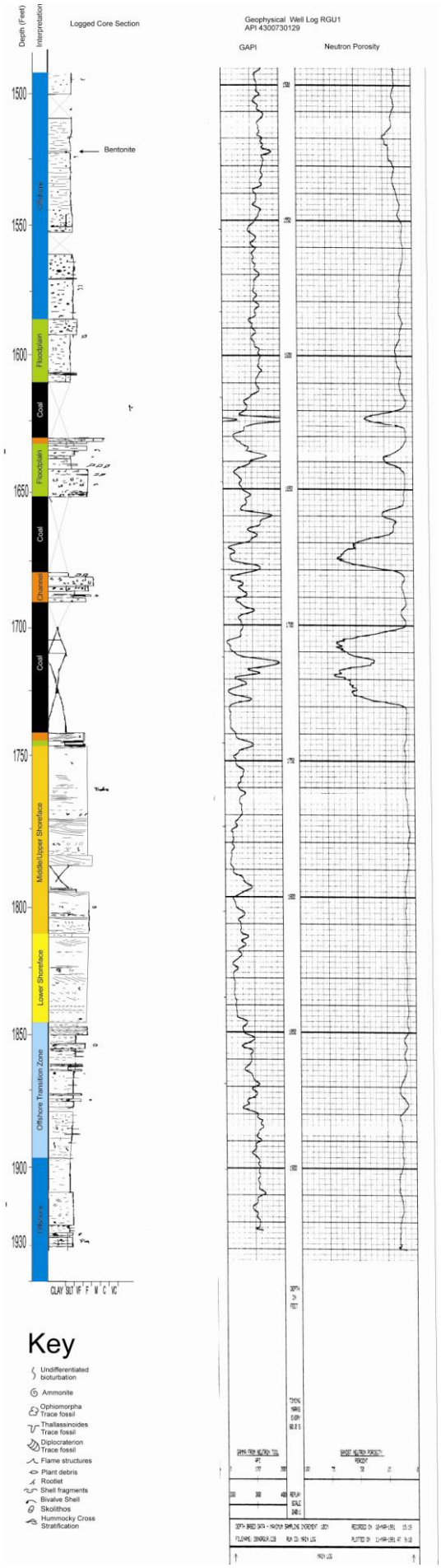

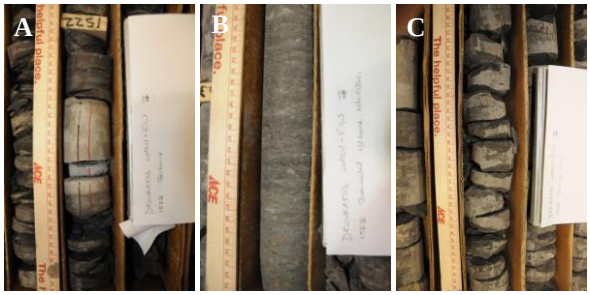

Figure 3.3: Offshore heteroliths and bentonite layer (A) sat in offshore shales. Depths: A) 1522', B) 1562', C) 1906'.

Figure 3.2: Organic rich, bioturbated siltstone (B) to clean sandstone (A)with low degree of bioturbation. Depths: A) 1644', B) 1684'.

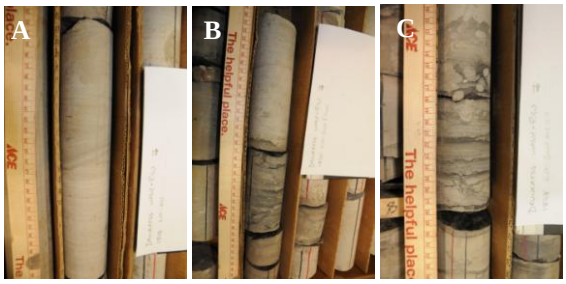

Figure 3.1: Lower shoreface sandstone of variable degree of bioturbation. Depths: A) 1806', B) 1814', C) 1849'.

Figure 3.4: Cored well section together with associated geopphysical well log response Gamma Ray and Neutron porosity. A selection of pictures from the core are included above, the complete set of photos from the core is included in Appendix II, along with a high quality jpg-version of the log.

Table 1: Facies associations for the lithofacies logged in the cored section from RGU1.

Facies Association	Lithofacies description	Bioturb. Index	Depositional Environment	Example Log Interval
Offshore	Bioturbated to laminated shaley silt with sparse organic matter, transitional boundary to overlying package. Ammonite fossil	3-4	Offshore, marine shelf. Uninterrupted by storms	588-578m
Offshore Transition Zone	Marine heteroliths. Interbedded siltstone with very-fine sandstone tempestites (HCS). Upwards coarsening package, ranging from siltstone (sand content about 5-10%) to sandy siltstone (sand 20-30%). V.f. sandstone layers ranging from a couple of cm to about 15 cm, thickness increase upwards. Soft sediment deformation. Ophiomorpha trace fossils and general undifferentiated bioturbation Scattered shell fragments throughout. Gradual transition to overlying package.	4-6	Storm affected offshore marine deposits. Below fair-weather wave-base.	578-562m
Lower Shoreface	Very fine to fine sandstone with hummocky cross stratification and bioturbation, interbedded siltstone with wave ripples (sand content about 40%), Planolites, Ophiomorpha and Thalassinoides trace fossils. Truncated low angle cross bedding (HCS) and wavey lamination, beds contain some siltstone interlamina, silt content never exceeds 10%.	3-4	Storm affected marine shoreface deposits. Periods of inter-storm quiescence	562-553m
Middle Shoreface	Very fine to fine sandstone with wave ripples. Ophiomorpha, palaeophycus, trace fossils. Internal structures: truncated low-angle lamination, planar lamination and HCS structures. Silty lenses and breaks	1-2 4-5	Storm dominated, wave influenced marine shoreface deposits. Above fair-weather	553-532m

	at irregular intervals, less than 5 cm thick. Abundant shell fragments occur locally. Sparse organic matter. Gradual transition to overlying layer.		wave-base.	
Upper Shoreface	Fine to medium sandstone with wavey to planar lamination and through cross bedding, dish structures at the bottom. Ophiomorpha, Thalassinoides and Skolithos trace fossils. Silt locally as drapes on low angle lamina of sandstone, silt < 20 %. Scattered shell fragments.	1-4	Wave dominated upper shoreface setting	
Coastal plain	Non-marine heteroliths. Laminated shale and siltstone interbedded fine to very fine sandstone with current ripples ripples (crevasse splays). Carbonaceous shale. Large coal fragments and plant debris, bioturbation is absent.	0	Non-marine deposits with brackish, lagoons, floodplains, swamps and mires. Minor tidal channels.	532-531m 503-498m 490-483m
Channel	Fine to Medium sandstone, generally very well sorted. Sparse shell and plant debris were found scattered in the section. Intervals containing plant debris, capped by a rootlet surface.	0-1	Fluvial channels, typically interpreted as meandering	531-530m 516-512m 498-497m
Coal	Carbonaceous shale grading into coal. Typical absent in the core due to prior sampling by previous workers.		Peat swamp, thicker intervals interpreted as raised mires	530-516m 512-503m 497-490m

The interpreted logged core section reflects facies associations characteristic for a prograding wave dominated shoreline and its non-marine deposits. The log shows an upwards coarsening trend from shale to sandstone, overlain by fluvial deposits. Several sections from within the fluvial interval are missing; these sections are thought to be removed for destructive sampling, a process in which the coal is tested for microfractures, volatile content, vitrinite reflectance, sulphuric content and so forth. Geophysical well logs accompanying the cored section were used as a way of determining the nature of these missing sections as coals, as explained in the following sub-chapter. The character of the coal itself could thus not be determined. As an analogue to the coal seams in Drunkards Wash, the outcrop from I-70 (Last Chance Delta) provided some insight to the coal characteristics for the Turonian Ferron Sandstone Member. The logged core yields a sedimentary facies succession close to similar to the Upper Ferron logged at Ivie Creek/I-70, to be discussed in more detail in the outcrop-chapter, and is characteristic for a prograding shoreline. It shows offshore marine shales and siltstone that coarsen upwards into shoreface sands, followed by sheltered marine and floodplain clays, with coal deposits capping each cycle of deposition. Sparse and thin occurrences of channel sands suggest that the well is drilled in the proximity of one or more channels. Grain-size as large as those found in the outcrop analogue was not identified, and no record of coal was preserved within the cored section. The intervals in which the coal layers were expected (based on the accompanying geophysical well log) were not available at the UGS Core Research Centre.

Four parasequences are interpreted within the cored section, the lowermost parasequence record the lithofacies stacking pattern characteristic for a prograding parasequence from offshore transition zone through shoreface to fluvial deposits, its upper limit is a flooding surface defined by a thick coal layer. The two following parasequences within the core are only recorded by their most proximal deposits, that is coastal plain and fluvial deposits capped by coal. The coal layers are interpreted to be the up-dip expression of marine flooding surfaces that separates individual parasequences within a highstand system tracts parasequence set (Bohacs and Suter, 1997).

3.2 Wireline facies associations

The principal geophysical well logs used in this study were the Gamma Ray and Neutron Porosity. The GR was used to qualitatively assess the silt content of the facies and the NPI was used to identify the coal intervals. The Gamma Ray cut-off, i.e. the value separating silt from sand, was set to 75 API with lower values indicative of cleaner and typically coarser sandstones and higher values indicative of more silt and mud rich facies. Neutron porosity data was used to identify coal layers by a marked, decrease in the log response (Rider, 1986). While the actual response is used to determine the lithology the log motif and trends are used to distinguish the depositional environment. This was calibrated by comparison to the cored section. An example of a typical well log data source used for this study is shown in the logged core section in Figure 3.4. The wireline facies are summarised in Table 2.The RGU1 core contains missing core sections due to the removal for destructive sampling of coal.

After comparison of the core and wireline logs from well RGU1, the geophysical well logs from the other wells in Drunkards Wash were interpreted in terms of the depositional settings. An example of how the facies associations for the geophysical well logs are divided is showed in Figure 3.5.

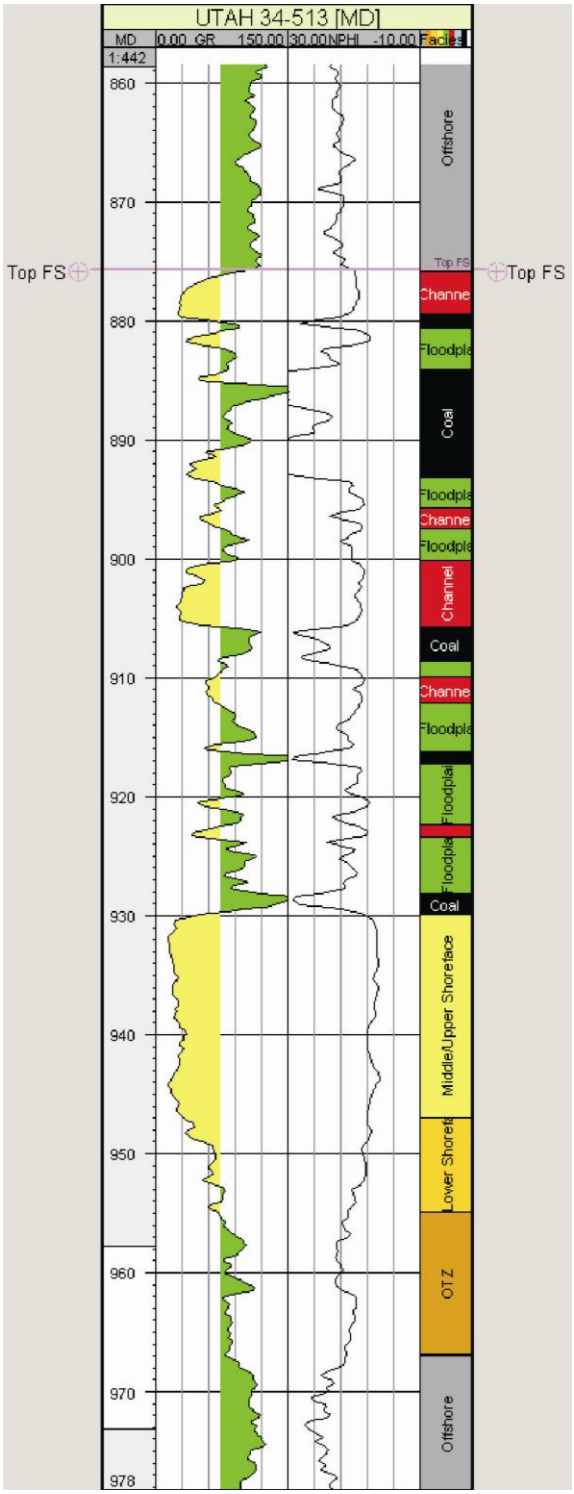

Figure 3.5: Wireline facies associations, as summarized in Table 2, from the uncored well Utah 34-513 in the northern part of the Drunkards Wash CBM-field.

Table 2: Facies associations for geophysical well logs.

Facies Association	Log Motif	Inferred Depositional Environment
Offshore	Thick sections of high GAPI values, no pronounced spikes towards lower values, indicative of sandstone.	Offshore shelf deposits
Offshore Transition Zone	Spikes in the Gamma Ray response towards lower values in between high responses from shale intervals. Upwards decline in bulk GAPI values	Storm affected offshore shelf deposits, above storm weather wave base.
Lower shoreface	Low Gamma Ray values compared to preceding responses. Gamma Ray spikes indicate presence of shale at narrow intervals	Above fair-weather wave base, more sand-dominated motif
Upper/Middle Shoreface	Upwards coarsening Gamma Ray log profile with rare shale spikes. Generally very low GAPI values.	Marginal marine deposits, daily wave action, constant reworking of sediments
Coastal plain	Significantly more heterolithic profile compared to offshore shales, no obvious trend like the upwards coarsening GR motif of the OTZ.	Proximity to channels and the reoccurring incidents of levee breaks associated with these.
Channel	Blocky to upwards fining Gamma Ray response.	Non-marine sandstone deposits
Coal	Coals are identified by a sharp, leftward kick in the Neutron porosity log.	Non-marine organic deposit

3.3 Log correlations

The data input were considered in light of the conceptual model proposed for the Ferron by earlier workers: prograding shoreline in a shallow ramp active margin in a foreland basin, as discussed in the previous chapters. Conceptual models are essential to give the model an appropriate expression. It serves as the basis for interpretations and extrapolating surfaces.

Identified surfaces include top flooding surface, which represent the regional transgression event that ended the hyatti sequence. Tectonic uplift during the Laramide Orogeny initiated the uplift of the San Rafael Swell, and the Ferron Sst. Member was tilted in response. The bentonite identified in outcrops and in the cored section of RGU1 show a similar dip-relationship when correlated.

Well section panels have served as the basis for understanding horizons and facies association relationship within the subsurface. Multiple panels are presented below, representing both depositional strike profiles (W, X, Y, Z panels), trending north-northeast to south-southwest and depositional dip profiles (A, B, C, D, E, F, G panels) trending northwest to southeast. The locations of the respective panels are marked in Figure 3.6. The panels displaying depositional strike show more homogeneous geophysical well log responses compared to the depositional dip profiles. Facies associations for the latter pinch out to the east and west i.e. both in the landward and seaward direction. The wells have been flattened on the top flooding surface horizon, which has an eastward dip away from the SRS, since this is the most regionally traceable marker. It also serves as a chronostratigraphic surface, as it represents a relatively rapid event of transgression.

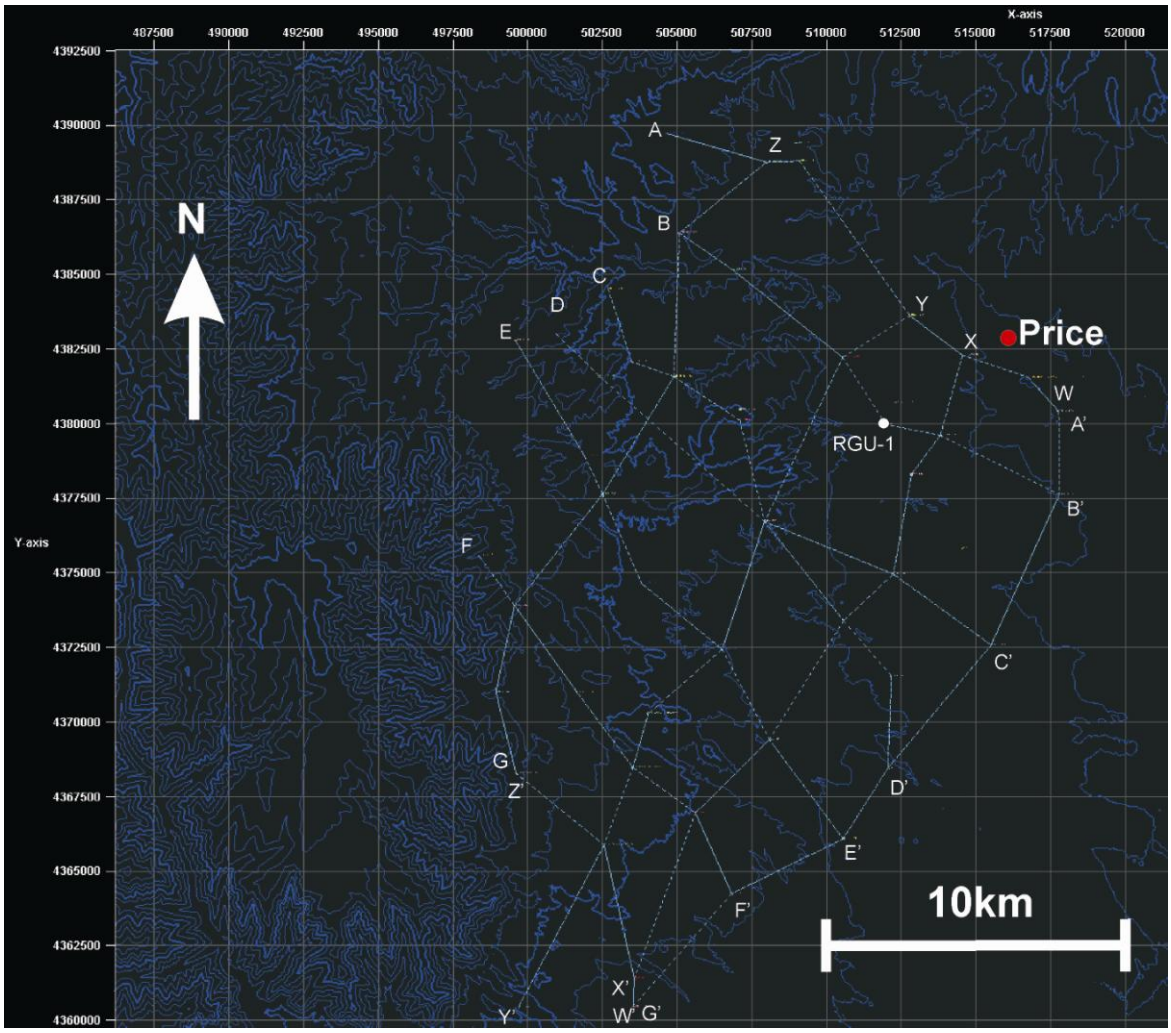

Figure 3.6: Overview map showing the well correlation panels underneath a contour map of northern Castle Valley.

The following correlation panels show the depositional dip from in the order from north to south through the Drunkards Wash field. A complete set of correlation panels is found in Appendix I.

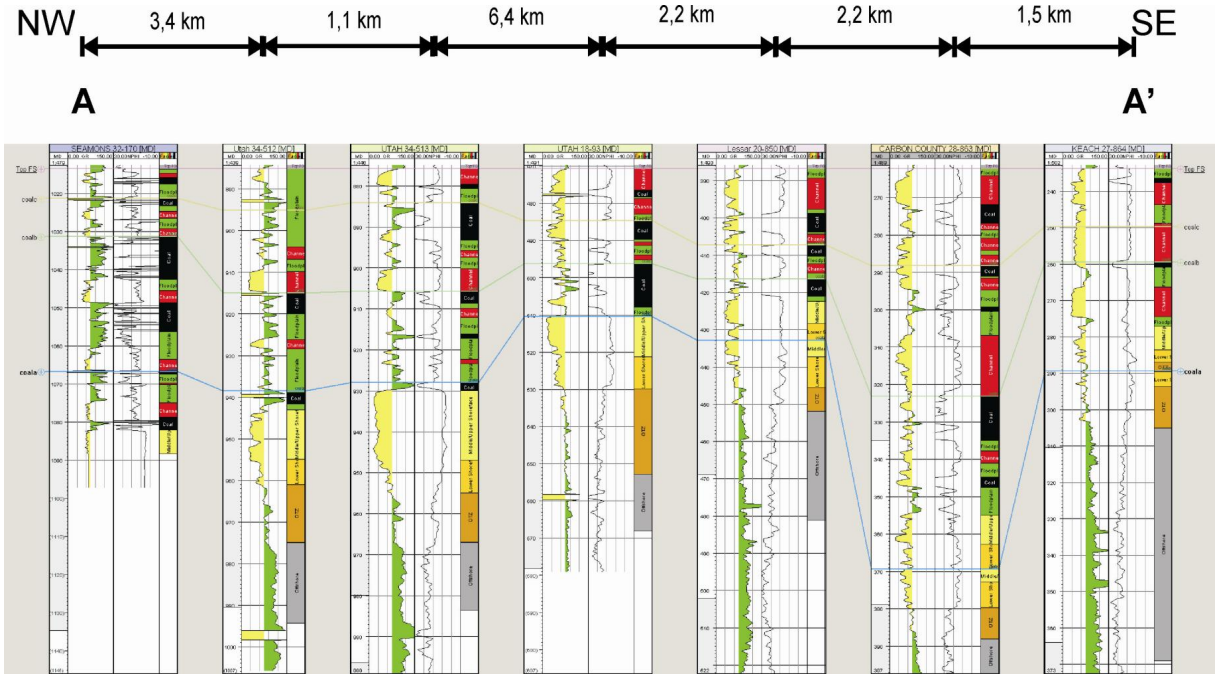

Figure 3.7: Northernmost depositional dip oriented correlation panel from Drunkards Wash.

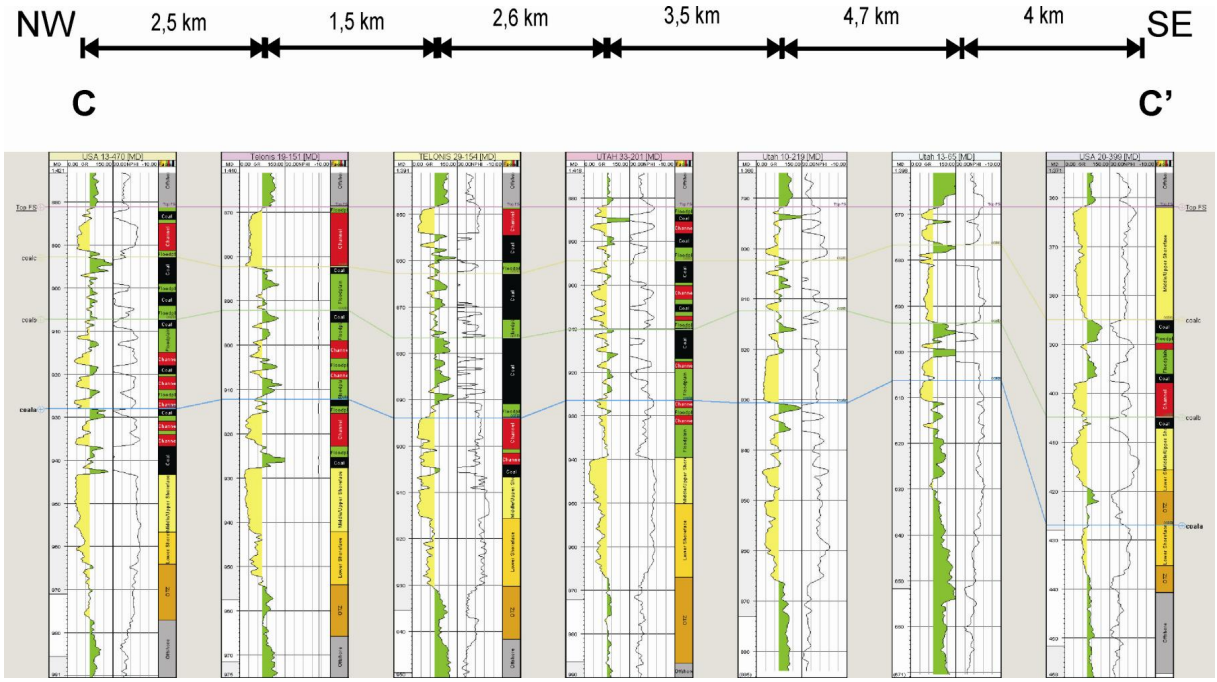

Figure 3.8: Depositional dip oriented correlation panel.

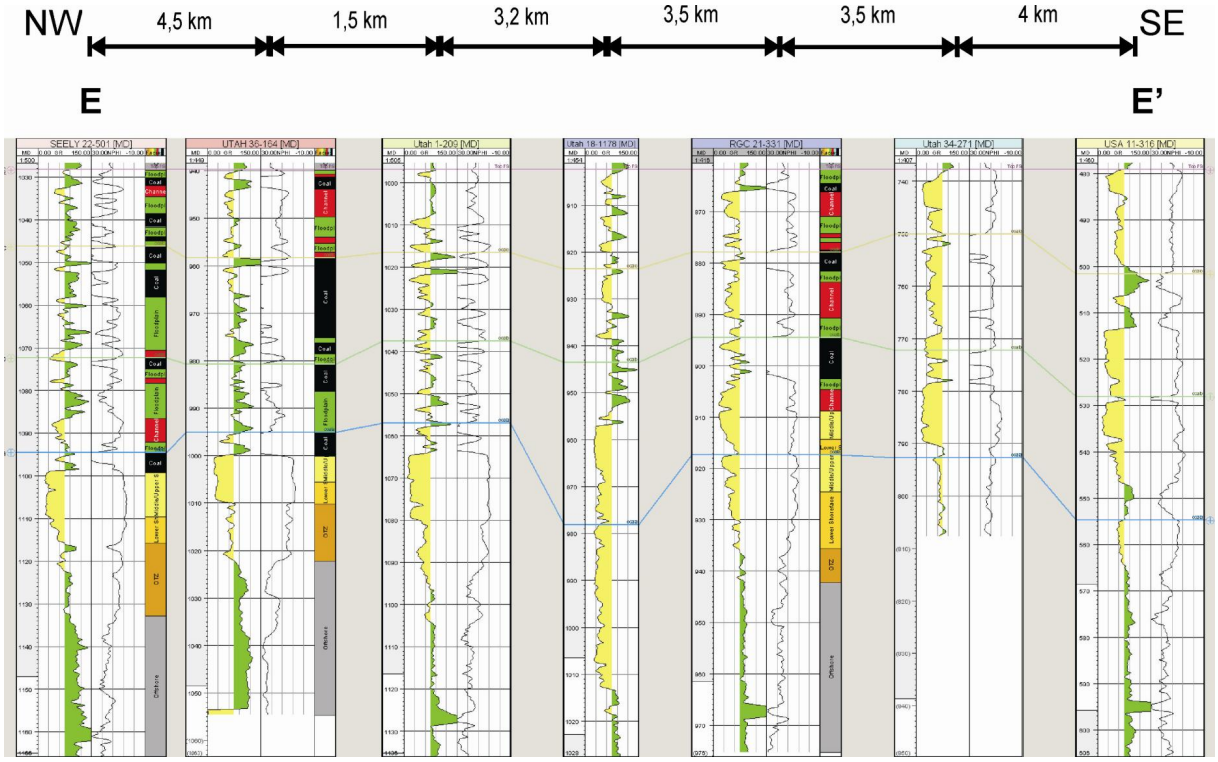

Figure 3.9: Depositional dip oriented correlation panel.

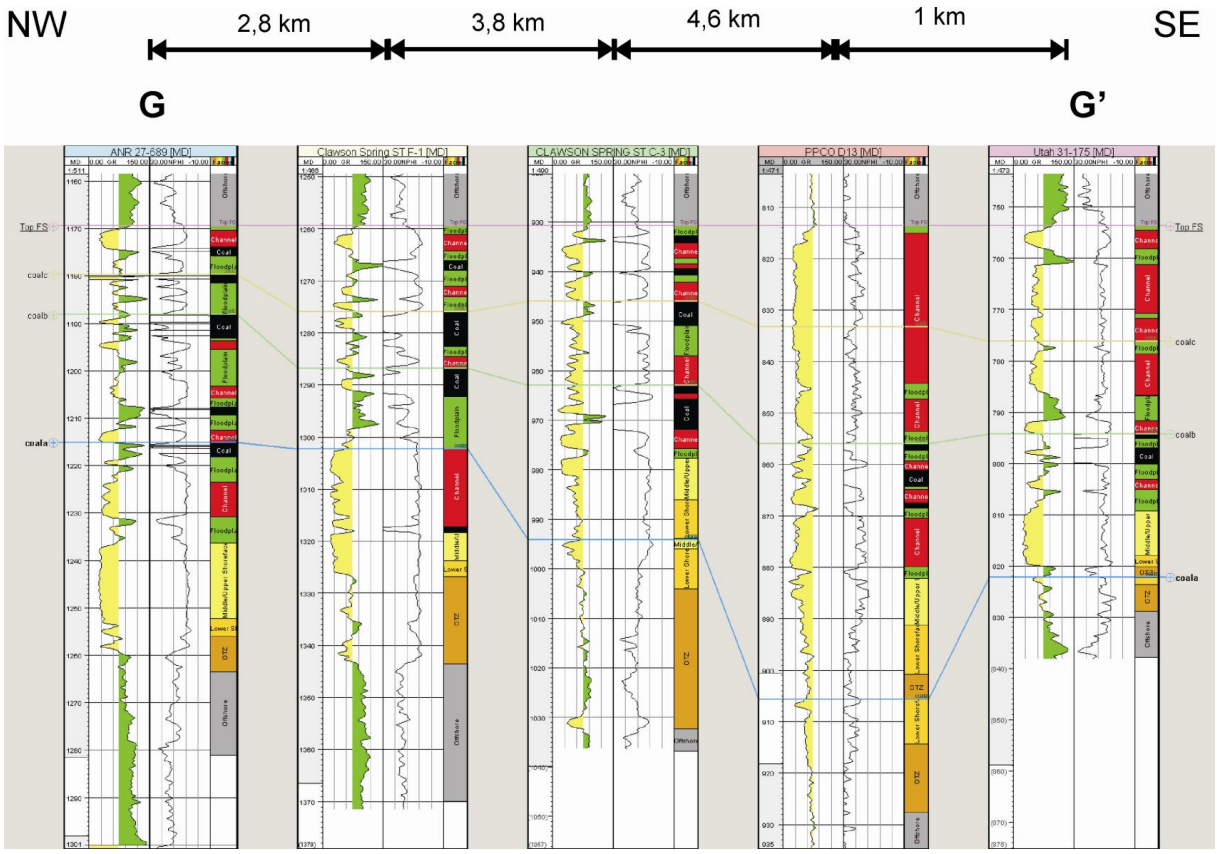

Figure 3.10: Depositional dip oriented correlation panel.

The succession seen in the correlation panels illustrates a large scale progradation of the succession, passing upward from offshore to coastal plain deposits. The top of the succession is marked by sharp transition back to offshore which is interpreted as a major flooding surface. The succession can be further subdidvided into 4 distinct phases of progradation, each represented by an upward shallowing of facies. These have been interpreted as parasequences (sensu Van Wagoner et al 1990). The lower three of these parasequences (PS1-PS3) are stacked into a progradational parasequences set, while the upper one (PS4) shows a backstepping pattern. The system prograded towards the SE and there is little difference in facies along depositional strike, although some marked thickness changes can be observed in the NE-SW panels. The correlations form the basis for sequence stratigraphic interpretation and model building and are discussed in more detail below.

Parasequence boundaries were identified initially in the down-dip portion of the dip orientated panels (e.g. Figure 3.7, Figure 3.8, Figure 3.9 and Figure 3.10). Surfaces were defined by a rapid upward transition from shallow to deeper water deposits, based primarily on the facies interpretation of the gamma ray log. The surfaces where then traced landward, though the shoreface successions and into the coastal plain dominated part of the succession.

The correlative conformity to the marine flooding surfaces in the non-marine part of the succession was typically expressed as a coal seam. Coal seams have commonly been correlated with marine flooding surfaces since they are associated with a rise in base level and more water logged conditions on the floodplain. Various authors have proposed different correlations for the position of the surface within the coal from the base of seam (e.g. Flint et al., 1995; Hampson, 1995) to the top (Diessel et al., 2000) or even within the coal (Davies et al., 2006). The latter authors illustrated that determining the exact position of the correlative conformity required detail petrographic study of the coal and was not possible just with wireline log data. Therefore for practicality the top of the coal seam was picked as the parasequences boundary. This uncertainty has little impact on the final correlations.

The coal layers thins and disappear to the southeast, (basinward) and it is possible to map out the downdip pinch of the major seams. This has direct implications for the CBM fields and is discussed in the modelling chapter.

Depositional strike panel, ordered from west to east:

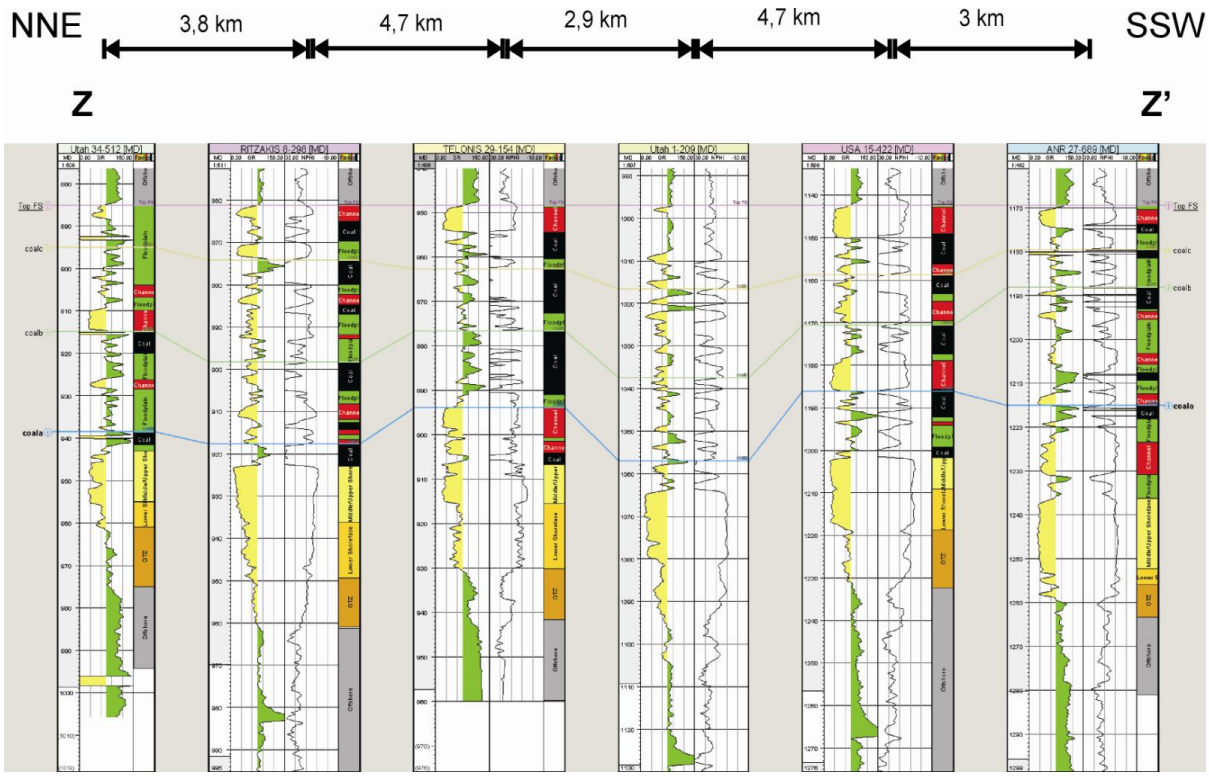

Figure 3.11: Easternmost depositional strike oriented correlation panel.

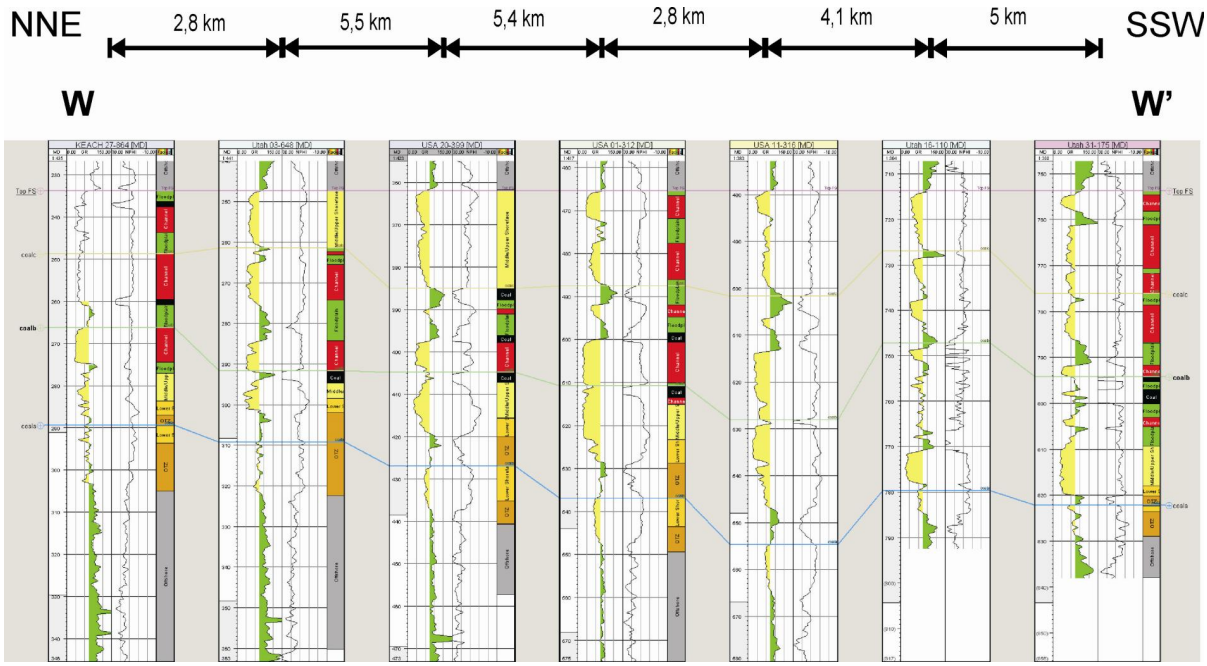

Figure 3.12: Westernmost depositional strike oriented correlation panel.

The panels illustrates that depositional dip is towards the SE and that there is little along-strike change in the facies. This is consistent with the observation from the cored well that the system is a wave dominated shoreline system. The lowermost parasequence (PS1) pinches out within the panels, while the progradational stacked PS2 and PS3 extend out of the subsurface study area and extend towards the outcrops. The correlation with the outcrop is discussed below. While there is little change in the distribution of the facies along strike there are some marked changes in thickness especially in the back stepping upper parasequence. This is also discussed in the context of the correlation to the outcrop in Chapter 6.

The parasequences stacking pattern of progradational to retrogradational may suggest the presence of a sequence boundary (sensu Van Wagoner et al., 1990) at the top of PS3. Such a surface was suggested by Edwards et al. (2005) who studied the outcropping Farnham unit and other deposits on the east side of the SRS. However, based upon the subsurface data alone no clear evidence for such a surface was observed.

For the 3D geocellular model the parasequences boundaries were used as zone boundaries. The base of the model was arbitrarily picked in the underlying Tununk Shale, just below the first obvious indication of upwards coarsening. The upper boundary for the model was defined by the regional flooding surface that overlies the Lower Ferron unit (Top PS4). In cases where the lower boundary was not identifiable, especially for those wells not drilled deep enough to record the transition from the Tununk into Ferron Sst., the boundary was set to best fit the thickness recorded in the neighbouring well. An example of such an instance may be viewed in Figure 3.7, in the north-westernmost well. Remaining zone boundaries were set to the top of each shallow marine parasequences or at their correlative conformity in the coastal plain. During the gridding a proportional grid with 6 equally thick layers was used to allow the individual facies in each zone to be captured.

3.4 Summary Sequence stratigraphy

The interpreted subsurface data show that the Drunkards Wash CBM-field is composed of a progradational to aggradational succession that includes 2 parasequences sets. The lowermost parasequence set includes 3 progradationally stacked parasequences (PS1 – PS3). Parasequence (PS1) prograded over the underlying offshore shale package and the transition from the Tununk to the Ferron Sandstone Member is conformable. PS1 pinches out within the area of the CBM field. Parasequences 2 and 3 are progradational to aggradational, and represent the most basinward expression of the Ferron Sandstone Member in Drunkards Wash. The second parasequences set is comprised of just 1 parasequence, PS4, which is aggradational and locally shows a back-stepping stacking pattern. The Ferron sandstone member is capped by a regional flooding surface that marks the onset of the overlying Blue Gate Shale Member, made up of the offshore shale package above the clastic wedge.

The interpreted parasequence boundaries along with the facies associations interpreted in each well suggests that there should be age-equivalent distal deposits in the basinward dip direction of the Drunkards Wash deposits. The correlation panels also suggest that the two parasequences that prograded the farthest basinward are PS2 and PS 3. Given the westward dip of the strata, it is possible that the distal expression of at least some of these parasequences may be present in the outcrop 15-20 km to the SE along the northern San Rafael Swell escarpment.

The following chapter addresses the outcrops and their relationship to the subsurface data. This is followed by a reconstruction of the palaeogeography and the building of reservoir models.

4 Outcrop Study

Outcrops along the northwestern rim of the San Rafael Swell and around the Farnham Dome, has been studied from Wellington in the north to Castle Dale further south. Lower Ferron outcrops are referred to as the GPS way point which was taken at their location. They are hence numbered WP1, WP2 etc. In addition to the Lower Ferron which lacks the upper shoreface and coastal plain deposits at outcrop, work was also udertaken on the Upper Ferron Sandstone in Ivie Creek which allows study of analogues for these more proximal deposits (Figure 4.1).

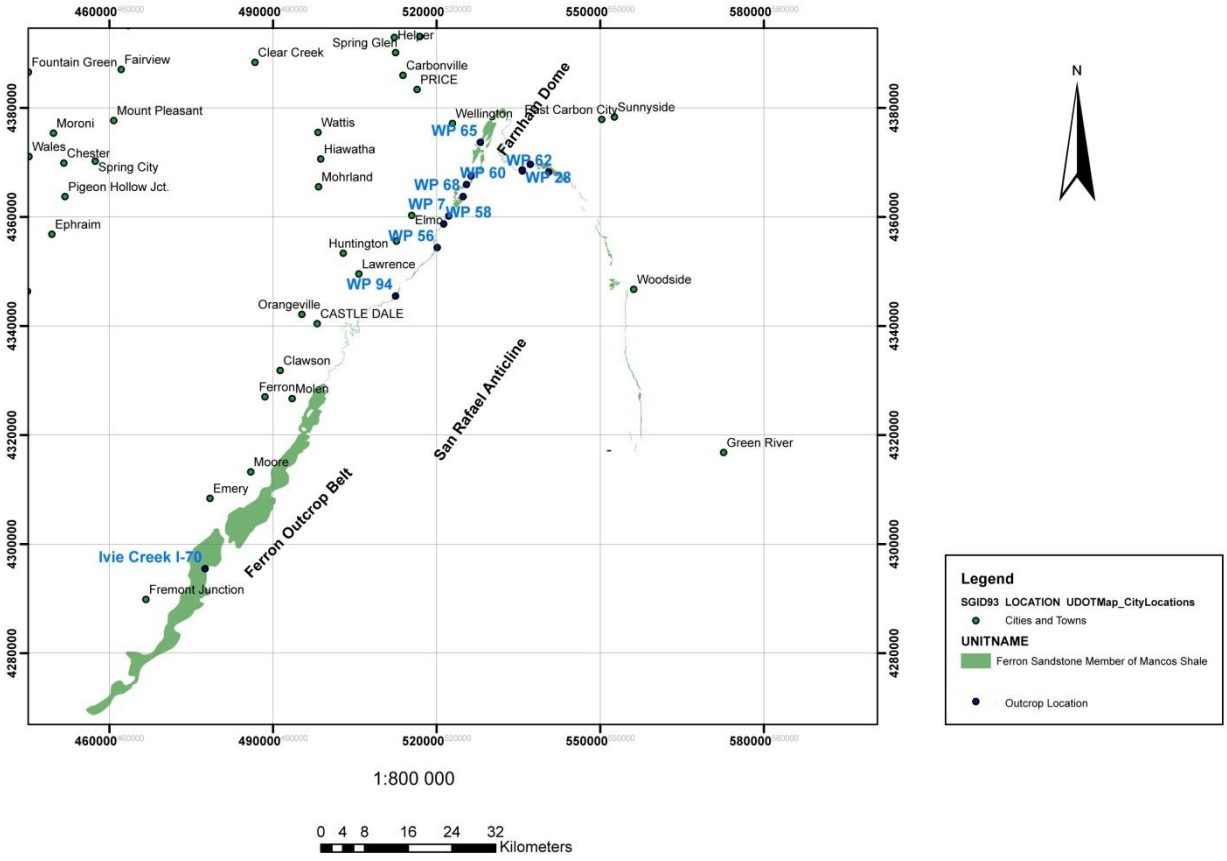

Figure 4.1: Overview map of Castle Valley and the San Rafael Swell. Outcrop locations are indicated in bold blue. Ivie Creek location to the south indicates where the Upper Ferron was studied.

Standard field methods were used to capture the lithofacies variation and parasequence boundaries in outcrops. Parasequences boundaries were traced to establish the stratigraphic relationship, both in the field and using Google Earth. In addition to the parasequences

boundaries which occur as sharp topped ridges in the outcrop, several bentonite ash layers were also identified and correlated in the field and into the subsurface.

4.1 Outcrop Analogue: Uppper Ferron

Outcrops of the Upper Ferron Sandstone were studied along Interstate 70 in the vicinity of Ivie Creek. The outcrops contains more than 120 m of upwards coarsening offshore to fluvial deposits representing three, west-east prograding parasequences that have been termed by Anderson et al., 2004, as Kf-2-Ivie Creek-a , Kf-2-Ivie Creek-b and Kf-2-Ivie Creek-c from the base upward.

The Kf-2 parasequence set represent a north-south trending, eastward prograding, wave-dominated shoreline. Interstate 70 follows the depositional dip profile of this parasequence set and have been logged from the offshore deposits near the informally named Ivie Creek Amphitheatre and into the fluvial deposits of Kf-2-Ivie Creek-c. Figure 4.2, below, show the top of parasequence Kf-2-IC-a, represented by shoreface deposits, and the overlying Kf-2-IC-b.

The outcrops were studied with the intention of comparing the resulting log to that of the cored well section in Drunkards Wash and using the geometries observed in the outcrops to constrain the models. Additionally, the outcrop as a whole provides a good insight into the relative distribution of facies associations found in shallow marine to fluvial depositional environments. Although the Upper Ferron is considered a fluvial to wave dominated shoreline with a prominent deltaic feature, the deposits are closely related to those found in the subsurface Drunkards Wash field.

Non-marine deposits investigated at this locality were of particular interest due to the fact that parts of the non-marine intervals in the RGU-1 cored section was absent. Coal seams in the outcrop along I-70 thus allowed for an improved understanding of the Cretaceous coal deposits from the Ferron Sandstone Member.

Channel bodies and coastal plain deposits were also studied along with the upper to middle shoreface facies associations occupying the interval between outcrops of the Lower Ferron and the Drunkards Wash CBM-fields easternmost margin.

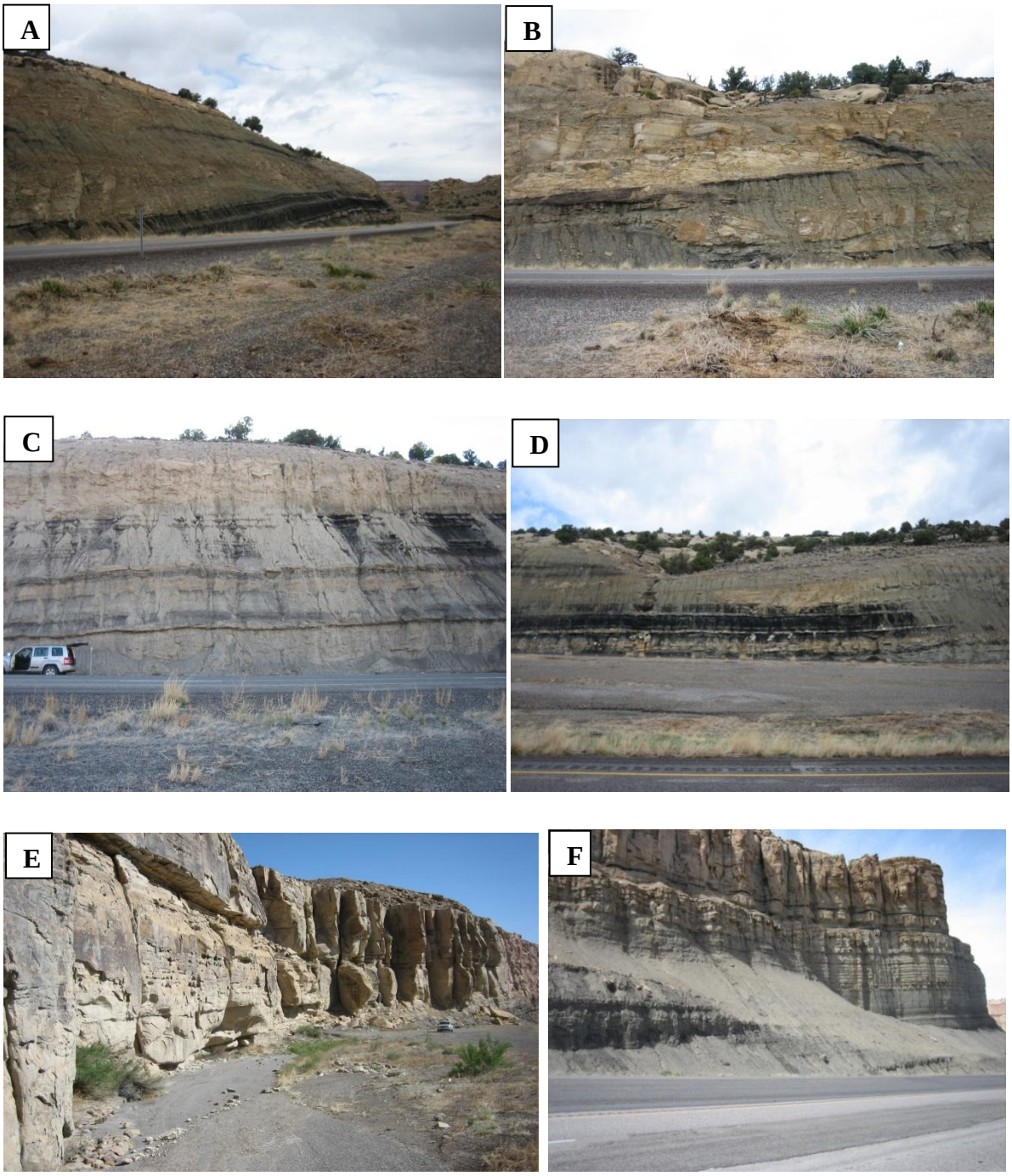

Figure 4.2: Upper Ferron Sandstone outcrop along Interstate 70. Kf-2-Ivie Creek –a, -b and –c, parasequences. A) Non-marine deposits from the uppermost section of the parasequences. B) Channel sandstone cut into coastal plain heteroliths. C) Vertical alteration of channel sands, coal seams (partly covered in scree) and coastal plain heteroliths. D) Coal seams as they appear along the I-70. E) Upper to Lower shoreface depsits. F) Lower shoreface to offshore deposits.

Garrison and van den Bergh (2004) carried out a similar sedimentological description in their work on high-resolution depositional sequence stratigraphy, where they include a detailed description of this outcrop.

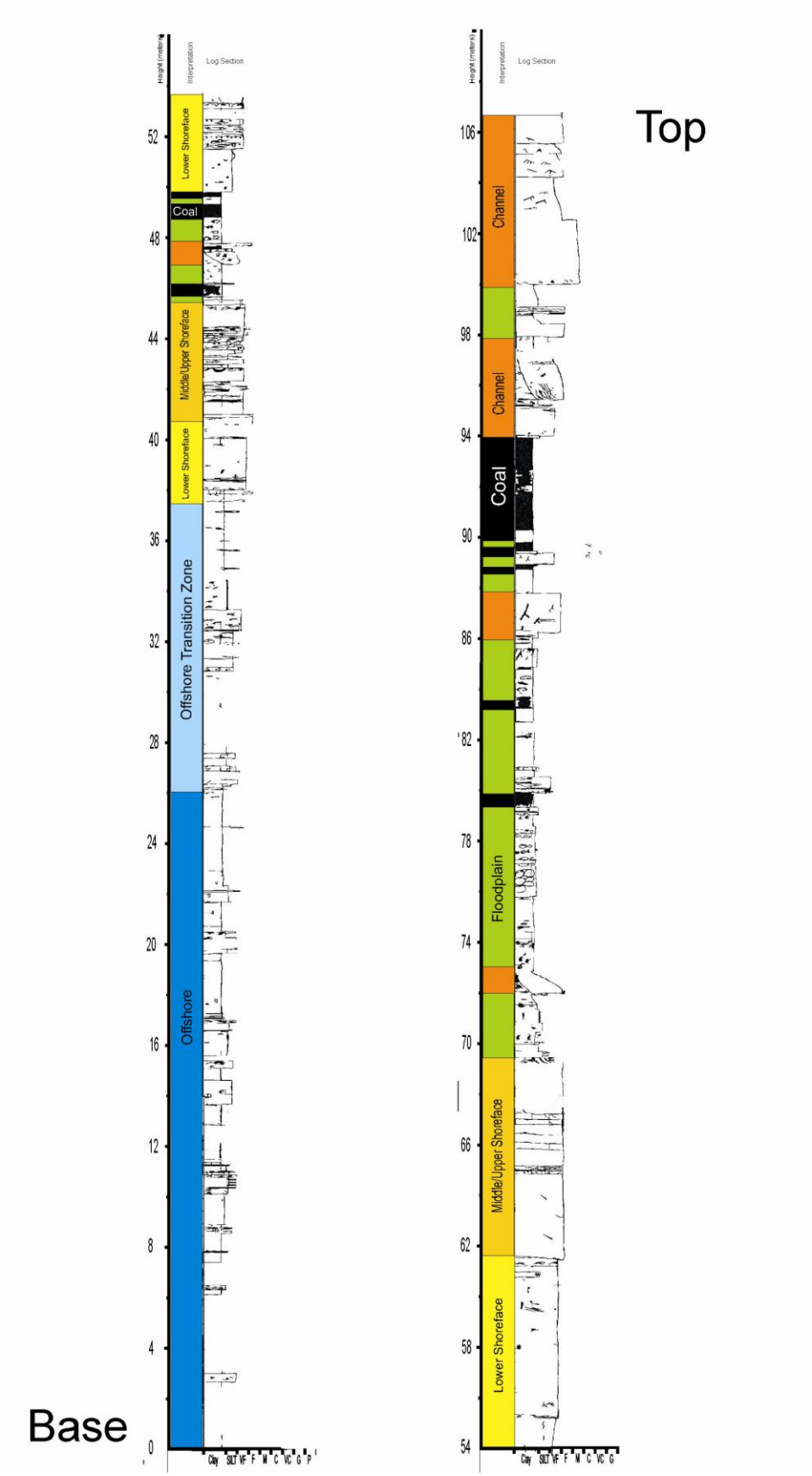

Figure 4.4.3: Ivie Creek I-70 log. Vertical stacking of three progradational parasequences. The facies recorded in this log is summarized in the following table.

Table 3: Summary of facies associations and brief description of their lithofacies for the Upper Ferron Ivie Creek outcrop study.

Facies Association	Lithofacies description	Bioturb. Index	Depositional Environment
Offshore	Siltstone dominated by undifferentiated bioturbation The siltstone weathers in a nodular fashion. Shale sections tend to form slopes. Sand content never exceeds 15%. Undifferentiated bioturbation	5-6	Deposited below storm wave base from suspension fall-out of sediments.
Offshore Transition Zone	Marine heteroliths: interbedded siltstone and vf sand. Silt lenses are present in the generally highly bioturbated sand. Silt or shale drape low angle lamina of sandstone in some intervals in which bioturbation have not obliterated the structures. Sharp boundary to overlying layer. Ophiomorpha, Thalassinoides trace fossils.	1-2 5-6	Deposited between storm- and fair-weather wave base. Sandstone deposited rapidly during centennial to millennial storms. Rapid sedimentation retards bioturbation.
Lower shoreface	Very fine sandstone with a sharp, undulatory boundary, internal structure HCS deposit. Horizontal Ophiomorpha burrows. Some intervals within the sandstone section are highly bioturbated, leaving no visual trace of internal	4-5	Deposited above fair-weather wave base, affected by annual storms. Shale and siltstone deposited in inter-storm periods of quiescence.

	structures. Ophiomorpha trace fossils are the most prominent and shifts to vertical burrows towards the top, where shell fragments starts to occur.		
Middle shoreface	Fine sand with truncated low angle lamination. undifferentiated vertical burrows, and sharp contact with under- and overlying layer. Scattered shell fragments were observed. 10 and 15 cm thick intervals with visible internal lamination identified as HCS.	1-3	Deposited above fair-weather wave base. Sediments thoroughly reworked by daily wave motion.
Upper Shoreface	Fine to medium sand, TXS and PPS to truncated low angle lamination. Shell fragments.	0	Deposits affected by the surf of fair-weather waves.
Coastal plain	Non-marine heteroliths: shales to carbonaceous shale interbedded with thin interbedded current-rippled vf-f sandstone (Crevasse splays). Rootlets.	0-1	Deposited on a low-gradient plain protected from fair-weather waves by the shoreline. Levee-breaks and storms contribute sand.
Channel	Through cross stratification to waning flow current ripples, unidirectional. Erosive base with lag conglomerates, organic debris and rip-up mudclasts. Rootlets.	0-1	High- to waning –energy unidirectional currents scour the coastal plain and deposit sands of

The coal seams show a yellow discoloration which is associated with the presence of sulphur. The seams contain numerous cleats which are analogues to those along which the gas in Drunkards Wash is produced. The cleats have an orientation close to perpendicular to the outcrop face in a northerly direction, with a possible cross-cutting secondary cleat set that is oriented close to perpendicular to the first set of cleats. These conjugate cleat sets appear as vertical and horizontal secondary mineral growth surfaces in Figure 4.4 A) and B). Cleats are described in the chapter concerning the geological setting, sub-chapter tectonic setting. Elevated sulphur content in coals suggest an increased marine influence which in turn is linked to marine flooding events (Holz et al., 2002) suggesting that the occurrence of the coal is related to the parasequences boundaries as described for the nearby Blackhawk Formation by Davies et al (2004). The sulphur content decreases upwards suggesting that while the initiation of mire growth is allocyclic, the majority of the coal accumulated while the parasequence prograded. Coal thicknesses measured range from a few tens of centimetres to 1,3 m and varied along strike.

Coastal plain heteroliths include interbedded crevasse splay sandstones and carbonaceous siltstones that occur in close proximity to the coal seams, often with a gradual transition through coaly silt and silty coal depending on the relative content of organic matter (Figure 4.4 D).

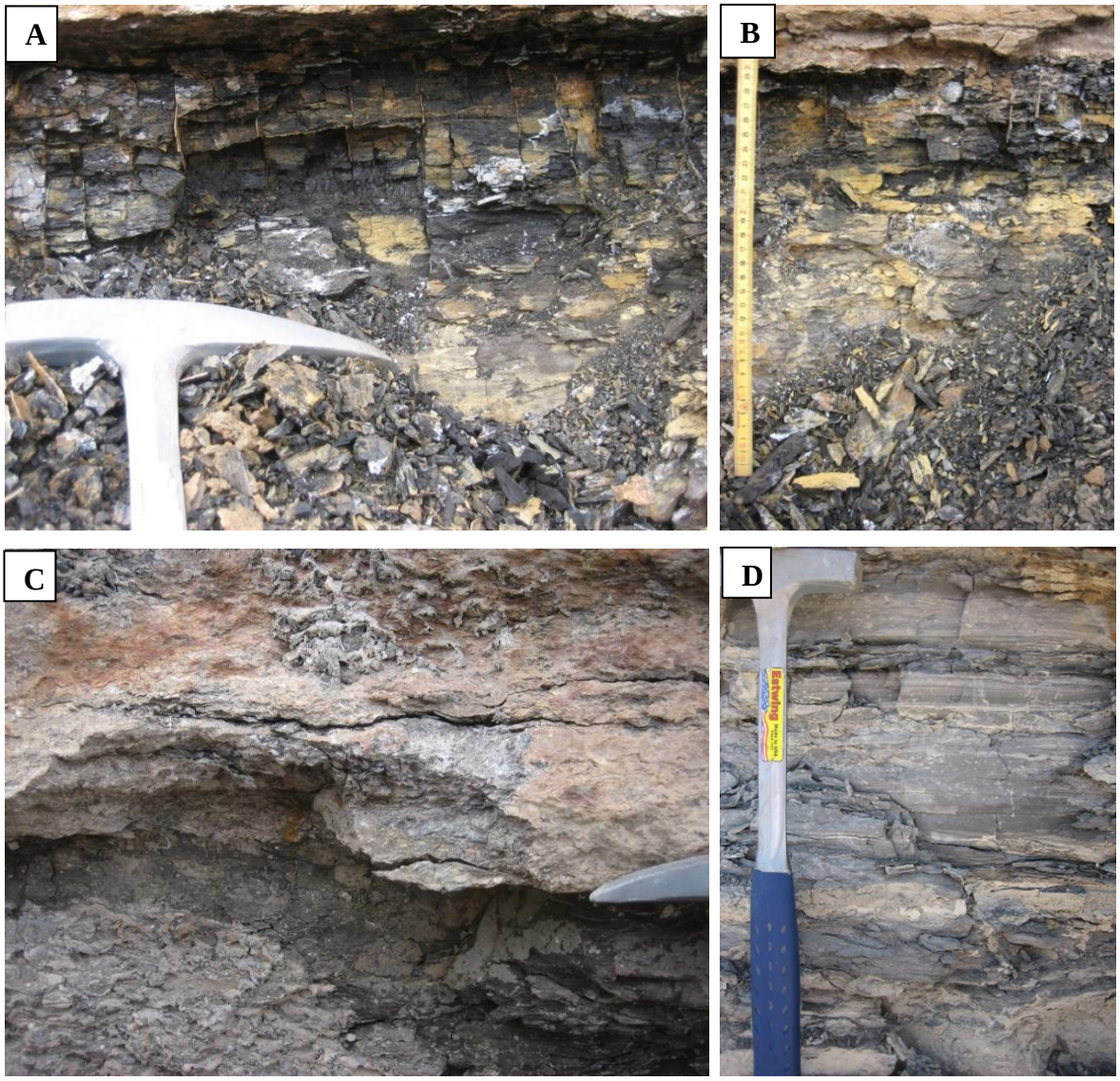

Figure 4.4: A) Carbonaceous siltstone and coal. The coal seam show clear evidence for cleating, one of the prime requirements for high gas recovery from the impermeable coal layers in Drunkards Wash. B) Sulphur is found along with the coal seams in this outcrop. C) Relationship between coal layer underlying channel sands. D) Carbonaceous shale found both below and underneath coal layers and channels, indicative of low-energy coastal plain depositional environments.

In addition to the coal and heterolithic overbank deposits the non marine interval also inlcudes channel belt deposits. Channel thicknesses recorded in outcrop range from 1 – 15 m. The erosive base of these showed scours of up to 2,5 metre. Sedimentary structures include trough cross stratification, current ripples and lag-conglomerates along base. Organic matter and mud-clasts were found within the channel-sands. The channels showed a general upwards fining trend.

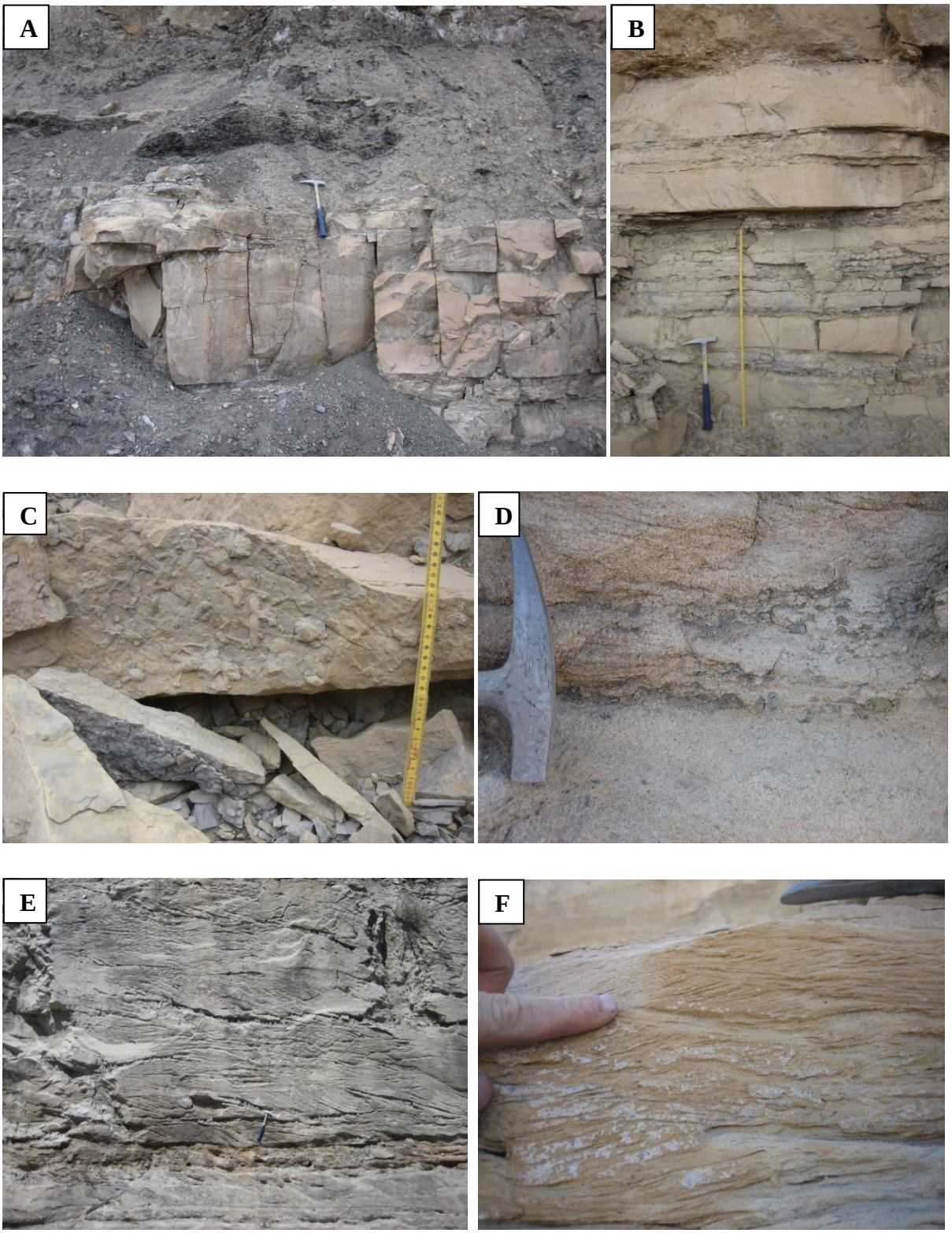

Figure 4.5: A selection of channel sandstone deposits from the outcrop at I-70. A) Channel body in coastal plain heteroliths, joint fracture planes cut the deposit. B) Amalgamated upwards fining channel sandstones. C) Vertical trace fossils of the type Ophiomorpha found at the base of the channel deposits in B). D) Coarse sand in the basal part of a channel body, rip-up mud clasts of the eroded coastal plain incorporated at its base. E) Large scale through cross stratification. F) Current ripples.

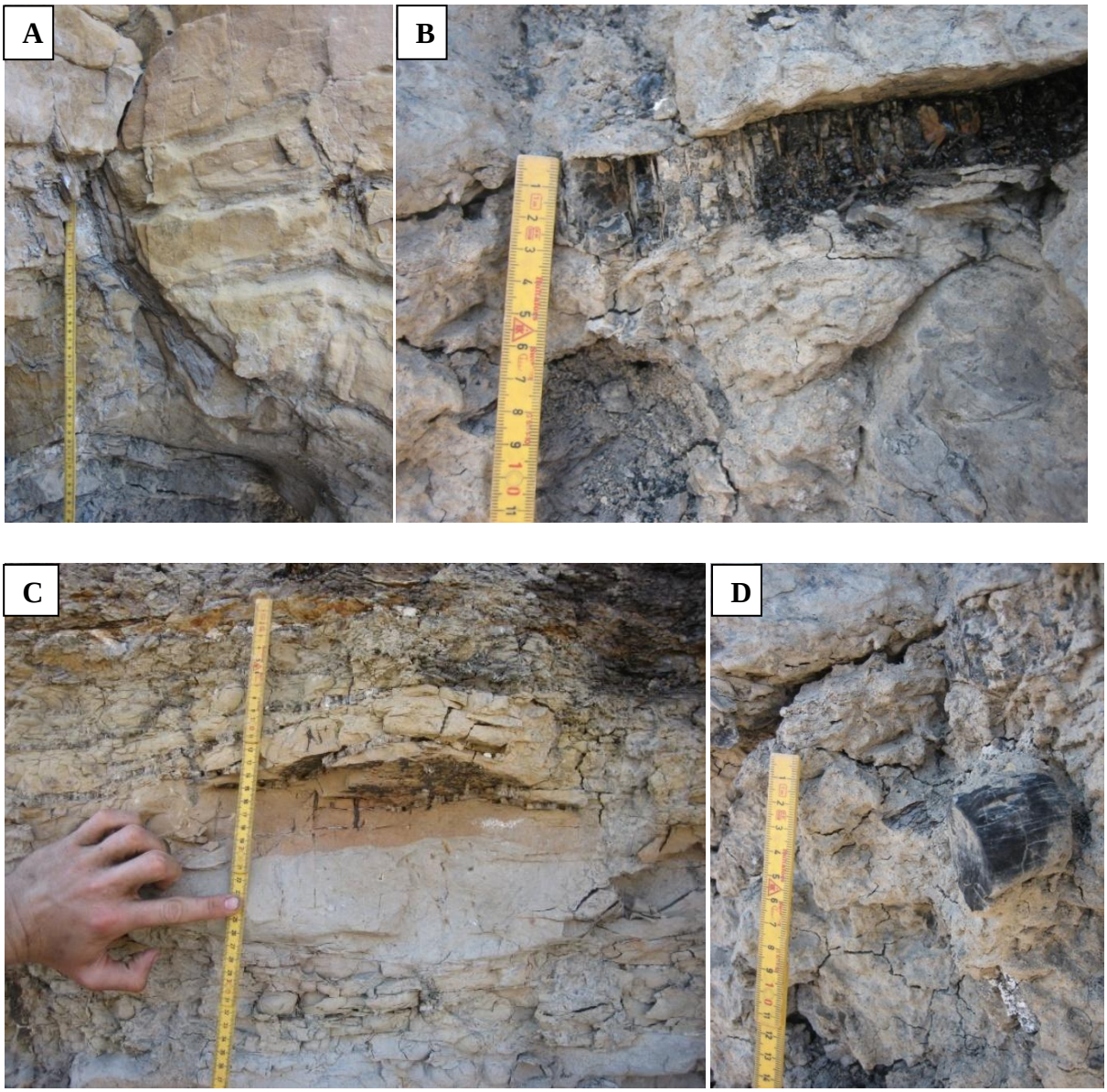

Figure 4.6: A selection of non-marine trace fossils and organic matter. A) Tree rootlet cut through channel sandstone. B) Small-scale coal seam. C) Rootlets of plants in coastal plain heteroliths. D) Petrified tree trunk.

4.2 Lower Ferron

Outcrops of the Lower Ferron extend from the Farnham Dome in the north to a locality east of the town of Moore in the southern Castle Valley (Figure 4.7). These outcrops were investigated as they were located close to the subsurface Drunkards Wash CBM-field and because stratigraphic project suggests that they may be time equivalent strata.

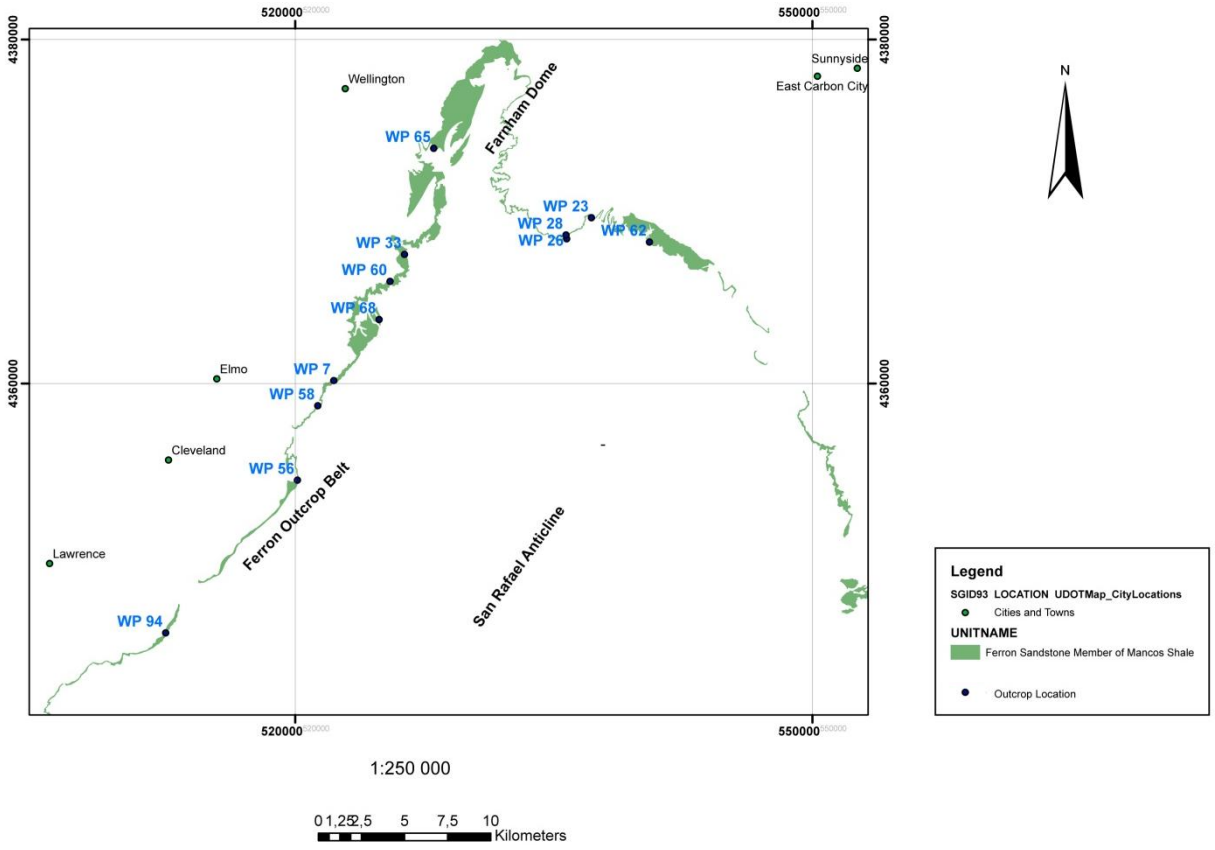

Figure 4.7: Overview map Lower Ferron outcrop locations in northern Castle Valley.

4.2.1 Geological background to the Lower Ferron outcrops

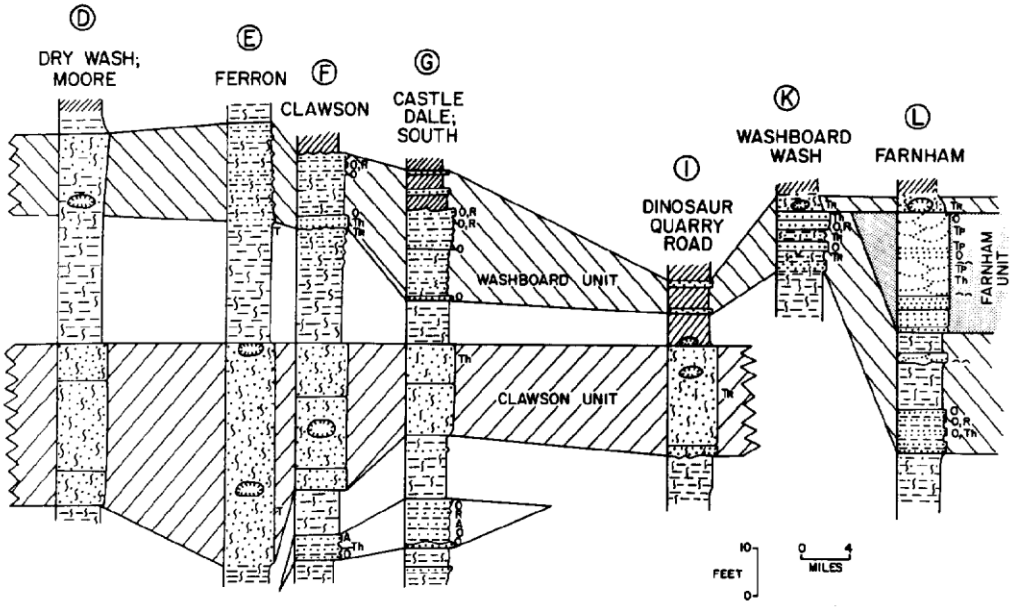

Figure 4.8: The original sequence stratigraphic panel for the Lower Ferron in Castle Valley, by Cotter (1975)

The Lower Ferron deposits were originally described by Cotter (1975) as a series of units (Figure 4.8) that represent the earliest sandstone deposits within the Mancos Shale. The units are capped by a regional transgressive surface that marks the end of the Lower Ferron Sandstone deposition, the hyatti sequence of Gardner (1995a) and the onset of the Upper Ferron Sandstone further south.

The units were described by Cotter (1975) as follows:

The Clawson unit is described as a poorly sorted, very fine grained sandstone with admixed clay, silt and organic matter to sandy siltstone at some locations. It pinches out in Tununk shale to the south, and its northern continuation is not determined. Large carbonate concretions occur at different intervals within the Clawson.

The Washboard unit is lithologically similar to the underlying Clawson unit, but interbedded with laminated sandstone. The unit shows an upwards coarsening trend in general towards laminated to wavy sandstone. The most proximal part of the outcrop is located to the north, based on an increased amount of laminated sandstone, and around Farnham Dome it encases the Farnham unit. The limits of the Washboard unit is not defined, but traced south past Moore, and southeast towards Cedar (near WP 62 in Figure 4.7).

The Farnham unit crops out near Wellington were it lies within the Washboard unit. It consists of very fine to fine sandstone with trough cross stratification and abundant shell fragments and preserved valves.

Cotter acknowledges an offshore sand bar deposit, which he names the Woodside Unit, stratigraphically lower than the shoreface deposits discussed above. The Woodside Unit was not covered in this study as the focus is directed towards the deltaic part of the Lower Ferron. Edwards et al. (2005) describes the Woodside Unit of Cotter in great detail and interprets the deposits to be turbidites fed from the Lower Ferron shoreline in the vicinity of present day Wellington.

The flooding surface capping the Lower Ferron interval is described by Garrison and van den Bergh (2004) to consist of a condensed section of the Ammonite Prionocyclus hyatti (Gardner, 1995a), this horizon marks the end of their hyatti sequence (Lower Ferron Sandstone) The flooding surface is characterized by the distinct ‘cannonball’-concretions.

4.2.2 Lower Ferron outcrop description

Three upward coarsening successions interpreted as parasequences belonging to the Lower Ferron, hyatti sequence, have been identified from the outcrop study. These are exposed in a NNE-SSW trending escarpment which runs broadly parallel to the depositional strike direction.

Figure 4.9: Lower Ferron Parasequences and flooding surface along the escarpment southeast of Price. View towards southwest. Note carbonate concretions in the uppermost sandstone ledge. The log named WP 30 cover this outcrop interval.

Due to the nature of the outcrop distribution, depositional dip sections are rare on the western side of the San Rafael Swell. Edwards et al. (2005) studied the down-dip distal marine equivalent for the Lower Ferron along the northern and eastern rim of the San Rafael Swell. The deposits where described as channelized turbidites of a sustained hyperpycnal flow from the Lower Ferron shoreline, and were identified by the authors as far south as Green River. Depositional dip sections for the Lower Ferron are restricted by the westward dip of this feature into the subsurface of Castle Valley, which limits these sections to narrow and laterally restricted canyons and ravines not suitable for a sequence stratigraphic reconstruction of the shoreline. The main sections on the western side of the SRS are oblique to depositional strike section, allow study of changes in the paleoshoreline orientation.

The height of the Lower Ferron outcrops range from around 30 m in the northernmost exposed Lower Ferron outcrop in the area around the Farnham Dome, to less than 6 m in the south. In the southernmost record of these distal parasequences of the Lower Ferron, only one parasequence could be distinguished directly beneath the regional flooding surface.

Figure 4.10: Two upper parasequences of the Lower Ferron, as in Figure 4.9, seen from a different angle. Carbonate concretions are visible as blocks atop the outcrop.

In the area around Jackass Flat south of the small town of Cleveland, the parasequences disappears and the only evidence for the stratal surface is the presence of large ‘cannonball’-concretions in the Mancos Shale. Cotter (1975) also noted this disappearance and saw this location as the southern limit of his Clawson Unit. Units attributed to the Lower Ferron appear further south, although the exact nature of the correlation is contensious. This will be discussed further below.

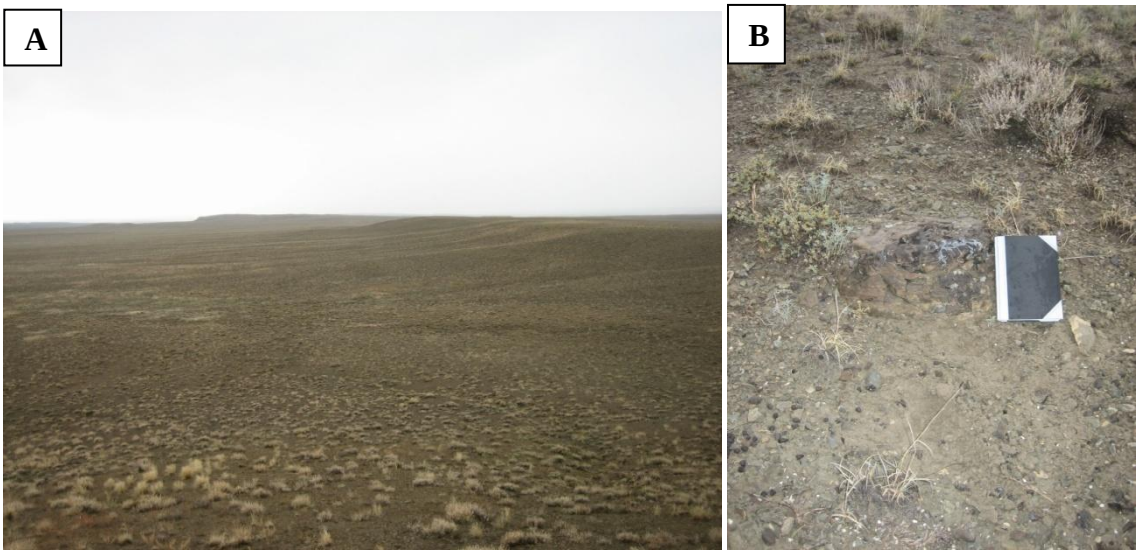

Figure 4.11: A) The surface expression of the Lower Ferron sandstone at Jackass Flat. The pronounced escarpment observed further north is reduced to a gentle hill. Reoccurence of Ferron sandstones can be seen in the far distance. B) Carbonate concretion sat in mudstone.

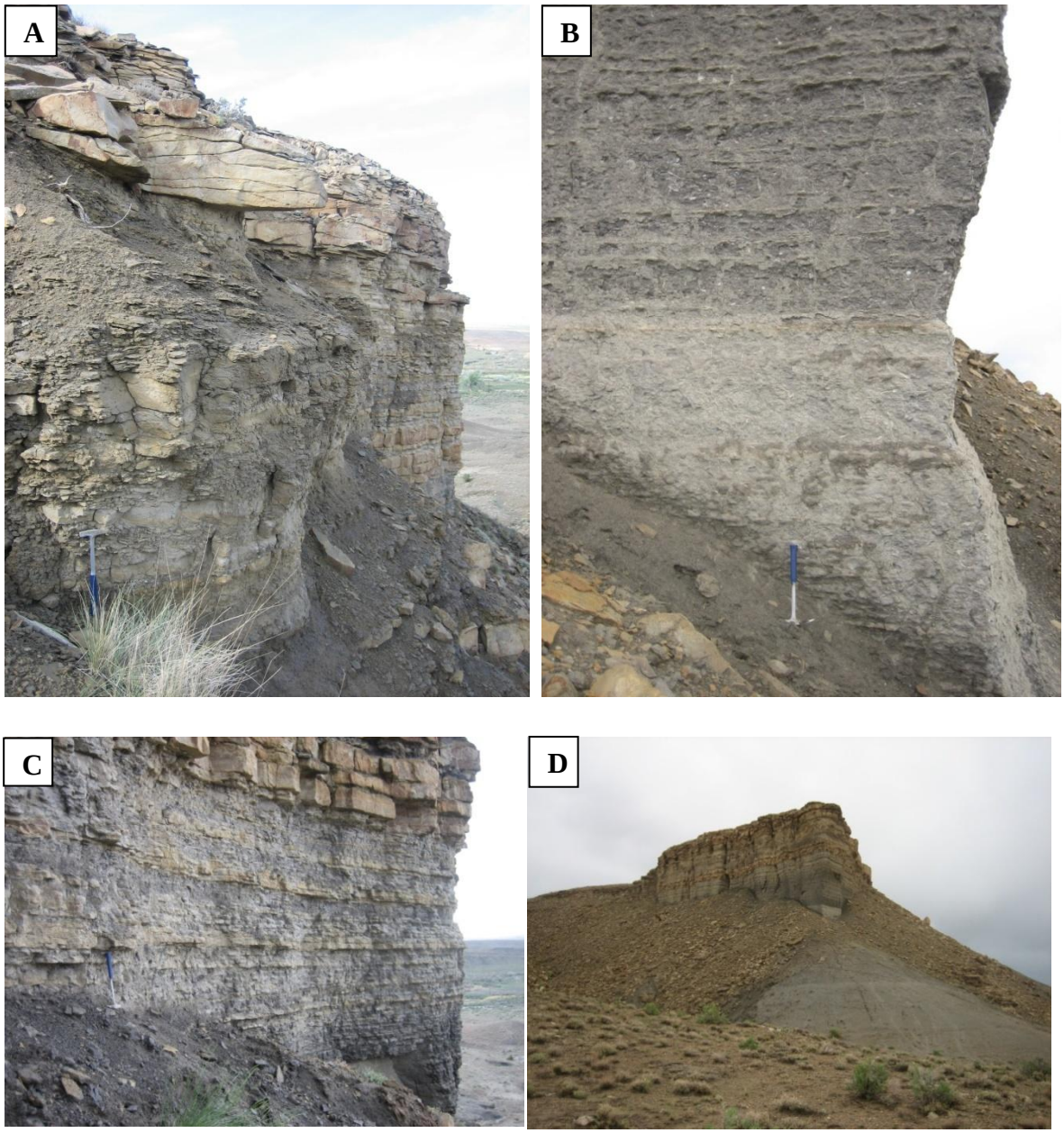

Figure 4.12: Lower Ferron outcrop near Farnham Dome Railroad crossing, WP 65.

4.2.3 Bentonite layers

Sat in the Blue Gate Shale, overlying the upper hyatti sequence boundary, a layer of bentonitic ash was identified approximately 25 m above the topmost parasequence of the Lower Ferron. This layer was also identified in the logged core section, to be discussed in more detail, at the same stratigraphic level relative to the Lower Ferron.

Obradovich (1993) dated the widespread volcanic ash layer overlying the Lower Ferron, hyatti sequence, to be 90,5 Ma. This bentonitic ash layer is underlying the condensed section

to which Gardner (1993) assigned the boundary between the hyatti and the ferronensis sequence.

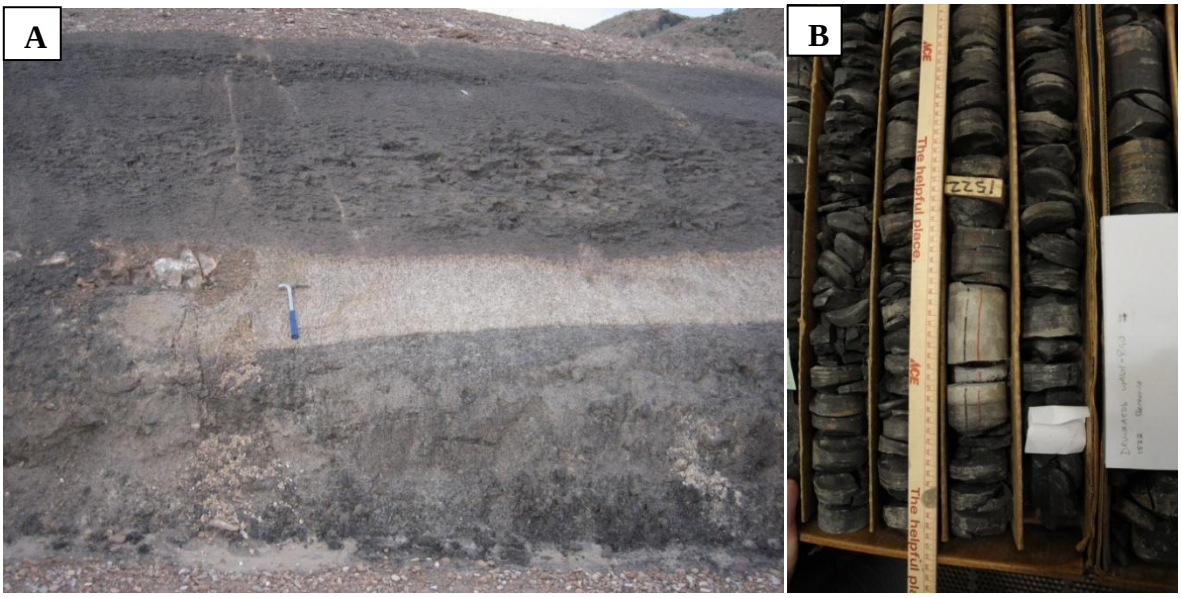

Figure 4.13:A) Bentonite layer, indicated by hammer, sat in Blue Gate Shale atop Lower Ferron outcrops near Farnham Dome. B) Bentonite from the cored section in RGU-1, identified at the same stratigraphic level in the core as in outcrop, approximately 25 meters above the Lower Ferron deposits.

4.3 Facies Description Lower Ferron Outcrops

A summary of the lithofacies observed in the outcrops of the Lower Ferron and their interpreted depositional environments is summarised in Table 4. This table includes information gathered from both the Upper Ferron and the Lower Ferron.

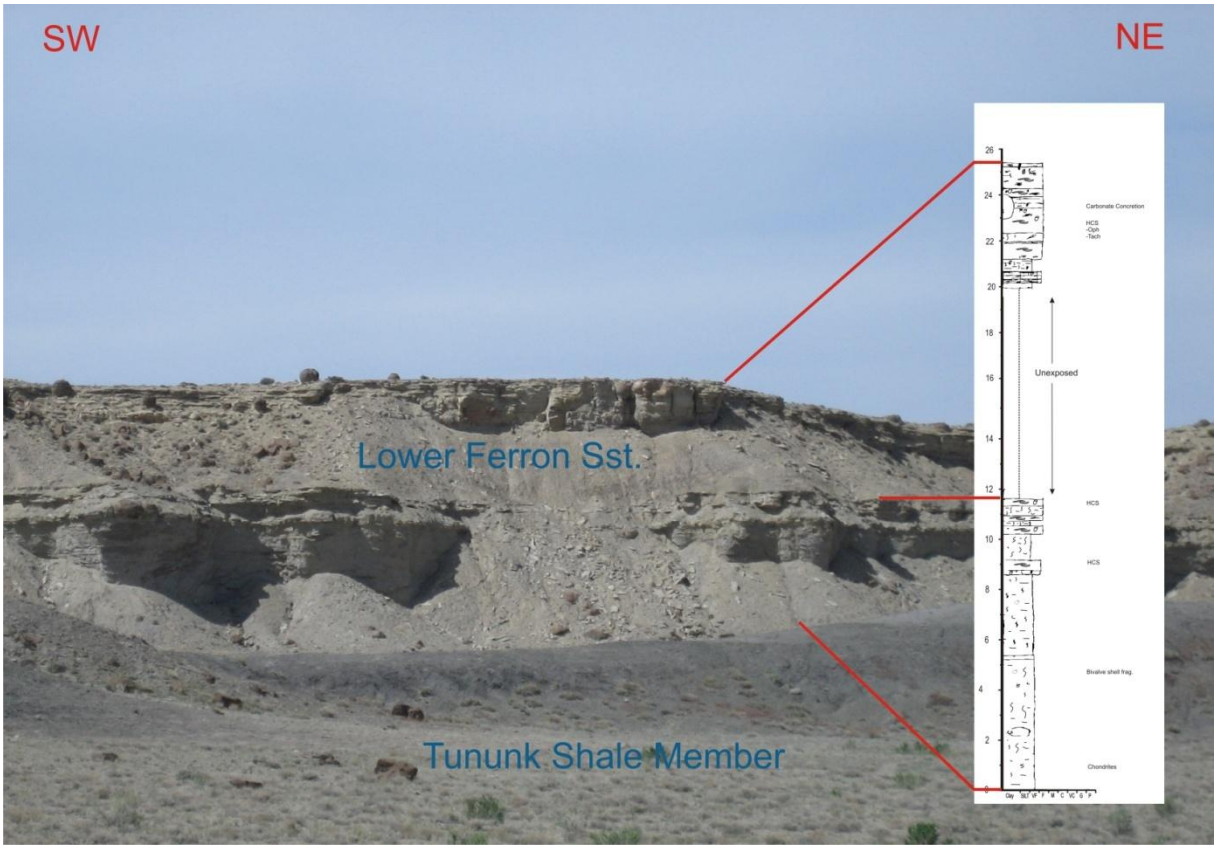

Figure 4.14: Example of an outcrop location along the San Rafael Swell. WP 30. Two parasequences are visible

Table 4: Facies associations from the Lower Ferron Sandstone outcrop study.

Facies Association	Lithofacies description	Bioturb. Index	Depositional Environment	Logs
Offshore	Siltstone dominated by undifferentiated bioturbation The siltstone weathers in a nodular fashion. Shale sections tendto form slopes. Sand content never exceeds 15%. Undifferentiated bioturbation	5-6	Deposited below storm wave base from suspension fall-out of sediments.	WP-ALL
Offshore Transition Zone	Marine heteroliths: interbedded siltstone and vf sand. Silt lenses are present in the generally highly bioturbated sand. Silt or shale drape low angle lamina of sandstone in some intervals in which bioturbation have not obliterated the structures. Sharp boundary to overlying layer. Carbonate concretions of varying size, 30 cm to 1,5 m in diameter. Ophiomorpha, Thalassinoides trace fossils.	1-2 5-6	Deposited between storm- and fair-weather wave base. Sandstone depositedrapidly during centennial to millennial storms. Rapid sedimentation retards bioturbation.	WP-ALL
Lower shoreface	Very fine sandstone with a sharp, undulatory boundary, internal structure HCS deposit. Horizontal Ophiomorpha burrows. Some intervals within the sandstone section are highly bioturbated, leaving no visual trace of internal structures. Ophiomorpha trace fossils are the most prominent and shifts to vertical burrows towards the top, where shell fragments starts to occur. Large carbonate concretions.	4-5	Deposited above fair-weather wave base, affected by annual storms. Shale and siltstone deposited in inter-storm periods of quiescence.	WP 68 WP 60 WP 33 WP 65 WP 28 WP 23
Tidal Inlet Channel	Through cross stratification. Erosive base with lag conglomerates, organic debris. Abundant shell fragments and oyster shells.	0-1	High–energy unidirectional currents that scour the Lower Shoreface	WP 65

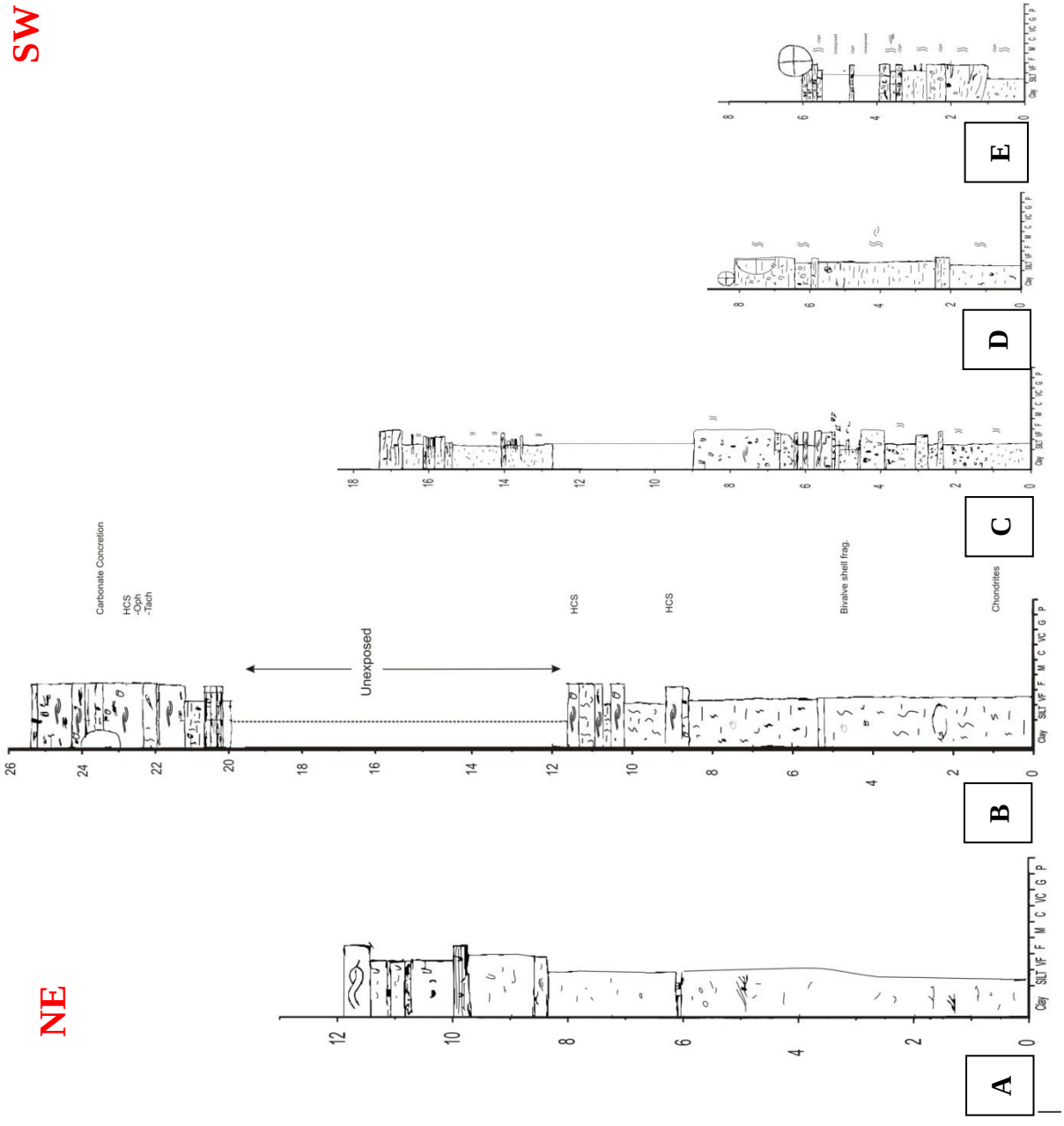

Figure 4.15: Logged outcrop intervals from the two uppermost parasequences of the Lower Ferron in northern Castle Valley. The log locations may be seen on the overview map (figure 1), where they span northeast – southwest. The log named WP 23 (A) is located in a relatively more basinward position than WP 30 (B) and WP 7 (C), and in between them the Lower Ferron is broken by faults. However, the basinward thinning trend is clearly observable. Note the severe southward thinning accompanied by the disappearance of one parasequence. Distances are shown in the correlation panel at the end of the chapter.

A) WP 23, B) WP 30, C) WP 7, D) WP 58, E) WP 56.

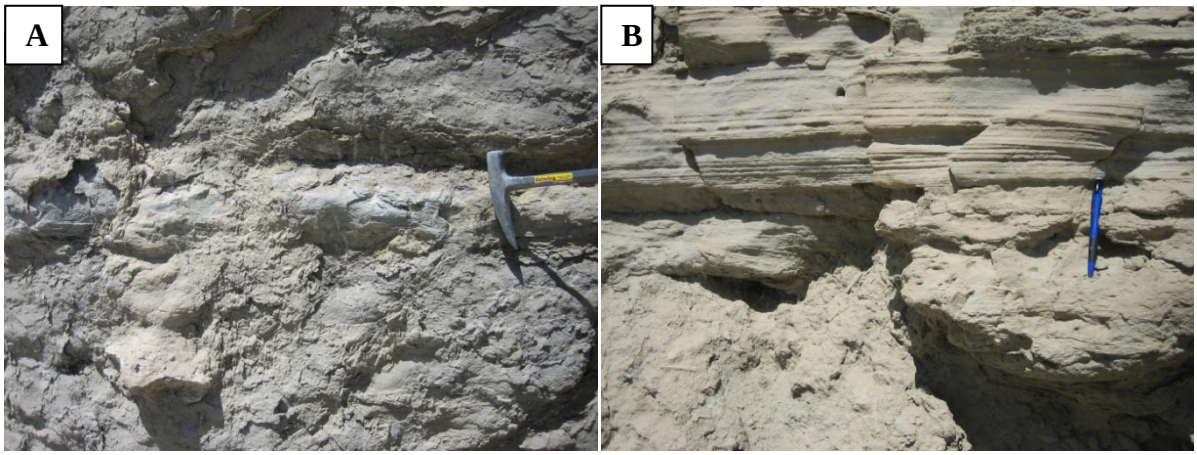

Figure 4.16: A) Nodular weathering expression of highly bioturbated siltstone. B) 30 cm thick laminated to swaley sandstone with sharp base to underlying bioturbated, nodular weathered siltstone.

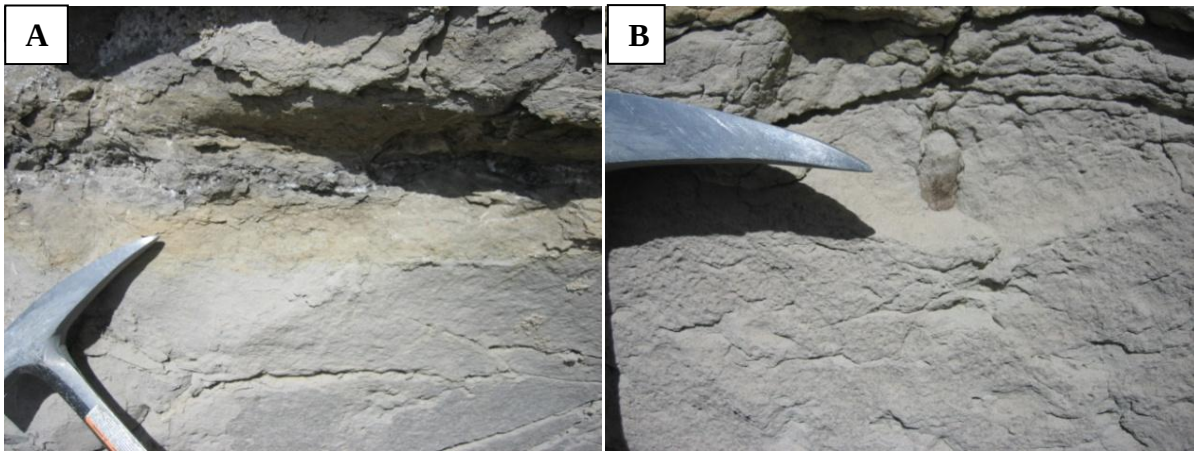

Figure 4.17: A) Secondary mineral growth. B) Ophiomorpha trace fossil.

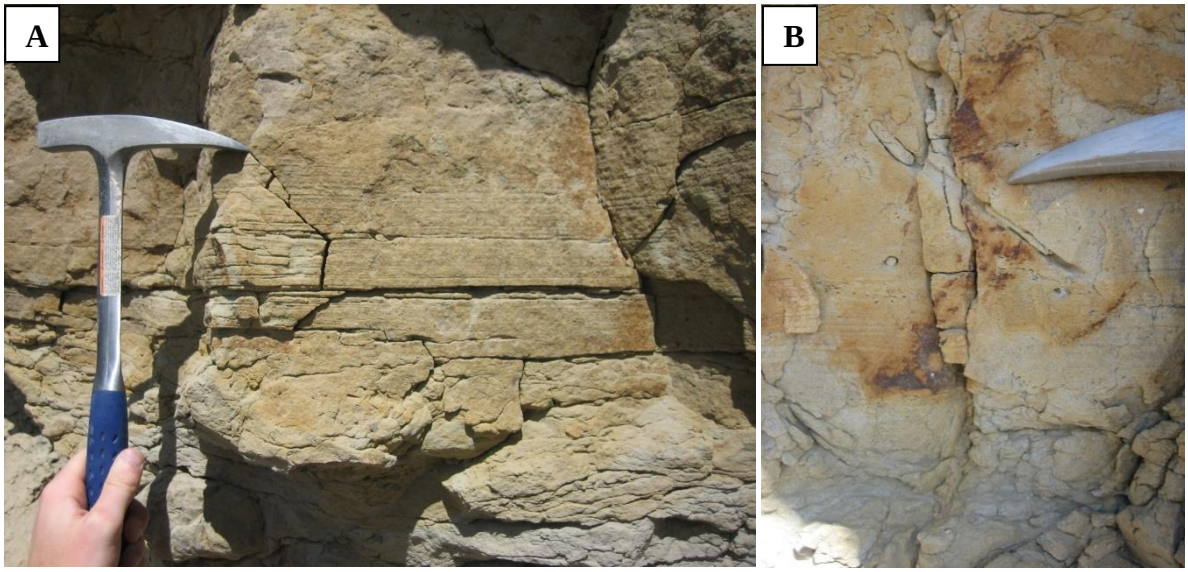

Figure 4.18: A) Laminated fine sandstone. B) Ophiomorpha trace fossil towards the top of the fine sandstone layer.

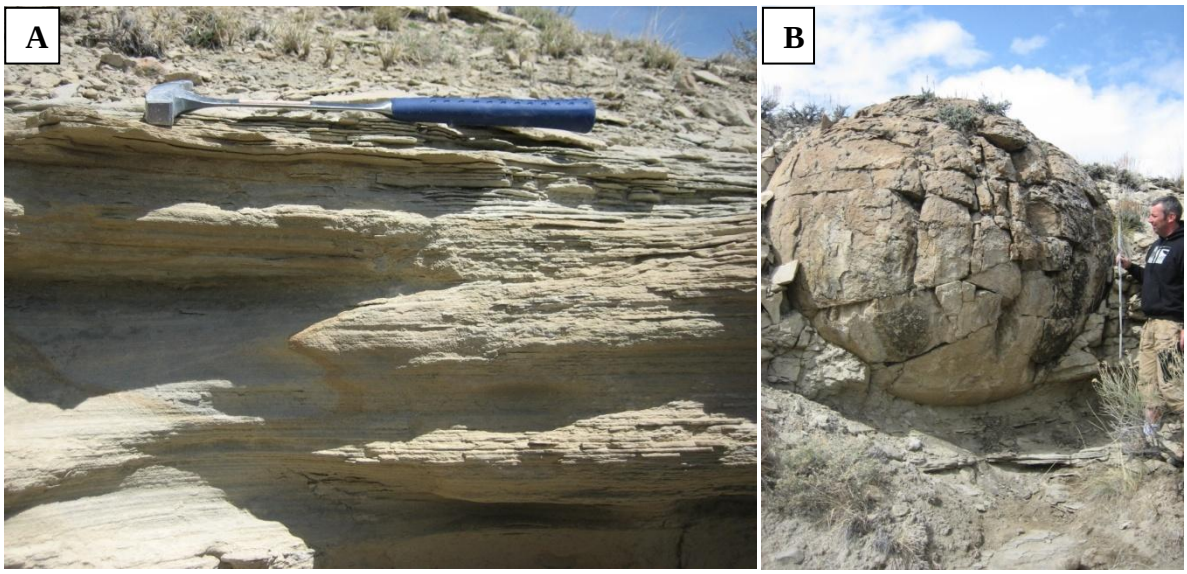

Figure 4.19: A) Planar parallel lamination in fine sandstone capping the outcrop interval. B) Carbonate concretion in upper part of outcrop WP 7. Popularly named cannonball concretions, these features are found along the entire stretch of the Lower Ferron outcrop along the western rim of the San Rafael swell. Typically situated at the top of the outcrops.

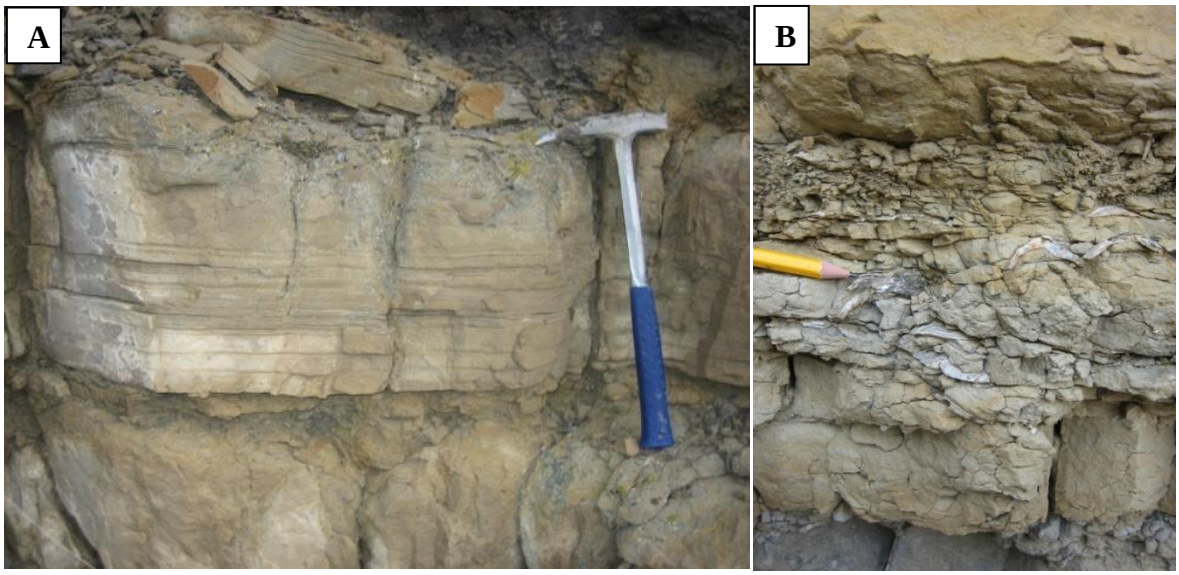

Figure 4.20: The Tidal Inlet Facies Association attributed deposits near Farnham Dome. Through cross stratified sandstone A), and intact oyster shells both scattered (B) but also found along horizontal layers.

4.4 Sequence stratigraphy

The outcropping part of the Lower Ferron is interpreted to comprise deposits that belong to the distal part of a low-energy, wave dominated shoreline. They record the progradation of three parasequences, the lower two parasequences are present across much of the area and are progradationally stacked. The third is only present in the northern part of Castle Valley and is back stepping.

The lower parasequence in outcrop rests conformably on the underlying Tununk Shale Member and grades upwards initially into bioturbated siltstones, which are overlain by bioturbated, very fine sandstone with wavy lamination to hummocky cross stratification. The parasequence is interpreted to represent progradation from offshore to offshore transition zone facies associations. The parasequence can be observed along the lower escarpment along the Dinosaur Quarry road, east of Cleveland. It thins southward and dives into the subsurface at Jackass Flat (Figure 4.21). Cotter (1975) noted a thin basal sandstone in his stratigraphic correlation panel underneath his Clawson and Washboard units at locality G and F in Figure 4.8. which suggests a southern pinchout just east of the towns Clawson and Castle Dale.

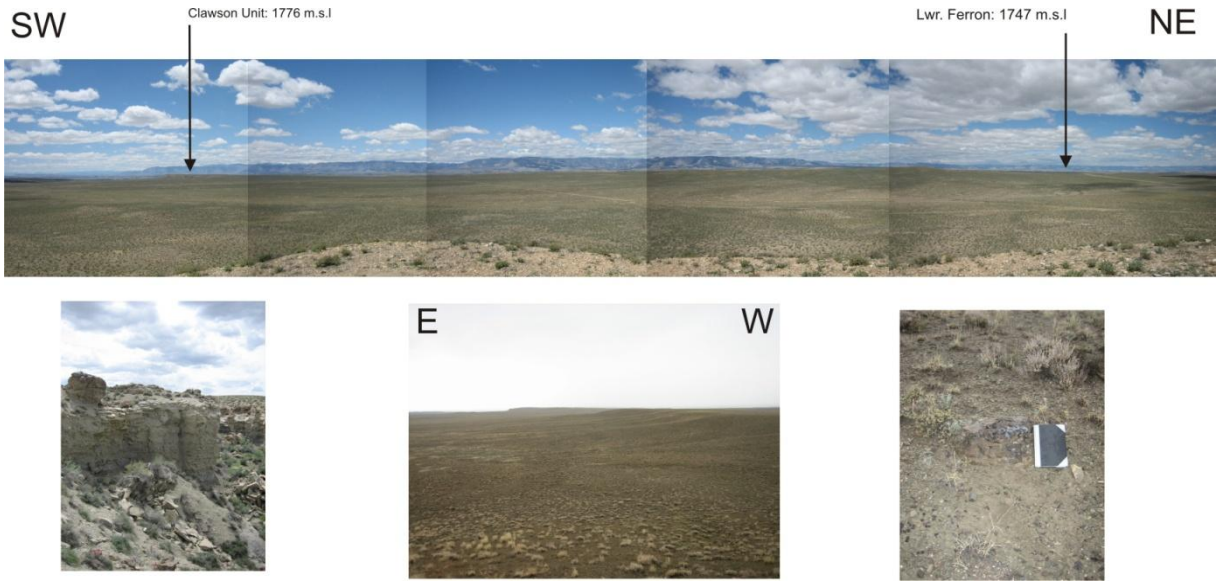

Figure 4.21: Overview mosaic overlooking the Jackass Flat. The Lower Ferron escarpment has thinned to siltstone and shale, and make out gentle slopes rather than the northern escarpments. Distance between the two arrows is approximately 11 km.

To the north this lowermost parasequence disappears into the subsurface before Washboard Wash, the northern type locality of the Washboard unit.

The parasequence is interpreted to re-appear southeast of the Farnham Dome due to local uplift around the faulted Farnham Dome.

The second Lower Ferron parasequence to crop out along the western San Rafael Swell escarpment shows a similar upward coarsening trend from offshore deposits through offshore transition zone deposits into lower shoreface sandstones. It does, however, generally show more amalgamated sandstones than the underlying parasequences suggesting a more basinward progradation. In the north around WP 65 (Figure 4.22) this parasequences is capped by a succession of tidal inlet deposits which overlie and cut into the lower shoreface deposits. .

To the north this parasequence dives into the subsurface, and underneath the Book Cliffs. Its southward continuation, assuming the stratigraphic relationship of Cotter (1975), Ryer (1994), Fisher et al. (1993, Figure 2.8) and Barton et al. (2004), would extend to the escarpment east of Clawson and continue further south to pinch out in the Tununk Shale Member, underneath the Upper Ferron Last Chance Delta.

Overlying this second parasequence, there is a further upward coarsening unit, separated from the preceding parasequence by a thick marine shale interval. The sandstones are thin and less amalgamated than those at the top of the underlying pararsequence and consequently this upper paraesquence is interpreted to illustrate a back-stepping stacking pattern. A bentonite horizon illustrated in Figure 4.13 A) lies with the Mancos Shale 26 m above this upper parasequences. This bentonite is correlated to the bentonite observed 25 m above the top of the PS4 in the cored well section in RGU-1, described in the previous chapter. This provides an additional datum for correlating the subsurface with the outcrop sections

The deposits of the Lower Ferron pinch out towards the southwest in the area around Jackass Flat (Figure 4.22). This will be discussed further in the discussion chapter. The proposed stratigraphic relationship between the outcrops of the Lower Ferron and their inferred relationship to the Upper Ferron deposits is summarised in Figure 4.26, and will be discussed further in Chapter 6.

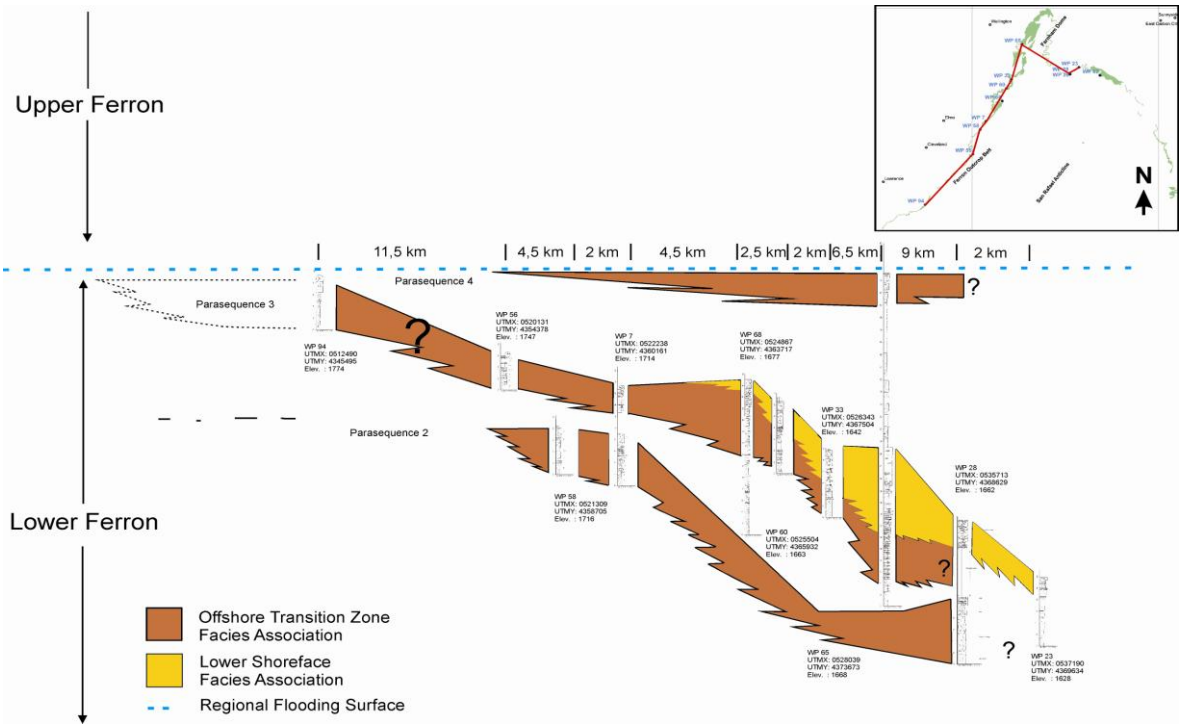

Figure 4.22: Correlation panel of the logged outcrop sections after surface tracing.

4.4.1 Outcrop to Subsurface correlation

The three parasequences observed in the outcrop have been correlated to the four parasequences observed in the subsurface in the Drunkards Wash CBM field (Chapter 3). The outcrops lie to the east and SE of the CBM field and the progradation direction observed from the subsurface data was towards the SE, hence the outcrops lie some 10+ km down depositional dip of the CBM field. Parasequence 1 is observed to pinch out within the subsurface data and is not present in the outcrops. Parasequence 2 and 3 are correlated to the two stacked parasequences observed in the field. The tidal inlet observed at the top of the Clawson unit is related to the maximum progradation of the clastic wedge and may be a distal expression of the proposed sequence boundary, as proposed by Edwards et al. (2005).

Parasequence 4, which back steps in the subsurface data is correlated to the uppermost, upward coarsening interval which is only local present in the outcrops in the north of the area.

The following schematic palaeogeographic maps summarise the combined outcrop and subsurface observations and highlights a direct link between the coastal plain deposits of the CBM field and distal lower shoreface deposits in the outcrops. This corresponds to the

existing published models (e.g. Cotter 1975) which suggest a source for the Clawson and Washboard units to the north and NE. The model suggests that the Lower Ferron shoreline prograded as a more or less straight wave dominated shoreline from the northwest to the southeast. The direction of shoreline progradation is possibly related to a well documented bulge in the Turonian shoreline related to the ancestral Uinta uplift and as such the Lower Ferron is a part of the Vernal Delta complex (Ryer and Lovekin, 1986), which is by this study suggested to be a more pronounced depositional feature than previous suggested.

Progradation was followed by a transgression before ultimate abandonment and the subsequent southern evolution of the Upper Ferron Last Chance Delta in the south.

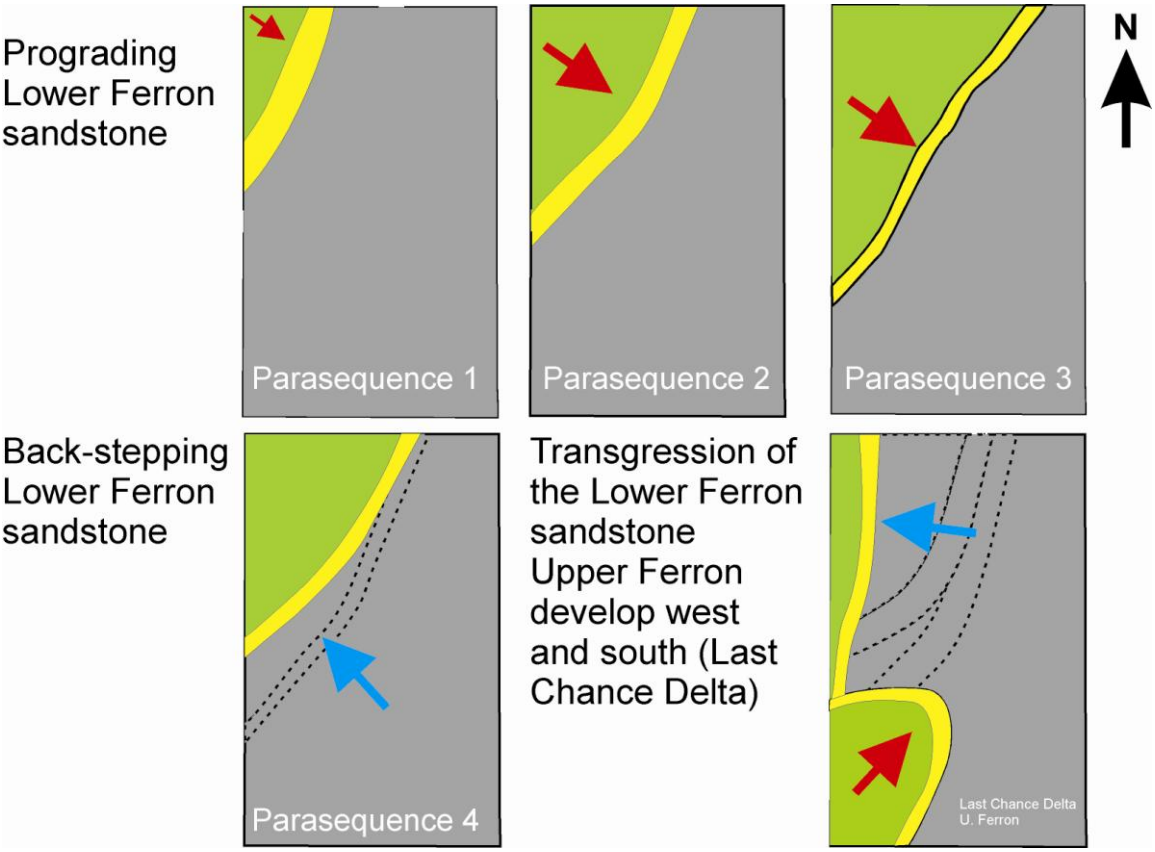

Figure 4.23: Schematic palaeogeographic map suggested for the Lower Ferron Sandstone of Castle Valley, and their paralic subsurface deposits. This map is based mostly on the outcrop studies, and the first subsurface correlation panels. Upper Ferron shoreface is based on Henry and Finn (2003) and Anderson and Ryer (2004), though only relatively positioned for comparison.

4.4.2 Relationship to the existing lithostratigraphy

The existing lithostratigraphy for the outcropping part of the Lower Ferron is confusing and somewhat contradictory. The lower parasequence of the present outcrop study is thought to coincide with the Clawson unit of Cotter (1975). The sandstones are overlain by an interval of finer grained material related to the overlying parasequences which corresponds to the Washboard unit of Cotter (1975).

However, the proposed relationship between the units he names Clawson and Washboard in northern Castle Valley does not fit with the conceptual model for the Lower and Upper Ferron units towards the south. The Washboard and Clawson both thin and become more distal up to Jackass Flat and then disappear. A unit also called the Washboard reappears south of Castle Dale and thickens and becomes more sand rich towards the south before eventually thinning and pinching out underneath the Upper Ferron to the south.

Further, the present study of the terminology of Cotter (1975), were he names the units after type localities along the Lower Ferron escarpment is not descriptive of the parasequences actually exposed there. For example, the unit he names the Clawson unit is the most inconspicuous feature east of Clawson according to the present study. The terminology of Ryer (1994), Kf-Washboard, is the best fit with the correlation panel presented above, as it describes the unit of Cotter (1975) as a parasequence, and also notes that it is the most basinward expression of the Lower Ferron.

The relationship between the various outcropping units, the Lower Ferron in the subsurface and the Upper Ferron outcropping around Ivie Creek is ambiguous. Visualizing the succession in 3D is a useful way to full investigate some of the facies trends spatially and to relate the various data sets. This relationship will be discussed further (Chapter 7) after the 3D model has been described and presented.

5 Model

Over the last decade, 3D geocellular modelling has, become a standard routine when dealing with subsurface petroleum reservoirs, and is currently widely applied within the petroleum industry. More recently the same software packages have also been used to study outcrops (e.g. Howell et al., 2008; Enge and Howell, 2010). The software and workflows have significant application for understanding sequence stratigraphic architecture and facies distribution. There are no previous studies that include both subsurface and outcrop data in a single model

The model presented in the current study was built using Schlumberger's Petrel 2009 software. The goals of building the model were: 1) to understanding and visualise the sequence stratigraphy and facies architecture within the Drunkards Wash CBM field; 2) to facilitate detailed correlation between the outcrops and the subsurface; 3) to visualise a largely unstudied clastic wedge in 3D, in order to further understand the detail of sediment transport and stacking patterns. The data used for building the model were the extensive well and outcrop log database and the surfaces mapped at outcrop. No seismic data were used since none were available. The following chapter explains how the model was built, what data were used and finally the results.

Given the high density of wells data within the proximal part of the model, it can be considered highly deterministic and the extrapolated facies associations did not extend far from each given input data.

5.1 Constructing the model

The model was constructed in Petrel and includes a 10 m Digital Elevation Model (DEM) obtained from the USGS, well log data from the Utah Geological Survey and outcrop data collected during the first field season in spring 2009.

The first stage was to recreate the topography of Castle Valley. 10 m DEM data were downloaded from http://seamless.usgs.gov/website/seamless/viewer.htm. The data were converted from a raster dataset to a text format through the use of ArcGIS, before they could be imported to Petrel. This dataset provided the geographic framework for constructing the model (Figure 5.1).

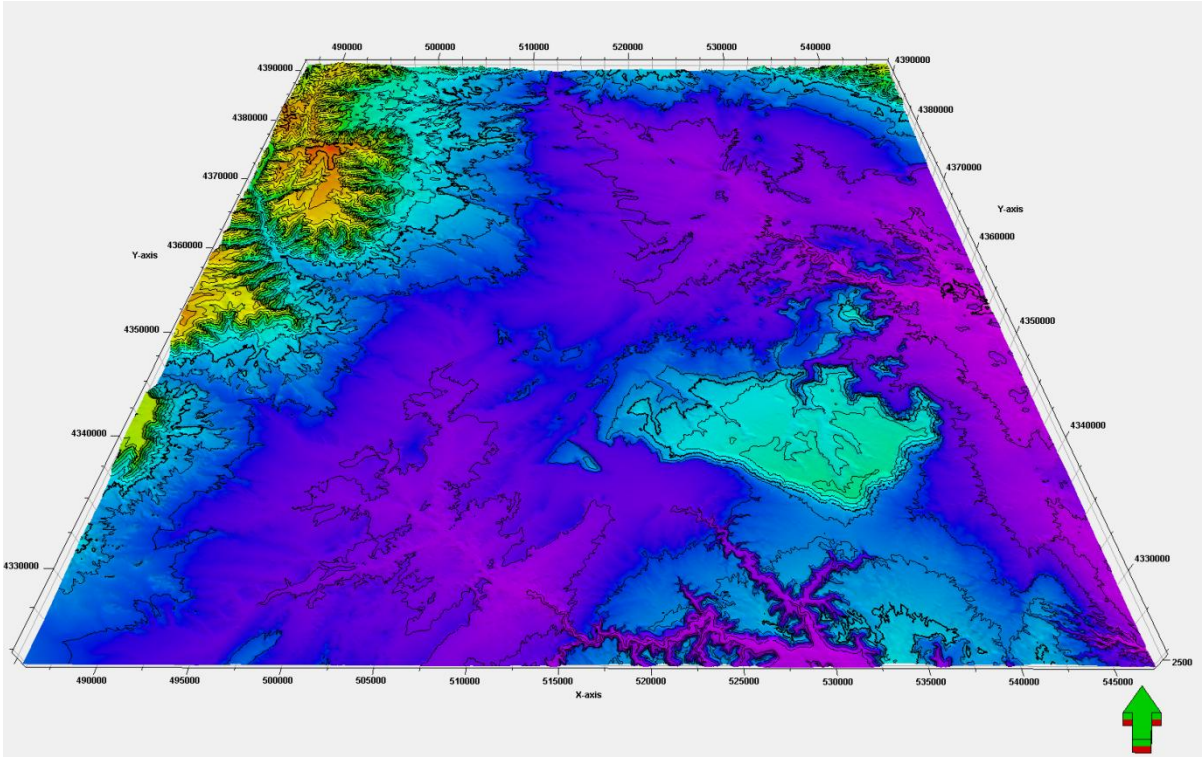

Figure 5.1: Topography of northern Castle Valley, representing the model-framework and geo-reference frame. No vertical exaggeration, contours every hundred meters. The ticks along the x-axis are spaced by 5km, along the y-axis by 10km.

Quality control of the gridded surface was carried out by comparing the topography with Kelly Bushing values for the wells and the location of the logged outcrops. The topographic dataset proved an exact match with the vast majority of wells, and all logged outcrops. Some Kelly Bushing values given in the datasets had to be edited manually.

The Drunkards Wash field contains over 250 wells. Fifty five of these were selected and downloaded from the database of the state of Utah's Division of Oil, Gas and Mining (http://oilgas.ogm.utah.gov/index.htm 11/04-2010). The prerequisite for the chosen wells was that some of these wells should follow the outer rim of the CBM-field, the remaining wells where chosen to provide a representative sample. Well RGU-1 was selected because it contains the cored section through the Lower Ferron.

All downloaded well logs had to be manually digitized before they could be imported to the Petrel program as discussed previously. Outcrops logs were scanned and imported as jpg files and later digitised. Facies association logs were created for all of the well logs and for the outcrop sections. A zone log was also generated for the 4 parasequences for both the subsurface and the outcrop sections as discussed in Chapter 3 and Chapter 4.

5.2 Surfaces and Grid design

The parasequences boundaries were used as the surface framework for the model. The surfaces were interpolated away from the data points (logs and outcrop locations) and gridded. A number of gridding algorithms are available and after gridding the surfaces were visually inspected to ensure that they matched the conceptual geological understanding. For the purpose of this study a Convergent Interpolation algorithm gave the best results. Figure 5.2 shows the 5 key surfaces with respect to topography and associated well logs along an oblique-to depositional dip profile (EW oriented J-section). Figure 5.3 shows the detail of the surfaces within the model and how they relate to the wells.

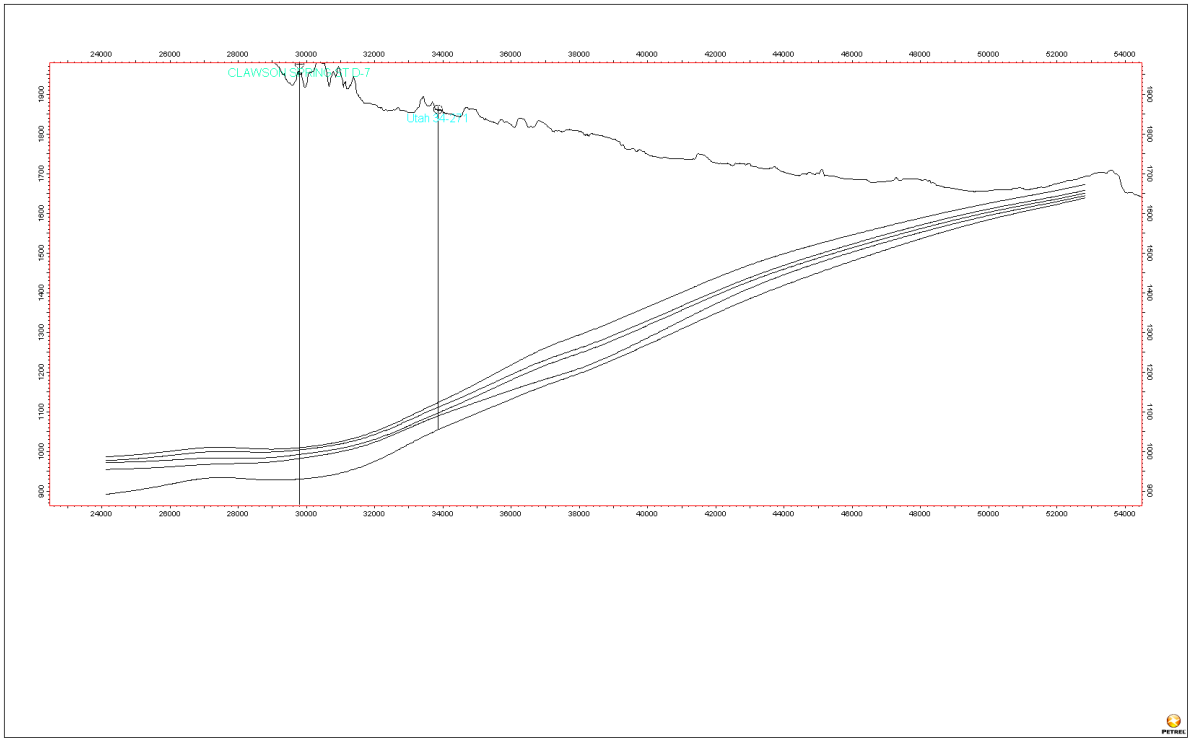

Figure 5.2: Key surfaces in an east-west directed cross section with vertical exaggeration 15. Well trajectories and topography included for reference.

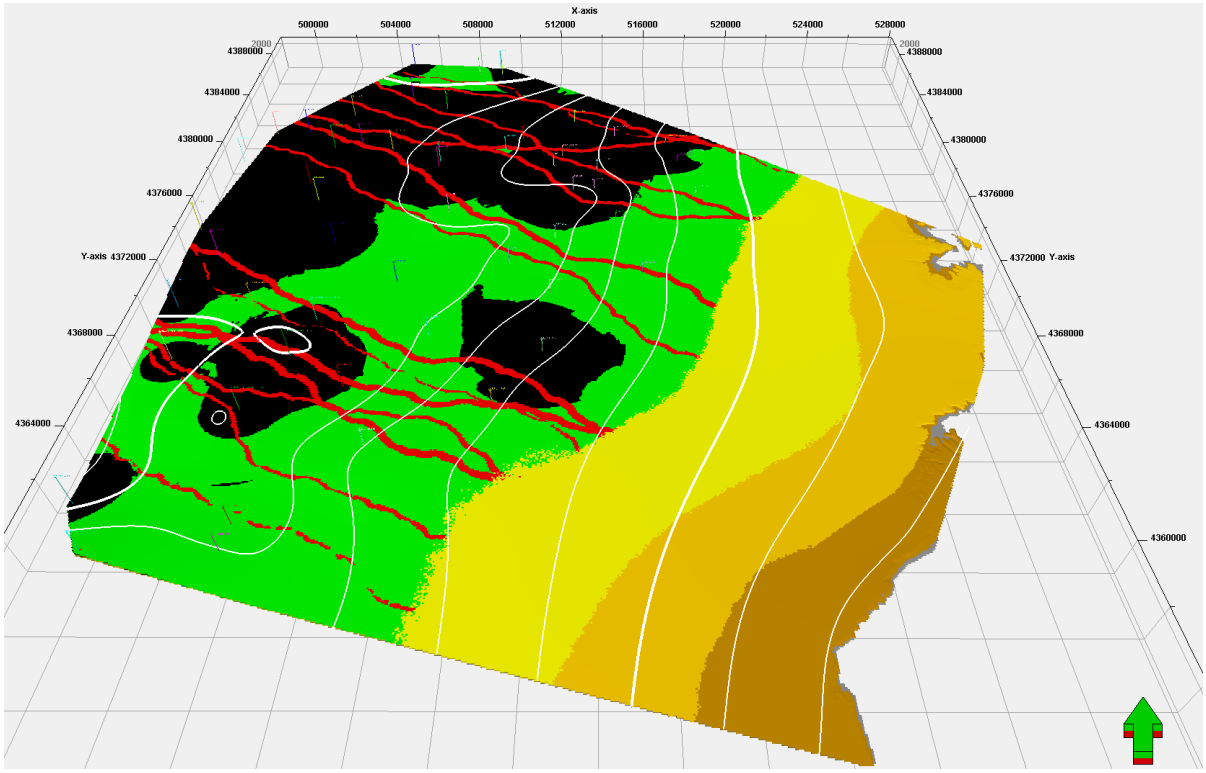

Figure 5.3: Oblique aerial view of the top of parasequence 3, white contour lines every 100 meters.

Facies are represented in the model as grid cells. A number different grid designs can be used to optimize the number of cells and the resolution. Given that no obvious onlap or truncation were, expected a proportional grid with 6 layers for each zone was used. This produced a typical vertical resolution of 2,5 m. The lateral resolution of the grid was 597 x 710 and the grid was orientated to the north by default. The gird contains a total of 12.23 million cells.

5.3 Populating the Grid

Facies property modelling used the facies association (FA) scheme described in Table 5, in the facies description chapter. On the basis of this scheme, a facies log was generated for each well or outcrop section and then upscaled to the grid. The upscaling procedure is based on a discrete modal average recording the most abundant facies within a cell. For the later facies modelling it was necessary to generate two upscaled facies logs, one which included the channels and coals with the coastal plain as “undifferentiated coastal plain” and one in which these three association were kept separate (Figure 5.4).

Table 5: Facies associations for the model building, their modelling method and appearance.

Code	Facies Association	Modelling Method	Colour Code	
0	Offshore	Truncated Gaussian with trends	Grey	Blue
1	Offshore Transition Zone		Brown	Light Blue
2	Lower Shoreface		Deep Yellow	Yellow
3	Upper/Middle Shoreface		Yellow	Orange
4	Coastal Plain		Green	Green
5	Channel	Stochastic Object Modeling	Red	
6	Lagoon	N/A	Pale Light Blue	
7	Coal	Indicator Kriging	Black	
8	Bakground	Aiding Stochastic Object Modeling	White	

Three different property modelling techniques were used to capture the geometries of the different facies associations. The detail of these is described below.

5.3.1 Shoreface Facies modelling, Truncated Gaussian with trends:

Parallel belts of facies are typically modelled using a property modelling tool which is based upon a series of "linear expectation planes" with added Gaussian noise. The plane represents the mean position of the facies boundary and the noise provides a stochastic representation of the bed scale inter-fingering (see MacDonald and Aasen 1994 for a full description). The approach was used to model s series of belts which included the undifferentiated CP, the USF, LSF, OTZ and offshore. The thickness of the USF, LSF and OTZ were determined from the upscaled geophysical well logs and the mapping of the facies tracts. The Undifferentiated Coastal plain and Offshore facies associations populated the remaining facies property model in the landward and basinward direction respectively. The trend option allows the user to

define the limits of each facies belt according to the predicted shoreline trend. In the case for the model and Drunkards Wash in general the trend was set to northeast-southwest to NNE-SSW. The Gaussian simulation calculates the relative position of each FA according to user-defined parameter, resulting in an interfingering, prograding distribution of FA. The input parameters include general trend for aggradation angle, whether the shoreline is progradational or retrogradational. Quality control was important to ensure that the trend input did not override the well log data input. A few re-runs of the property modeling was necessary in addition to some manual editing at small scale.

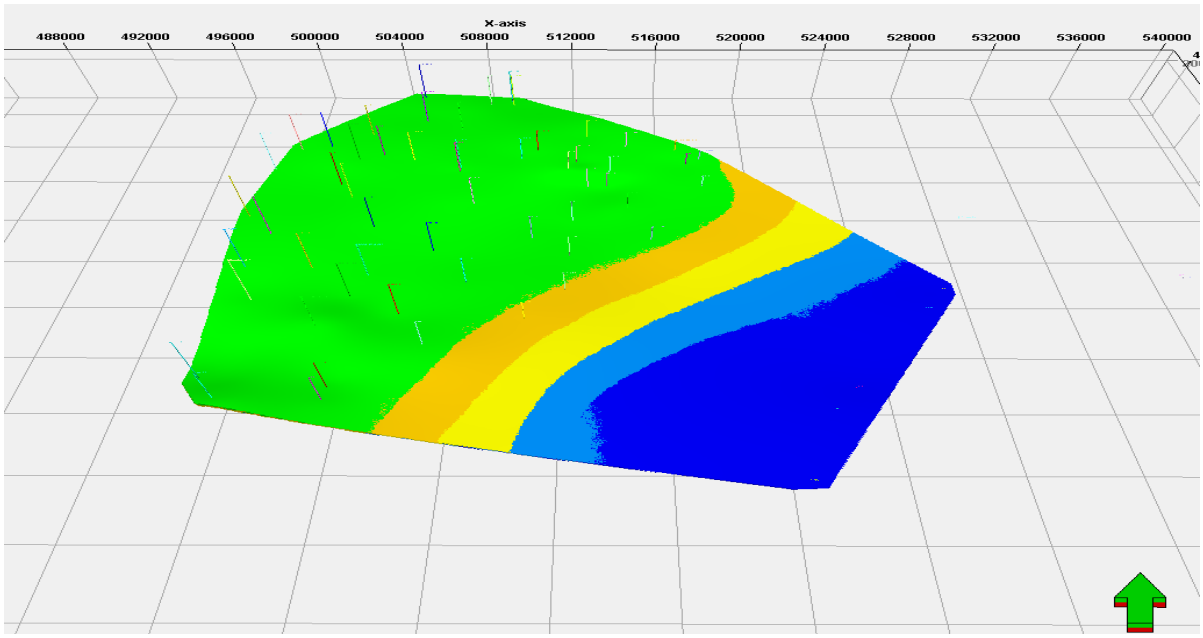

Figure 5.4: Facies belt modelling, here represented by the top of parasequence 2. Facies codes differ from that of the final, merged model as explained in the text.

5.3.2 Coal seam modelling, Indicator Kriging:

Indicator Kriging was used to model facies properties for the coal seams. This is a deterministic approach for kriging discrete properties that prevents over interpreting the upscaled well logs from input. The input data is honoured in terms of position of coal layers close to the wells and the relative percentage of coal within the layered zones. The input data is extrapolated using kriging with manually set variance and distribution. This produced a series of well constrained laterally continuous coal seams that honoured the observations in the wells.

5.3.3 Fluvial Channels, Stochastic Object Modelling:

Stochastic object based modelling was employed for the fluvial channel bodies. This approach places objects with a pre-define shape (e.g. channel) into a background. The proportions of object vs background are defined by the user and the object dimensions and orientation are drawn stochastically from a user defined distribution. The position is random, but can be set to condition to the observation in the wells.

The main input for the modelling was the upscaled well logs which provide data on the relative percentage of FA and the distribution of individual channel sands. The input parameters determining the shape of the channel body was set according to channel data from similar environments including observations made in the outcrops of the Upper Ferron and from the published literature (Reynolds, 1999; Gibling, 2006). The parameters for channel body morphology in Petrel include: orientation, amplitude, width, height and the drift for each of these. Input data allowed for min, max and mean values for each parameter, as shown below.

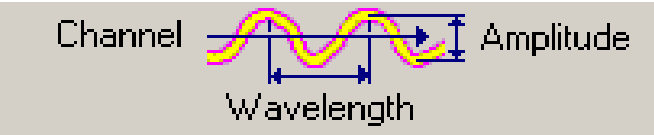

	Drift [0-1]	Min	Med/mean	Max/std
Orientation	0,2	110	120	130
Amplitude	0,2	600	800	1000
Wavelength	0,2	10000	15000	20000

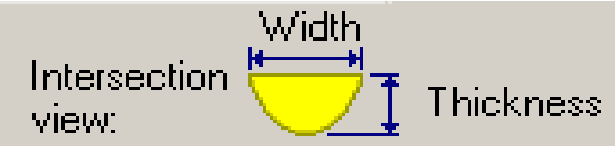

	Drift [0-1]	Min	Med/mean	Max/std
Width	0,2	150	300	450
Thickness	0,2	1	3	15

5.3.4 Merging Facies Properties

Given that different facies modelling tools were used to model different parts of the system it was then necessary to merge the realisations into a final model. This was done using the merge facies tool. Firstly the facies associated with the coastal plain environment were added together, the channels were set to truncate the coal seams were these coincided. The resulting property modelling may be viewed in Figure 5.6.

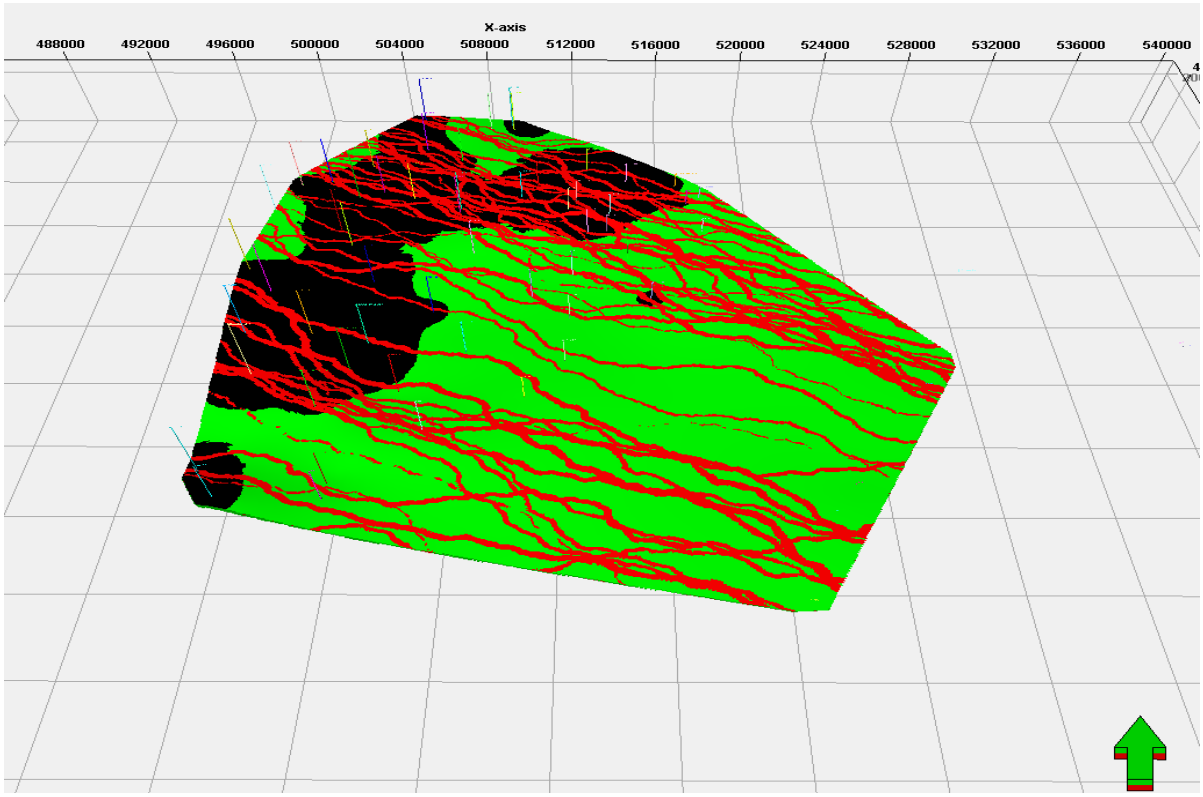

Figure 5.5: Fluvial and coal facies combined with the background undifferentiated coastal plain facies. Top parasequence 2.

These specific coastal plain facies were then merged with the CP, from the Truncated Gaussian simulation. In this case the coal and channels replaced the undifferentiated CP but not any of the other facies. The final result is a model that includes 3 facies (coal, channel and background) in the coastal plain and then a series of parallel belts in the marine setting.

This stepwise approach enabled the modelling of facies with different geometries. Howell et al. (2008) describe a similar workflow for shallow marine reservoirs.

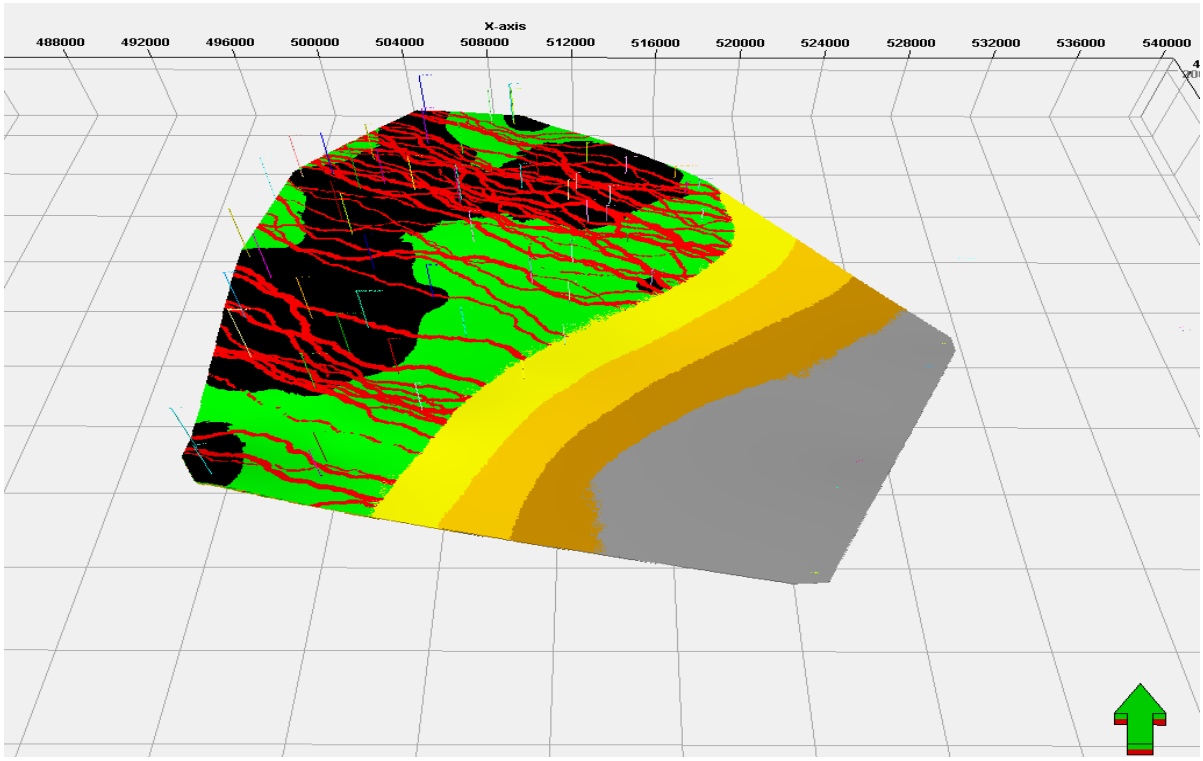

Figure 5.6: Fluvial facies set to replace the coastal plain facies from the initial facies belt modelling step. Top parasequence 2.

5.3.5 Faults in the model interval

The dense grid of well data is excellent for generating the surfaces, however it is difficult to identify and predict the position of faults, unless the wells are cut or if the faults significantly displace the layers. Seismic data enable the more accurate mapping of faults but were not available to this study. Seismic data is described in the literature on the Drunkards Wash CBM-field. However, only one article exemplifies such a dataset. The poor quality of this seismic image does not allow for reliable interpretation at reservoir scale (Figure 5.7).

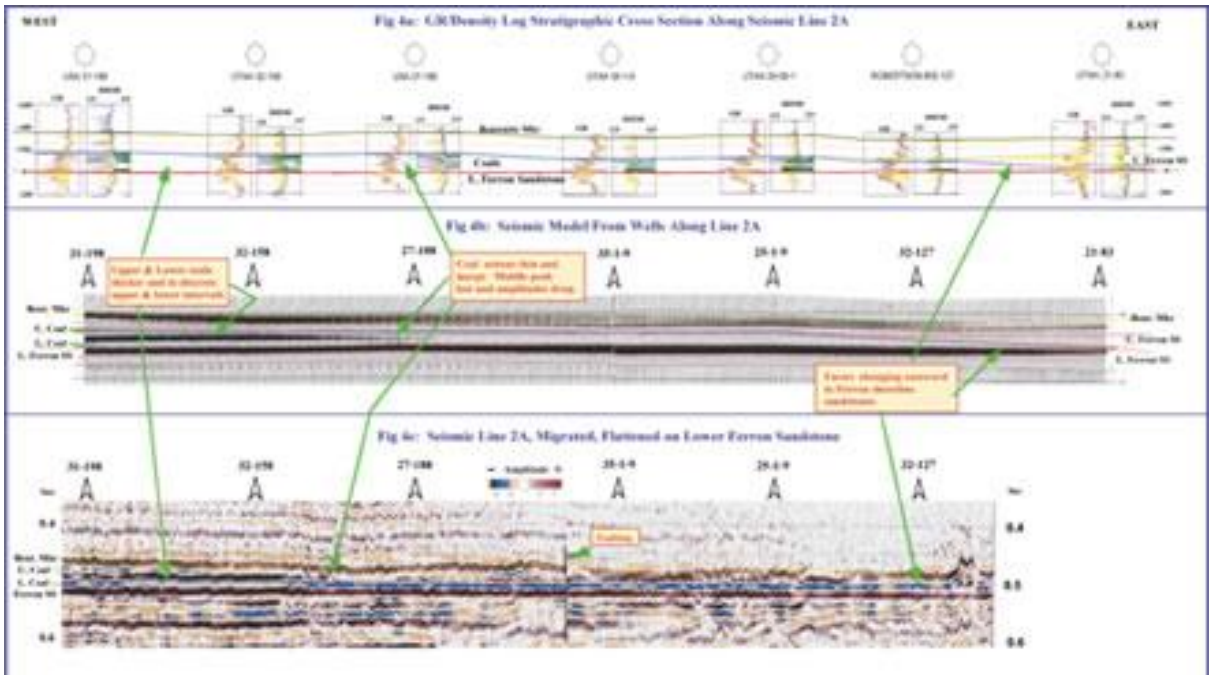

Figure 5.7: Seismic line, as described by Lyons (2001). URL: http://www.aapg.org/explorer/geophysical_corner/2001/12gpc.cfm

Given the goal of this study was to investigate the stratigraphy architecture a decision was made to ignore the structures, although a couple of small (c. 10m) faults were observed at outcrop. Figure 2.5 provides an overview of earlier work on the Drunkards Wash tectonic features. A brief review of inferred fault surface locations within the model is given in the following results chapter.

Other short comings include the lack of discrete crevasse splay deposits in the model because of the grid resolution and the potential for extending the model further into adjacent CBM fields, neither of these would significantly alter the conclusions that are presented in the following chapter.

6 Results from model building

Representing a 3D model on a 2D page is challenging. This chapter includes a series of screen shots which include 3D views, maps of surfaces and cross sections which are used to support the observations described and the discussion in the subsequent chapter. The model is included on a DVD in appendix II. Given that it is difficult to include a scale on a view of a 3D volume it should be noted that the area covered by the DEM is 61 x 67,5 km. The geocellular model covers an area of 28 x 31 km and the Lower Ferron interval is 90 m thick on average. The maximum depth of burial, seen where the model diverges the most from the DEM is 1843,31 m.

6.1 Summary

The model (Figure 6.1) shows a westward dipping package of strata which dives into the subsurface at a tectonic dip of 1-3 degrees and then flattens underneath the Wasatch Plateau away from the SRS. Minor bulges in the model are most probably related to small scale reverse faults documented by Burns and Lamarre (1997, Figure 2.5). No apparent repeated sections have been observed in the well data, but more data from more closely spaced wells would offer a good restraint on the fault distribution throughout the CBM-field. The faulted appearance becomes clearer when the vertical exaggeration is increased which is to be discussed in a following sub-chapter.

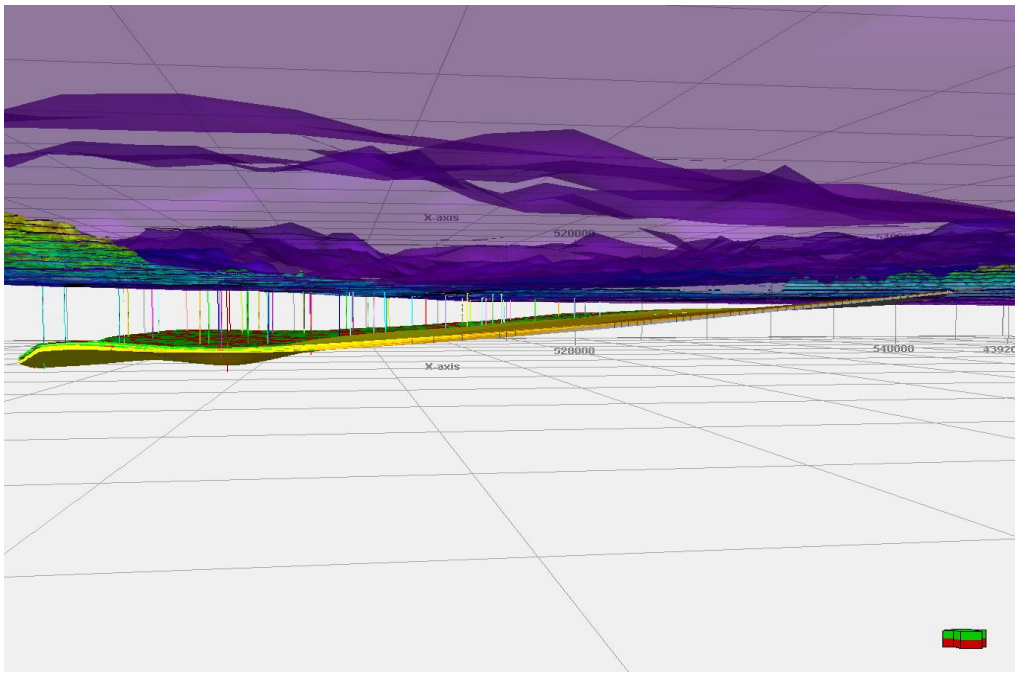

Figure 6.1: The model and its spatial relationship to the topography in Castle Valley. Westward dip away from the San Rafael Swell, view looking north-northeast. Vertical exaggeration is X3.

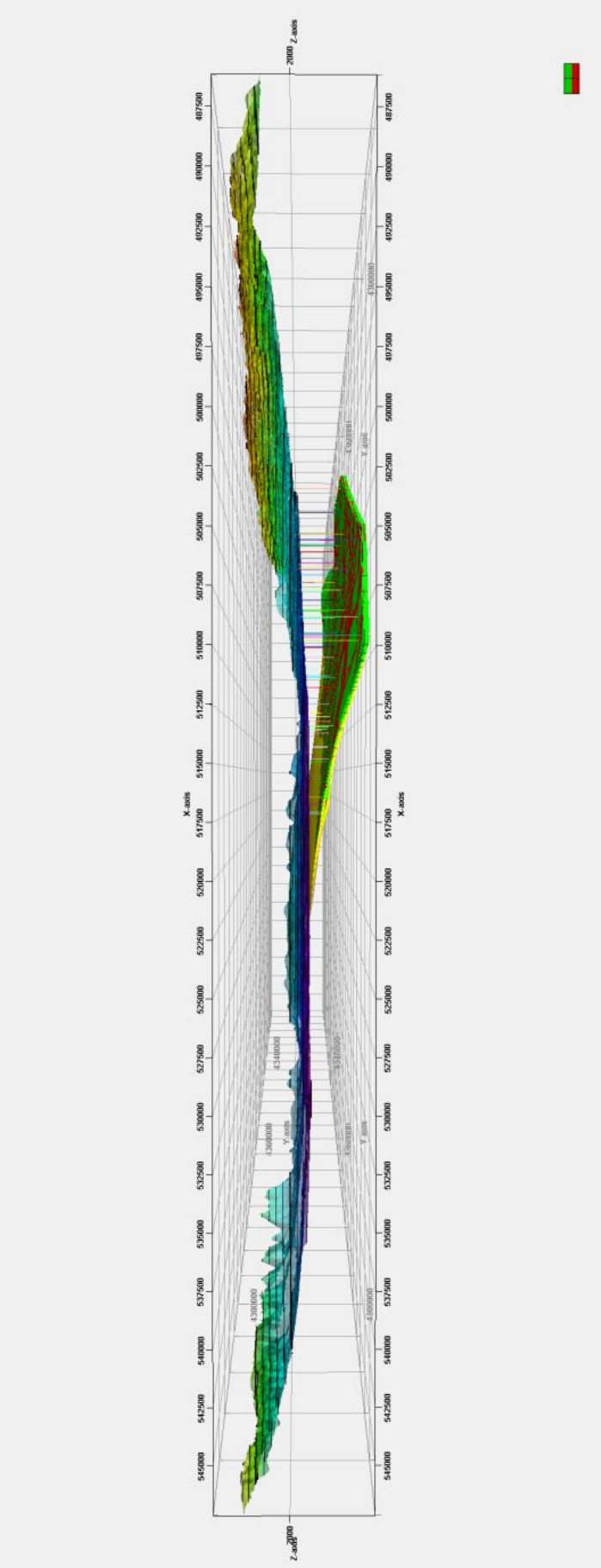

Figure 6.2: View looking south, entire model. Vertical exaggeration X3.

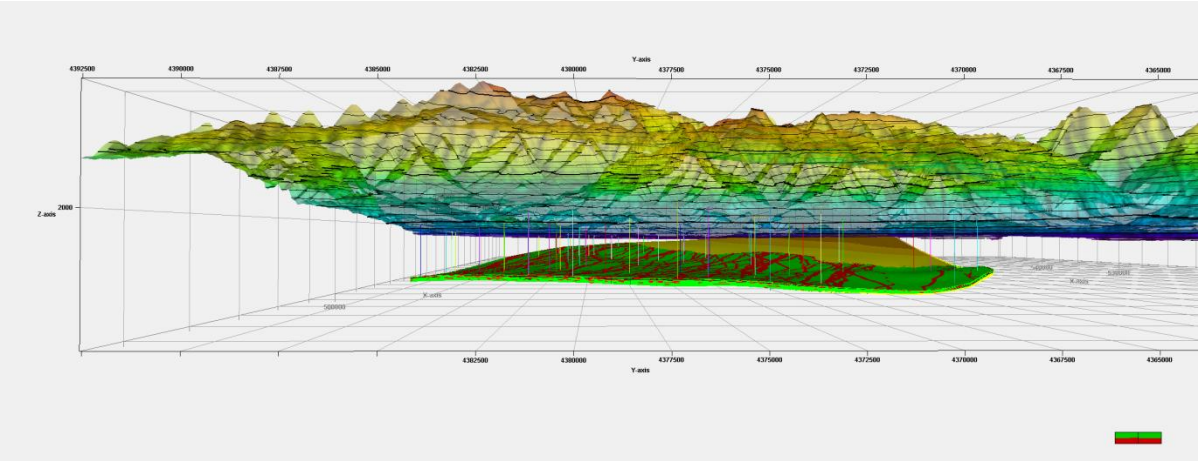

Figure 6.3: Entire model, viewed from the Wasatch Plateau looking south. Ferron Sandstone Member deposits continue underneath the Wasatch and are thought to be the source rock for conventional HC-production from sandstone reservoirs produced from the Clear Creek field on the Plateau. Vertical exaggeration X3.

The thickest part of the model occurs where the shoreface intervals of the 4 parasequences are stacked. The model thins slightly landward, due to coal compaction and significantly basinward due to facies thinning. The model ranges in thickness from about 5-30 m in the outcrop section at the most distal reaches to 90 m. Localised thickening to around 140 m is attributed to post-depositional tectonic events.

6.2 Geological features:

Individual parasequences are up to 60 m thick and the facies belts within them are up to 4 km wide (Figure 6.4) The shorelines follows a relatively straight, north-northeast to south-southwest trend, in accordance with the conceptual model. Lateral variations along the strike of the shoreline are highlighted in the areas where the model is conditioned to a lot of well data: Away from the wells the boundaries are extrapolated and should be treated with more caution.

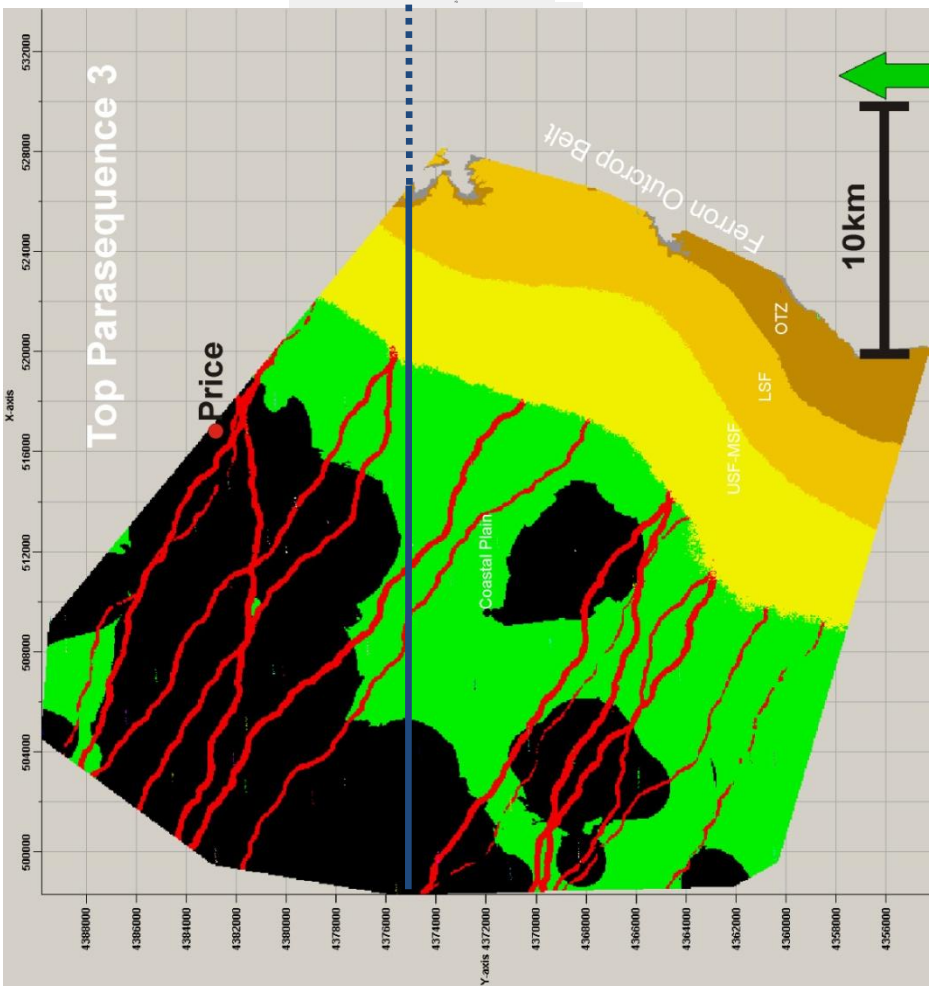

Figure 6.4: Plan view of the top of parasequence 3.

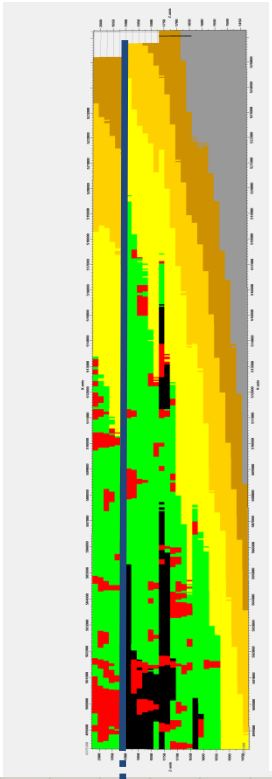

Figure 6.5: Simbox view of the parasequence stacking pattern in cross section as indicated by blue line. Simbox view is to be explained in the following sub-chapter.

6.2.1 Facies stacking patterns and stratal architecture

Various cross sections (in the I- and J- direction – SN and EW respectively) through the model show the facies stacking patterns and stratal architecture. Given that the thickness to length ratio of the model is relatively low, the geometries are difficult to display in a complete cross-section. Some of the cross sections are displayed with a simbox-grid. The simbox option is a way to simplify the 3D-model so that it is uniformly flattened, faults (if any are present) are neglected and the depth of the model is averaged. The result is a rectangular cube that does not correspond with the well log depth (Figure 6.8), but offer a unique way to view and evaluate the cross sections. For the current model this results in the removal of the post-sedimentary deformation and tilt of the Lower Ferron, which enables a view into how the sedimentary package would have looked like at the time of deposition. It is important to bear in mind that these views of the model are flattened.

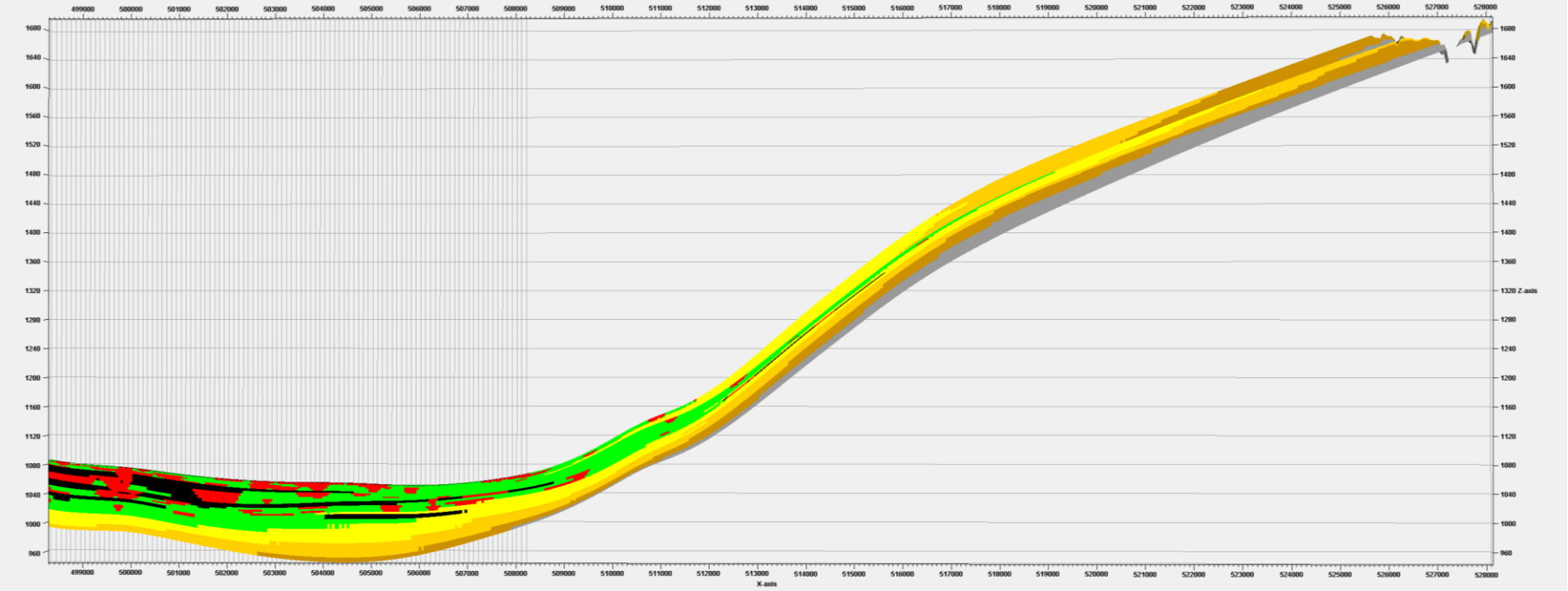

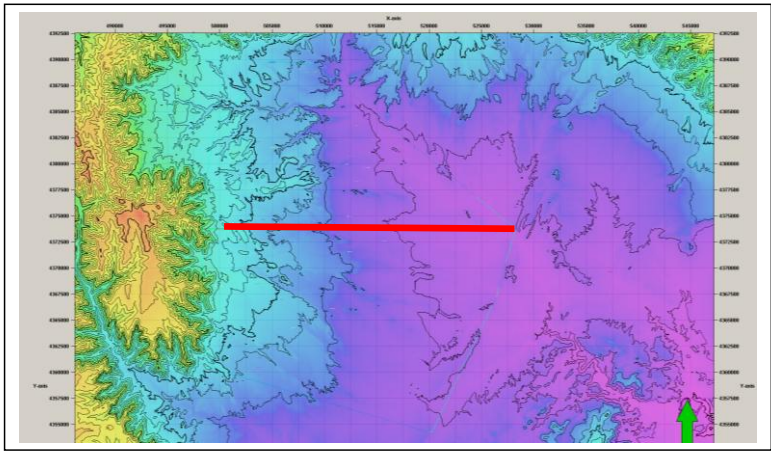

Figure 6.6: E-W -section with overview map. The cross section shows the southward pinchout of the Lower Ferron and the uplift caused by the San Rafael Swell to the southeast..Vertical exaggeration is X15.

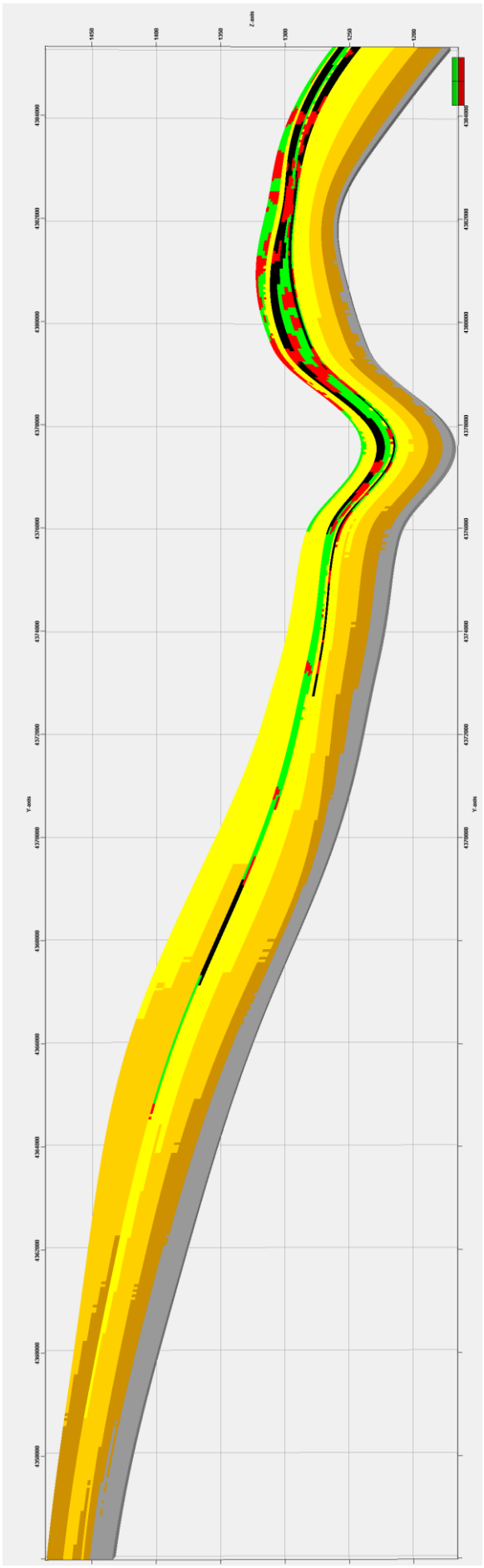

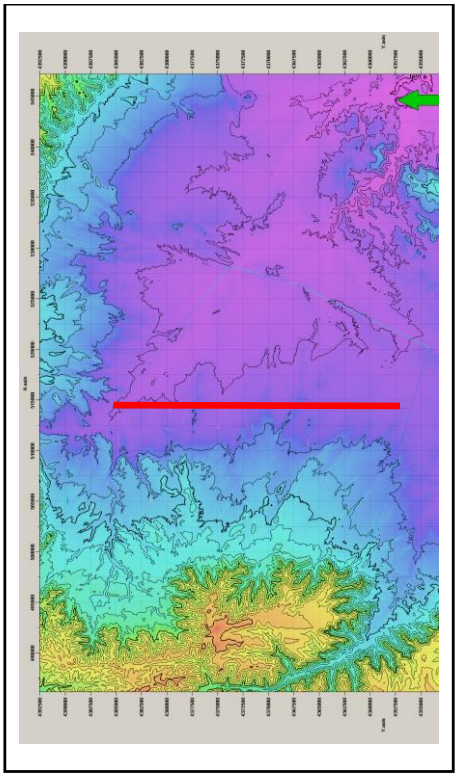

Figure 6.7: S-N-section and overview map. Lower Ferron dips to the north, away from the San Rafael Swell and flattens underneath the Book Cliffs. Suspected reverse faulting to the north. Vertical exaggeration is X25.

The following figures present the model in a simbox grid. In the three immediately following figures, I-Section view, an option to scroll through the cross-sections of the model is briefly portrayed.

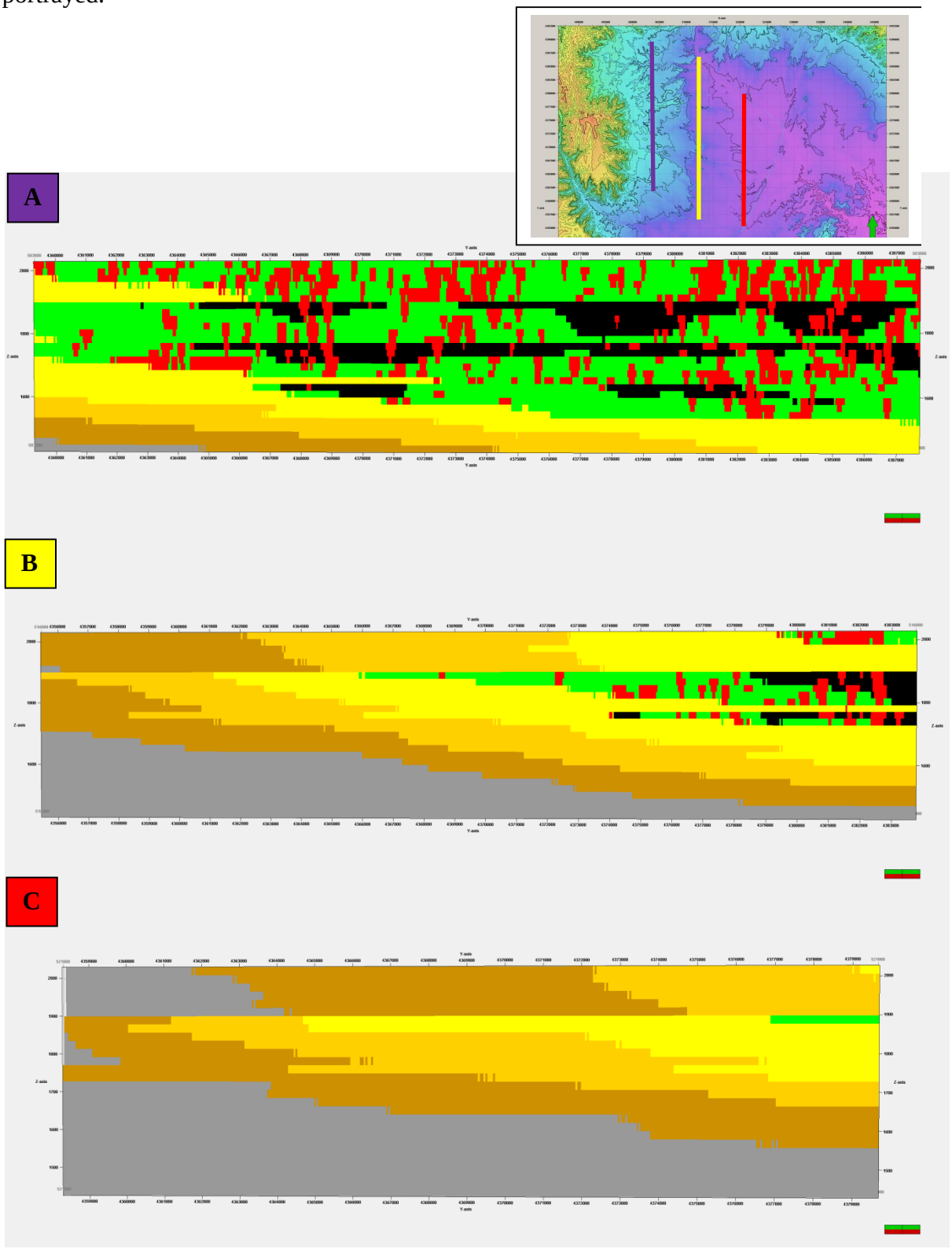

Figure 6.8: I-section Simbox view from east (A) to west (C).

The various cross sections and maps highlight that the stacking patterns the progradational stacking patterns observed in PS1-PS3 are captured in the model. The models also show the back-stepping to aggradtionally stacked PS4 at the top of the Lower Ferron. Note that PS4 contains a high proportion of channel bodies. This model differs from that proposed by Henry and Finn (2003), who suggested that sandstone in PS4 was all comprised of a transgressive shoreface deposit.

The model also highlights the distribution of coal within the model. The major coal intervals are associated with PS2 and PS3. Coal layers are almost completely absent in the upper part of the model, where the channel sands dominate. This suggests that the rate of accommodation may have been too great for coal formation (Diessel et al., 2000).

6.2.2 Fault surfaces

As already mentioned, thrust faults are reported in the Drunkards Wash CBM-field (Tripp, 1989; Burns and Lamarrre, 1997; Montgomery et al., 2001). While these were not modelled discreetly, their location can be inferred from rapid changes in bed dip and local thickness changes within the model (Figure 6.9). A number of fault surfaces were created (Figure 6.10, Figure 6.11 and Figure 6.12) although not included in the final models.

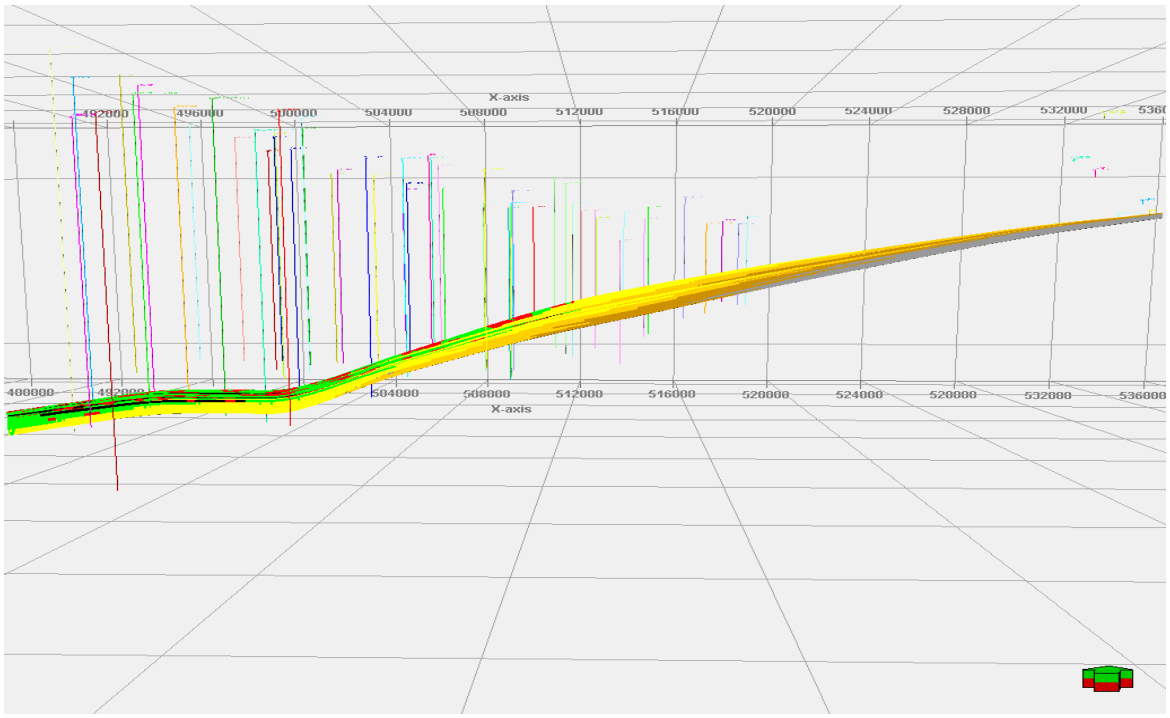

Figure 6.9: J-section, west-east, showing the prograding stacking patten of the Lower Ferron. Dip is to the west, away from the San Rafael Anticline. Vertical exaggeration is X10. Individual parasequences dip basinward. The profile at this exaggeration suggests the relative location of a fault, evident from the kink in the profile.

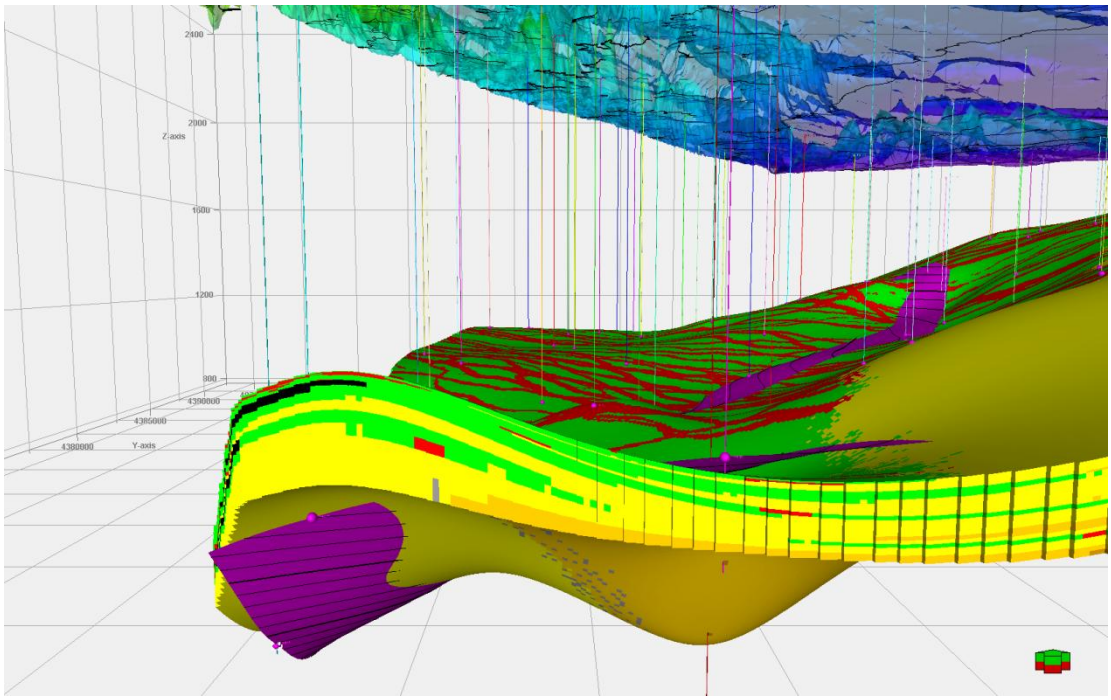

Figure 6.10: Extrapolated fault surfaces in relation to an unfaulted 3d grid. Fault surfaces are picked from neighbouring wells. Reverse faulting. Vertical exaggeration X10.

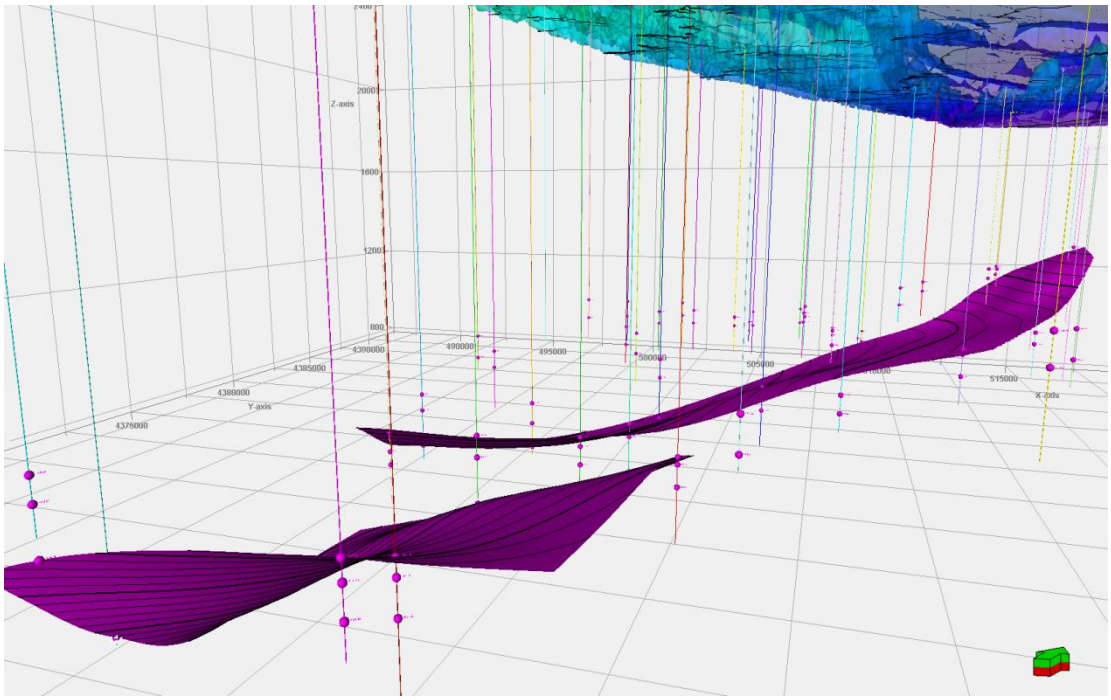

Figure 6.11: Fault surfaces without 3d-model, shows relation to well input. Vertical exaggeration x10.

The fault surfaces derived from this model are low angle thrust faults. The offset could not be quantified, but previous work has recorded offset of about 45 meters (Burns and Lamarre, 1997).

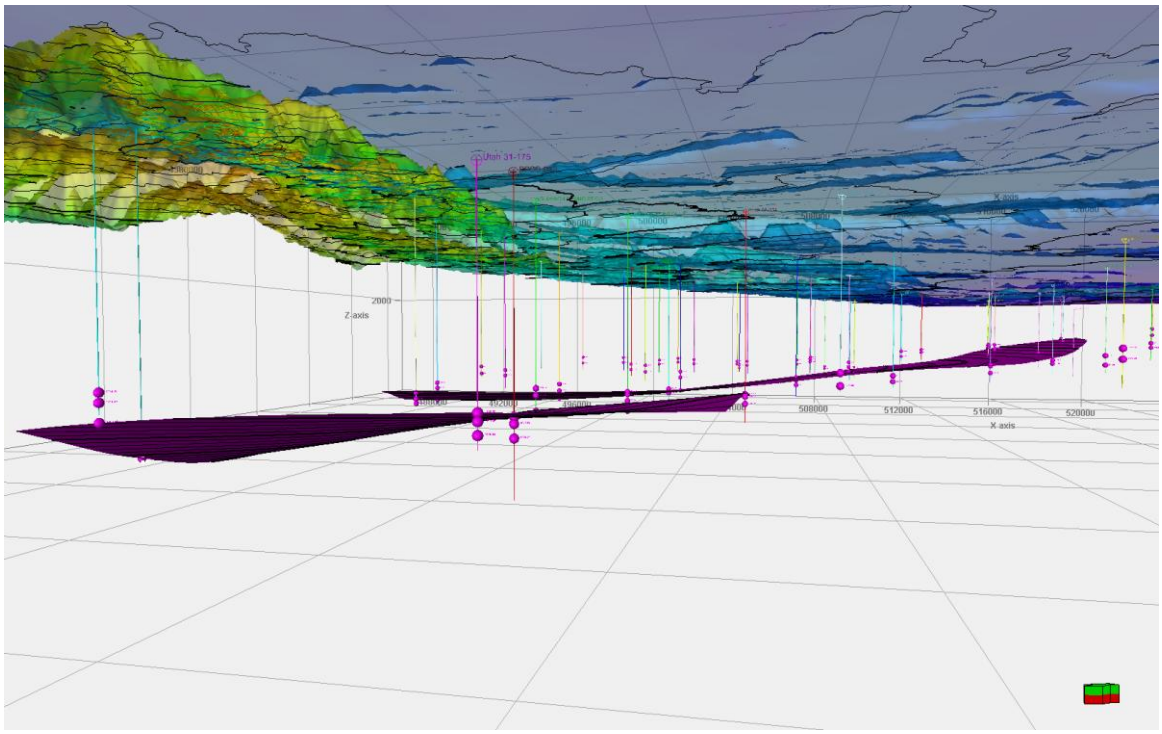

Figure 6.12: Gently dipping fault surfaces as above, vertical exaggeration x3.

6.3 Correlation of the subsurface and the outcrop

The model includes data that have been taken from both the subsurface and the adjacent outcrops. Using the model it is possible to visualize and QC the proposed relationships (Figure 6.13). There model illustrates that there is good conformity between the geocellular model, the field observations, and our conceptual understanding of shoreface architecture.

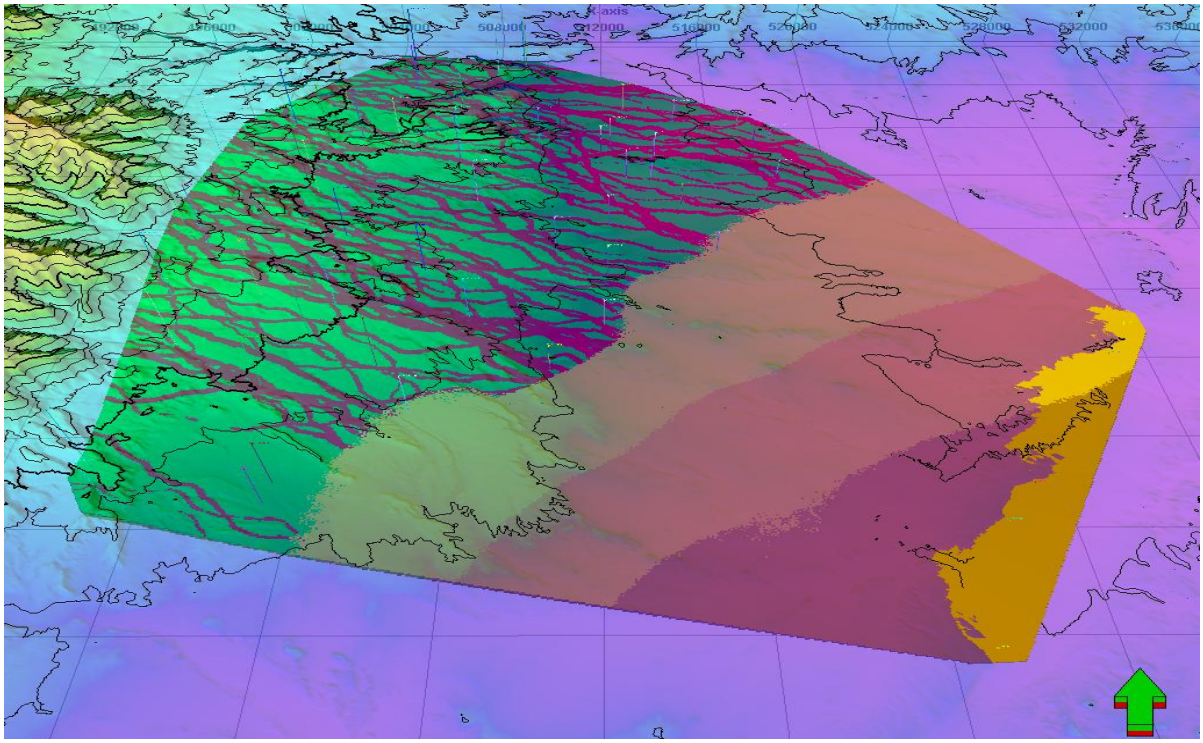

Figure 6.13: Oblique aerial view of the Lower Ferron Drunkards Wash deposits exposed underneath a transparent topography. The bright colours along the eastern margin of the model show where the Ferron model intersect the surface, and predictive position of outcrops.

6.3.1 Implications of the model for understanding the Sequence Stratigraphy

Visualising the strata in 3D has implications for understanding the spatial relationships of the different stratigraphic elements. The present model suggests that the subsurface Drunkards Wash CBM-field is readily correlated to the outcrops in the northern part of Castle Valley.

As discussed previously the lowermost parasequences pinches out within the CBM field and does not extend to the surface. The three uppermost parasequences all extend to the Lower Ferron (Clawson and Washboard) outcrops which is a new correlation, not previously proposed by former workers (e.g. Cotter 1975; Ryer 1986; Henry and Finn, 2003)

To highlight this correlation some of the correlation panels presented previously were extrapolated schematically to the logged outcrops to illustrate their relation.

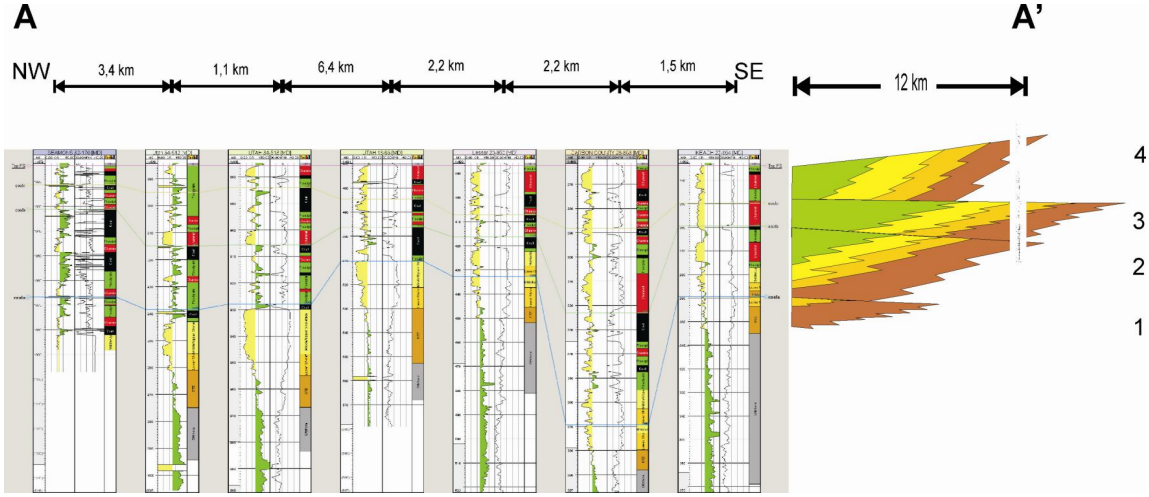

Figure 6.14: Northern correlation panel, extrapolated to WP 65.

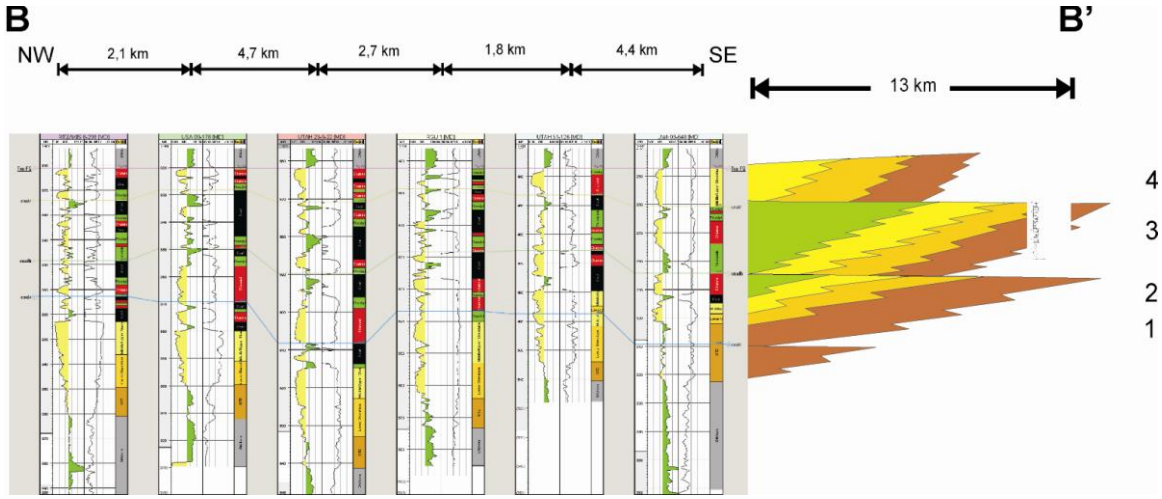

Figure 6.15: Second correlation panel from north, extrapolated to WP 33.

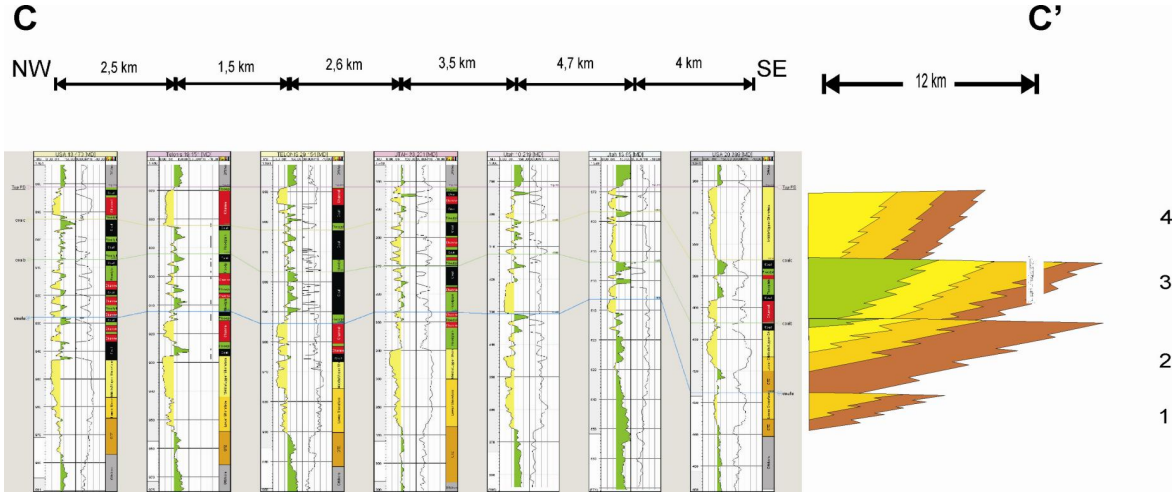

Figure 6.16: Third correlation panel from north, extrapolated to WP 60.

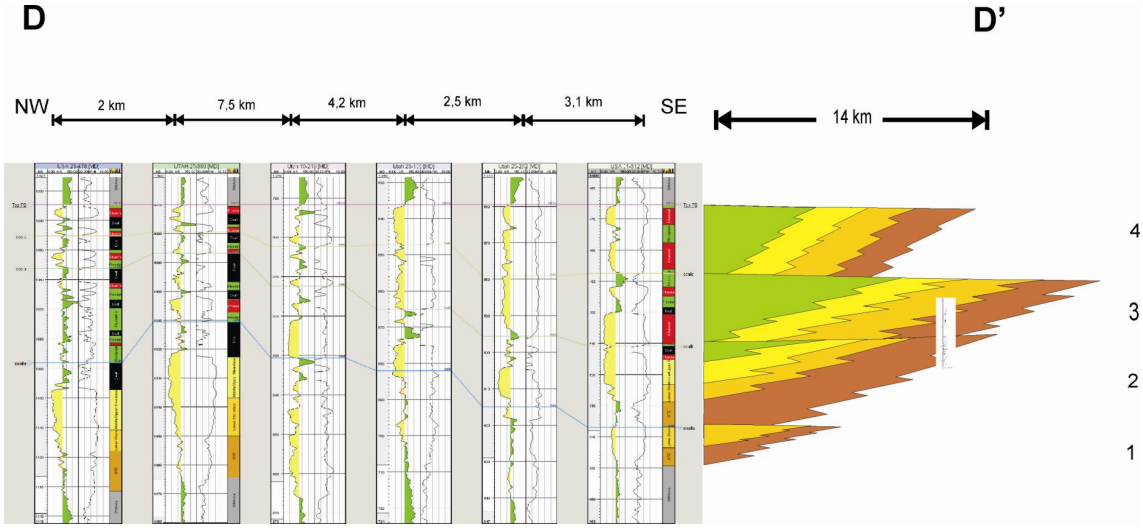

Figure 6.17: Fourth correlation panel from north, extrapolated to WP 7.

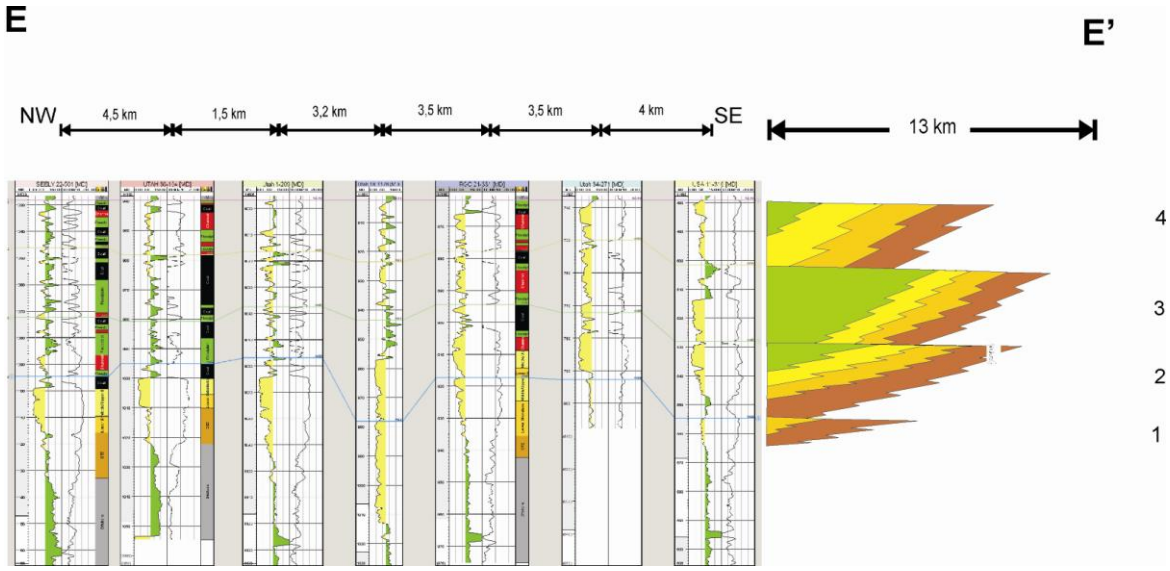

Figure 6.18: Fifth correlation panel from north, extrapolated to WP 58.

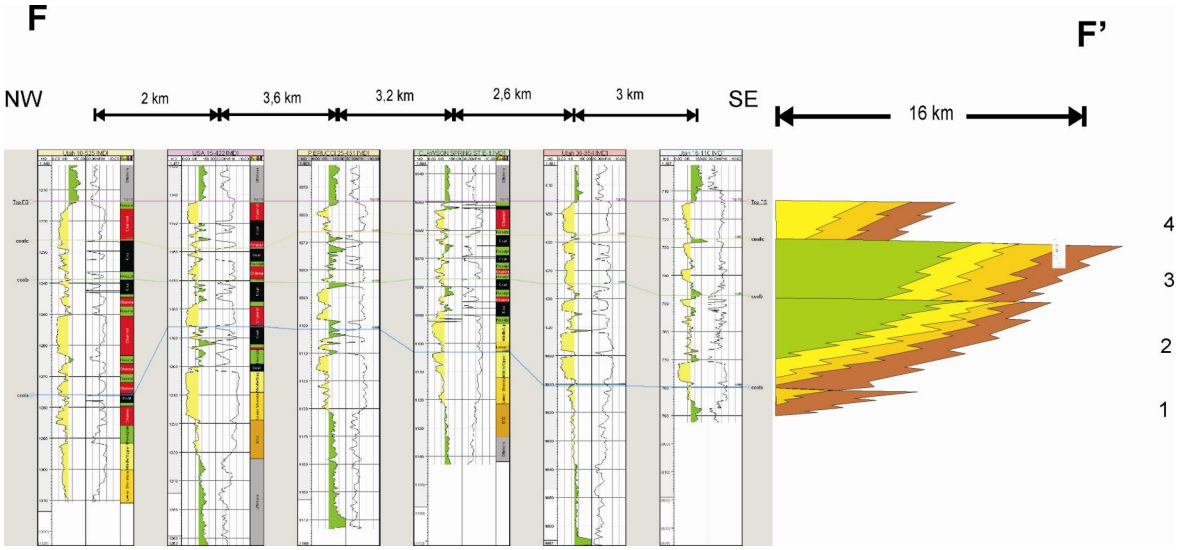

Figure 6.19: Sixth correlation panel from north, extrapolated to WP 56.

The model and correlation differ from that proposed by Henry and Finn (2002) who did not correlate the subsurface with the outcrops and did not recognize the upper most, back stepping parasequence. Parasequence 4 highlights some unusual geometries which are evident from the model isochore maps (on the following page) and cross sections from the model. Firstly the PS appears to show a change in shoreline orientation. The southern panel (Figure 6.20) shows a more aggradational stacking pattern, suggesting that the shoreline may have shifted closer to N-S. The implications of this are discussed in the next chapter.

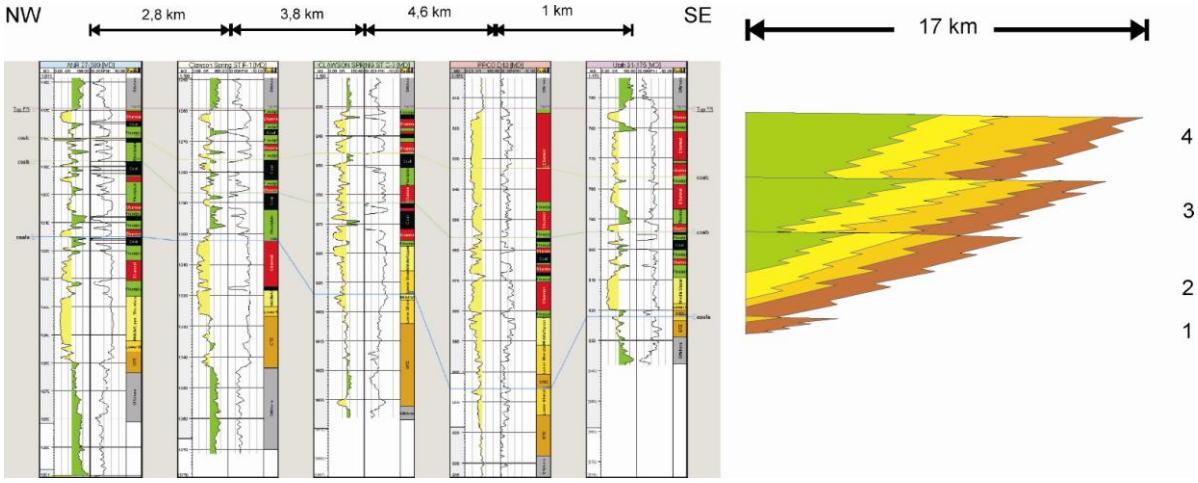

Figure 6.20: Southernmost correlation panel (G-G') and its schematic extrapolation to an arbitrary point. The 17 km are measured to the southernmost outcrop (WP94), its implications are discussed further in the following chapter.

There is also a marked thickening of PS 4 towards the centre of the model (Figure 6.21), which is expressed as a thickening of the individual facies tracts. It is common for transgressive systems tracts parasequences to illustrate a more steeply climbing shoreline trajectory which results in thicker facies tracts that do not prograde as far basinward. The along strike thickness changes occurs over too short a distance to be associated with changes in flexural subsidence (c. 10km).

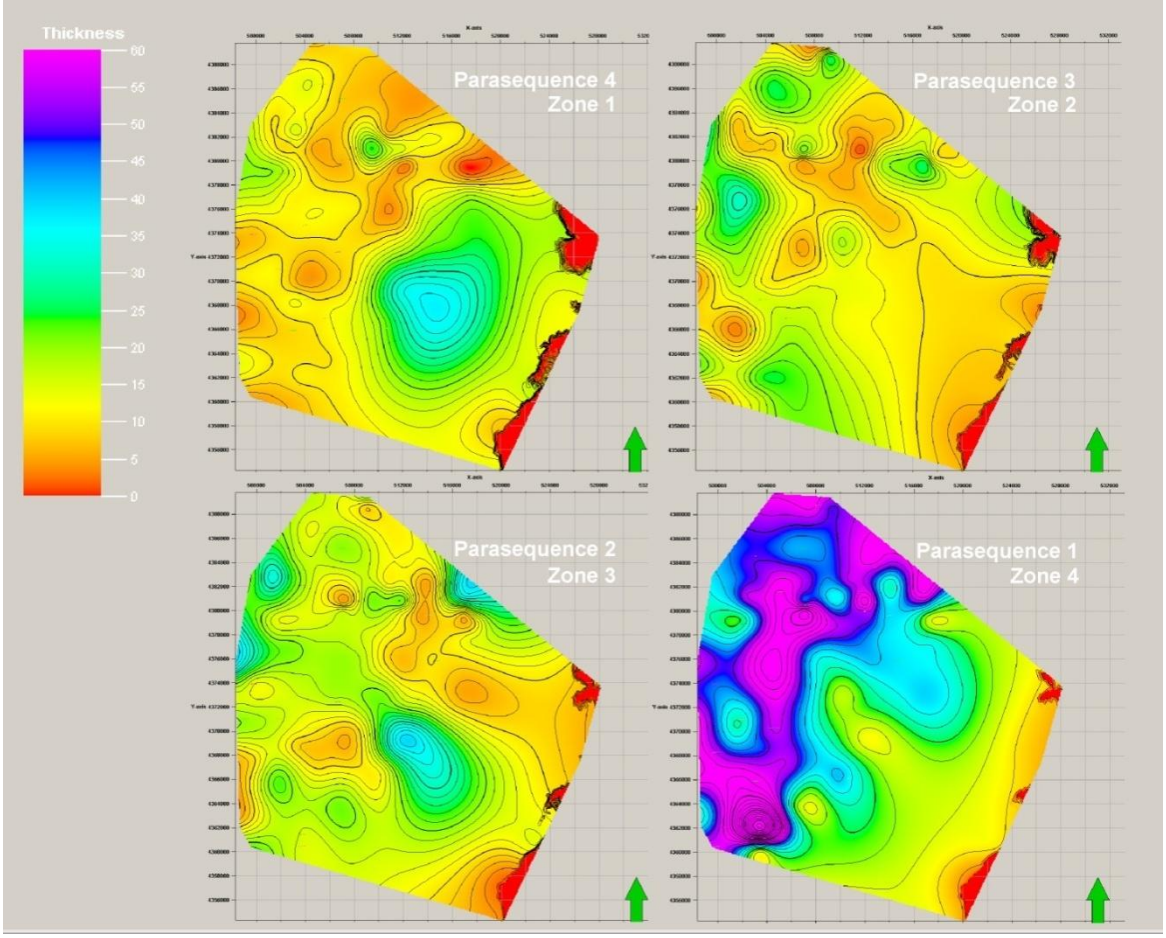

Figure 6.21: Isochore representation of the parasequences described above. Light contours every 2 meters, heavy contours every 10 meters. Colour scheme illustrates the range and magnitude of thickness differences.

6.3.2 Stratal archictecture, palaeogeography and sequence stratigraphy

A series of plan view screen grabs from the different zones within the model illustrate the mapped palaeogeography (Figure 6.22 and Figure 6.23).These maps show progradation of a series of broadly parallel facies belts towards the SE. This is in accordance with the regional palaoegeographic model and a north-westerly source from the Vernal delta complex as discussed in Chapter 2.

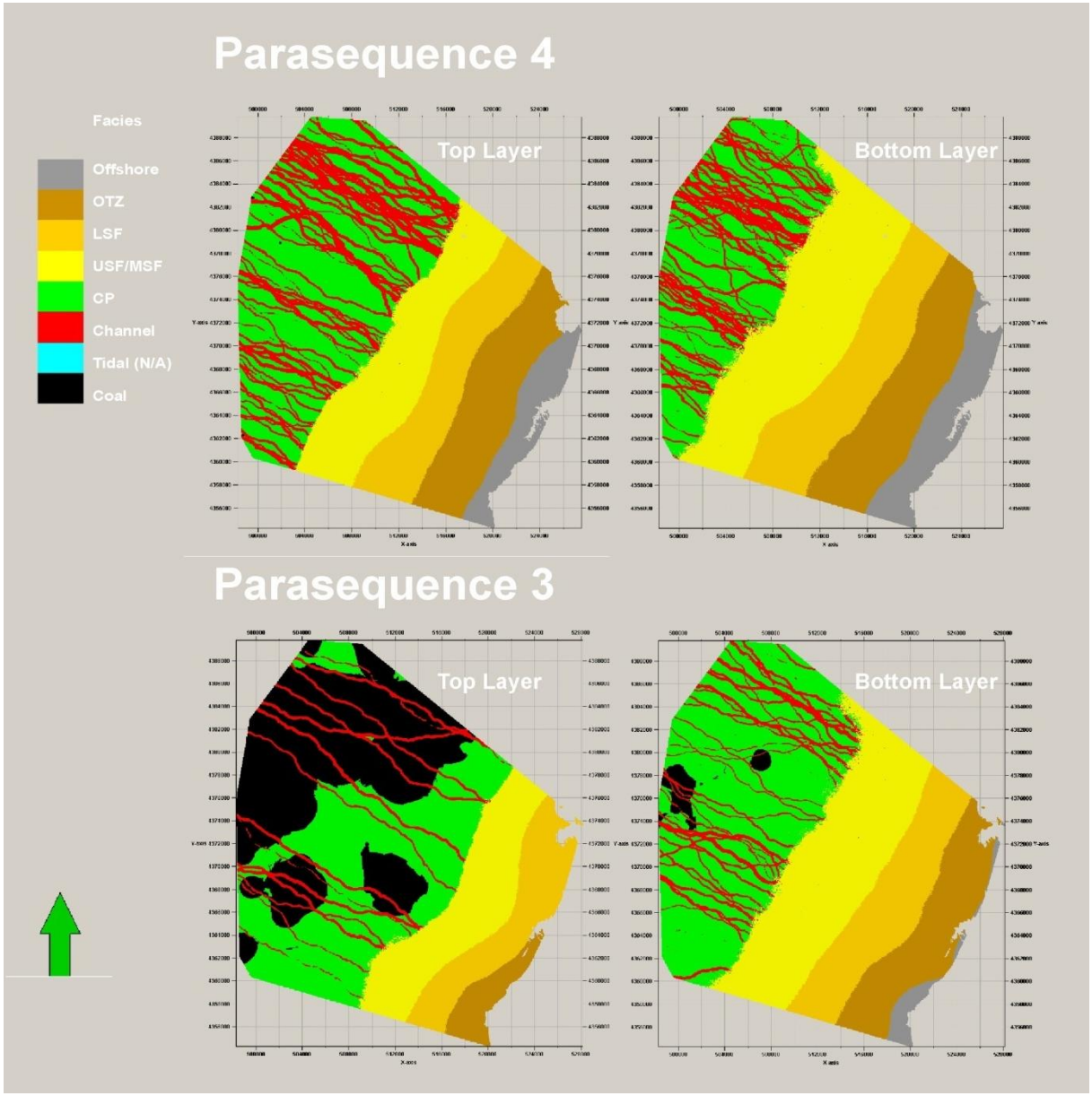

Figure 6.22: Progradational stacking of parasequences 3 and 4 (uppermost) in plan view. Layers in Petrel corresponds roughly to clinoforms. Tidal flat/Lagoonal facies have not been clearly defined, and remains as an artifact from the model building.

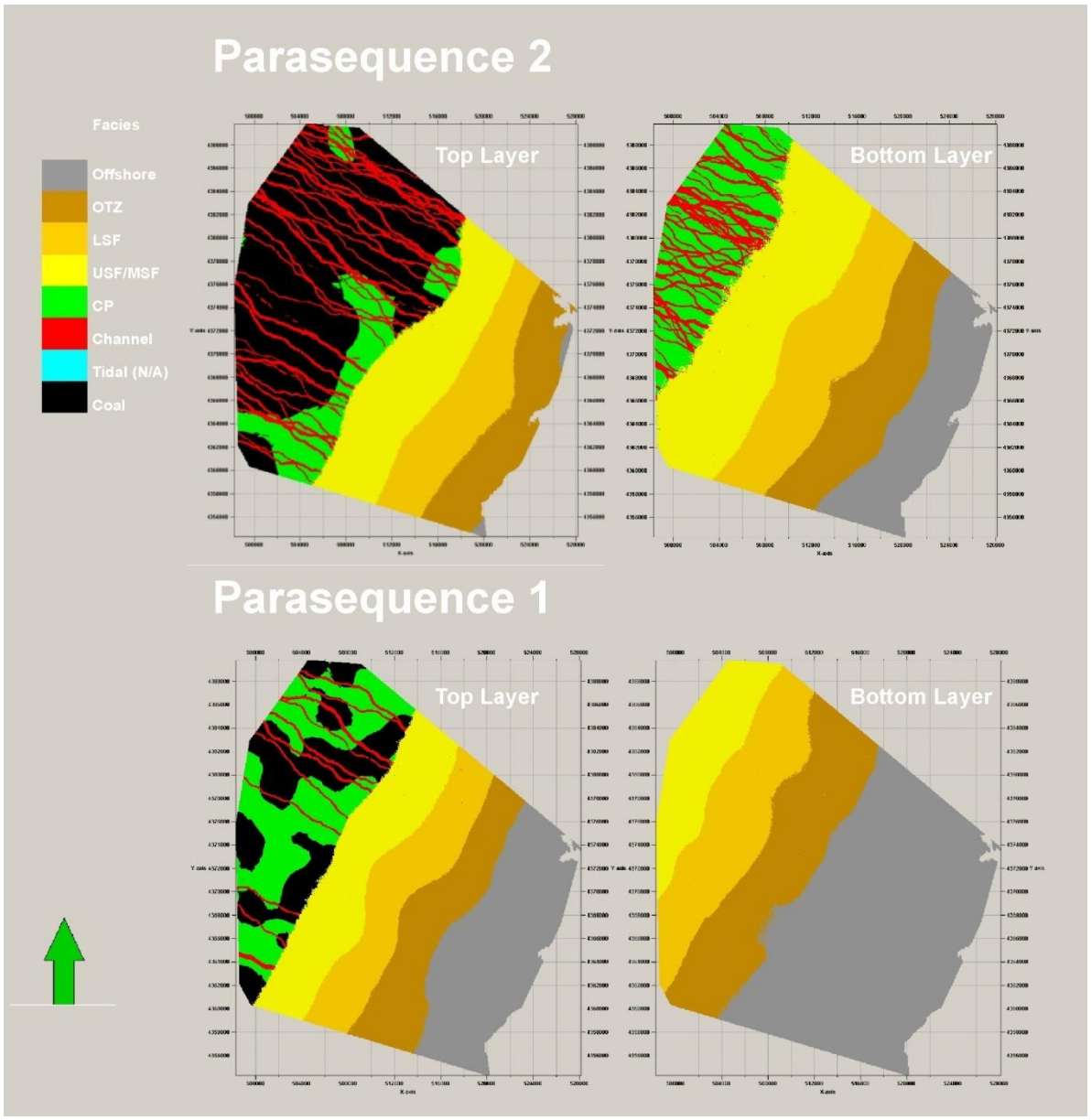

Figure 6.23: Progradational stacking of parasequences 1 and 2 (lowermost) in plan view. Layers in Petrel corresponds roughly to clinoforms. Tidal flat/Lagoonal facies have not been clearly defined, and remains as an artifact from the model building.

The map views of the model facies, conditioned to the well data and outcrop show a detailed palaeogeographic evolution. While the overall trend is consistent with the models of Ryer and Lovekin (1986) there is a level of detail that would be extremely difficult to capture using conventional maps and sections. This detail includes suitable changes in the width of facies belts and the presence of a series of minor embayments and kinks along the shoreline that are comparable to the variability seen along modern coastlines.

The model also has implications for the larger scale correlation between the Lower Ferron in the subsurface, the Clawson and Wash Units and the Upper Ferron to the south. This is discussed further in the following chapter.

7 Discussion

The 3D geocellular model constructed for this study illustrates the application of modelling to improve understanding of sequence stratigraphy. The 3D model provides more insight into facies stacking patterns than, more widely applied, 2D representation such as correlation panels and maps.

The model shows a progradational to aggradational to backstepping, *ascending shoreline* (Helland-Hansen and Martinsen, 1996) divided into four distinct parasequences. The lowermost parasequence pinches out in the subsurface, while the three uppermost, prograding to backstepping shorelines are visible at outcrop-level, where they manifest themselves as the Clawson and Washboard units defined by Cotter (1975). The model illustrates how these parasequences and the facies within them are distributed.

Based on the model, this study has shown that the subsurface interval in the Drunkards Wash CBM-field has its down-dip marine equivalent exposed along the western escarpment of San Rafael Swell in Castle Valley. The relationship of these deposits to the distal deposits that occur beneath the Upper Ferron outcrops to the south will be discussed in more detail below. Katich (1953) suggested that they were time equivalent and the lower Ferron shoreline was embayed, this was later disproved by Ryer and McPhillips (1983). Although not directly stated, such a model would suggest that further coal deposits lie beneath the Wasatch Plateau in the south east. Other authors such as Thompson et al. (1986) have suggested that the outcropping Clawson and Washboard units represent the south extent of long shore transported plumes derived from the north. The correlation of the outcrop and the subsurface undertaken in the present study and the relationship between the upper and lower Ferron are discussed in the following section.

7.1 Sequence stratigraphic relationship

During the course of the current study two possible sequence stratigraphic models have been considered. Both of these consider the Lower Ferron as a depositional system with a non-marine portion in the subsurface CBM field and more distal deposits in the outcrop. The key issue to be discussed here is the detail of the correlation between the outcrop and the subsurface and the correlation of the outcropping units from north to south.

One of the proposed sequence stratigraphic models has already been described in the outcrop chapter (Figure 4.22). That model suggested that the upper and lower Ferron are two distinct and unrelated depositional systems. An alternative model (Figure 7.4) suggests a greater degree of linkage between the upper most parasequence in the Lower Ferron which is retrogradationally stacked and the overlying initiation of the Last Chance Delta in the south.

7.1.1 Alternative Outcrop Correlation

The uppermost parasequence modelled in the subsurface Drunkards Wash Field (PS4) is correlated to the outcrop where it has been extended south to the escarpment near the town of Clawson (Washboard Unit of Cotter, 1975, and Kf-Washboard of Ryer, 1994). This locally back-stepping parasequence to the north (PS4) is interpreted to be accompanied to the south by a regressive part of the same parasequence.

From the town Castle Dale and southward this upper parasequence becomes the most prominent feature of the Lower Ferron and is reported as far south as Mesa Butte south of I-70 by Anderson and Ryer (2004). The more proximal expression of the shoreline east of Castle Dale and Clawson and southward is the basis for interpreting PS4 as locally transgressive in the north (seen in the well logs of Drunkards Wash), with a regressive contemporaneous component to the south.

In the correlation panel in chapter four, PS3 was correlated to that escarpment, in accordance with the published literature. Such a correlation implies a more sinuous shoreline, a more rapid transgression and a close to complete reversal of depositional direction of the Lower Ferron. If the escarpment is related to PS 4 then a series of thin basal sandstones at localities F and G in Cotter (1975, Figure 4.8) would link to PS3, suggesting that PS3 pinches out towards the south. This is more consistent with the depositional trends and facies belts width suggested by the model, especially the occurrence of the proximal tidal channel deposits of the Farnham Unit of Cotter (1975) to the north of the SRS.

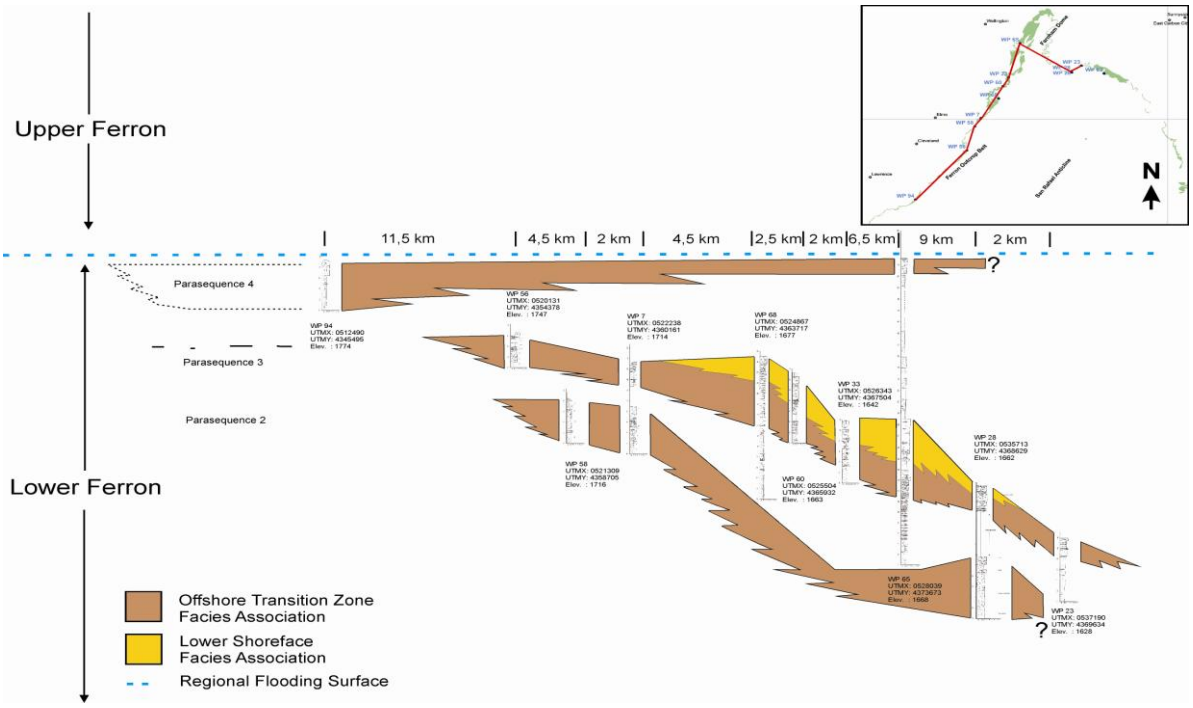

Figure 7.1: The proposed stratigraphic relationship for the Lower Ferron sandstone in outcrop.

This new model suggests a southward shift of the depositional system between PS3 and PS4 and a greater degree of linkage between the deposits of the Lower and Upper Ferron with a gradual southward migration of the main depositional system, rather than two discreet systems with highly sinuous shorelines and long distance, geostrophic currents on a shelf.

7.1.2 Lower Ferron terminology and lithostratigraphy

The previous work carried out by Cotter (1975) identified the lithological units of the Lower Ferron outcrops and placed them in a stratigraphic relationship. The current study suggests that the existing lithostratigraphy is ambiguous and inconsistent. The current lithostratigraphy includes 2 (sometimes 3) units in which the Washboard overlies the Clawson. The Washboard locally includes a third unit "the Farnham".

The Washboard unit alters between proximal to distal deposits over short distances although there is an overall proximal to distal trend towards the south for both the Clawson and Washboard. This trend is then reversed in the Washboard south of the town of Clawson where

the Washboard unit become more proximal and extends southward as far as I-70. The lower Clawson unit pinches out in the Tununk shale near the town of Emery.

The correlation panel in this chapter suggests that in the north the Clawson is equivalent to PS2 and the overlying Washboard is equivalent to PS3. The Farnham unit which includes the tidal channel complex within the Washboard is a possible expression of the sequence boundary at the stratigraphic turn-around between progradation and retrogradation (c.f. Edwards et al., 2005).

To the south, the main escarpment east of Castle Dale and the town of Clawson is the distal expression of PS4 rather than PS3. In that case the lithostratigraphic Clawson unit is now assigned to PS3 and the Washboard is PS4. PS2 does not extend this far south. This revised correlation has implications for understanding the stratigraphic evolution of the area.

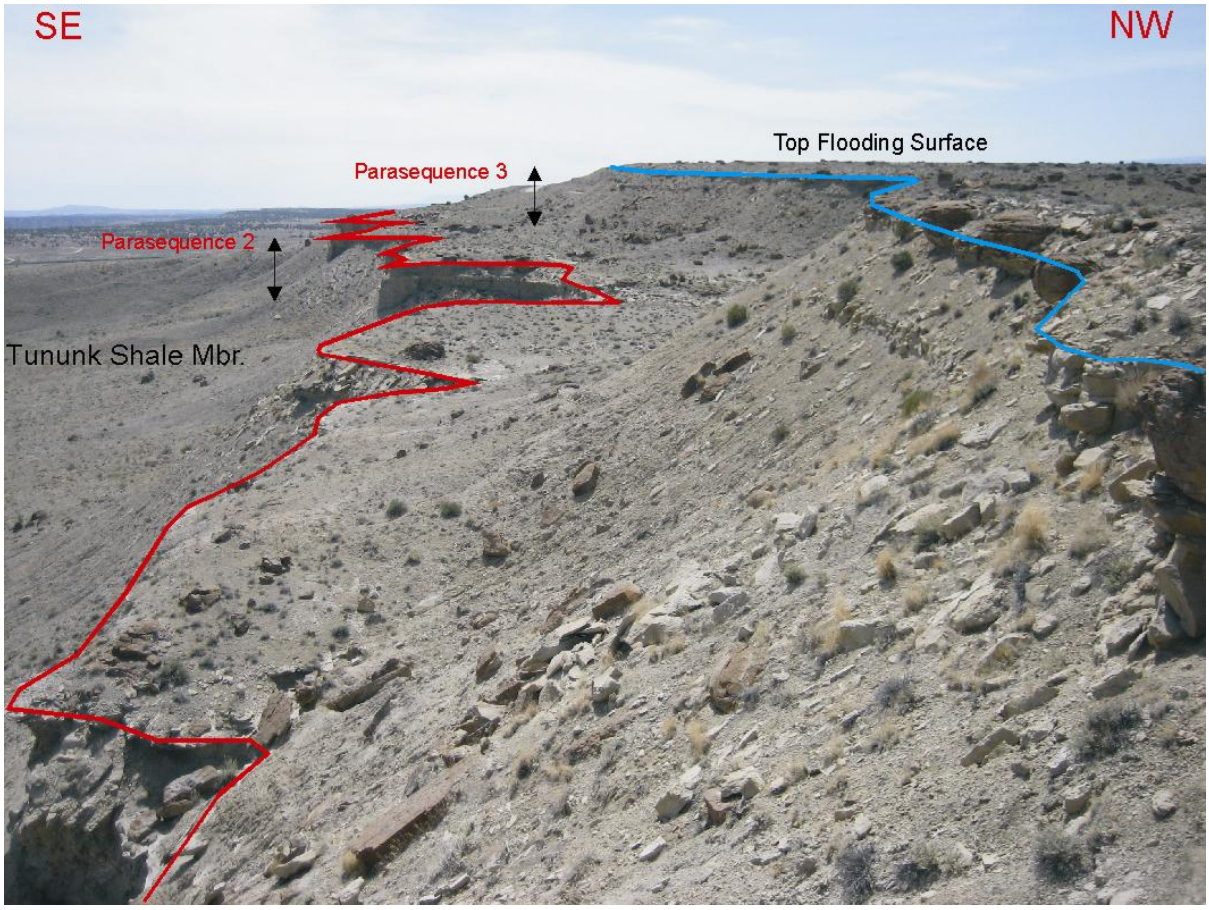

Figure 7.2: Lower Ferron parasequences in northern Castle Valley. Parasequence boundary in red, transgressive top flooding surface in blue.

A comparison between the parasequences of the present study, and the Lower Ferron lithostratigraphy is summarised in the table below:

Table 6: Summary of the interpreted parasequences and their relation to the previous work.

Parasequence	Unit (Cotter, 1975)	Ryer (1994)	Barton et al. (2004)	Type
PS1	N/A	N/A	N/A	Progradational
PS2	Clawson	Kf-Clawson	Washboard	Progradational
PS3	Washboard/Farnham	Kf-Washboard	Clawson	Progradational to Aggradational
PS4	Washboard			Aggradational Back-stepping

7.2 Evolution of the Lower Ferron depositional system

This study has suggested two significant changes to the understanding of the Lower Ferron depositional system: 1) the updip correlation of the outcrops to the subsurface deposits in the CBM fields and, 2) the along strike re-correlation of the outcrops and the southward migration of the depositional system.

The old conceptual model states that the Lower Ferron sandstone was deposited during rapid regression over an area of low subsidence rates. The non-marine, coal bearing deposits above this thin, basal sandstone are part of an aggradational to retrogradational depositional system related to the Upper Ferron sandstone, implying that the 30- 60 meter thick Lower Ferron sandstone deposits are traceable from the outcrops along the San Rafael Swell to the subsurface beneath the Wasatch Plateau without any associated paralic deposits. This supposed rapid regression must then be accompanied by a rapid transgression that quickly ended the widespread Lower Ferron depositional cycle and marked the onset of Upper Ferron coal bearing deposits. The correlation panel constructed by Henry and Finn (2003) for the U.S. Geological Survey exemplifies the errors that follow the conceptual model originally envisaged for the Ferron Sandstone Member. The first occurrence of sandstone is correlated

over a broad area and does not interfinger in the palaeolandward direction, as one would assume for such a depositional system. Additionally, the correlation panels presented therein must assume much broader facies tracts to account for the prograding distance than what is proposed in the present study.

Rather than abrupt changes in style and direction of deposition, this study highlights the possibility of a more pronounced Lower Ferron depositional system, including a continental depositional environment with coal accumulation. This model is supported by the improved correlation that is facilitated by the 3D model. Furthermore the facies tract thicknesses and belt widths suggested by this new depositional systems model are consistent with those observed from other Upper Cretacoeus systems in Utah (Howell and Flint 2003; Hampson and Howell 2005; Sømme et al 2008 and others).

The re-evaluation of the along strike correlation of the outcrops also has implications for understanding the relationship between the Lower and Upper Ferron systems. The study of the Lower Ferron suggests that the system migrated southward through time and that PS4 represented a transition from a shoreline system linked to the Vernal Delta Complex in the north to the younger, Upper Ferron, Last Chance Delta to the south.

This study offer means for understanding the Lower Ferron as a distinct part of the Vernal deltaic complex, non-contemporary with the overlying Last Chance Delta of the Upper Ferron, but with a gradual transition between them. Whereas previous work have interpreted the Lower Ferron to be a thin, seaward stepping sandstone package with associated southward distribution of marine shelf sands by geostrophic currents, the current study suggests that the Lower Ferron has a non-marine equivalent in the Drunkards Wash, Helper Field and most likely the Buzzard Bench CBM fields, and a gradual transition to the Upper Ferron through autogenic cyclicity. Such a shift may be autocyclic, related to the switching of fluvial input points, it may also be explained by the uplift of an ancestral SRS/Farnham Dome proposed by Edwards et al. (2005), similar to the mechanism proposed by Ryer and Lovekin (1986) to explain anomalous bulges in the Vernal shoreline.

The palaeogeographic maps (Figure 7.3) are updated from those presented chapter four (Figure 4.22). The notable difference is the southward bulge in the shoreline of PS4. This is a plan view representation of the proposed correlation panel presented above.

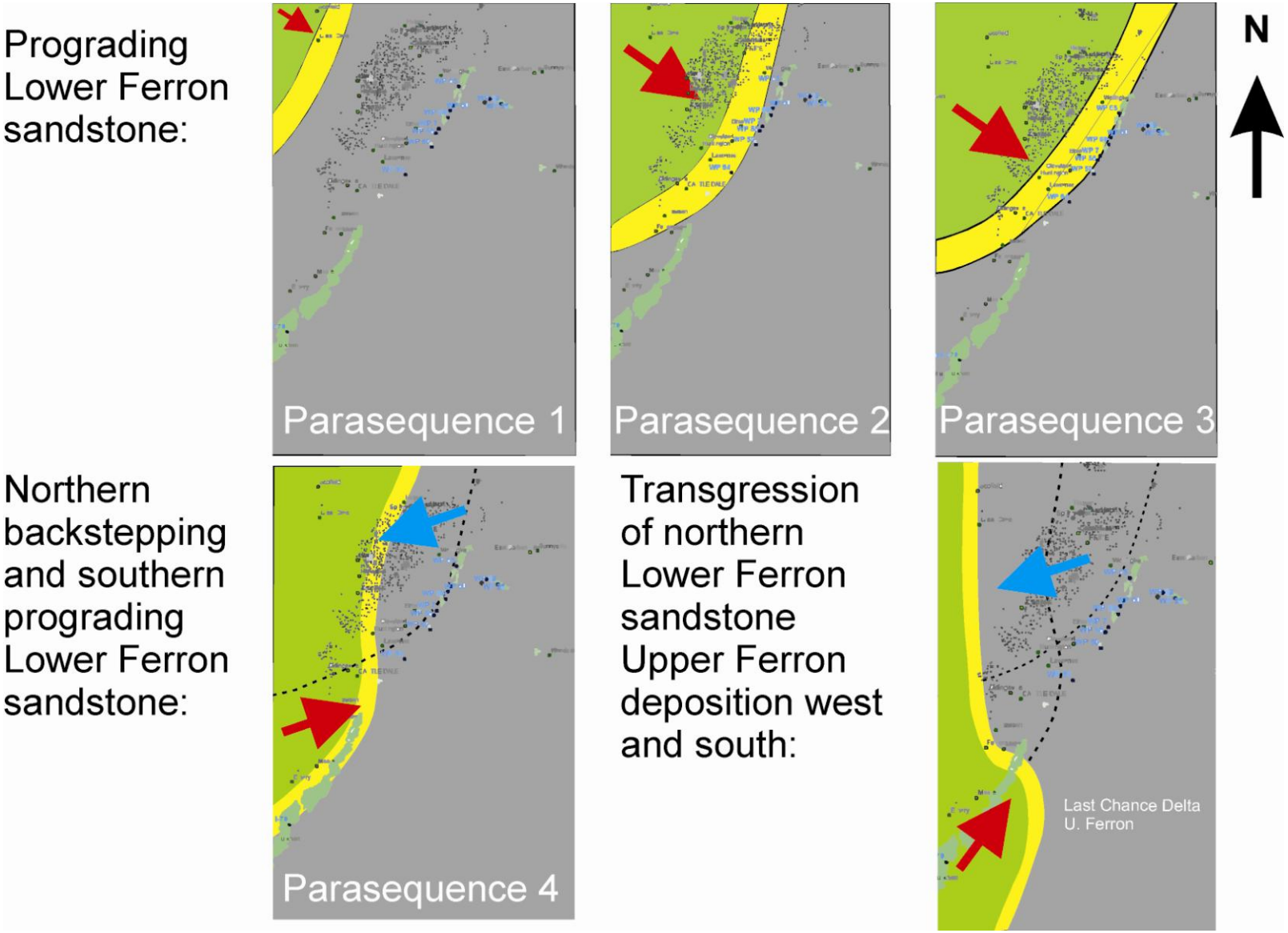

Figure 7.3: Schematic palaeogeo-graphic map illustrating the newly proposed depositional model for the Lower Ferron and its dynamic transition to the overlying Upper Ferron Last Chance Delta. Superimposed on the palaeogeogrphy are the geological features and outcrop locations from the maps presented in previous chapters (e.g. Figure 2.7), to offer a reference frame for the schematic shorelines.

The figure below illustrates the relative relationship between the Upper Ferron and the newly proposed stratigraphy for the Lower Ferron:

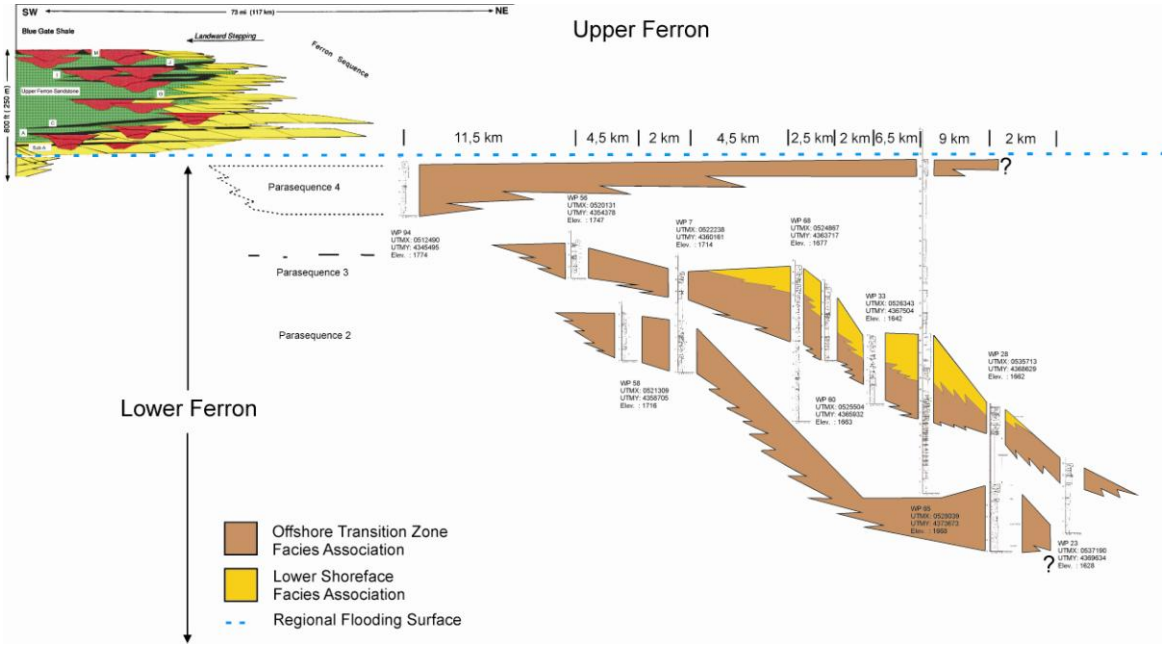

Figure 7.4: The alternative explanation for the stratigraphic relationship between the Upper and Lower Ferron. Schematic outcrop model not to scale, Upper Ferron stratigraphy by Fisher et al. (1993, Figure 2.8).

7.3 Future work

There are three key aspects of this study that could be improved with further work.

1. Mapping of faults within the CBM field. This could be achieved by using more of the available well data or having access to the seismic data. While this would not change the understanding of the stratigraphic relations but it would add to the utility of the model.

2. During the course of the work, numerous bentonites were observed in the field. Sampling, mapping and geochemical correlation of these would greatly improve the confidence in the new correlations

3. There are numerous intervals associated with very large "cannonball" concretions. There is significant scope for petrographic and isotopic work to understand their genesis and correlation.

7.4 Conclusions

- The Drunkards Wash CBM-field was successfully modelled from geophysical well logs, core and outcrop data.
- The model yielded four distinct parasequences comprising the Lower Ferron. Three of which were proven to extend to the surface of northern Castle Valley, where they crop out along the San Rafael Swell.
- The combined data presented in this study suggest that the Lower Ferron was a more prominent feature during its deposition than previously assumed.
- The present study offers a different explanation for the southward extent of the Lower Ferron sandstone, and a more dynamic evolution from the northern Vernal deltaic complex to the southern Last Chance Delta.

References

Anderson, P.B., and Ryer, T.A., 2004, Regional Stratigraphy of the Ferron Sandstone, *in* Regional to Wellbore Analog for Fluvial-Deltaic Reservoir Modeling: The Ferron Sandstone of Utah: *AAPG Studies in Geology 50* T.C. Chidsey, Jr, R.D. Adams, and T.H. Morris (eds.) p. 211-224

Anderson, P.B., Chidsey, Jr, T.C, Ryer, T.A., Adams, R.D., and McClure, K., 2004, Geological Framework, Facies, Paleogeography, and Reservoir Analogs of the Ferron Sandstone in the Ivie Creek Area, East.Central Utah, *in* Regional to Wellbore Analog for Fluvial-Deltaic Reservoir Modeling: The Ferron Sandstone of Utah: *AAPG Studies in Geology 50* T.C. Chidsey, Jr, R.D. Adams, and T.H. Morris (eds.) p. 331-356

Armstrong, R.L., 1968, Sevier orogenic belt in Nevada and Utah: *Geological Society of America Bulletin*, v. 79, p. 429-458

Barker, C.E., 2004, Analysis of coal from the Ferron Sandstone Member of the Mancos Shale near Emery, Utah: *USGS Open-File Report 2004-1279,* p. 1-4

Barker, C.E., and Dallegge, T.A., 1998, Approaches to coalbed methane gas-in-place analysis using sorption isotherms and burial history reconstruction – an example from the Ferron Sandstone, Utah: *15th Annual International Pittsburgh Coal Conference, Technical Papers*, unpaginated

Barton, M.D., Angle, E.S., and Tyler, N., 2004, Stratigraphic Architecture of Fluvial-Deltaic Sandstones from the Ferron Sandstone Outcrop, East-Central Utah, *in* Regional to Wellbore Analog for Fluvial-Deltaic Reservoir Modeling: The Ferron Sandstone of Utah: *AAPG Studies in Geology 50* T.C. Chidsey, Jr, R.D. Adams, and T.H. Morris (eds.) p. 193-210

Beaumont, C., 1981, Foreland basins: *Geophysical Journal of the Royal Astronomical Society,* v. 65

Bhattacharya, J.P., and Tye, R.S., 2004, Searching for Modern Ferron Analogs and Application to Subsurface Interpretation, *in* Regional to Wellbore Analog for Fluvial-Deltaic Reservoir Modeling: The Ferron Sandstone of Utah: *AAPG Studies in Geology 50,* T.C. Chidsey, Jr, R.D. Adams, and T.H. Morris (eds.) p. 39-57

Bhattacharya, J.P., and MacEachern, J.A., 2009, Hyperpycnal rivers and prodeltaic shelves in the Cretaceous Seaway of North America: *Journal of Sedimentary Research,* v.79, p. 184-209

Blakely, R.C., Paleogeographic maps, URL: http://jan.ucc.nau.edu/~rcb7/index.html

Bohacs, K., and Suter, J., 1997, Sequence stratigraphic distribution of coaly rocks: Fundamental controls and paralic examples: *AAPG Bulletin,* v. 81, no. 10, p. 1612-1639

Burns, T. D., and R. A. Lamarre, 1997, Drunkards Wash project: coalbed methane production from Ferron coals in east-central Utah: *Proceedings of the International Coalbed Methane Symposium, University of Alabama, Tuscaloosa*, paper 9709, p. 507–520

Chidsey, Jr., T.C., Adams, R.D., and Morris, T.H., eds., 2004, Regional to Wellbore Analog for Fluvial-Deltaic Reservoir Modeling: The Ferron Sandstone of Utah: *AAPG Studies in Geology 50,* 568 p.

Chidsey, Jr., T.C., Wakefield, S., Hill, B.G., and Hebertson, M., 2004, Oil and Gas Fields Map of Utah: *Utah Geological Survey,* Map 203 DM

Condon, S.M., 2003, Fracture network of the Ferron Sandstone Member of the Mancos Shale, East-Central Utah, USA: *International Journal of Coal Geology*, v. 56, p. 11-139

Corbeanu, R.M., Soegaard, K., Szerbiak, R.B., Thurmond, J.B., McMehan, G.A., Wang, D., Snelgrove, S., Forster, C.B., and Menitove, A., 2001, Detailed internal architecture of a fluvial channel sandstone determined from outcrop, cores, and 3-D ground penetrating radar: Example from the middle Cretaceous Ferron Sandstone, East-Central Utah: *AAPG Bulletin,* v. 85, no. 9, p. 1583-1608

Cotter, E., 1975, Late Cretaceous sedimentation in a low-energy coastal zone: The Ferron Sandstone of Utah: *Journal of Sedimentary Petrology,* v. 45, no. 3, p. 669-685

- 1976, The role of deltas in the evolution of the Ferron Sandstone and its coals: *Brigham Young University Geology Studies*, v. 22, pt. 3, p. 15-41

Davies, R., Howell, J., Boyd, R., Flint, S., and Diessel, C., 2006, High-resolution sequence-stratigraphic correlation between shallow-marine and terrestrial strata: Examples from the Sunnyside Member of the Cretaceous Blackhawk Formation, Book Cliffs, eastern Utah: *AAPG Bulletin,* v. 90, no. 7, p. 1121-1140

Davis, L.J., 1954, Stratigraphy of the Ferron Sandstone: *Intermountain Association of Petroleum Geology Fifth Annual Field Guidebook,* p. 55-58

DeCelles, P.G., and Mitra, G., 1995, History of the Sevier orogenic wedge in terms of critical taper models, northeast Utah and southwest Wyoming: *GSA Bulletin,* v. 107, no. 4, p. 454-462

DeCelles, P.G., 2004, Late Jurrasic to Eocene evolution of the cordilleran thrust belt and foreland basin system, western U.S.A.: *American Journal of Science,* v. 304, p. 105-168

Dietz, R.S, and Holden, J.C., 1970, Reconstruction of Pangaea: Breakup and dispersion of continents, Permian to present: *Journal of Geophysical Research,* v. 75, no. 26, p. 4939-4956

Diessel, C., Boyd, R., Wadsworth, J., Leckie, D., and Chalmers, G., 2000, On balanced and unbalanced accommodation/peat accumulation ratios in the Cretaceous coals from Gates Formation, Western Canada, and their sequence stratigraphic significance: *International Journal of Coal Geology,* v. 43, p. 143-186

Edwards, C.M., Hodgson, D.M., Flint, S.S., and Howell, J.A., 2005, Contrasting styles of shelf sediment transport and deposition in a ramp margin setting related to relative sea-level change and basin floor topography, Turonian (Cretaceous) Western Interior of central Utah, USA: *Sedimentary Geology,* v. 179, p. 117-152

Enge, H.D., and Howell, J.A., 2010, Impact of deltaic clinothems on reservoir performance: Dynamic studies of reservoir analogs from the Ferron Sandstone Member and Panther Tongue, Utah: *AAPG Bulletin,* v. 94, no.2, p.139-161

Fisher, R.S., Barton, M.D., and Tyler, N., 1993, Quantifying reservoir heterogeneity through outcrop characterization – 2. Architecture, lithology, and permeability distribution of a seaward-stepping fluvial-deltaic sequence, Ferron Sandstone (Cretaceous), central Utah: *Topical Report GRI-93-0023 for Gas Research Institute, Contract No. 5089-260-1902,* 83 p.

Flint, S., Aitken, J., and Hampson, G., 1995, Application of Sequence Stratigraphy to Coal-Bearing Coastal Plain Successions: Implications for the UK Coal Measures, *in* European Coal Geology: *Geological Society of London Special Publication No 82,* M.K.G. Whateley, and D.A. Spears (eds.), p. 1-16

Forster, C.B., Snelgrove, S.H., Lim, S.J., Corbeanu, R.M., McMechan, G.A., Soegaard, K., Szerbiak, R.B., Crossey, L., and Roche, K., 2004, 3-D Fluid-Flow Simulation in a Clastic Reservoir Analog: Based on 3-D Ground-Penetrating Radar and Outcrop Data from the Ferron Sandstone, Utah, *in* Regional to Wellbore Analog for Fluvial-Deltaic Reservoir Modeling: The Ferron Sandstone of Utah: *AAPG Studies in Geology 50* T.C. Chidsey, Jr, R.D. Adams, and T.H. Morris (eds.) p. 405-425

Gardner, M.H., 1993, Sequence stratigraphy of the Ferron Sandstone (Turonian) of east-central Utah: *Ph.D. dissertation, Colorado School of Mines, Golden*, 528 p.

-1995a, Tectonic and Eustatic Controls on the Stratal Architecture of Mid-Cretaceous Stratigraphic Sequences, Central Western Interior Foreland Basin of North America: *in* Stratigraphic Evolution of Foreland Basins: *Society of Sedimentary Geology (SEPM) Special Publication 52,* S. Dorobek, and J. Ross (eds.), p. 283-303

- 1995b, The Stratigraphic Hierarchy and Tectonic History of Mid-Cretaceous Foreland Basin of Central Utah: *in* Stratigraphic Evolution of Foreland Basins: *Society of Sedimentary Geology (SEPM) Special Publication 52,* S. Dorobek, and J. Ross (eds.), p. 283-303

Gardner, M.H., Cross, T.A., and Levorsen, M., 2004, Stacking Patterns, Sediment Volume Partitioning, and Facies Differentiation in Shallow-Marine and Coastal Plain Strata of the Cretaceous Ferron Sandstone, Utah, *in* Regional to Wellbore Analog for Fluvial-Deltaic Reservoir Modeling: The Ferron Sandstone of Utah: *AAPG Studies in Geology 50,* T.C. Chidsey, Jr, R.D. Adams, and T.H. Morris (eds.), p. 95-124

Garrison, Jr, J.R., and van den Bergh, T.C.V., 1997, Coal Zone and High-Resolution Depositional Sequence Stratigraphy of the Upper Ferron Sandstone, *in* Mesozoic to Recent Geology of Utah: *Brigham Young University Geology Studies*, v. 42, pt. 2, p.160-178

- 2004, High-Resolution Depositional Sequence Stratigraphy of the Upper Ferron Sandstone Last Chance Delta: An Application of Coal-Zone Stratigraphy, *in* Regional to Wellbore Analog for Fluvial-Deltaic Reservoir Modeling: The Ferron Sandstone of Utah: *AAPG Studies in Geology 50* T.C. Chidsey, Jr, R.D. Adams, and T.H. Morris (eds.) p. 125-192

Gibling,M.R., 2006, Width and thickness of fluvial channel bodies and valley fills in the geological record: a literature compilation and classification: *Journal of Sedimentary Research*, v. 79, p. 731-770

Hale, L.A., 1972, Depositional history of the Ferron Formation, central Utah, *in* Plateau-Basin and Range transition zone, central Utah: *Utah Geological Association Publication 2,* J.L. Baer, and E. Callaghan (eds.), p. 29-40

Hale, L.A., and Van de Graaff, F.R., 1964, Cretaceous stratigraphy and facies patterns, northeastern Utah and adjacent areas: *Intermountain Association of Petroleum Geologists Guidebook,* 13th Annual Field Conference, p. 115-138

Hampson, G., 1995, Discrimination of Regionally Extensive Coals in the Upper Carboniferous of the Pennine Basin, UK using High Resolution Sequence Stratigraphic Concepts, *in* European Coal Geology: *Geological Society of London Special Publication No 82,* M.K.G. Whateley, and D.A. Spears (eds.), p. 79-97

Hampson, G.J. and Howell, J.A., 2005, Sedimentologic and geomorphic characterization of ancient wave-dominated deltaic shorelines; Upper Cretaceous Blackhawk Formation, Book Cliffs, Utah, USA., *in* River Deltas – Concepts, Models and Examples: *Society for Economic Paleontologists and Mineralogists Special Publication* L. Giosan and J.P. Bhattacharya (eds.), v. 83, p 133–154.

Haq, B.U., Hardenbol, J. and Vail, P.R., 1987, Chronology of fluctuating sea levels since the Triassic: *Science,* v. 235, no. 4793, p. 1156-1167

Hay, W.W., DeConto, R.M., and Wold, C.N., 1997, Climate: Is the past the key to the future: *Geol Rundsch*, v. 86, p. 471-491

Helland-Hansen, W., and Martinsen, O.J., 1996, Shoreline trajectories and sequences: Description of variable depositional dip scenarios: *Journal of Sedimentary Research,* v. 66, no. 4, p. 670-688

Henry, M.E., and Finn, T.M., 2003, Evaluation of undiscovered natural gas in the Upper Cretaceous Ferron Coal/Wasatch Plateau Total Petroleum System, Wasatch and Castle Valley, Utah: *International Journal of Coal Geology*, v. 56, p. 3-37

Hintze, L. F., 1988, Geologic history of Utah: *Brigham Young University Geology Studies Special Publication 7*, 202 p.

Hintze, L.F., Willis, G.C., Laes, D.Y.M., Sprinkle, D.A., and Brown, K.D., 2000, Digital Geological Map of Utah: *Utah Geological Survey*

Holz, M., Kalkreuth, W., and Banerjee, I., 2002, Sequence Stratigraphy of paralic coal-bearing strata: an overview: *International Journal of Coal Geology*, v. 48, p. 147-179

Howell, J.A., and Flint, S.S., 2003, Siliciclastics Case Study: The Book Cliffs, *in* The Sedimentary Record of Sea-Level Change: *Cambridge University Press*, A.L. Coe (ed.), pt. 3, p. 135-197

Howell, J.A., Skorstad, A., MacDonald, A., Fordham A., Flint, S., Fjellvoll, B., and Manzocchi, T., 2008, Sedimentological parameterization of shallow-marine reservoirs: *Petroleum Geoscience*, v. 14, p. 17-34

Jordan, T.A., 1981, Thrust loads and foreland basin evolution, Cretaceous, Western United States: *AAPG Bulletin*, v. 65, no. 12, p. 2506-2520

Katich, Jr, P.J., 1953, Geological notes: source direction of Ferron Sandstone in Utah: *AAPG Bulletin*, v. 37, no. 4, p. 858-862

Kauffman, E.G., 1984, Paleobiogeography and Evolutionary Response Dynamic in the Western Interior Seaway of North America, *in* Jurassic-Cretaceous Biochronology and Paleogeography of North America: *Geological Association of Canada Special Paper 2*, G.E.G. Westerman (ed.), p. 273-306

Laubach, S.E., Marrett, R.A., Olson J.E., and Scott A.R., 1997, Characteristics and origins of coal cleat: a review: *International Journal of Coal Geology*, v. 35, p. 175-207

Li, H., and White, C.D., 2003, Geostatistical models for shales in distributary channel point bars (Ferron Sandstone, Utah): From ground penetrating radar data to three-dimensional flow modeling: *AAPG Bulletin*, v. 87, p. 1851-1868

Lupton, C.T., 1916, Geology and coal resources of Castle Valley in Carbon, Emery, and Sevier Counties, Utah: *U.S. Geological Survey Bulletin*, v. 628, p. 1-88

Lyons, W.S., 2001, Seismic Maps Ferron Coalbed Sweetspots, *in* Seismic Guides Interpretation in the Ferron Coalbed Methane Play: *AAPG Explorer, Geophysical Corner*, R. R. Ray (ed.) URL: http://www.aapg.org/explorer/geophysical_corner/2001/12gpc.cfm

MacDonald, A.C., and Aasen, J.O., 1994, A prototype procedure for stochastic modeling of facies tract distribution in shoreface reservoirs, *in* Stochastic modeling and geostatistics; principles, methods, and case studies: *American Association of Petroleum Geologists Computer Applications in Geology*, J.M. Yarus, and R.L. Chambers (eds.), p. 91–108.

Montgomery, S.L., Tabet, D.E., and Barker, C.E., 2001, Upper Cretaceous Ferron Sandstone: major coalbed methane play in central Utah: *AAPG Bulletin*, v. 85, no. 2, p. 199-219

Miller, E.L., Gans, P.B., and Garing, J., 1983, The Snake River Décollement: An exhumed mid-Tertiary ductile-brittle transition: *Tectonics*, v. 2, no. 3, p. 239-263

NASA image, URL: http://eol.jsc.nasa.gov/sseop/images/EFS/lowres/STS61C/STS61C-40-96.jpg

NASA World Wind – Maps of study area (Chapter One)

Neuhauser, K.R., 1988, Sevier-age ramp-style thrust faults at Cedar Mountain, northwestern San Rafael Swell (Colorado Plateau), Emery County, Utah: *Geology*, v. 16, p. 299-302

Obradovich, J.D., 1993, A Cretaceous Time Scale, *in* Evolution of the Western Interior Basin: *Geological Association of Canda Special Paper 39*, W.G.E. Caldwell, and E.G. Kauffman (eds.), p. 379-396

Pang, M., and Nummedal, D., 1995, Flexural subsidence and basement tectonics of the Cretaceous Western Interior Basin, United States: *Geology*, v. 23, no. 2, p. 173-176

Reynolds, A.D., 1999, Dimensions of Paralic Sandstone Bodies: *AAPG Bulletin*, v. 83, no. 2, p. 211-229

Rice, C.A., 2003, Production waters associated with the Ferron coalbed methane fields, central Utah: Chemical and isotopic composition and volumes: *International Journal of Coal Geology*, v. 56, p. 141-169

Rider, M.H., 1986, Geological Interpretation of Well Logs: *John Wiley and Sons*, 175 p.

Ryer, T.A., 1980, Deltaic Coals of the Ferron Sandstone Member of the Mancos Shale – Predictive Model for Cretaceous Coals of the Western Interior, *in* Proceedings of the Fourth Symposium on the Geology of Rocky Mountain Coal: *Colorado Geological Survey Resource Series no. 10*, L.M. Carter (ed.), p.4-5

-1981, Deltaic coals of the Ferron Sandstone Member of Mancos Shale: Predictive model for Cretaceous coal-bearing strata of Western Interior: *AAPG Bulletin*, v. 65, no. 11, p. 2323-2330

- 1984, Transgressive-Regressive Cycles and the Occurrence of Coal in some Upper Cretaceous Strata of Utah, U.S.A.: *in* Sedimentology of Coal and Coal-Bearing Sequences: *International Association of Sedimentologists, Special Publication*, R.A. Rahmani, and R.M. Flores (eds.), v. 7, p. 217-227.

- 1994, Interplay of tectonics, eustasy, and sedimentation in the formation of mid-Cretaceous clastic wedges, central and northern Rocky Mountain regions: *Rocky Mountain Association of Geologists Unconformity Controls Symposium*, p. 35-44

- 2004, Previous studies of the Ferron Sandstone, *in* Regional to Wellbore Analog for Fluvial-Deltaic Reservoir Modeling: The Ferron Sandstone of Utah: *AAPG Studies in Geology 50* T.C. Chidsey, Jr, R.D. Adams, and T.H. Morris (eds.) p. 3-38

Ryer, T.A., and Lovekin, J.R., 1986, The Upper Cretaceous Vernal Delta of Utah – Depositional or paleotectonic feature?, *in* Paleotectonics and Sedimentation in the Rocky Mountain Region, United States: *AAPG Memoir 41*, J. Peterson (ed.), p. 497-510

Ryer, T.A., and McPhillips, M., 1983, Early Late Cretaceous Paleogeography of East-Central Utah, *in* Mesozoic Paleogeography of the West-Central United States: *Society of Economic Paleontologists and Mineralogists, Rocky Mountain Paleography Symposium 2*, M.W. Reynolds, and E.D. Dolly (eds.), p. 253-272

Sinclair, H.D., Coakley, B.J., Allen, P.A., and Watts, A.B., 1991, Simulation of foreland basin stratigraphy using a diffusion model of mountain belt uplift and erosion: an example from the central Alps, Switzerland: *Tectonics*, v. 10, no. 3, p. 599-620

Stokes, W.L., 1988, Geology of Utah: *Occasional Paper Number 6, Utah Museum of Natural History*, 280 p.

Sømme, T.O., Howell, J.A., Hampson, G.J. and Storms, J.E.A., 2008, Genesis, architecture, and numerical modeling of intra-parasequence discontinuity surfaces in wave-dominated deltaic deposits: Upper Cretaceous Sunnyside Member, Blackhawk Formation, Book Cliffs, Utah, USA. *in* Recent Advances in Models of Siliciclastic Shallow-Marine Stratigraphy: *SEPM Special Publication*, G.J. Hampson, R.J. Steel, P.M. Burgess and R.W. Dalrymple (eds.) , v. 90, p. 421–441.

Tabet, D.E., Hucka, B.P., and Sommer, S.N., 1995, Depth, vitrinite reflectance, and coal thickness maps, Ferron Sandstone, central Utah: *Utah Geological Survey, Open-File Report 329*, 3 plates

Tabet, D. E., 1998, Migration as a process to create abnormally high gas contents in the Ferron Sandstone coal beds, central Utah: *AAPG Annual Convention, Abstracts with Program,* v. 2, paper A646.

Thompson, S.L., Ossian, C.R., and Scott, A.J., 1986, Lithofacies, Inferred Processes, and Log Response Characteristics of Shelf and Shoreface Sandstones, Ferron Sandstone, Central Utah, *in* Modern and Ancient Shelf Clastics – A Core Workshop: *Society for Sedimentary Geology (SEPM) Core Workshop No. 9*, T.F. Moslow and E.G. Rhodes (eds.), p. 325-361

Tripp, C.N., 1989, A hydrocarbon exploration model for the Cretaceous Ferron Sandstone Member of the Mancos Shale, and the Dakota Group in the Western Wasatch Plateau and Castle Valley of east-central Utah, with emphasis on post-1980 subsurface data: *Utah Geological Survey Open-File Report 160,* 81 p

United States Geological Survey database, URL: http://seamless.usgs.gov/website/seamless/viewer.htm.

Utah Government databases, URL: http://oilgas.ogm.utah.gov/index.htm, and: http://oilgas.ogm.utah.gov/Statistics/PROD_CBM_field.cfm

Van Wagoner, J.C., Mitchum, R.M., Campion, K.M., and Rahmanian, V.D., 1990, Siliciclastic sequence stratigraphy in well logs, cores, and outcrops: Concepts for high-resolution correlation of time and facies: *AAPG Methods in Exploration Series, no. 7*

Vail, P.R., Mitchum, Jr., R.M., and Thompson, III, S., 1977, Global Cycles of Relative Changes in Sea Level, *in* Seismic Stratigraphy – Applications to Hydrocarbon Exploration: *AAPG Memoir 26,* C.E. Payton (ed.), p. 83-98

Willis, G.C., 1999, The Utah Thrust System – An Overview, *in* Geology of northern Utah and vicinity: *Utah Geological Association Publication 27*, L.E. Spangler (ed.), p. 1-9.

Winn, Jr., R.D., 1991, Storm deposition in marine sand sheets: Wall Creek Member, Frontier Formation, Powder River Basin, Wyoming: *Journal of Sedimentary Petrology*, v. 61, no. 1, p. 86-101

Appendix I

This appendix includes information mentioned in, or relevant, to the thesis. Petrel files, las-files, pictures, correlation panels, core log and maps are all included in Appendix II on a DVD.

In the following pages one will find:

- Well correlation panels, depositional dip and strike
- Overview maps of the correlation panels and the extrapolated correlations
- Well correlation panels extrapolated to outcrop
- Statistics from the final model
- Well log information table containing the specs for the well logs included in the model
- Waypoint information table that accounts for the various localities visited in the field, listed with UTM-coordinates and purpose of locality.
- Outcrop logs, either raw or processed in CorelDraw.

Well correlation panels

Well correlation panels NW-SE (depositional dip), panels ordered from north to south:

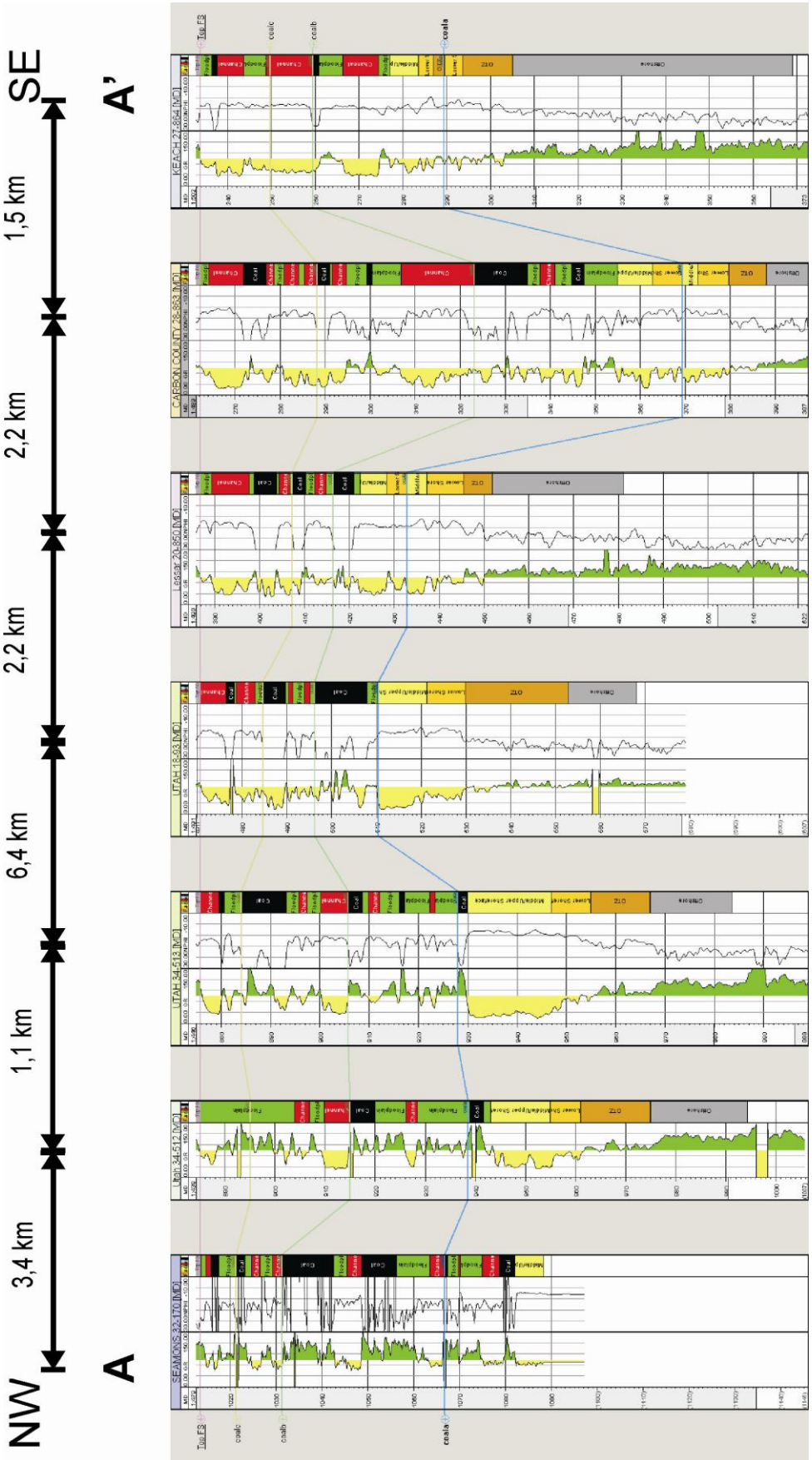
NW
SE
A
A'
3,4 km
1,1 km
6,4 km
2,2 km
2,2 km
1,5 km

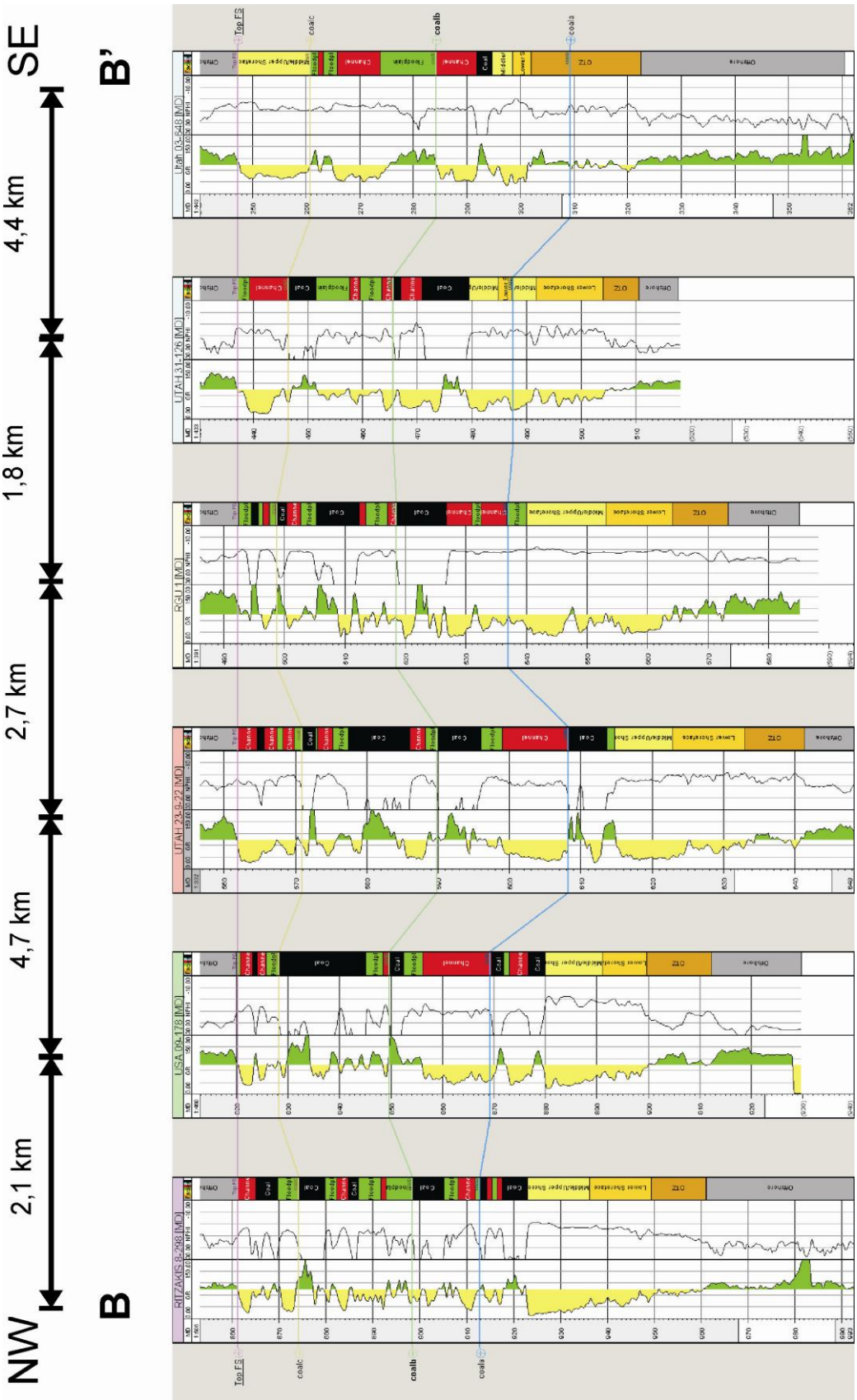
NW
SE
B
B'
2,1 km
4,7 km
2,7 km
1,8 km
4,4 km
Top FS
coalc
coalb
coala

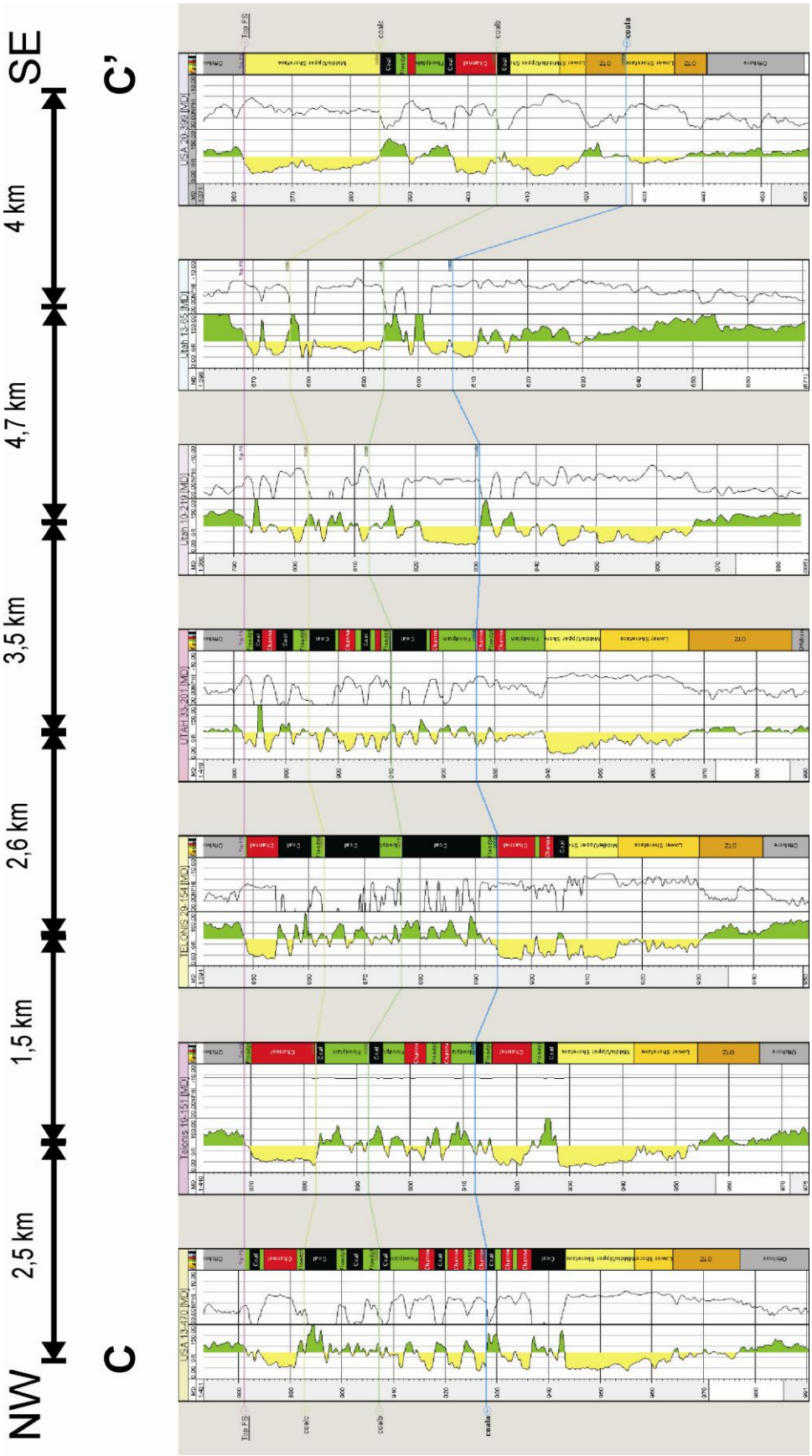
NW
SE
C
C'
2,5 km
1,5 km
2,6 km
3,5 km
4,7 km
4 km
USA 20-396 (MD)
Utah 13-55 (MD)
Utah 10-219 (MD)
UTAH 33-201 (MD)
TELONIS 29-154 (MD)
Telonis 16-151 (MD)
USA 13-470 (MD)
Top ES
coals
coala

NW
SE
D
D'
2 km
7,5 km
4,2 km
2,5 km
3,1 km
Top FS
coalc
coalb
coala
USA 23-478 [MD]
UTAH 25-368 [MD]
Utah 10-219 [MD]
Utah 23-106 [MD]
Utah 25-252 [MD]
USA 01-312 [MD]

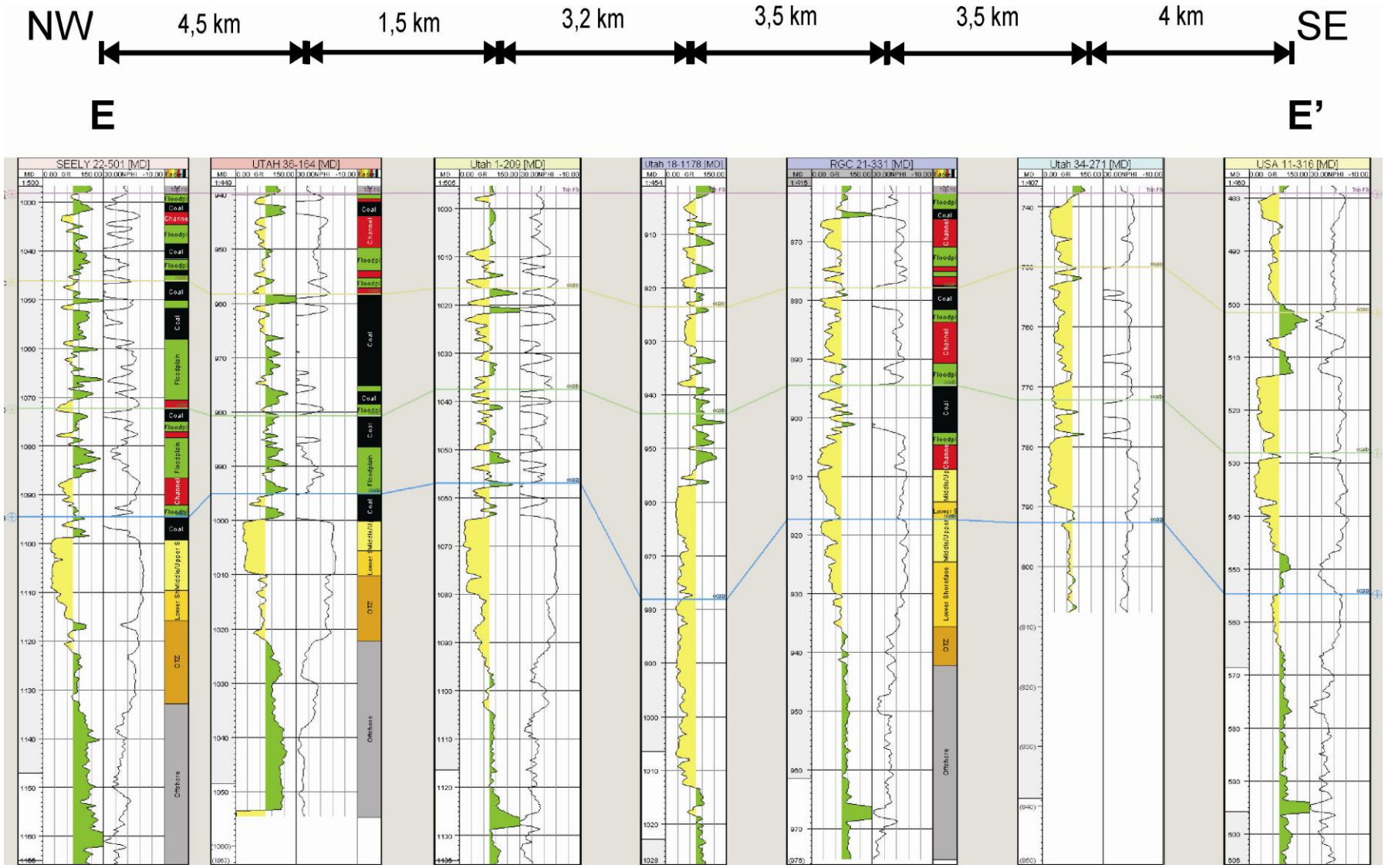
NW
4,5 km
1,5 km
3,2 km
3,5 km
3,5 km
4 km
SE
E
E'
SEELY 22-501 [MD]
UTAH 36-164 [MD]
Utah 1-209 [MD]
Utah 18-1178 [MD]
RGC 21-331 [MD]
Utah 34-271 [MD]
USA 11-316 [MD]
Coal
Floodplain
Channel
Lower Shoreface
Middle/Upper Shoreface
OTZ
Offshore

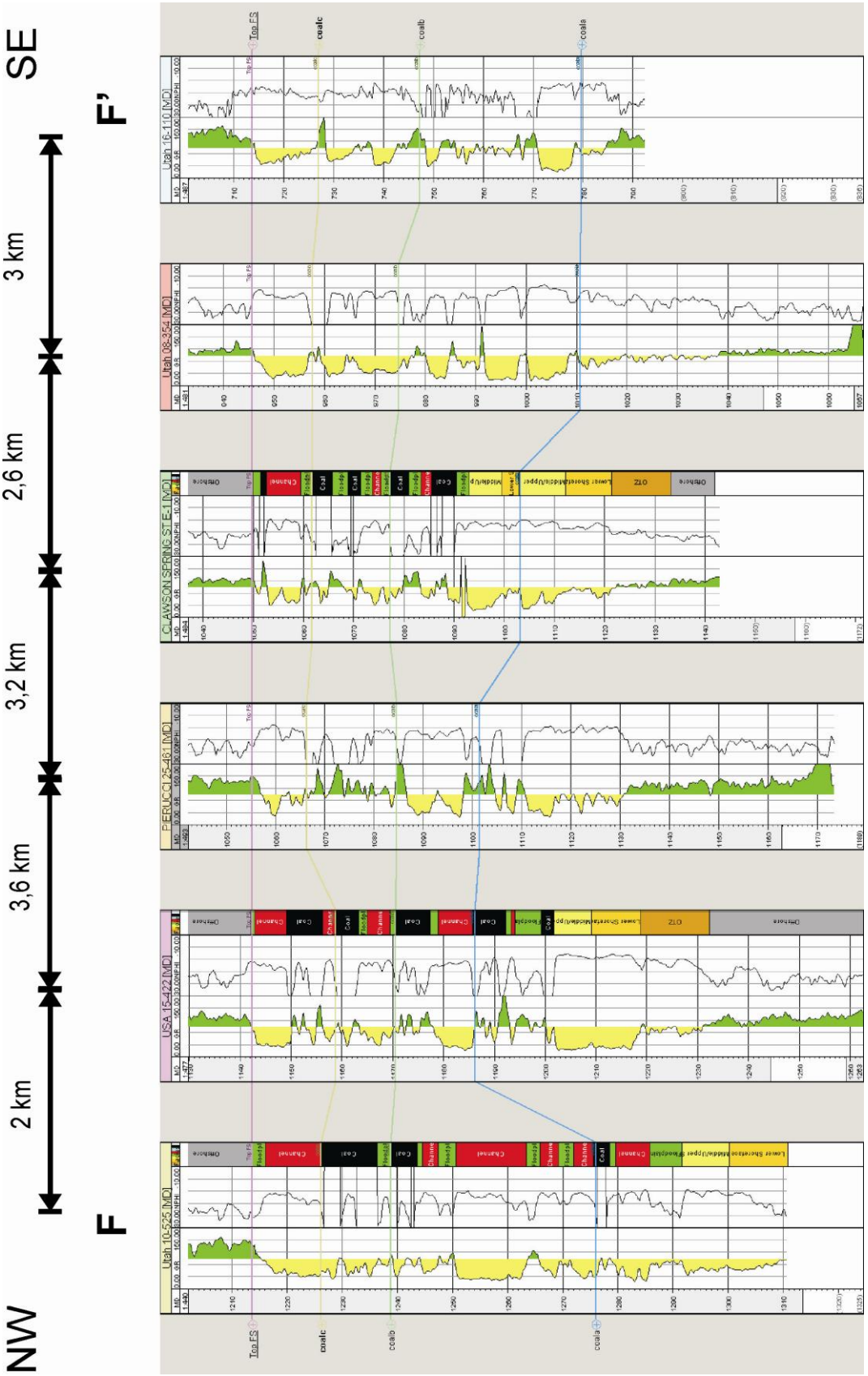
NW
SE
F
F'
2 km
3,6 km
3,2 km
2,6 km
3 km
Top FS
coalc
coalb
coala
Utah 10-525 [MD]
USA 15-422 [MD]
PERUCCI 25-461 [MD]
CLAWSON SPRNG ST E-1 [MD]
Utah 08-354 [MD]
Utah 16-110 [MD]

Correlation Panels NNE-SSW (depositional strike), panels ordered from east to west:

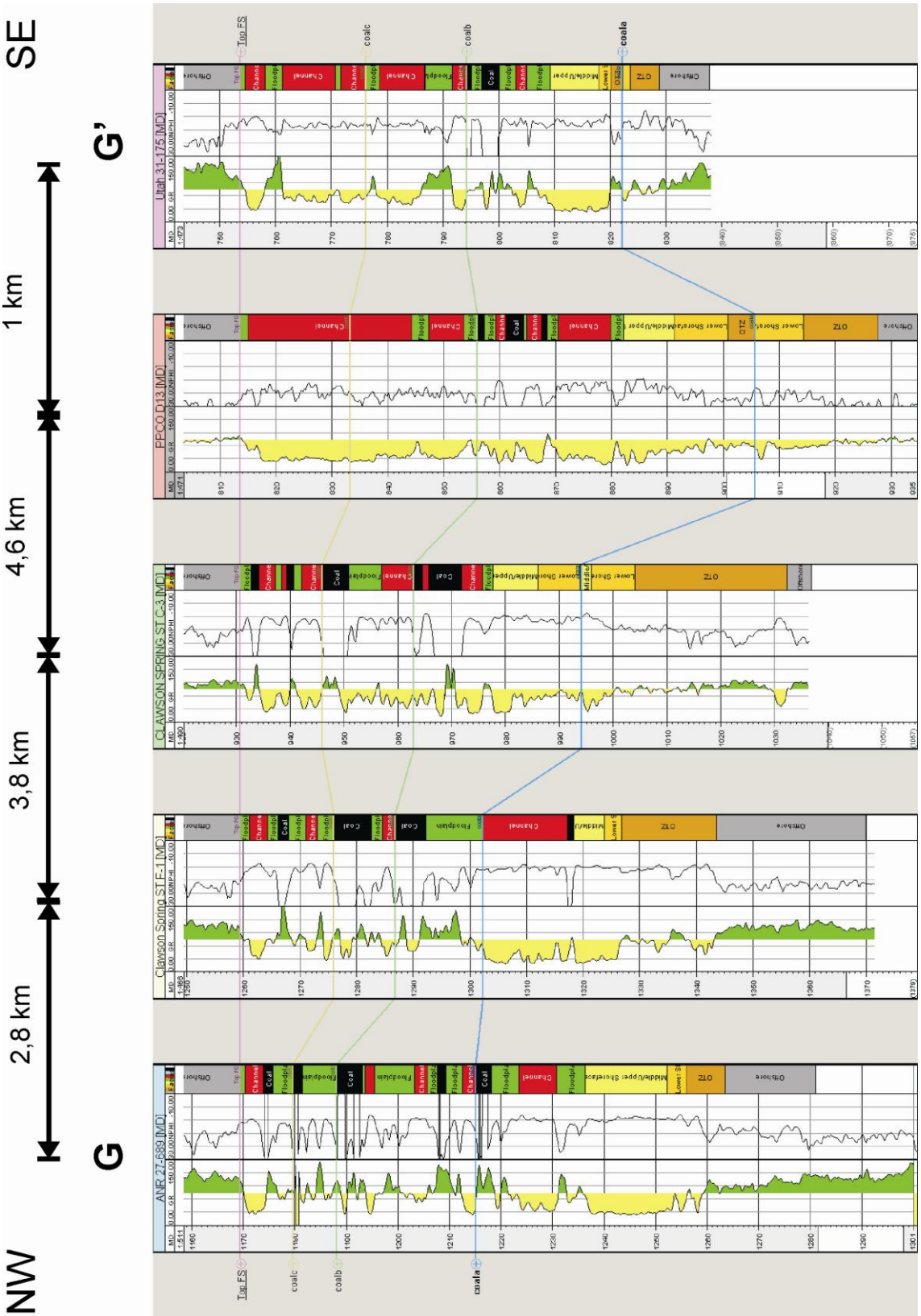

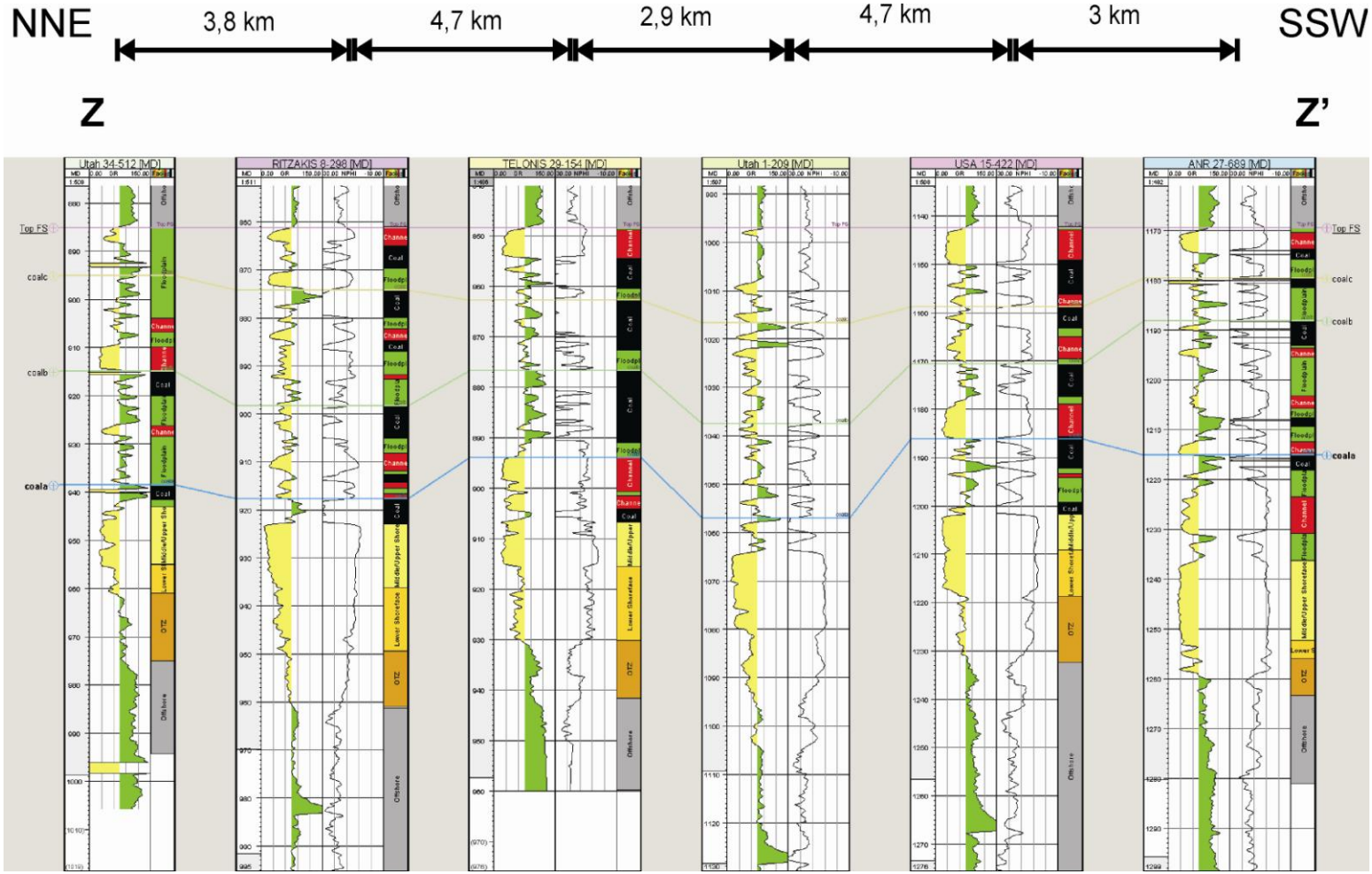
NNE
3,8 km
4,7 km
2,9 km
4,7 km
3 km
SSW
Z
Z'
Utah 34-512 [MD]
RITZAKIS 8-298 [MD]
TELONIS 29-154 [MD]
Utah 1-209 [MD]
USA 15-422 [MD]
ANR 27-689 [MD]
Top FS
coalc
coalb
coala

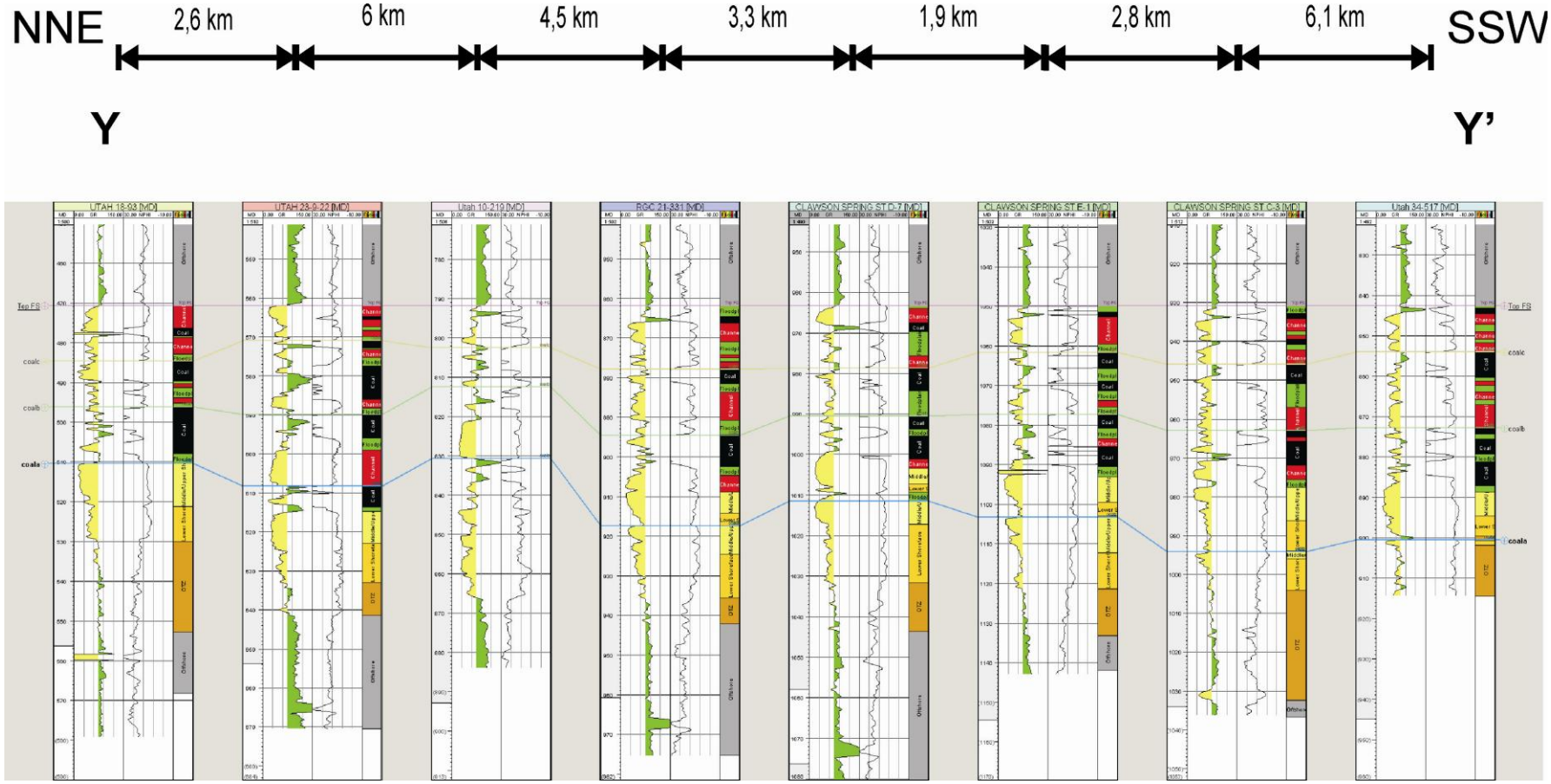
NNE
2,6 km
6 km
4,5 km
3,3 km
1,9 km
2,8 km
6,1 km
SSW
Y
Y'
UTAH 18-93 [MD]
UTAH 23-9-22 [MD]
Utah 10-219 [MD]
RGC 21-331 [MD]
CLAWSON SPRING ST D-7 [MD]
CLAWSON SPRING ST E-1 [MD]
CLAWSON SPRING ST C-3 [MD]
Utah 34-517 [MD]
Top FS
coalc
coalb
coala

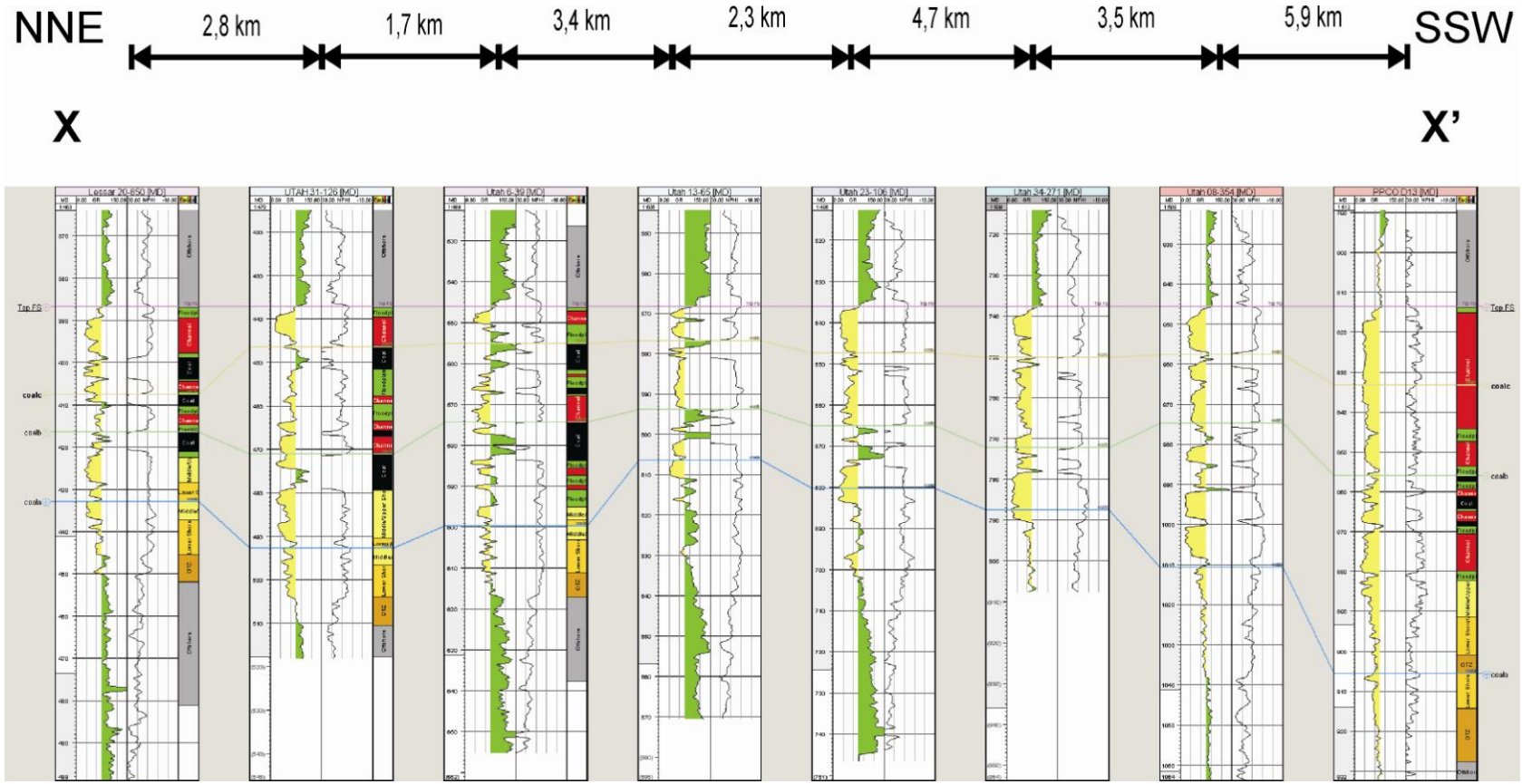
NNE
2,8 km
1,7 km
3,4 km
2,3 km
4,7 km
3,5 km
5,9 km
SSW
X
X'
Lessar 20-850 [MD]
LITAH 31-126 [MD]
Utah 6-39 [MD]
Utah 13-65 [MD]
Utah 23-106 [MD]
Utah 34-271 [MD]
Utah 08-354 [MD]
PPCO D13 [MD]
Top FS
coalc
coalb
coala

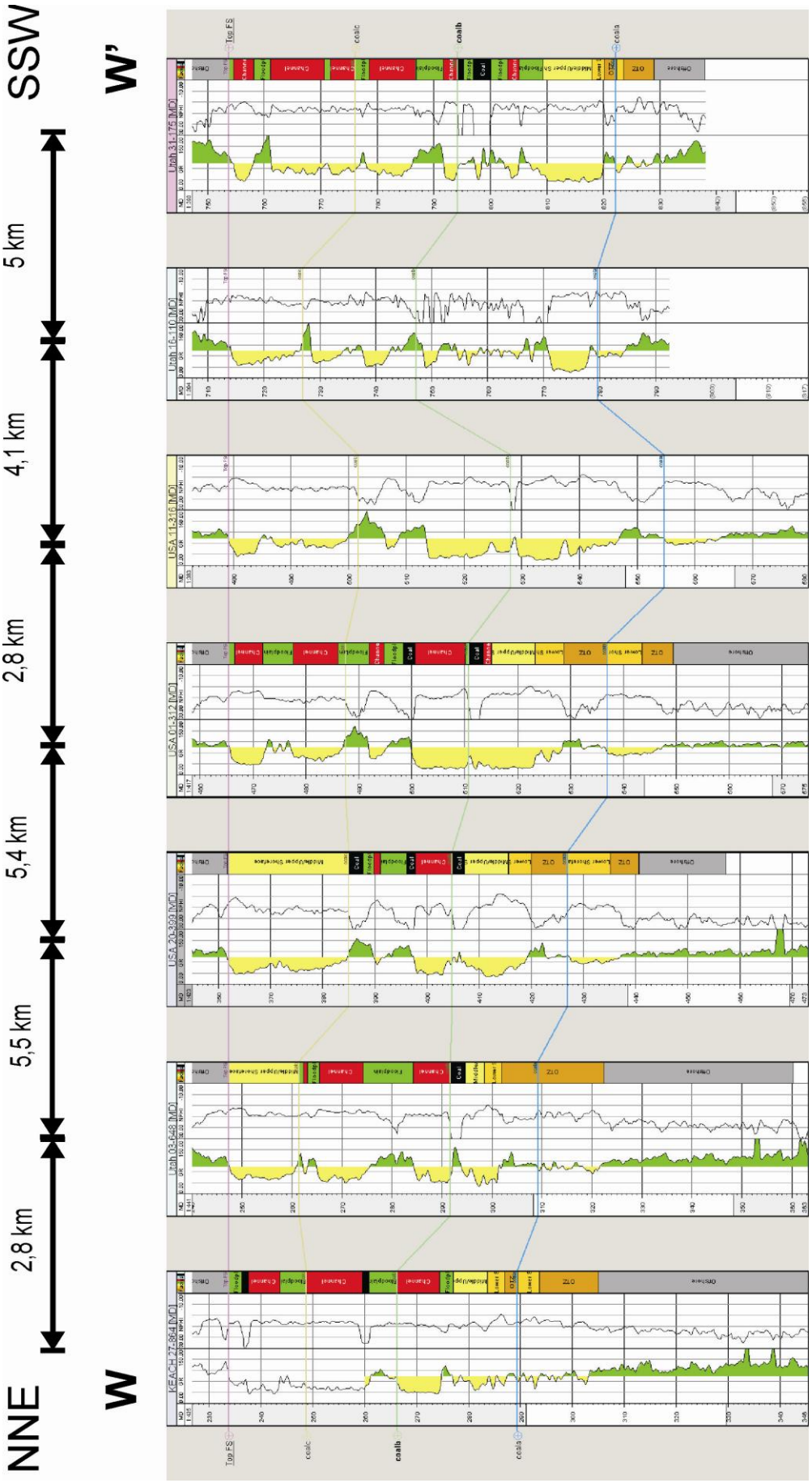
NNE
SSW
W
W'
2,8 km
5,5 km
5,4 km
2,8 km
4,1 km
5 km
Top FS
coalc
coalb
coala

Overview Maps Correlation panels

Overview map Correlation Panels

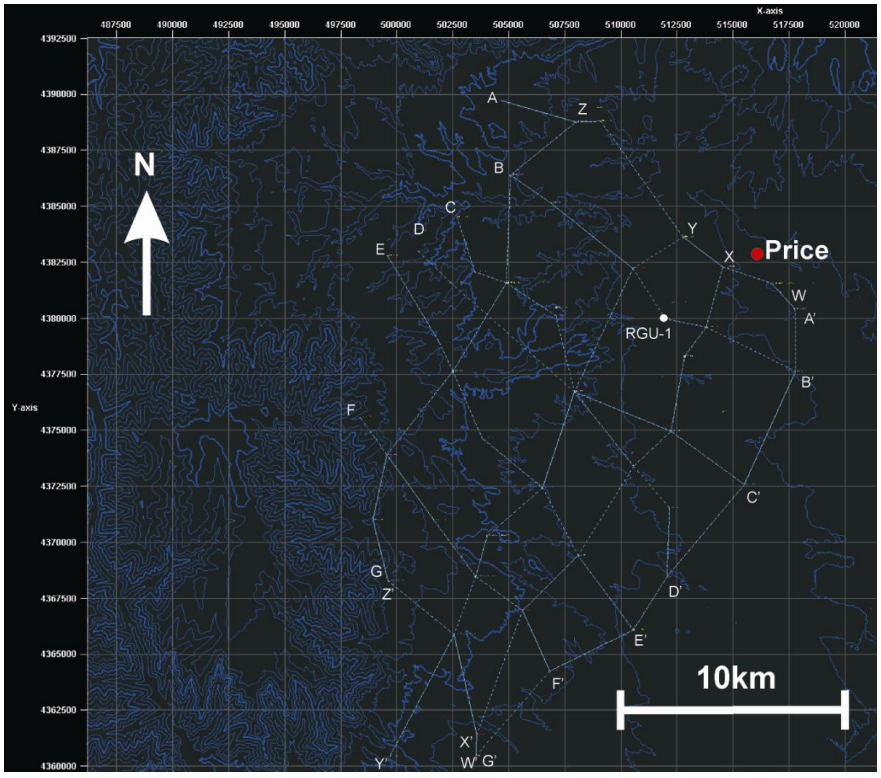

Overview map correlation panels extrapolated to outcrop:

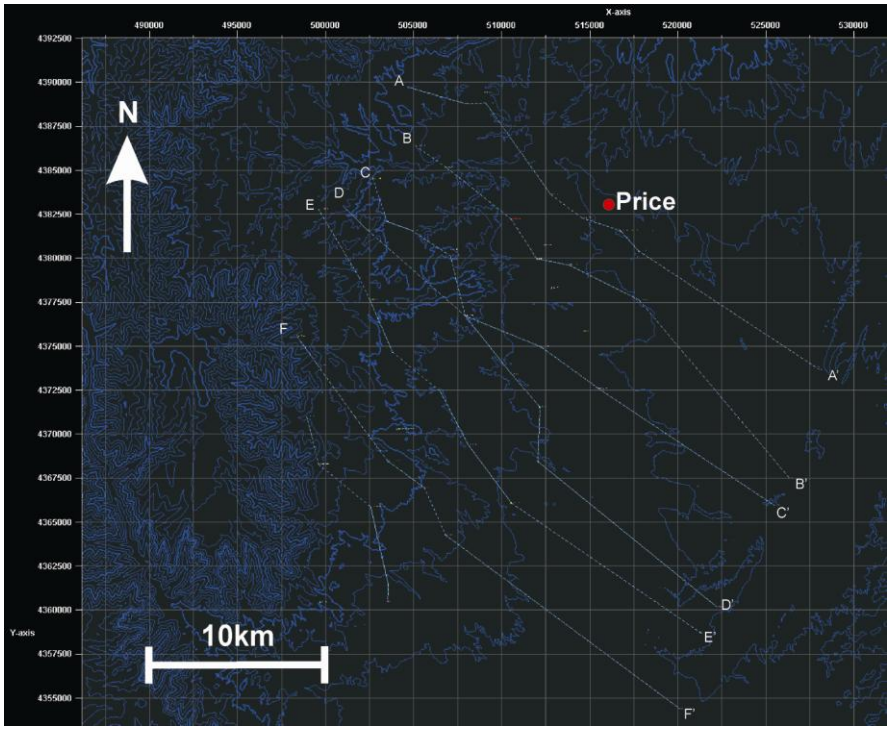

Correlation panels extrapolated to outcrop

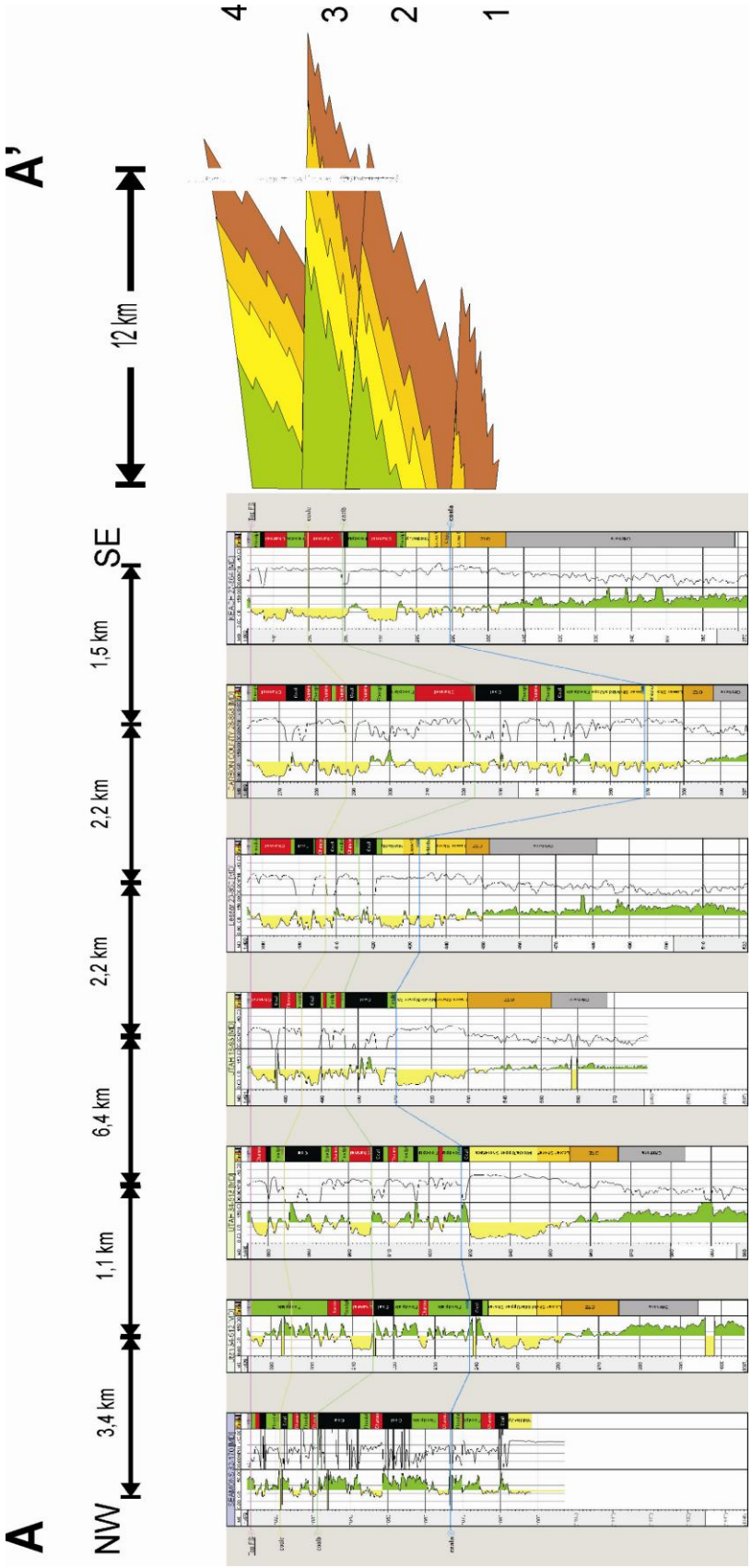

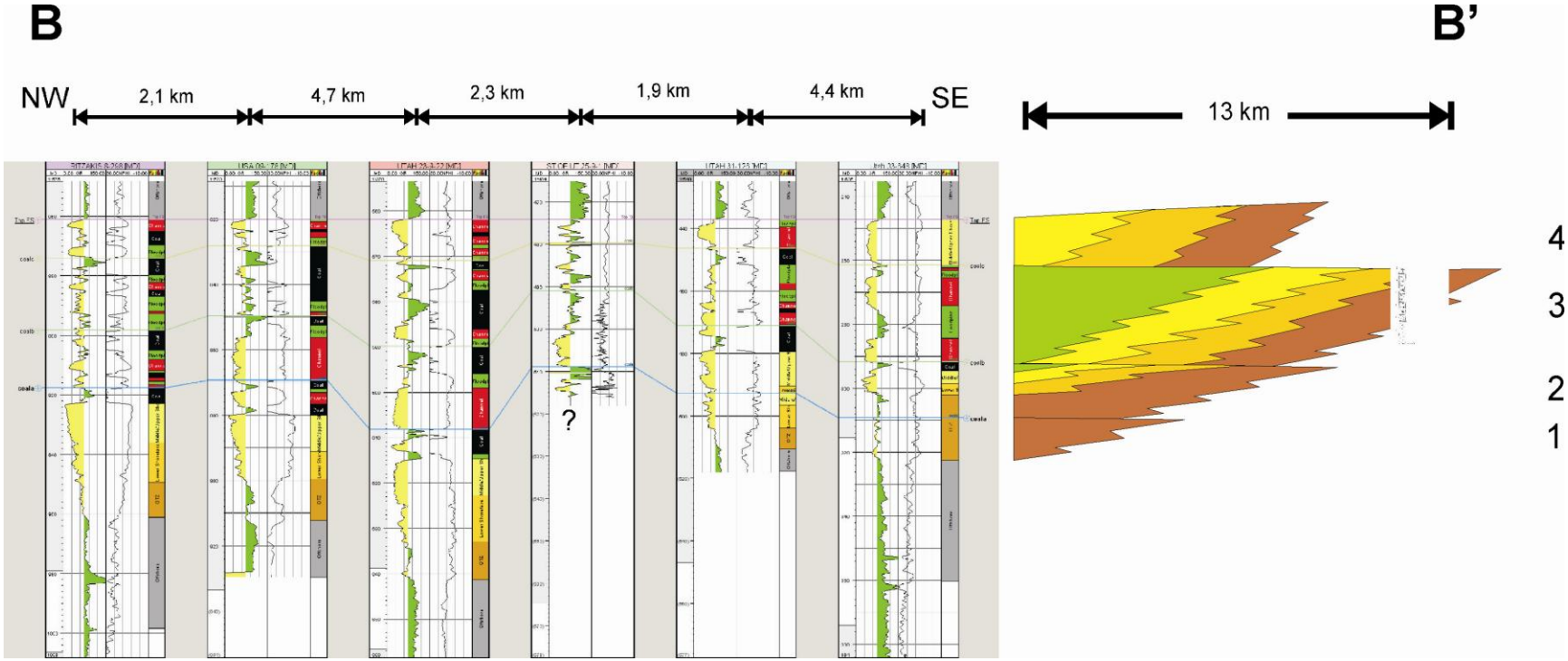
B
B'
NW
2,1 km
4,7 km
2,3 km
1,9 km
4,4 km
SE
13 km
?
4
3
2
1

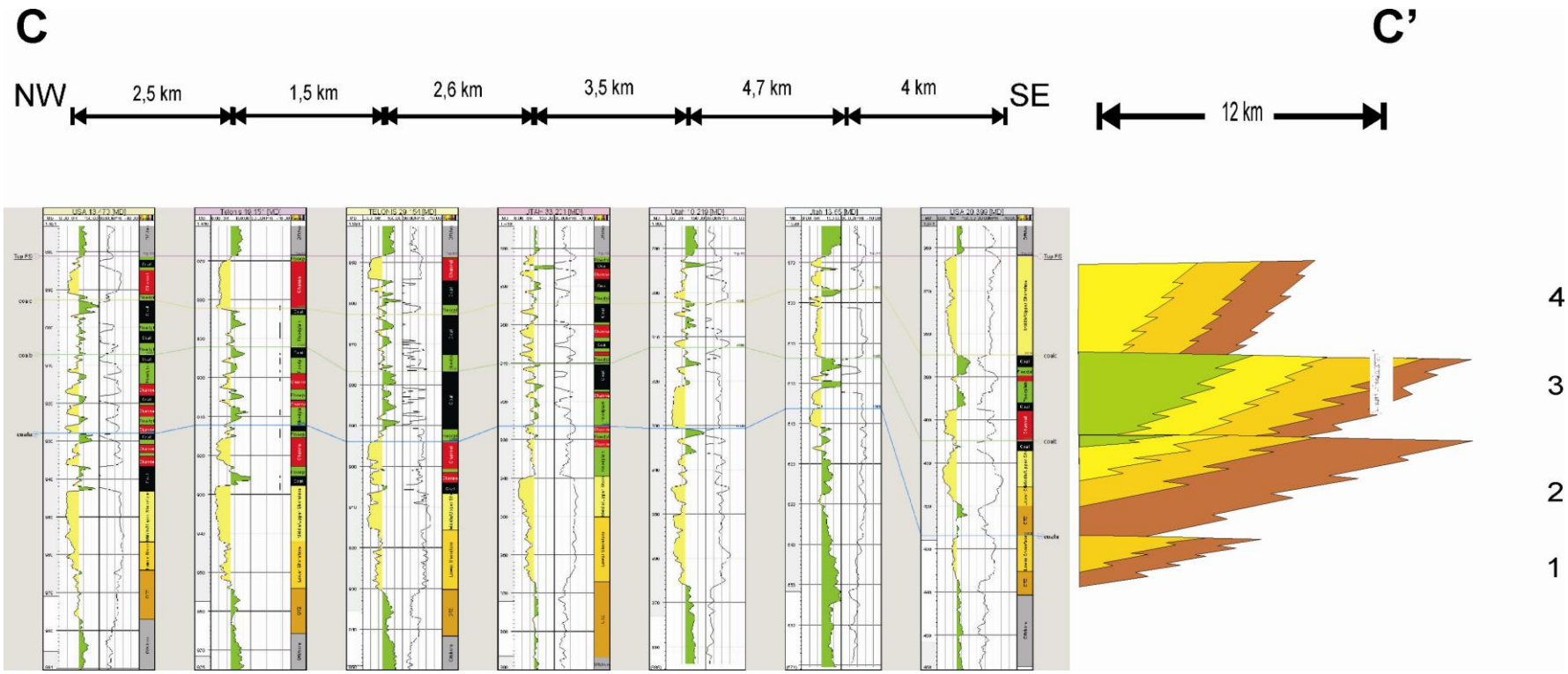
C
C'
NW
2,5 km
1,5 km
2,6 km
3,5 km
4,7 km
4 km
SE
12 km
4
3
2
1

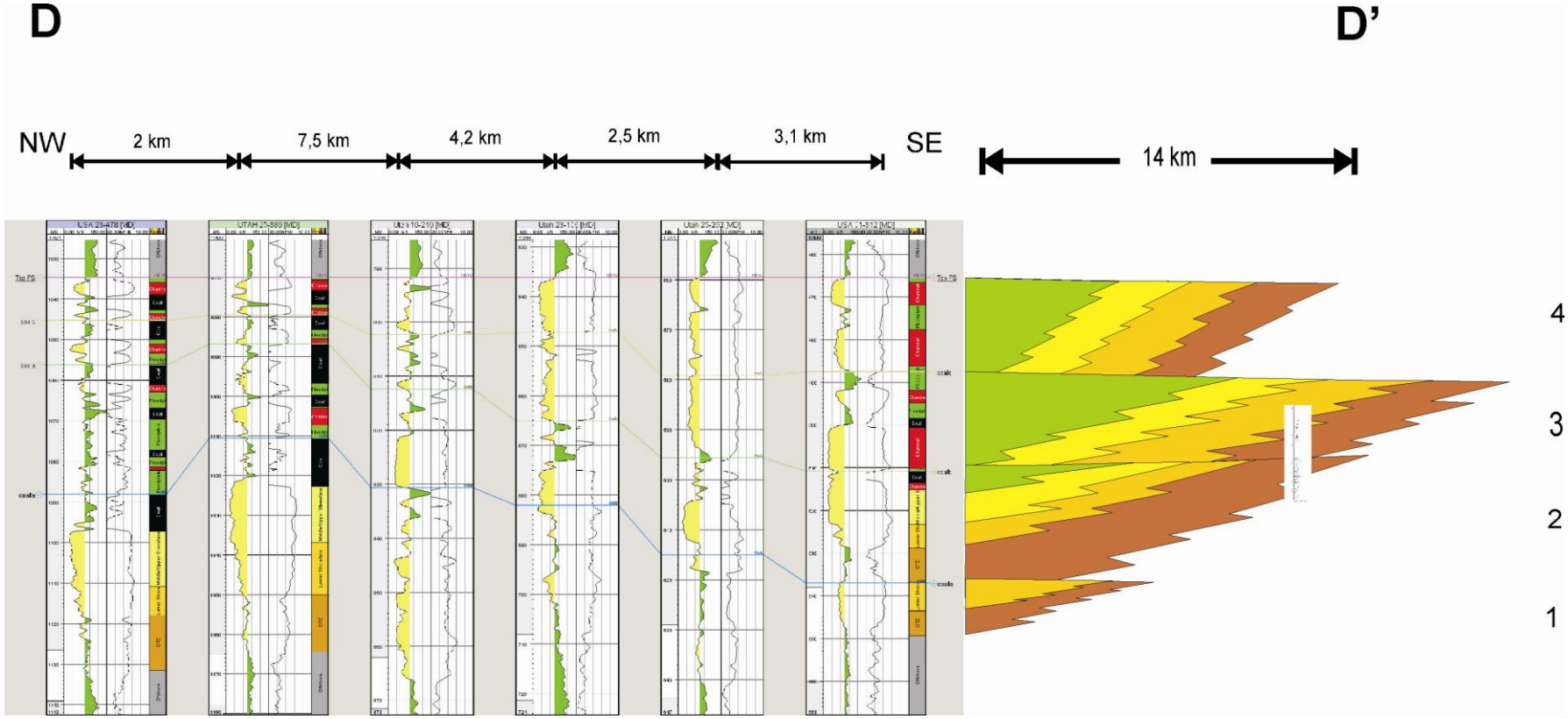
D
D'
NW
2 km
7,5 km
4,2 km
2,5 km
3,1 km
SE
14 km
4
3
2
1

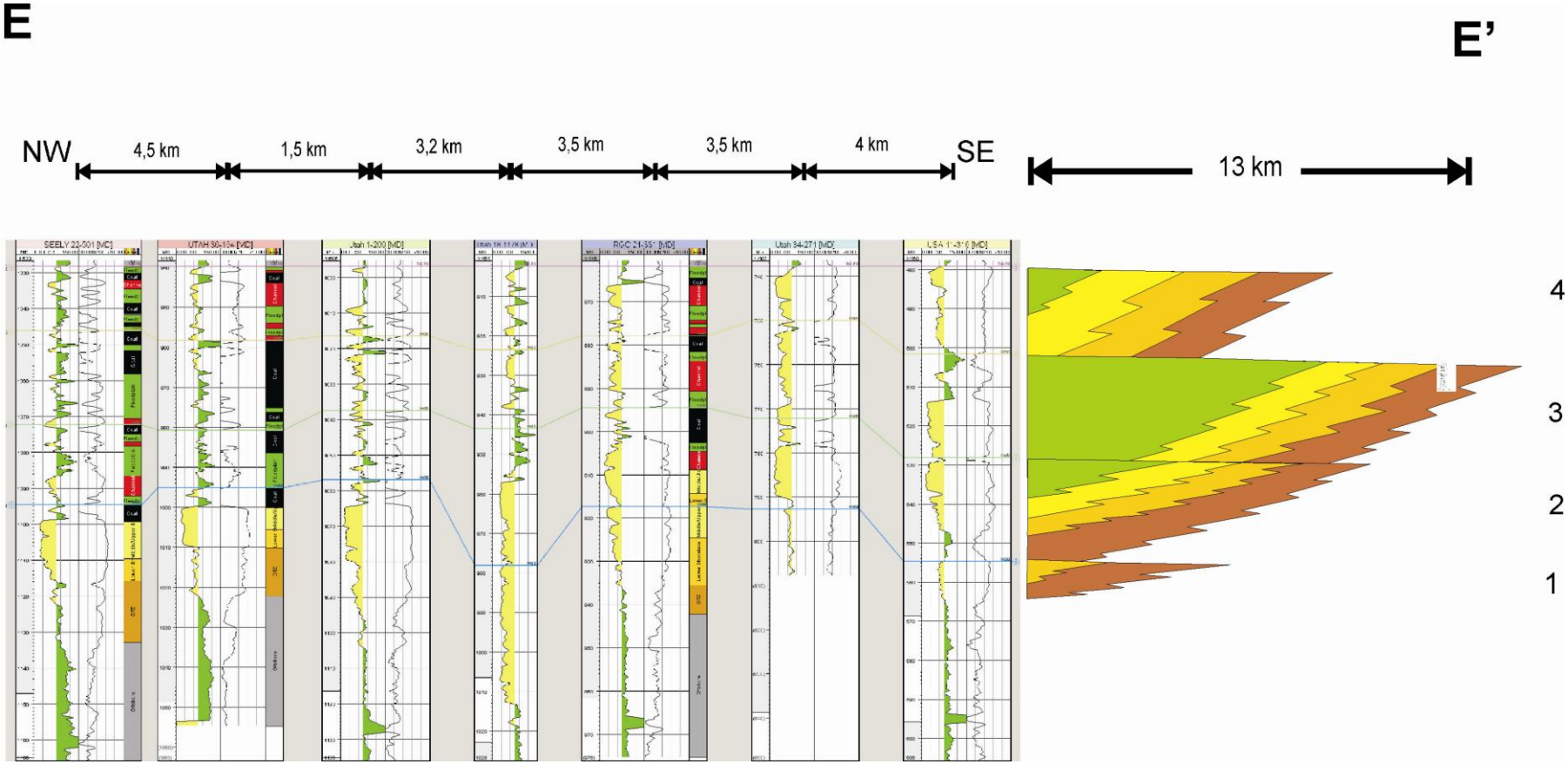
E
E’
NW
4,5 km
1,5 km
3,2 km
3,5 km
3,5 km
4 km
SE
13 km
4
3
2
1

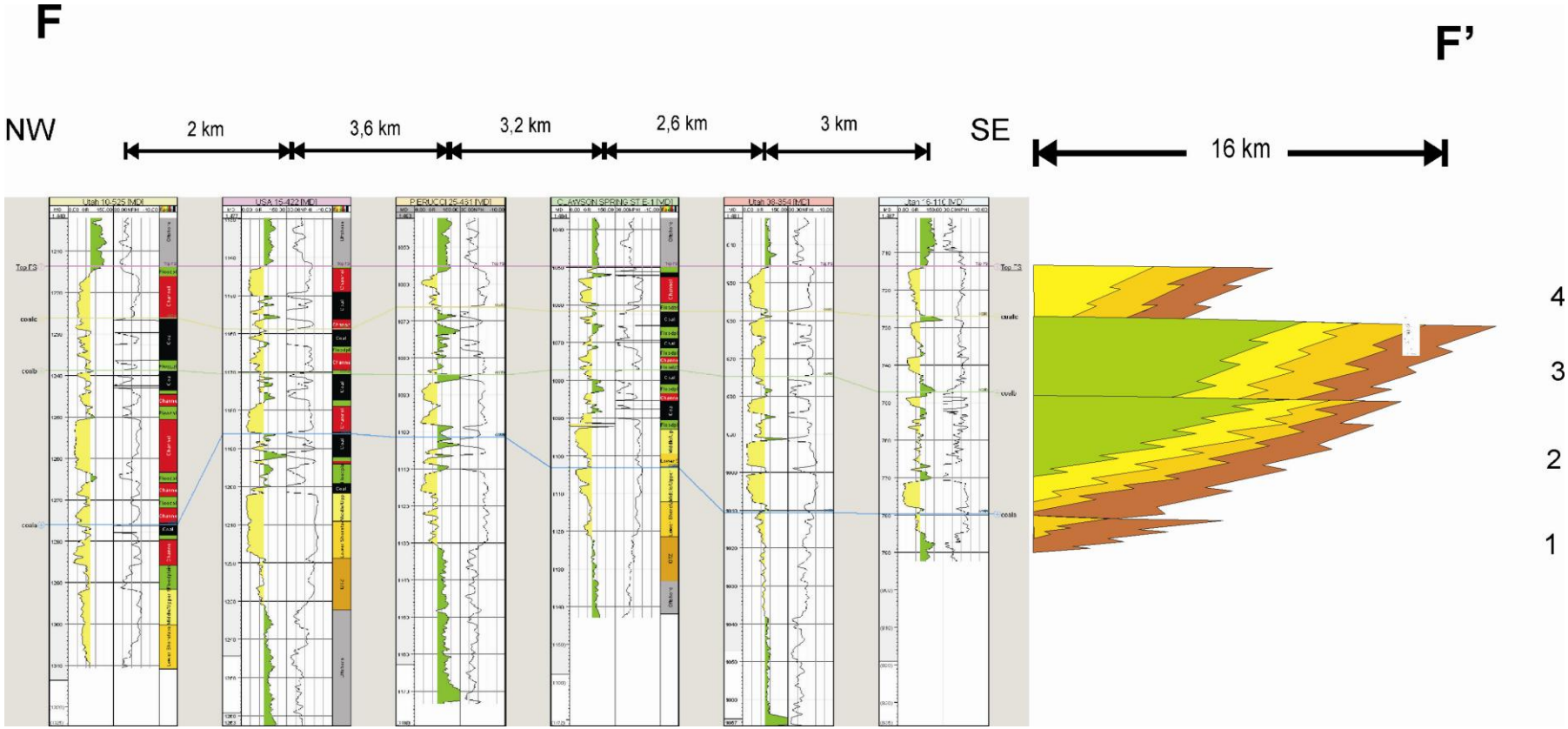
F
F'
NW
2 km
3,6 km
3,2 km
2,6 km
3 km
SE
16 km
4
3
2
1

Model statistics

Statistics for Merged3 (Unfiltered)

Code	Name	%	N	Intervals	Min	Mean	Max	Std
0	Offshore	12.53	874614	124845	0.0 (1)	13.4 (7.01)	33.3 (21)	8.092
1	OTZ	12.50	872318	242026	0.5 (1)	8.7 (3.6)	41.2 (12)	6.714
2	Lower Shoreface	11.18	780123	298179	0.4 (1)	8.7 (2.62)	54.4 (9)	6.56
3	Middle/Upper Shoreface	18.66	1302618	429891	0.2 (1)	14.4 (3.03)	96.4 (17)	13.72
4	Floodplain	29.22	2039050	640660	0.1 (1)	10.5 (3.18)	96.5 (24)	11.86
5	Channel	11.93	832840	409549	0.2 (1)	5.1 (2.03)	48.0 (18)	4.121
6	Lagoon/Embayment	0.00	1	1	6.4 (1)	6.4 (1)	6.4 (1)	0
7	Coal	3.97	277211	172427	0.2 (1)	5.1 (1.61)	28.4 (10)	3.145

Statistics for Merged3Final

Axis	Min	Max	Delta
X	498282.00	528132.00	29850.00
Y	4354283.00	4389783.00	35500.00
Z	811.03	2654.33	1843.31

Description	Value
Number of properties:	
In this folder:	5
Includes sub folders:	5
Cells (nI x nJ x nK)	597 x 710 x 29
Total number of cells:	12292230
Total number of cells in filtered area:	8092778
Unit:	

Name	Type	Min	Max	Delta	N	Mean	Std	Var	Sum
Facies [U]	Disc.	0	8	8	8092819	7	1	1	59654378
General discrete [U]	Disc.	0	4	4					
Coal	Disc.	7	8	1					
CoastalPlain	Disc.	4	8	4					
Merged	Disc.	0	7	7	8092830	3	2	4	21632904

Well log information table

API	Well Name	UTM E (NAD83)	UTM N (NAD 83)	Long	Lat	Z-min (feet)	Z-max (feet)	K.B.	Ground Level	Town -ship	Range	Meri -dian	Section	Surface Location	*.las?	Inc. Petrel?	Comments
4300730767	Utah 34-512	507991	4388767	-110.91	39.65	400	3300	6054	6047	13S	9E	S	34	1442 FSL 0855 FWL	Y	Y	Only GR
4300730820	UTAH 34-513	509100	4388810	-110.89	39.65	2100	3350	7320	7309	13S	9E	S	34	1582 FSL 0810 FEL	Y	Y	Wrong KB, corrected in Petrel: new KB at 1827,65 meters
4300730291	SEAMONS 32-170	504657	4389723	-110.94	39.66	3000	3600	6459	6452	13S	9E	S	32	0700 FNL 0500 FWL	Y	Y	
4300730506	Utah 34-510	508986	4389404	-110.89	39.65	2200	3430	5980	5973	13S	9E	S	34	1745 FNL 1185 FEL	Y	Y	
4300730777	Utah 27-520	498696	4380557	-111.01	39.57	400	3850	7109	7102	14S	8E	S	27	1253 FSL 2033 FWL	Y	Y	GR only
4300730800	SEELY 22-501	499582	4382798	-111	39.59	2600	3850	7020	7013	14S	8E	S	22	2184 FNL 0605 FEL	Y	Y	
4300730600	UTAH 25-389	502386	4381598	-110.97	39.58	2900	3950	7104	7097	14S	8E	S	25	0737 FNL 1976 FEL	Y	Y	
4300730706	USA 13-470	502688	4384507	-110.97	39.61	2300	3390	6471	6464	14S	8E	S	13	1741 FNL 0554 FEL	Y	Y	
4300730317	UTAH 36-164	501889	4378929	-110.98	39.56	3010	3460	6624	6617	14S	8E	S	36	1070 FSL 2000 FWL	Y	Y	Strange Neutron pororosity-reading at 3160ft, lacking part of trace?
4300730691	USA 15-422	499556	4373905	-111	39.51	3000	4250	7284	7277	14S	8E	S	15	0652 FSL 0535 FEL	Y	Y	
4300730793	USA 23-478	500966	4382993	-110.99	39.6	2600	3860	7028	7021	14S	8E	S	23	1509 FNL 0964 FEL	Y	Y	
4300730129	RGU 1	511986	4379969	-110.86	39.57	0	1930	N/A	5797	14S	9E	S	36	0755 FNL 1980 FEL	Y	Y	7' added to compensate for KB + CORE LOCATION
4300730130	ST OF UT 25-9-1	512319	4380712	-110.86	39.58	0	1700	N/A	5720	14S	9E	S	25	1683 FSL 0877 FEL	Y	Y	7' added to compensate for KB
4300730299	Telonis 19-151	503477	4382082	-110.96	39.59	400	3300	6450.5	6449.5	14S	9E	S	19	0860 FSL 2000 FWL	Y	Y	
4300730202	Utah 26-6-24	509836	4381369	-110.88	39.58	1700	2270	N/A	5863	14S	9E	S	26	1480 FNL 2000 FWL	Y	Y	
4300730178	Utah 36-1-2	512401	4380016	-110.85	39.57					14S	9E	S	36	0600 FNL 0620 FEL	N	N	Faint print/poor scan-> hard to read information
4300730199	Utah M-1	510171	4381058	-110.88	39.58					14S	9E	S	26	2500 FNL 2570 FEL	N	N	Test well, with no neutron porosity information (resistivity and GR only)
4300730419	USA 09-178	506843	4385169	-110.92	39.62	2500	3050	6222	6215	14S	9E	S	9	0428 FSL 2527 FWL	Y	Y	
4300730330	TELONIS 29-154	504890	4381577	-110.94	39.58	200	3150	6350	6343	14S	9E	S	29	0800 FNL 1500 FWL	Y	Y	
4300730201	UTAH 23-9-22	510540	4382222	-110.88	39.59	1650	2200	N/A	5820	14S	9E	S	23	1320 FSL 1320 FEL	Y	Y	
4300730386	UTAH 33-201	507094	4380116	-110.92	39.57	2300	3350	6601	6594	14S	9E	S	33	0317 FNL 1815 FEL	Y	Y	
4300730475	RITZAKIS 8-298	505075	4386391	-110.94	39.63	2300	3350	6247	6240	14S	9E	S	8	0798 FNL 2018 FWL	Y	Y	
4300730211	PRETTYMAN 10-15-34	508832	4385293	-110.9	39.62	2600	3850	7020	7013	14S	9E	S	10	0842 FSL 1419 FEL	Y	N	WRONG LAS deleted from petrel asit gave the wrong depth, revise
4300730294	UTAH 28-192	507117	4380483	-110.92	39.57	2560	3230	6573,9	6566,9	14S	9E	S	28	0888 FSL 1746 FEL	Y	Y	
4300731012	LDS 33-522	517186	4380033	-110.8	39.57	750	1300	N/A	5545	14S	10E	S	33	0636 FNL 0795 FEL	Y	Y	Incomplete neutron porosity log, lacks backup. 7' added to compensate for KB
4300730587	UTAH 18-93	512782	4383625	-110.85	39.6	1100	1900	5671	5664	14S	10E	S	18	0556 FSL 0673 FWL	Y	Y	
4300731332	CARBON COUNTY 28-863	516747	4381557	-110.8	39.58	500	1500	5536	5529	14S	10E	S	28	0952 FNL 2249 FEL	Y	Y	
4300731014	LESSAR 20-850	514554	4382291	-110.83	39.59	450	2000	5627,9	5620,9	14S	10E	S	20	1499 FSL 1164 FWL	Y	Y	
4300731292	KEACH 27-864	517777	4380410	-110.79	39.57	400	1300	5501,9	5494,9	14S	10E	S	27	0584 FSL 1110 FWL	Y	Y	
4300730305	UTAH 31-126	513810	4379608	-110.84	39.57	1100	1700	5693	5686	14S	10E	S	31	1954 FNL 1291 FEL	Y	Y	
4300730844	Utah 10-525	498364	4375580	-111.02	39.53	2500	4300	7541	7534	15S	8E	S	10	0880 FSL 0818 FWL	Y	Y	
4300730880	ANR 27-689	498930	4371005	-111.01	39.49	3000	4350	7191	7184	15S	8E	S	27	1640 FSL 2380 FWL	Y	Y	
4300730748	PIERUCCI 25-461	501655	4370985	-110.98	39.49	2700	3850	6820	6813	15S	8E	S	25	1575 FSL 1151 FWL	Y	Y	
4300730467	UTAH 1-209	502505	4377635	-110.97	39.55	2850	3750	6822	6815	15S	8E	S	1	2271 FSL 1251 FEL	Y	Y	
4300731124	Utah 18-1178	503803	4374646	-110.96	39.52	100	3500	6465	6456	15S	9E	S	18	2366 FNL 2423 FEL	Y	Y	GR only
4300730243	Utah 13-65	512236	4374958	-110.86	39.52	1660	2200	N/A	5710	15S	9E	S	13	1320 FNL 1200 FEL	Y	Y	7' added to compensate for KB, not found in Petrel
4300730653	RGC 21-331	506508	4372434	-110.92	39.5	2000	3200	6249	6242	15S	9E	S	21	1009 FSL 1148 FWL	Y	Y	
4300730496	UTAH 34-271	508087	4369405	-110.91	39.47	2200	2650	6114	6107	15S	9E	S	34	1693 FSL 0965 FWL	Y	Y	
4300730298	Utah 10-219	507927	4376719	-110.91	39.54	2400	2900	6308	6301	15S	9E	S	10	0805 FNL 0956 FWL	Y	Y	
4300730280	Utah 23-106	510572	4373393	-110.88	39.51	2000	2450	5835	5828	15S	9E	S	23	1400 FEL 1150 FNL	Y	Y	
4300730644	CLAWSON SPRING ST D-7	504033	4370278	-110.95	39.48	300	3650	6489	6478	15S	9E	S	31	0736 FNL 1634 FEL	Y	Y	
4300730400	Utah 25-252	512176	4371535	-110.86	39.49	1700	2200	5885	5878	15S	9E	S	25	1937FNL 1416 FEL	Y	Y	
4300730217	Utah 6-38	513682	4378313	-110.84	39.55	1550	1930	5220	5213	15S	10E	S	6	0899 FNL 1730 FEL	Y	Y	
4300730218	Utah 6-39	512844	4378302	-110.85	39.55	50	2150	N/A	5690	15S	10E	S	6	0934 FNL 0819 FWL	Y	Y	
4300730591	USA 20-399	515511	4372578	-110.82	39.5	750	1600	5722	5715	15S	10E	S	20	1445 FSL 1128 FEL	Y	Y	
4300730274	Utah 8-99	514565	4375831	-110.83	39.53	1200	1850	5678	5671	15S	10E	S	8	1500 FSL 1120 FWL	Y	Y	
4300730927	Utah 03-648	517793	4377624	-110.79	39.55	730	1350	5572.5	5565.5	15S	10E	S	3	2028 FSL 1075 FWL	Y	Y	
4301530546	Utah 27-585	498708	4362213	-111.01	39.41	3000	4300	7134	7127	16S	8E	S	27	0221 FNL 1708 FWL	Y	Y	
4301530487	Utah 34-517	499687	4360440	-111,00	39.39	1800	3000	6630	6623	16S	8E	S	34	0816 FNL 0347 FEL	Y	Y	
4301530463	CLAWSON SPRING ST C-3	502555	4365876	-110.97	39.44	2400	3400	6656	6645	16S	8E	S	12	1320 FSL 1320 FEL	Y	Y	
4301530473	CLAWSON SPRING ST F-1	499604	4368276	-111	39.46	250	4500	7320	7309	16S	8E	S	3	2071 FNL 0611 FEL	Y	Y	
4301530355	USA 11-316	510556	4366080	-110.88	39.44	1500	2150	5854	5847	16S	9E	S	11	1477 FSL 1713 FEL	Y	Y	
4301530464	Utah 08-354	505609	4366948	-110.93	39.45	2800	3550	6539.5	6532.5	16S	9E	S	8	1063 FNL 1924 FEL	Y	Y	
4301530317	Utah 31-175	503520	4360459	-110.96	39.39	2250	2750	6118	6110	16S	9E	S	31	0897 FNL 1731 FWL	Y	Y	
4301530531	PPCO D13	503565	4361407	-110.96	39.4	2300	3490	6192.5	6177	16S	9E	S	30	2217 FSL 1856 FWL	Y	Y	
4301530350	USA 01-312	512050	4368444	-110.86	39.47	1100	2000	5844	5837	16S	9E	S	1	1453 FNL 1881 FEL	Y	Y	
4301530404	CLAWSON SPRING ST E-1	503516	4368477	-110.96	39.47	300	3750	6770	6759	16S	9E	S	6	1394 FNL 1920 FWL	Y	Y	
4301530250	Utah 16-110	506828	4364245	-110.92	39.43	2250	2600	6312	6305	16S	9E	S	16	2000 FWL 0860 FSL	Y	Y	Too deep log-top to identify Top FS
	Carbon Canal					150	9600								Y		Drilled to Jurassic, just outside DW
Buzzard Bench																	
4301530286	Utah FED D 35-14	490215	4350544	-111.11	39.3	3000	4070	6943	6934	17S	7E	S	35	1249 FNL 0360 FWL	Y	Y	
Helper Field																	
4300730595	Helper Federal D-8	520361	4389794	-110.76	39.66	2500	3300	6235	6230	13S	9E	S	35	0546 FNL 1048FEL	Y	Y	

Waypoint information table

The table includes the most notable localities covered during the field work in Utah, 'missing' waypoint-number include start/end localities of logs after traversing (minor significance), bentonite that have not been sampled, localities of overview sketches and pictures. The strike/dip measurements were carried out to test for any eventual folding in the area of Jackass Flat, where the distal expressions of the southern Lower Ferron sandstone deposits disappear into the subsurface. These measurements did not yield any results to suggest such a feature, as expected, and are therefore not included in the thesis.

Waypoint	UTMX	UTMY	Elevation	Description
7	522233	4360161	1702	Logged outcrop
16	537301	4369920	1638	Bentonite sampling
17	537297	4369906	1637	Bentonite sampling
18	537334	4369950	1643	Bentonite sampling
23	537190	4369634	1628	Logged outcrop Lower Ferron
26	535754	4368409	1688	Logged outcrop Lower Ferron
29	535727	4368654	1690	Logged outcrop Lower Ferron
30	535689	4368657	1689	Logged outcrop Lower Ferron
33	526343	4367904	1642	Logged outcrop Lower Ferron
43	477072	4295152	1807	Logged outcrop Upper Ferron (Ivie Creek/I-70)
56	520131	4354378	1747	Logged outcrop Lower Ferron
58	521309	4358705	1716	Logged outcrop Lower Ferron
60	525504	4365932	1663	Logged outcrop Lower Ferron
65	528039	4373673	1668	Logged outcrop Lower Ferron
66	527106	4374607	1619	Bentonite sampling
68	524867	4363717	1677	Logged outcrop Lower Ferron
69	517599	4351728	1758	Bentonite sampling: highly weathered
70	517385	4351911	1753	Bentonite sampling: highly weathered
77	553910	4354730	1714	Bentonite sampling: highly weathered
84	526794	4375171	1661	Bentonite sampling: highly weathered
87	517405	4351382	1772	Strike-dip measurement Jackass Flat: 198/08
88	515807	4349656	1780	Strike-dip measurement Jackass Flat: 210/05
89	517940	4348640	1785	Strike-dip measurement Jackass Flat: 195/10
90	518257	4348632	1782	Strike-dip measurement Jackass Flat: 249/12
91	517573	4348000	1788	Strike-dip measurement Jackass Flat: 210/12
92	515427	4345534	1776	Strike-dip measurement Jackass Flat: 243/07
93	512555	4345851	1780	Strike-dip measurement Jackass Flat: 223/07
94	512490	4345495	1774	Logged outcrop 'Clawson' + Strike/dip: 240/07

Outcrop logs and raw log RGU-1

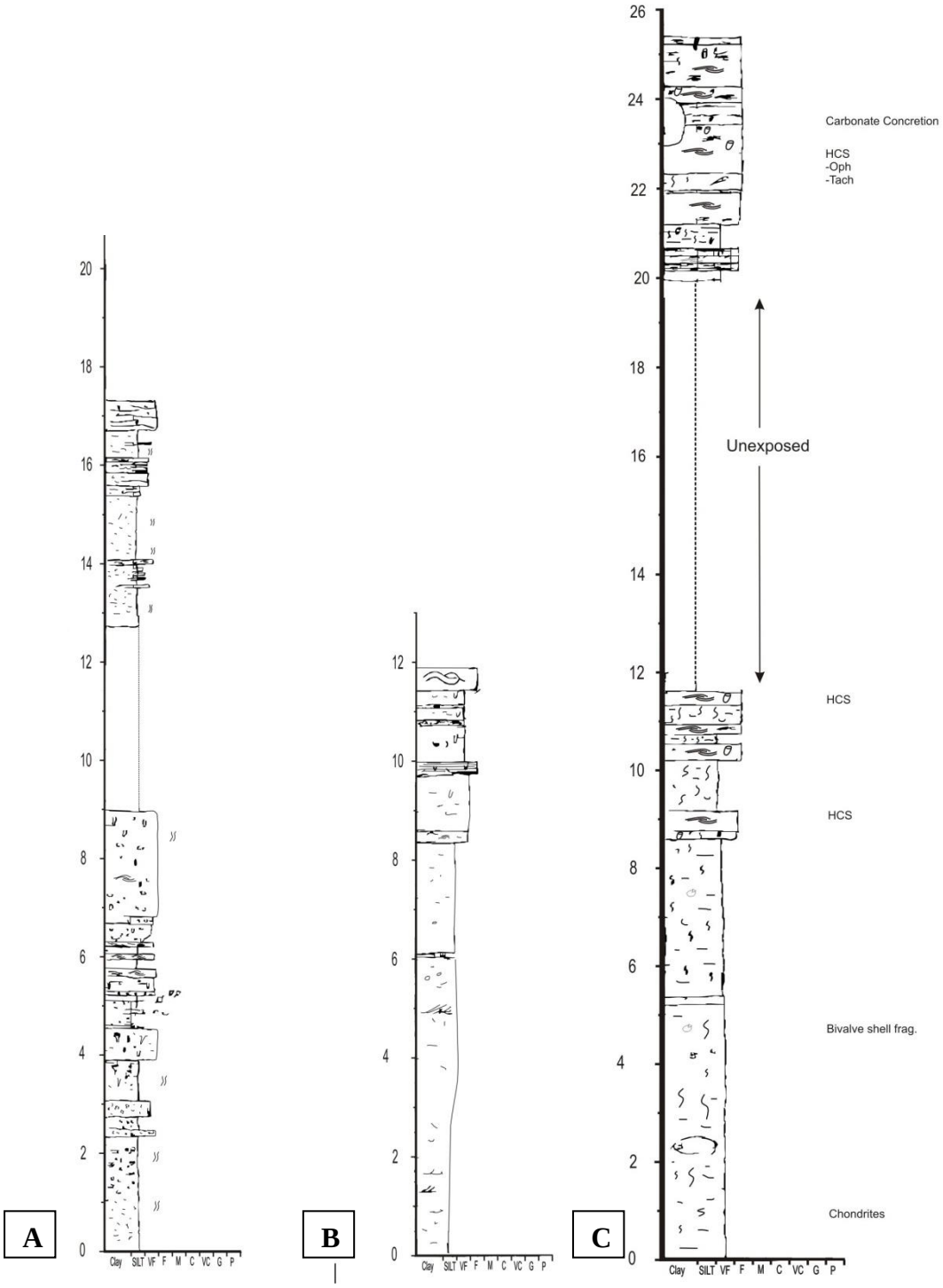

Figure A.5: A) WP 7, B) WP 26, C) WP 30

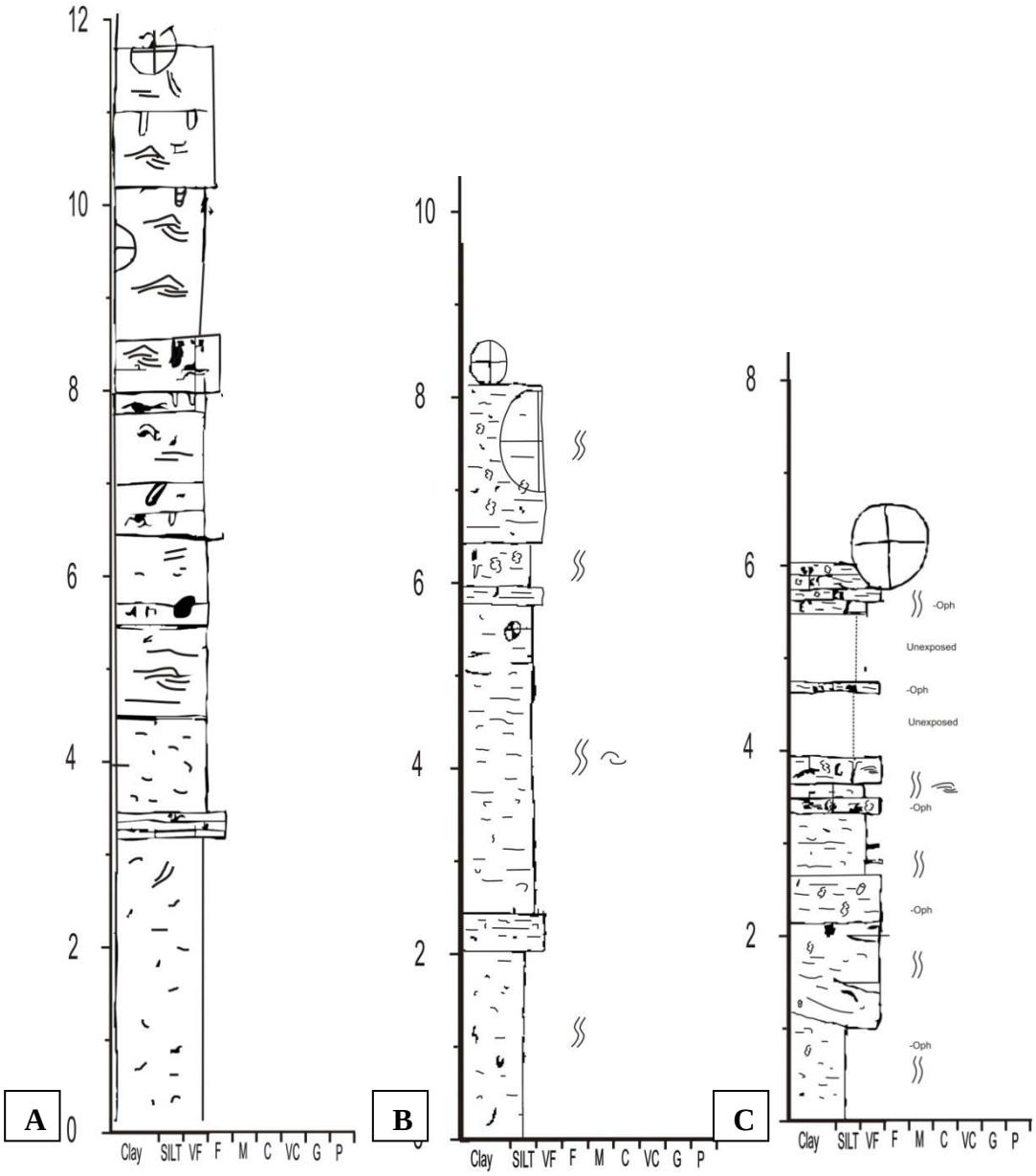

Figure A.6: A) WP 33, B) WP 56, C) WP 58

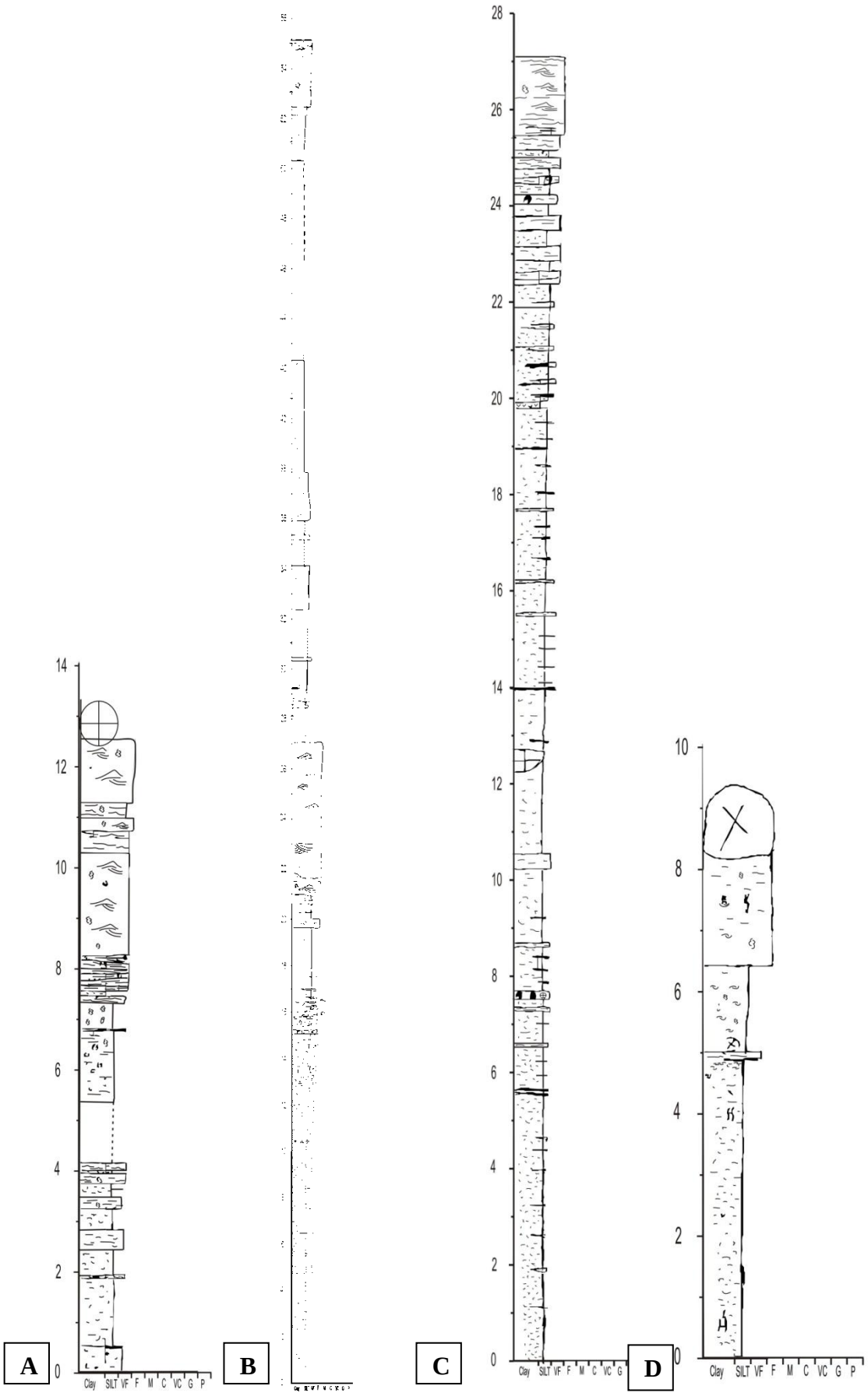

Figur A.7: A) WP 60, B) WP 65, C) WP 68, D) WP 94

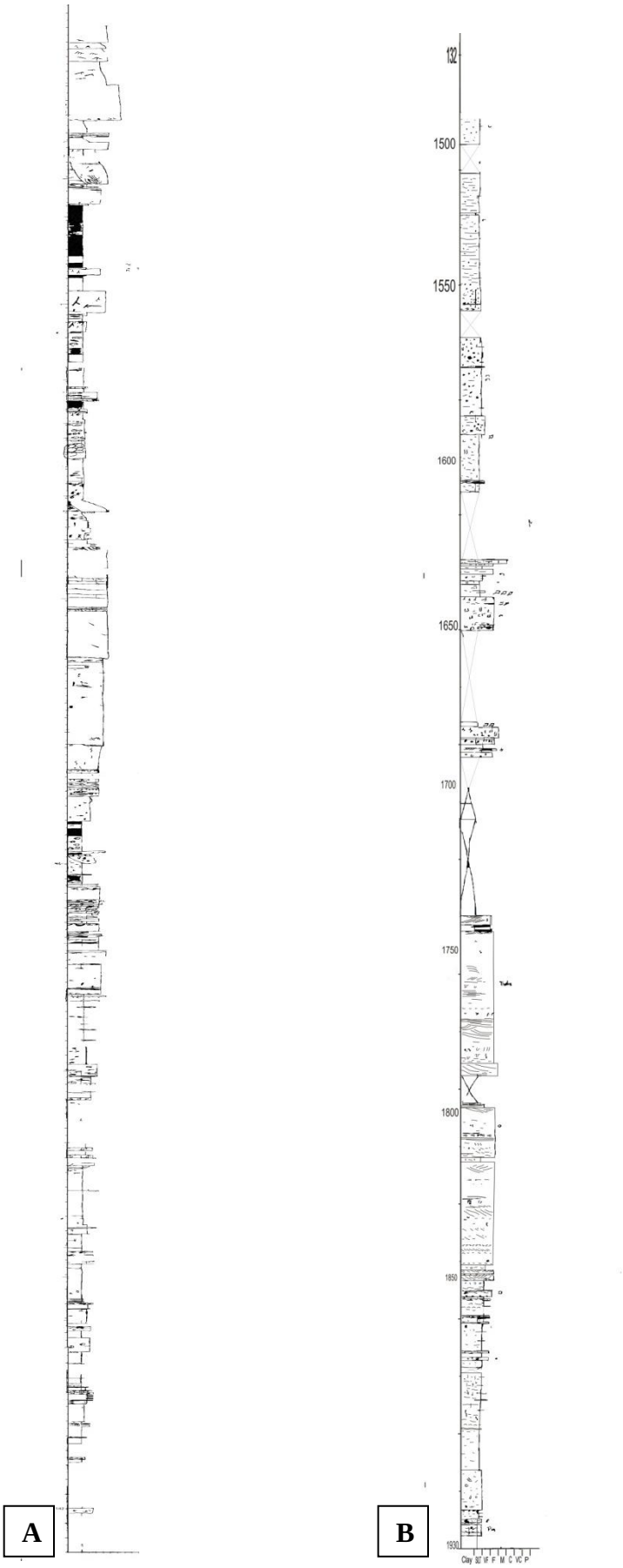

Figur A.8: A) Ivie Creek, B) RGU-1 (Depth given in feet)